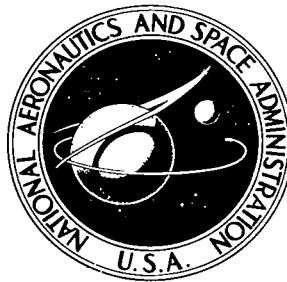


NASA TECHNICAL NOTE



NASA TN D-6011

C. 1

LOAN COPY: RET  
AFWL (WLO)  
KIRTLAND AFB,



NASA TN D-6011

AERODYNAMIC CHARACTERISTICS  
OF AIR-CUSHION MODELS AT  
VERY LOW GROUND CLEARANCES AND  
AT FREE-STREAM DYNAMIC PRESSURES  
EXCEEDING CUSHION PRESSURE

*by Kalman J. Grunwald and William G. Johnson, Jr.*

*Langley Research Center*

*Hampton, Va. 23365*



0132670

1. Report No. <b>NASA TN D-6011</b>		2. Government Accession No.		3. Recipient's Catalog No.	
4. Title and Subtitle <b>AERODYNAMIC CHARACTERISTICS OF AIR-CUSHION MODELS AT VERY LOW GROUND CLEARANCES AND AT FREE-STREAM DYNAMIC PRESSURES EXCEEDING CUSHION PRESSURE</b>				5. Report Date <b>October 1970</b>	
				6. Performing Organization Code	
7. Author(s) <b>Kalman J. Grunwald and William G. Johnson, Jr.</b>				8. Performing Organization Report No. <b>L-7369</b>	
				10. Work Unit No. <b>126-63-11-01</b>	
9. Performing Organization Name and Address <b>NASA Langley Research Center Hampton, Va. 23365</b>				11. Contract or Grant No.	
				13. Type of Report and Period Covered <b>Technical Note</b>	
12. Sponsoring Agency Name and Address <b>National Aeronautics and Space Administration Washington, D.C. 20546</b>				14. Sponsoring Agency Code	
15. Supplementary Notes					
16. Abstract  Air-cushion models employing peripheral jet and plenum cushions of circular, rectangular, and side-by-side planforms were tested in hovering and at forward speed in the 17-foot (5.18-meter) test section of the Langley 300-MPH 7- by 10-foot tunnel. The principal purpose of these tests was to study the characteristics of air cushions when free-stream dynamic pressure exceeded air-cushion pressure. Also examined were the hovering performance and the effects of moving ground belt, crosswind, height, and angle of attack. For the configurations tested, there was no significant loss in cushion performance when free-stream dynamic pressure exceeded cushion pressure.					
17. Key Words (Suggested by Author(s)) <b>Tracked air-cushion vehicle Air-cushion vehicle</b>			18. Distribution Statement <b>Unclassified - Unlimited</b>		
19. Security Classif. (of this report) <b>Unclassified</b>		20. Security Classif. (of this page) <b>Unclassified</b>		21. No. of Pages <b>127</b>	
				22. Price* <b>\$3.00</b>	

AERODYNAMIC CHARACTERISTICS OF AIR-CUSHION MODELS AT  
VERY LOW GROUND CLEARANCES AND AT FREE-STREAM  
DYNAMIC PRESSURES EXCEEDING CUSHION PRESSURE

By Kalman J. Grunwald and William G. Johnson, Jr.  
Langley Research Center

SUMMARY

Air-cushion models employing peripheral jet and plenum cushions of circular, rectangular, and side-by-side planforms were tested in hovering and at forward speed in the 17-foot (5.18-meter) test section of the Langley 300-MPH 7- by 10-foot tunnel. The principal purpose of these tests was to study the characteristics of air cushions when free-stream dynamic pressure exceeded air-cushion pressure. Also examined were the hovering performance and the effects of moving ground belt, crosswind, height, and angle of attack. For the configurations tested, there was no significant loss in cushion performance when free-stream dynamic pressure exceeded cushion pressure.

Although a variety of powered air-cushion configurations were tested, the results indicate that the cushion performance was independent of configuration. External forces and moments on the body or shell of the vehicle were measured and found to be representative of the unpowered configuration of the shape tested and also to be independent of the cushion.

Belt characteristics, such as permeability and surface roughness, caused unexpected results in hovering performance. When the experimental limitations which resulted in discrepancies in the data were isolated and corrected, hovering performance followed the exponential theory as expected.

Crosswind conditions in general did not produce any significant changes in the air-cushion characteristics. The data were also unaffected by large percentage variations in height. However, the use of the moving belt is required if accurate flow conditions under the air cushion are to be achieved.

INTRODUCTION

The Office of High-Speed Ground Transportation within the U.S. Department of Transportation (DOT) is interested in tracked air-cushion vehicles for possible future

high-speed ground transportation systems. The present investigation of the aerodynamics of cushions was undertaken by NASA at the request of DOT in order to provide some of the data needed for the design and evaluation of air-cushion vehicles.

Although considerable data and experience are available for untracked air-cushion vehicles (also referred to as ground-effect machines), these data do not extend to the very small clearances and high operating speeds at which the cushions of tracked air-cushion vehicles will be expected to operate. In particular, almost no data are available for conditions where the dynamic pressure due to vehicle speed significantly exceeds the cushion pressure.

The primary purpose of the present investigation was to study the characteristics of cushions operating at very small clearances at ratios of dynamic pressure to cushion pressure from zero to greater than 1. In order to evaluate the cushion characteristics properly, it was necessary to separate the cushion forces and moments from the aerodynamic forces and moments on the external surfaces of the models. This separation was accomplished by mounting a body shell and an air cushion on separate balances. Tests were conducted on a circular-shaped and a rectangular-shaped model, each with both peripheral jet and modified plenum air cushions. Another model with two rectangular peripheral jet air cushions mounted side by side was also tested. The rectangular-type and side-by-side models were also tested at various sideslip angles to simulate cross-wind conditions.

The tests were conducted in the 17-foot (5.18-meter) test section of the Langley 300-MPH 7- by 10-foot tunnel over the endless-belt moving ground plane (ref. 1). A significant, but secondary, part of the investigation was to determine the need for the moving ground plane for this type of testing. Therefore, some comparative tests were made with the belt moving and with the belt stopped.

TRW Systems Group was under contract to the Department of Transportation to assist the NASA Langley Research Center during the tests. They also conducted an independent analysis of the data, which is presented under separate cover in reference 2.

## SYMBOLS

An axis-system drawing indicating the positive direction of forces, moments, and angles is presented in figure 1. All the data have been presented about the moment reference center as shown in figures 1 and 2. The units used for the physical quantities in this paper are given in the International System of Units (SI). In some cases, equivalent values are given in the U.S. Customary Units.

A	planform area of air cushion, 0.46 m <sup>2</sup> (5 ft <sup>2</sup> )
A <sub>1</sub>	planform area over which the cavity pressure acts, 0.46 m <sup>2</sup> (5 ft <sup>2</sup> )
b	body width of rectangular-type model, 35.56 cm (14.0 in.)
C <sub>p</sub>	pressure coefficient, $\frac{\text{Local pressure} - \text{Atmospheric pressure}}{L_s/A}$
c	body length of rectangular-type model, 210.82 cm (83 in.)
d	diameter of air cushion for circular model, 79.96 cm (30.30 in.)
d <sub>e</sub>	diameter of circle whose area is equivalent to planform area of air cushion, 79.96 cm (30.30 in.)
F' <sub>D</sub>	drag (approximate), N (lb)
F <sub>L</sub>	lift, N (lb)
F <sub>Y</sub>	side force, N (lb)
H	plenum pressure as defined for exponential theory (ref. 3), N/m <sup>2</sup> (lb/ft <sup>2</sup> )
h	average height from model to ground, measured at moment reference center, m (ft)
L	total cushion length, cm (in.)
L <sub>s</sub>	static lift, N (lb)
l	distance from leading edge of cushion to local pressure orifice, cm (in.)
M <sub>X</sub>	rolling moment, m-N (ft-lb)
M <sub>Y</sub>	pitching moment, m-N (ft-lb)
M <sub>Z</sub>	yawing moment, m-N (ft-lb)

$P_c$	cushion pressure as defined for exponential theory (ref. 3), $L_s/A$ , $N/m^2$ (lb/ft <sup>2</sup> )
$P_{cav}$	cavity pressure, $N/m^2$ (lb/ft <sup>2</sup> ) (see fig. 5)
$P_{pl}$	settling-chamber pressure, $N/m^2$ (lb/ft <sup>2</sup> ) (see fig. 5)
$P_s$	free-stream static pressure, $N/m^2$ (lb/ft <sup>2</sup> )
$q$	dynamic pressure, $\frac{1}{2}\rho V^2$ , $N/m^2$ (lb/ft <sup>2</sup> )
$R$	Reynolds number
$t$	jet-exit thickness, cm (in.) (see fig. 4)
$V$	free-stream velocity, m/sec (ft/sec)
$W$	mass flow, kg/sec (lb/sec)
$X$	jet thickness parameter (ref. 3), $\frac{t}{h}(1 + \cos \theta)$
$\alpha$	angle of attack, deg
$\beta$	sideslip angle, deg
$\theta$	angle between jet-exit line and local horizontal (ref. 3), deg
$\rho$	free-stream density, kg/m <sup>3</sup> (slugs/ft <sup>3</sup> )

Subscripts:

$c$	center line
$L$	left pad
$R$	right pad

## MODEL DESCRIPTION

Three basic models tested during the research program were a circular model with a single circular air cushion, a rectangular model with a single rectangular air cushion, and a larger rectangular model with two rectangularly shaped cushions (referred to as the side-by-side model). Each air cushion was constructed of aluminum, and each was separately mounted to an internal strain-gage balance which was mounted to a strut support. The vehicle bodies of all three models were of glass-fiber construction and were supported by separate internal strain-gage balances mounted to the strut support. Drawings of the models giving pertinent dimensions are presented in figure 2, and photographs are presented in figure 3.

The circular air cushion and the rectangular air cushion were tested both as a modified plenum and as a peripheral jet. The two-cushion side-by-side model was tested only in the peripheral jet configuration. A drawing of the internal design is presented in figure 4. When the base plate, as shown in figure 4, is located nearly flush with the base of the outer ring, the peripheral jet gap is formed. The peripheral jet gap dimensions were as follows:

### Circular model:

Hovering . . . . .	0.064 cm (0.025 in.);	0.254 cm (0.100 in.)
Forward speed . . . . .	0.064 cm	(0.025 in.)

### Rectangular-type model:

Hovering . . . . .	0.051 cm (0.020 in.);	0.318 cm (0.125 in.)
Forward speed . . . . .	0.051 cm	(0.020 in.)

### Side-by-side model:

Hovering . . . . .	0.051 cm (0.020 in.)
Forward speed . . . . .	0.051 cm (0.020 in.)

If this base plate is moved to the higher location, shown as dashed lines in the figure, the annular-type plenum (modified plenum) is configured.

Although the internal construction was different for the circular and the rectangular-type air cushions, the method of providing air at the jet exit was essentially the same. The high-pressure air passed through the air lines and was dumped into a high-pressure chamber inside the air cushion. From this chamber it exited uniformly into a much larger chamber, which is referred to herein as the settling chamber (figs. 4 and 5), and finally exited through the converging jet exit around the perimeter of the model.

Base plates with a wider peripheral jet gap were constructed for both the circular and the rectangular-type models. The new base plates permitted these configurations to be tested with a jet having a Reynolds number about one order of magnitude higher than

the Reynolds number for the original base plates. A screen of 20 percent porosity was constructed for use inside the pressure chamber of the rectangular-type model with the larger jet.

The body shell was designed as an air shield for the air cushion and was mounted on a separate balance with a small clearance gap between the body and the air cushion at the model periphery (fig. 5). In this manner, forces and moments could be recorded separately for the body and the air cushion and then added to give total vehicle loads. Unfortunately, this installation resulted in an air leakage around the perimeter of the vehicle between the shell and the air cushion, and a region of varying pressure was created between the two (fig. 5). The pressure that developed therein was measured and then was used to adjust the data so that the cavity conditions were based on free-stream static pressure. This adjustment is discussed in more detail in the section on "Corrections to Lift."

The body shell for the side-by-side model could be tested with or without the air exhaust contoured channel located in its base. (See figs. 2(c) and 2(d).) Pressure orifices were located along the center line of the contoured channel and along the center line of the flat-bottom configuration. (See fig. 6(a).) Pressure orifices were located in the base of the rectangular-type air cushion (fig. 6(b)); the measured pressures are presented along with the force data.

## TESTING TECHNIQUES, ACCURACY, AND CORRECTIONS

### Testing Technique

Powered-model hovering tests were performed both over a smooth plastic ground surface in a large room (referred to as static room in the figures) and over the ground belt in the 17-foot (5.18-meter) test section of the Langley 300-MPH 7- by 10-foot wind tunnel. Belt material was fastened to the smooth plastic ground surface, and tests were conducted to determine the effect of the material surface and permeability on the performance of the air cushion.

The forward-speed tests were conducted over the moving belt in the 17-foot (5.18-meter) test section. Final leveling and height adjustments were made with the model power on and the desired static lift established. Following these adjustments, the required tunnel speed was established, and the moving ground belt was brought to an equivalent speed. Tunnel and belt speeds were varied to cover the desired ratios of free-stream dynamic pressure to cushion pressure (0 to approximately 6) while the jet mass flow was held constant.



## Accuracy Considerations

Throughout the test program, problems which degraded the accuracy of the results and led to scatter were encountered, particularly with determining the model height or the effective height. Most of these problems arose because the moving-belt ground plane was not originally designed for this type of operation. Prior to these tests, the belt backing plate was straightened, and subsequent contour checks indicated that it was flat to within  $\pm 0.03$  cm (0.01 inch). Measurements of the belt thickness indicated a variation of  $\pm 0.01$  cm (0.004 inch). During tests with model air and tunnel air flowing, additional variations in contour were introduced by the lifting of the belt. Other problems such as belt surface roughness and porosity also affected the results to a lesser, but undetermined, degree. The effects that these problems have on the results are discussed in appropriate parts of the text.

## Corrections to Lift

As previously mentioned, the vehicle body and air cushion were mounted on separate balances in order to measure the forces on each separately. This separation required a clearance gap large enough to eliminate contact between the body and the cushion. (See fig. 5.) The flow conditions in the region of the clearance gap resulted in reduced pressure inside the cavity. This reduced pressure acted over the entire upper surface of the air cushion and upon the inner surface of the vehicle body. Although a similar condition may exist on a full-size vehicle, the local pressure existing in the cavity would probably not be the same as experienced for these models.

In order to establish a common reference for the data, the cushion lift data were corrected to correspond to a condition of free-stream static pressure in the cavity. The following expression was used to correct the cushion lift:

$$\text{Lift}_{\text{corrected}} = \text{Lift}_{\text{measured}} + \Delta P_{\text{cav}} A_1$$

where  $\Delta P_{\text{cav}}$  is the difference between the pressure measured in the cavity and the free-stream static pressure, and  $A_1$  is the planform area over which the cavity pressure acts.

## PRESENTATION OF RESULTS

	Figure
Hovering performance (all configurations) . . . . .	7 to 12
Circular model (peripheral jet):	
Effect of forward speed . . . . .	13 to 14
Effect of ground boundary layer . . . . .	15

	Figure
Effect of height . . . . .	16
Unpowered data . . . . .	17 to 18
Effect of angle of attack . . . . .	19
Circular model (modified plenum):	
Effect of forward speed . . . . .	20 to 21
Effect of height . . . . .	22
Unpowered data . . . . .	23 to 24
Rectangular-type model (peripheral jet):	
Effect of forward speed (pressure measurements included) . . . . .	25 to 26
Effect of sideslip (pressure measurements included) . . . . .	27 to 28
Effect of ground boundary layer (pressure measurements included) . . . . .	29
Rectangular-type model (modified plenum):	
Effect of forward speed . . . . .	30 to 31
Effect of sideslip (pressure measurements included) . . . . .	32 to 33
Side-by-side model (contoured channel):	
Effect of forward speed . . . . .	34 to 35
Effect of sideslip . . . . .	36 to 37
Effect of ground boundary layer . . . . .	38
Effect of angle of attack . . . . .	39
Effect of differential pad pressure . . . . .	40 to 41
Side-by-side model (flat bottom):	
Effect of forward speed . . . . .	42 to 43
Effect of sideslip . . . . .	44
Effect of ground boundary layer . . . . .	45
Effect of height . . . . .	46
Unpowered data (flat bottom and contoured channel) . . . . .	47
Pressure distributions for channel and flat-bottom base center line . . . . .	48

## DISCUSSION

For the reader's convenience, the data have been separated into three categories according to configuration. However, the discussion will consider the configurations together because of the similarity in results and conclusions.

### Hovering

Tests were conducted on each peripheral jet cushion for the hovering (static) mode in a large room over a smooth plastic ground surface and then were repeated in the tunnel over the woolen belt used during moving-belt tests. These test data are compared in

figures 7 to 11 with the exponential theory of reference 3, which can be used to predict the performance of the peripheral jet in the hovering mode. This theory predicts the ratio of cushion pressure to settling-chamber pressure as a function of jet thickness and model height.

The different overall levels of performance for the three cushions, as can be seen in figure 7, were unexpected. These data were expected to fall slightly below the exponential-theory curve because of the low Reynolds number, and it was also expected that the three configurations would fall essentially together since they were tested at nearly the same Reynolds number. The particularly poor performance of the rectangular-type model when compared with the performance of the other configurations was, therefore, quite surprising. If the exponential theory is assumed to be representative, the considerably lower performance must be caused by the experimental setup and could be a result of poor air-flow supply distribution or inaccurate plenum pressure measurement. The latter possibility was ruled out after a series of check calibrations and a program to investigate the air-flow supply distribution were initiated.

In order to investigate the effect of Reynolds number, new base plates forming wider peripheral gap were constructed for both the circular and the rectangular-type models. A pressure-drop screen was constructed for installation in the air chamber of the rectangular-type model just ahead of the larger peripheral jet annulus (0.318 cm (0.125 inch)) to improve the flow distribution. The effect of this screen was evaluated, and the data indicate substantially improved performance. (See fig. 10.) No tests were conducted on the smaller gap model with the screen installed. Figures 11 and 12 show the effect of Reynolds number on cushion pressure and compare these data with some test data from reference 4.

Differences in performance due to the surface of the ground simulation and the vehicle configuration are presented in figures 8 and 9. It appears from these tests that a number of variables were being inadvertently introduced because of the test equipment used, particularly the belt. The most significant effect of the belt on the cushion was introduced by its surface roughness, which may have partially destroyed the peripheral jet curtain and thereby caused a reduction in the effectiveness of the curtain to maintain cushion pressure. Air passing through the belt during the tests caused some belt lifting and may also have affected cushion performance.

Unpublished test data of the modified plenum, which showed no measurable difference between the belt and smooth surface, tend to support the hypothesis that the peripheral jet curtain was being destroyed. The modified plenum does not require the jet curtain to maintain cushion pressure nor does it have the higher peripheral jet-exit velocities and, therefore, was not so dependent on the belt surface and permeability.

Hovering tests performed with the vehicle body installed over the rectangular-type peripheral jet cushion (fig. 9) did not give the same results as had been obtained with the cushion alone. The differences here may have resulted from the pressure field established about the body or the effect that the clearance-slot pressure field between the cushion and body had on the jet curtain.

The experience gained in this program indicates the importance of using a non-porous smooth surface in order to acquire meaningful static data.

### Forward Speed

Effects of forward speed on the air cushion.- As was previously mentioned, the principal purpose of the investigation was to determine if the peripheral jet air cushion would unload because of a breakdown of the jet curtain when free-stream dynamic pressure exceeded cushion pressure at very low ground heights. An examination of the peripheral jet cushion performance at forward speed with the ground belt moving can be made in figure 13 for the circular model, in figure 25 for the rectangular-type model, and in figures 34 and 42 for the side-by-side models. The lift, drag, and pitching-moment data for these models are presented as a function of free-stream dynamic pressure divided by hovering cushion lift per unit area ( $q/L_S/A$ ). For these tests, this pressure ratio was varied by holding cushion pressure constant and varying free-stream dynamic pressure. Therefore, when  $q/L_S/A > 1.0$ , the free-stream dynamic pressure exceeds cushion pressure. In all the cases examined in this investigation, the isolated air cushion maintained a lift value near or above the hovering lift up to values of free-stream dynamic pressure 5 times that of the cushion. Increases in total vehicle lift occurred because of the lift contribution from the external body.

The lift of the modified plenum air cushion (figs. 20 and 21 for circular model and figs. 30 and 31 for rectangular-type model) increased with increasing pressure ratio  $q/L_S/A$ . This increase is probably a result of the free-stream air ramming underneath the model and thereby increasing the bottom pressure. The same effect could not be achieved so readily with the peripheral jet model because the jet curtain would tend to restrict air from passing underneath the model.

The data for a peripheral jet cushion over a moving ground belt (such as fig. 27(a),  $\beta = 0^\circ$ ) in some cases displayed rapid increases in lift culminating in peak lift values at low pressure ratios ( $q/L_S/A = 0.75$ ). Other data taken through the same pressure-ratio range but at higher static-lift values (fig. 25) did not display this peaking tendency. The explanation of the lift peaks may be related to the effect of belt lifting and porosity and, therefore, should be ignored from operation considerations. In general, when a peripheral jet cushion is used close to the ground, where cushion pressure is less than free-stream dynamic pressure ( $q/L_S/A > 1.0$ ), lift values remain equal to or about the same level as hovering lift.

Effects of moving belt (ground boundary layer).- The data for the peripheral jet configuration over the moving belt and over the stopped belt are compared in figures 15, 29, 38, and 45. These data show pitching-moment differences between moving-belt and stopped-belt conditions. Base center-line pressure profiles similar to those presented in figures 29(b) and 29(c) were typical of the bulk of the data and indicated that the moving belt affected the flow by causing larger positive pressures at the rear of the model, which translated into greater negative pitching moments. The data of figures 26(c) and 26(d) also indicated the necessity of having the moving belt if the proper pressure profiles are to be present, as well as indicating that these profiles can be approached at zero forward speed as long as the belt is moving at an appropriate speed.

The modified plenum configuration was also tested with and without the moving belt; these data are presented for the circular model in figures 20 and 21 and for the rectangular-type model in figures 30 and 31. The trends of the data are very similar to those found in the peripheral jet model.

Channel vent between side-by-side air cushions.- The flat surface between the side-by-side cushions is a region wherein the air from the cushions was trapped and, therefore, could push against the surface. The result is an increase in lift on the vehicle. A method of providing venting by the use of a contoured channel (fig. 2(d)), designed to handle the free-stream ram air plus the increment due to cushion-air flow, was used for some of the tests. The data acquired for the model with this channel, which ran the full length of the vehicle, are presented in figures 34 to 41, and some center-line pressure distributions are presented in figure 48. The pressure data reveal that the channel adequately handled the cushion-air flow. The principal purpose of these tests was to show the usefulness of such a channel and not to recommend the use of the particular one tested.

Effects of height.- Height effects were examined for all configurations. The results are presented for the circular model in figures 16 and 22 and for the side-by-side model in figure 46. These data, which are representative of all the configurations tested, indicate that at small clearances, even large percentage changes in height did not result in any significant change in the effects of forward speed on the aerodynamic characteristics.

Effects of crosswind.- Crosswind operation was simulated by testing the rectangular-type (figs. 27, 28, 32, and 33) and side-by-side (figs. 36, 37, and 44) models at various sideslip angles. The cushion forces and moments showed little effect of crosswind. In general, the body forces (except drag) and moments increased with sideslip angle, as would be expected. The effects of crosswind on various cross-sectional configurations similar to those used herein are presented in reference 5, and the limitations of this method of crosswind simulation are discussed therein.

Effects of angle of attack.- The circular model (fig. 19) and the side-by-side model (fig. 39) were tested at small positive angles of attack. At these conditions large increases

in lift over the level condition were measured on the air-cushion pad. Such large changes in lift are significant and should be considered in the design of any air-cushion vehicle system.

Unpowered air-cushion and differential pad pressure.- A series of unpowered air-cushion (zero pad pressure) tests were conducted, and the results are presented for the circular model in figures 17, 18, 23, and 24 and for the side-by-side model in figure 47. These data indicate that the corrected forces and moments on the shell or body experienced only small changes regardless of the cushion pressure. This result, therefore, leads to the conclusion that the body and air cushion experience loads independent of each other. Tests were also conducted on the side-by-side model in which the left pad pressure was systematically reduced while the right pad was kept at full pressure. (See figs. 40 and 41.) No unusual results were evident for either group of tests.

### CONCLUDING REMARKS

Air-cushion models employing peripheral jet and plenum cushions of circular, rectangular, and side-by-side planforms were tested in hovering and at forward speed in the 17-foot (5.18-m) test section of the Langley 300-MPH 7- by 10-foot tunnel. The principal purpose of these tests was to study the characteristics of air cushions when free-stream dynamic pressure exceeded air-cushion pressure. Also examined were the hovering performance and the effects of moving ground belt, crosswind, height, and angle of attack. For the configurations tested, there was no significant loss in cushion performance when free-stream dynamic pressure exceeded cushion pressure.

Although a variety of powered air-cushion configurations were tested, the results indicate that the cushion performance was independent of configuration. External forces and moments on the body or shell of the vehicle were measured and found to be representative of the unpowered configuration of the shape tested and also to be independent of the cushion.

Belt characteristics, such as permeability and surface roughness, caused unexpected results in hovering performance. When the experimental limitations which resulted in discrepancies in the data were isolated and corrected, hovering performance followed the exponential theory as expected.

Crosswind conditions in general did not produce any significant changes in the air-cushion characteristics. The data were also unaffected by large percentage variations in

height. However, the use of the moving belt is required if accurate flow conditions under the air cushion are to be achieved.

Langley Research Center,  
National Aeronautics and Space Administration,  
Hampton, Va., August 20, 1970.

#### REFERENCES

1. Turner, Thomas R.: A Moving-Belt Ground Plane for Wind-Tunnel Ground Simulation and Results for Two Jet-Flap Configurations. NASA TN D-4228, 1967.
2. TRW Systems Group: Moving Ground Plane Wind Tunnel Tests on Several Tracked Air Cushion Vehicle (TACV) Models. 06818-6032-R0-00, U.S. Dep. Transp., Mar. 1, 1969.
3. Jones, R. Stanton: Some Design Problems of Hovercraft. Pap. No. 61-45, Inst. Aerosp. Sci., Jan. 1961.
4. Richardson, H. H.; and Captain, K. M.: Simplified Static Performance Characteristics of Low-Pressure Plenum and Peripheral Jet Fluid Suspensions. Rep. DSR 76110-8 (Contract C-85-65), Dep. Mech. Eng., Massachusetts Inst. Technol., Jan. 1968.
5. Grunwald, Kalman J.: Aerodynamic Characteristics of Vehicle Bodies at Crosswind Conditions in Ground Proximity. NASA TN D-5935, 1970.

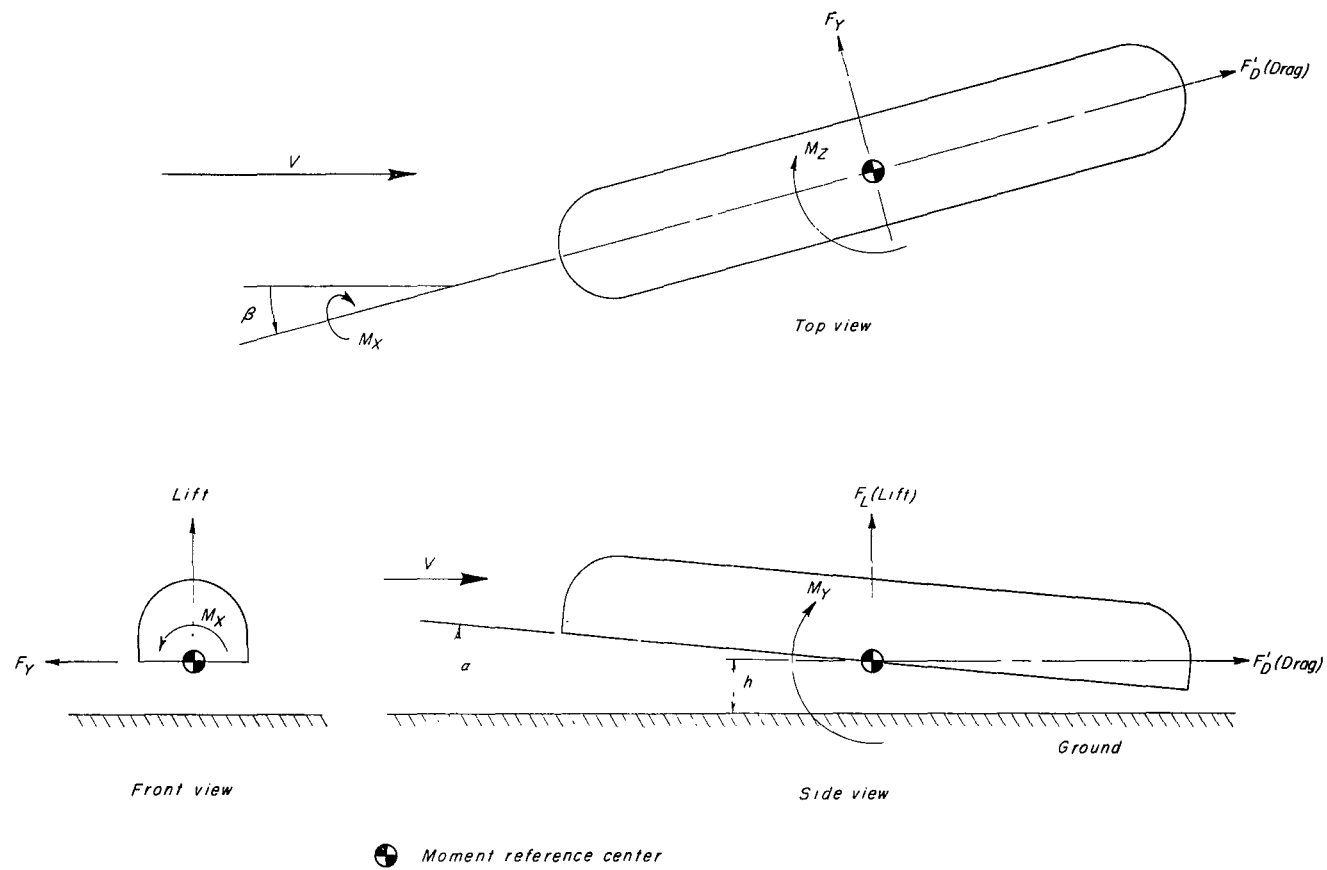
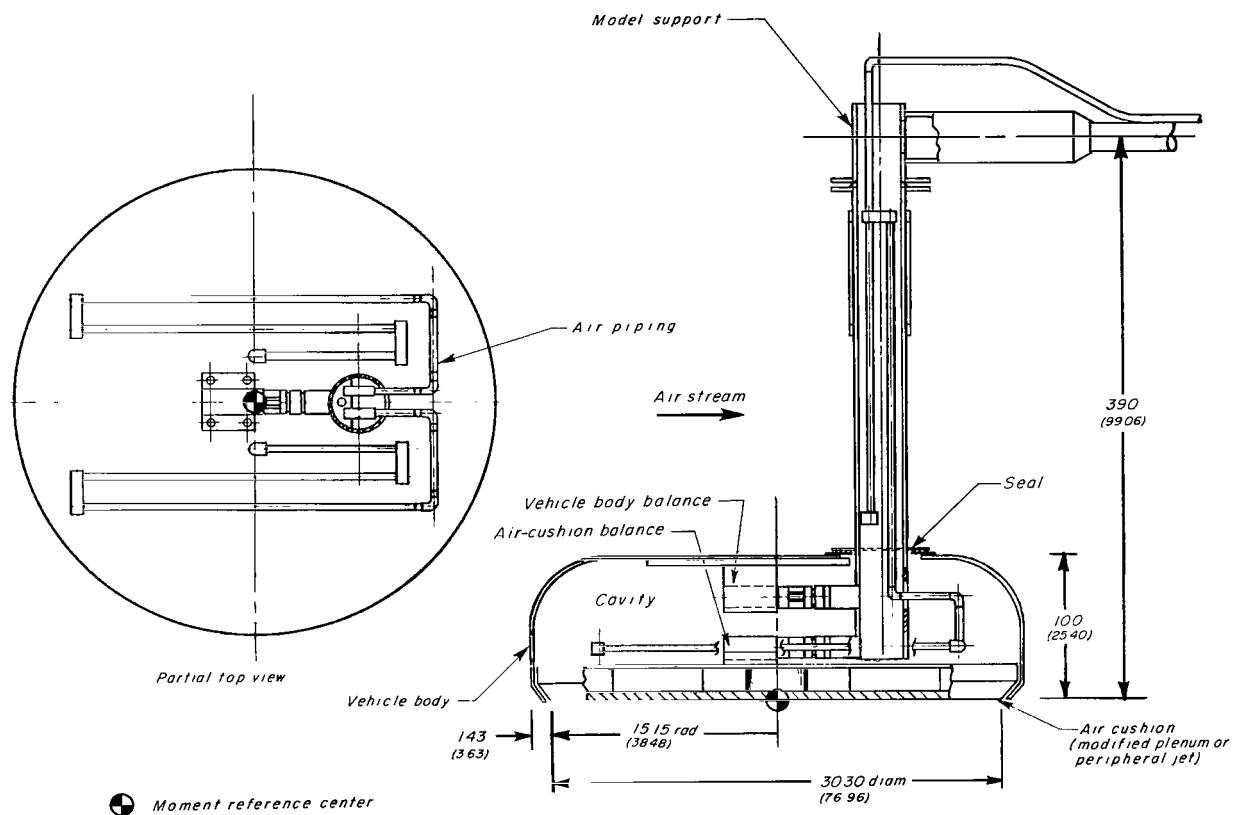


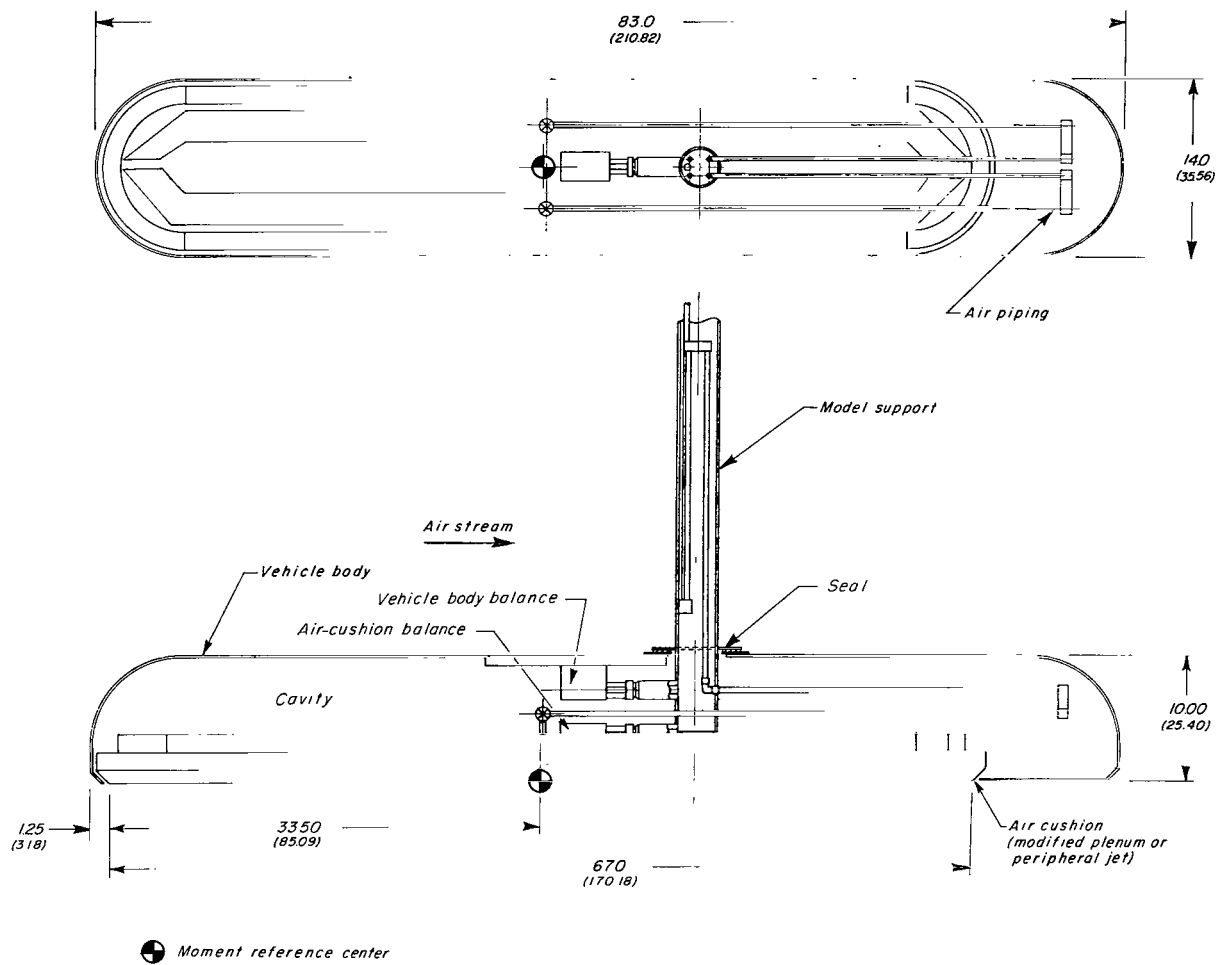
Figure 1.- Axis system drawing showing positive sense of forces, moments, and angles.





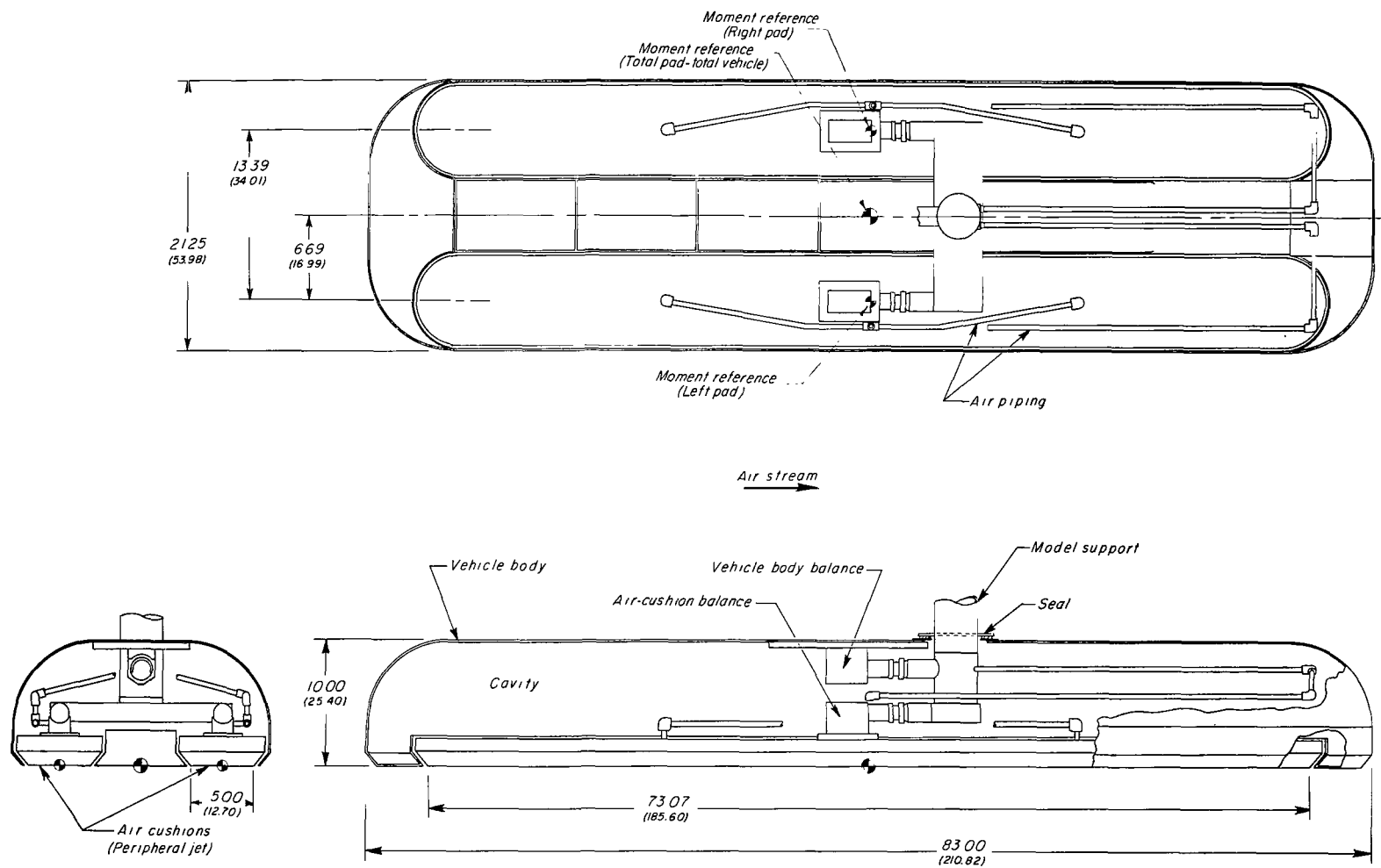
(a) Circular model.

Figure 2.- Drawings of models. All dimensions are in inches (centimeters).



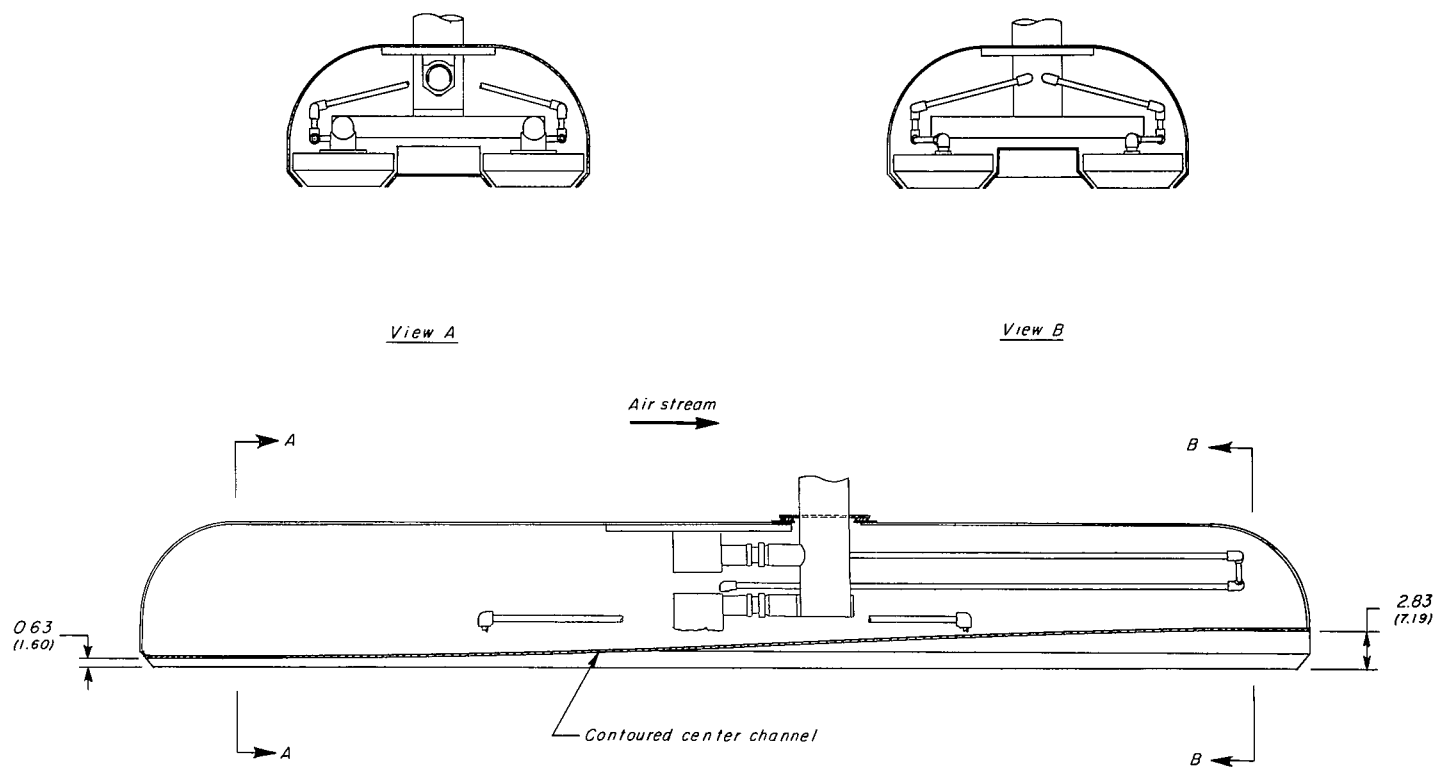
(b) Rectangular-type model.

Figure 2.- Continued.



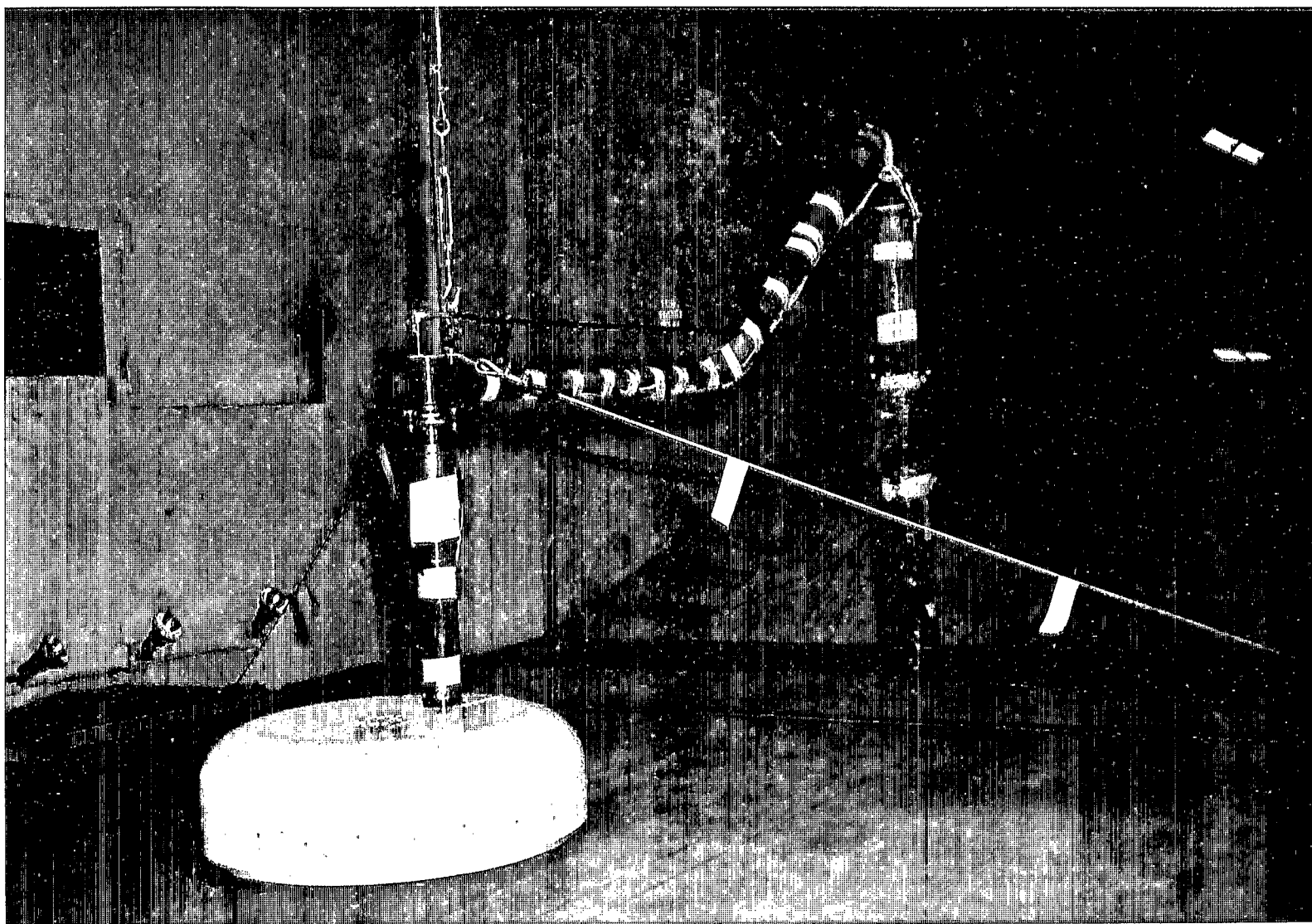
(c) Side-by-side model (flat-bottom configuration).

Figure 2.- Continued.



(d) Side-by-side model (contoured-channel configuration).

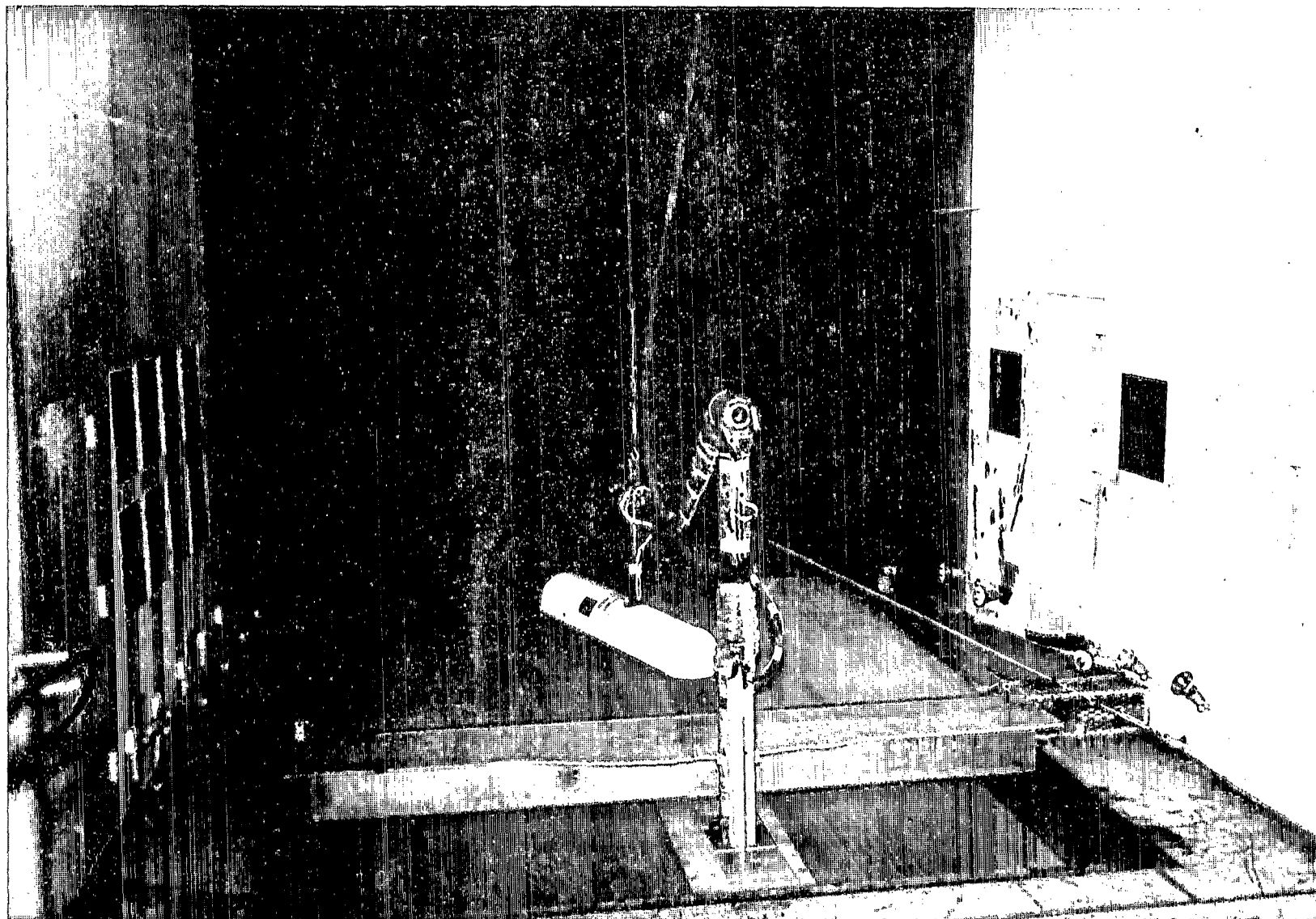
Figure 2.- Concluded.



L-67-9420

(a) Circular model.

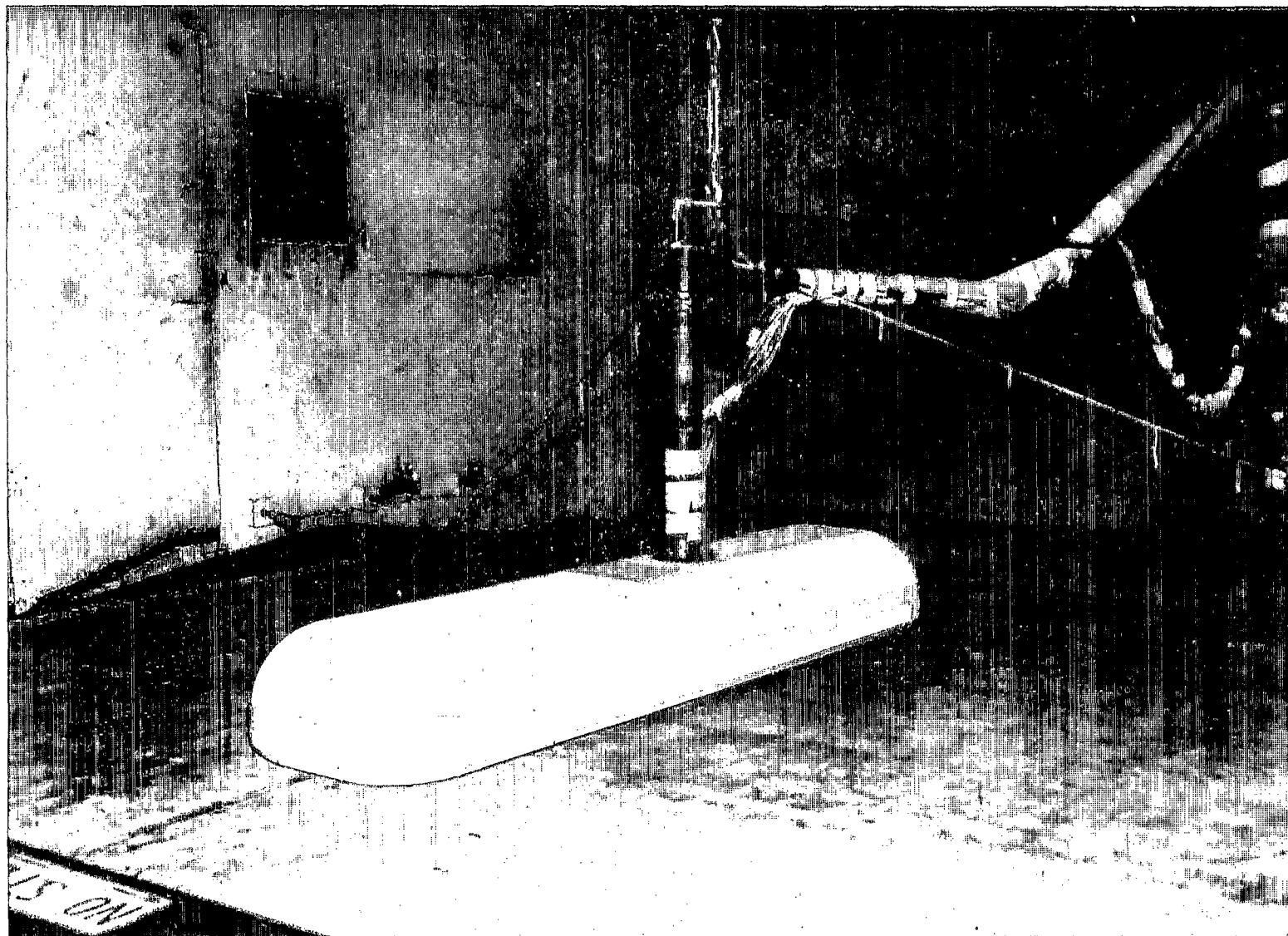
Figure 3.- Photographs of models over ground belt in the 17-foot (5.18-meter) test section.



L-67-9804

(b) Rectangular-type model.

Figure 3.- Continued.



L-68-5134

(c) Side-by-side model.

Figure 3.- Concluded.

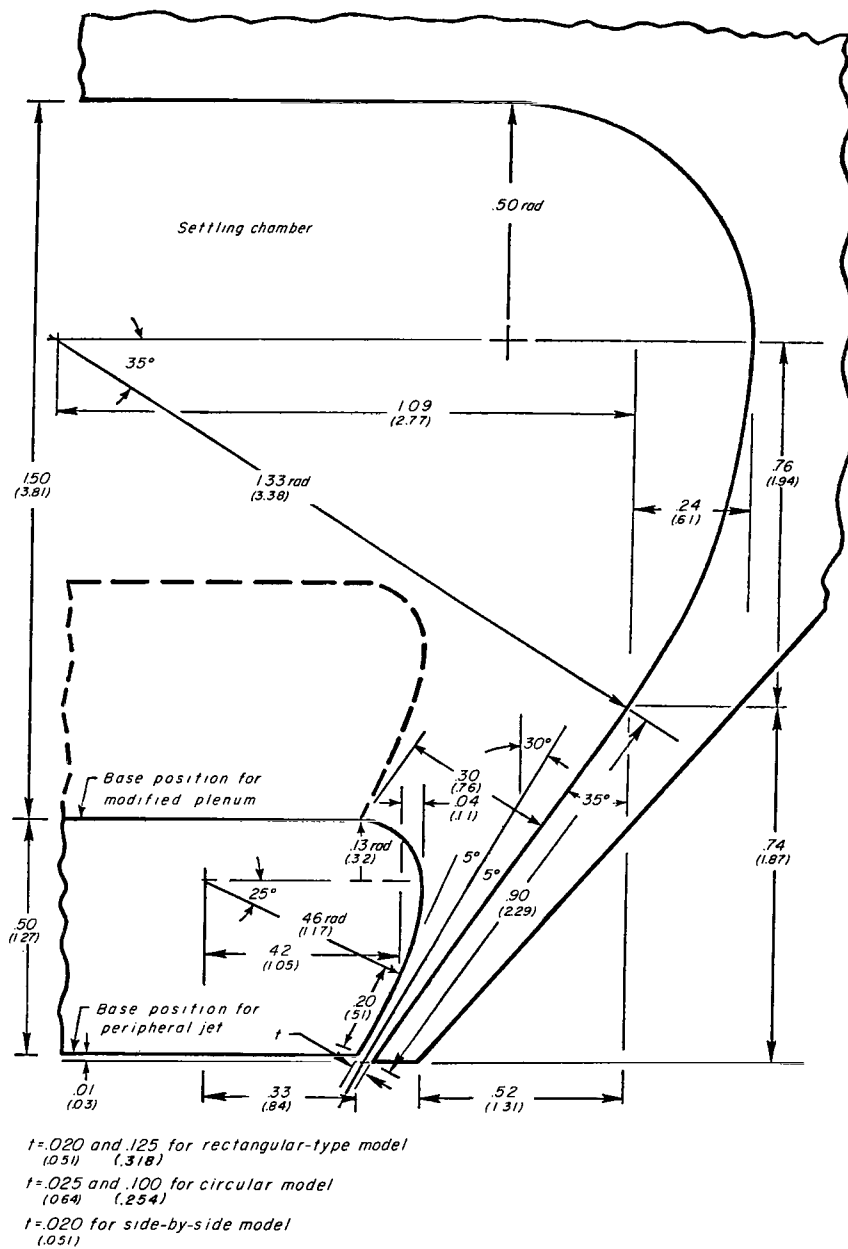


Figure 4.- Jet-exit detail for peripheral jet and modified plenum.  
All dimensions are in inches (centimeters).



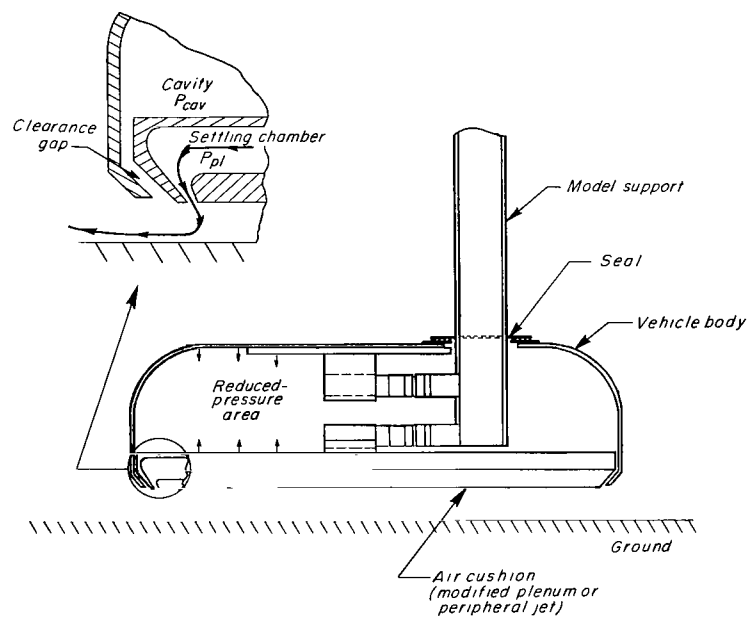
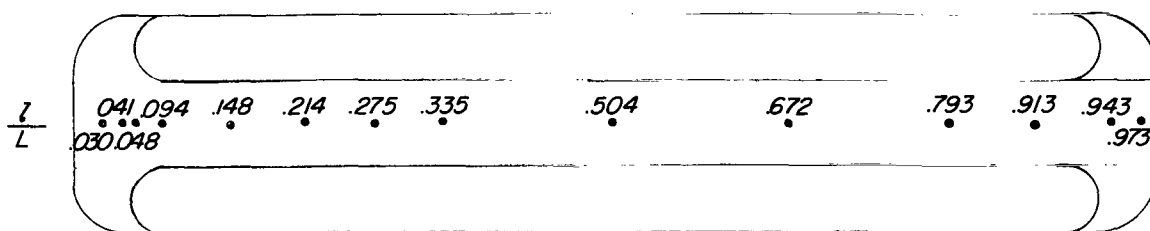


Figure 5.- Sketch of internal flow conditions.

*Pressure-orifice location in side-by-side model (Flat and contoured channel)*

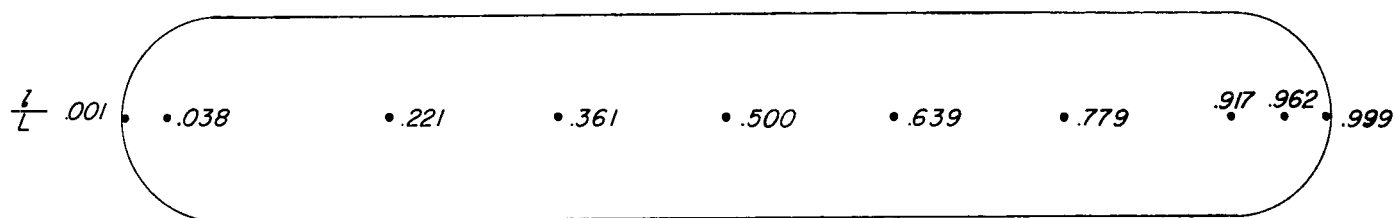


*Bottom view of body and air cushions*

(a) Center-line base of contoured and flat channel in side-by-side model.

Figure 6.- Pressure locations.

*Pressure-orifice location in rectangular-type cushion*



*Bottom view of air-cushion pad*

(b) Base of rectangular-type air cushion.

Figure 6.- Concluded.

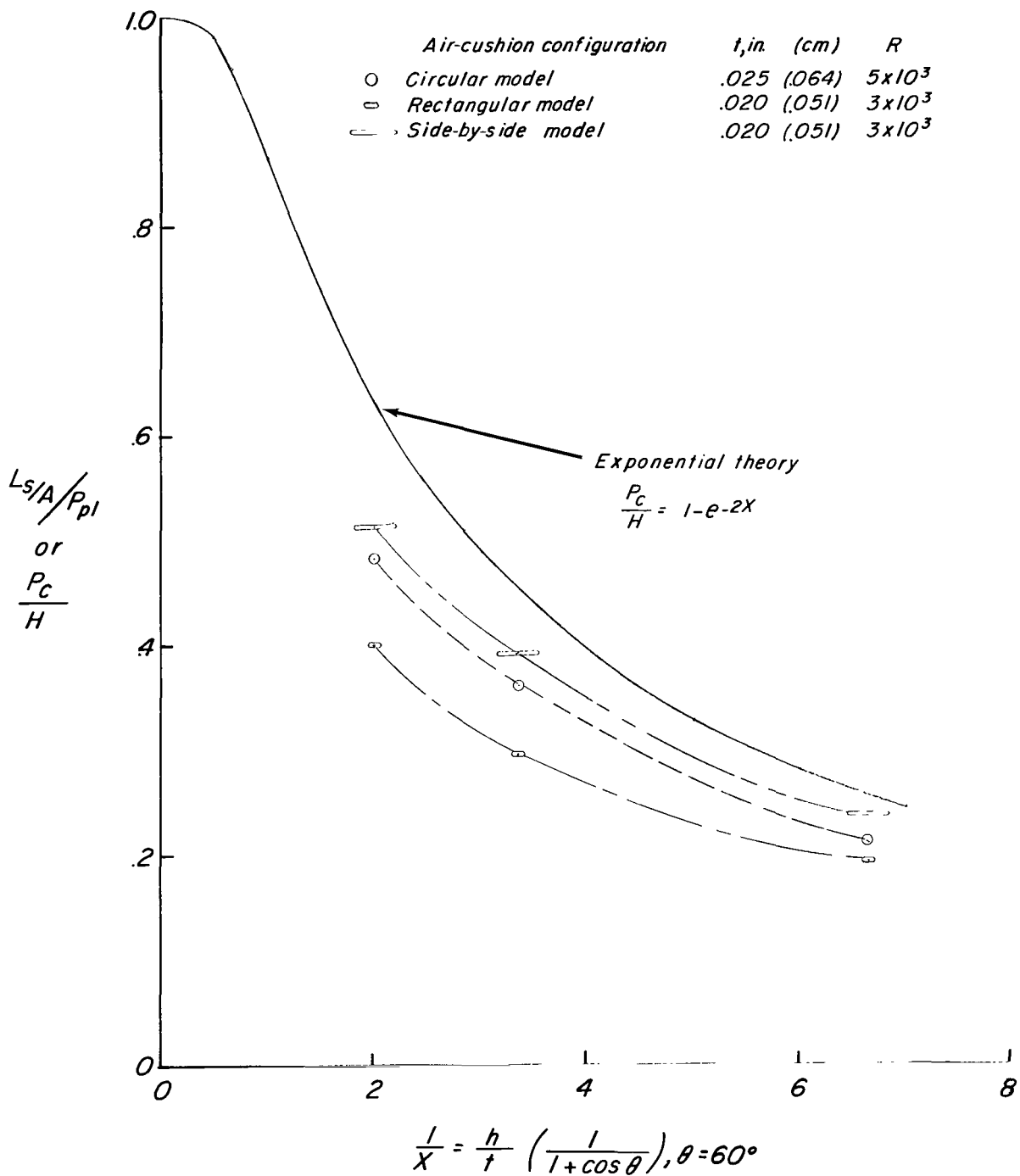


Figure 7.- Comparison of cushion effectiveness for original three configurations tested at zero speed over smooth plastic ground surface.

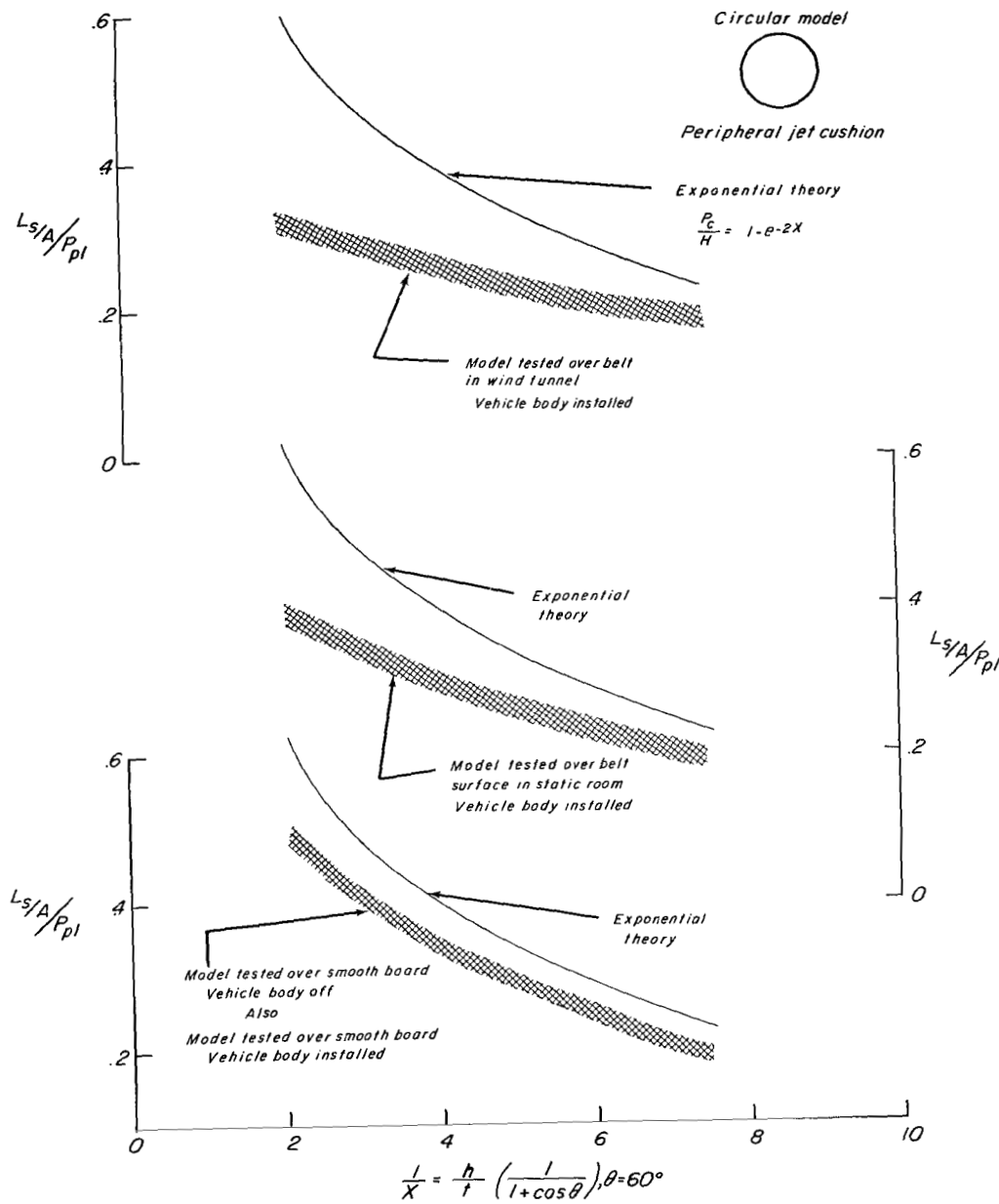


Figure 8.- Cushion effectiveness at zero speed for various circular model configurations and ground-surface conditions.

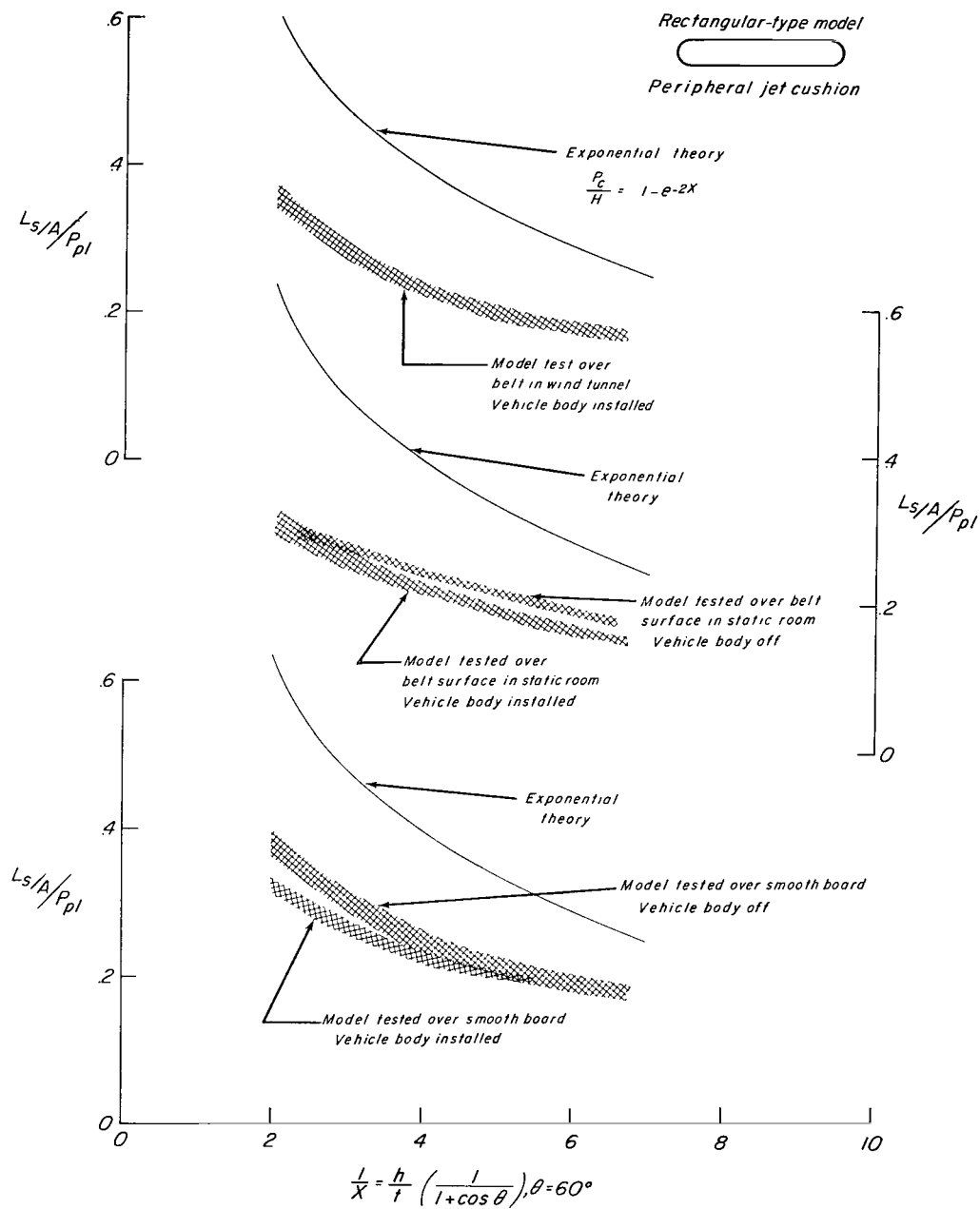


Figure 9.- Cushion effectiveness at zero speed for various rectangular model configurations and ground-surface conditions.

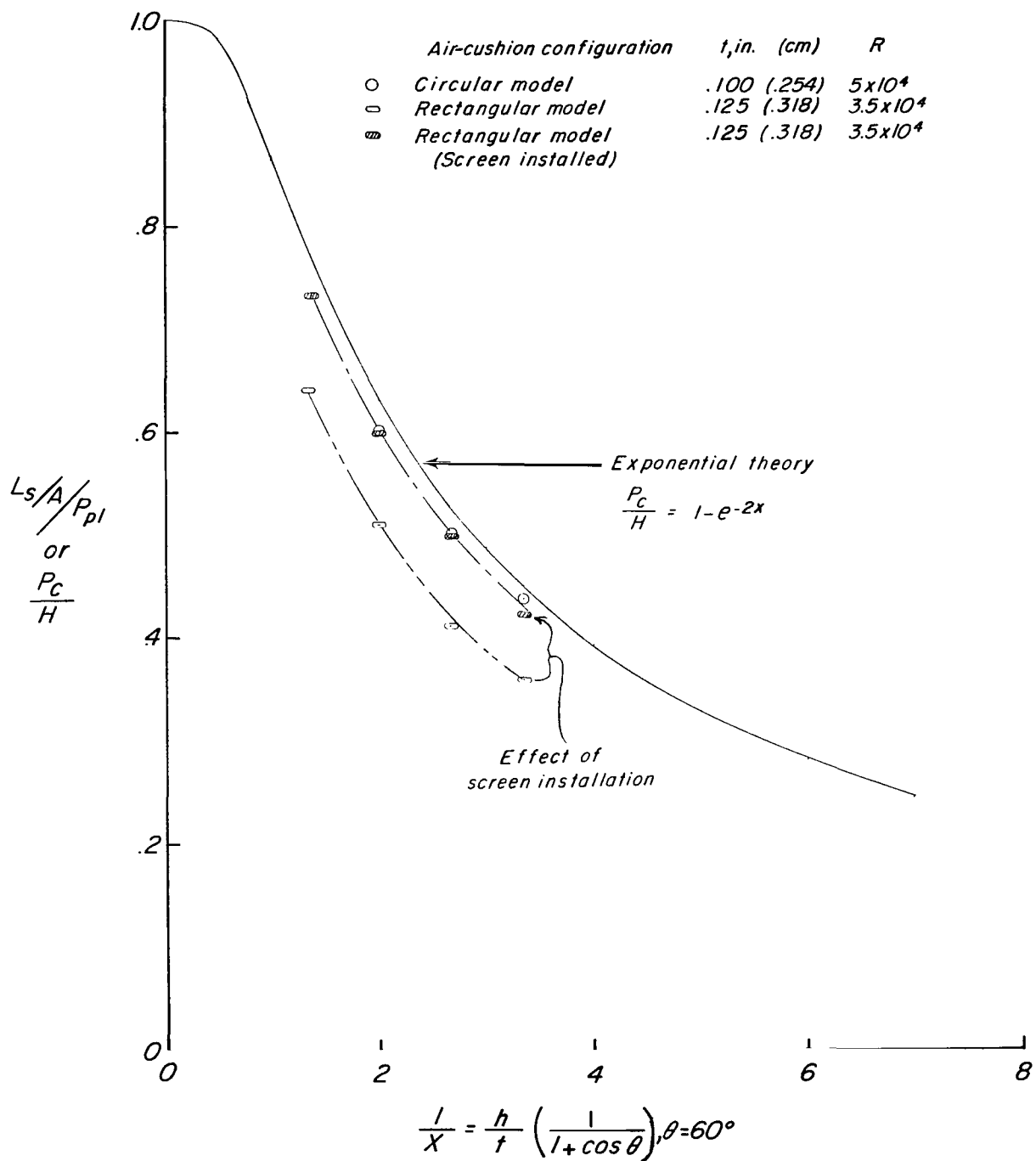


Figure 10.- Comparison of cushion effectiveness for circular and rectangular models with larger jet nozzles and effects of installation of screen in rectangular model.

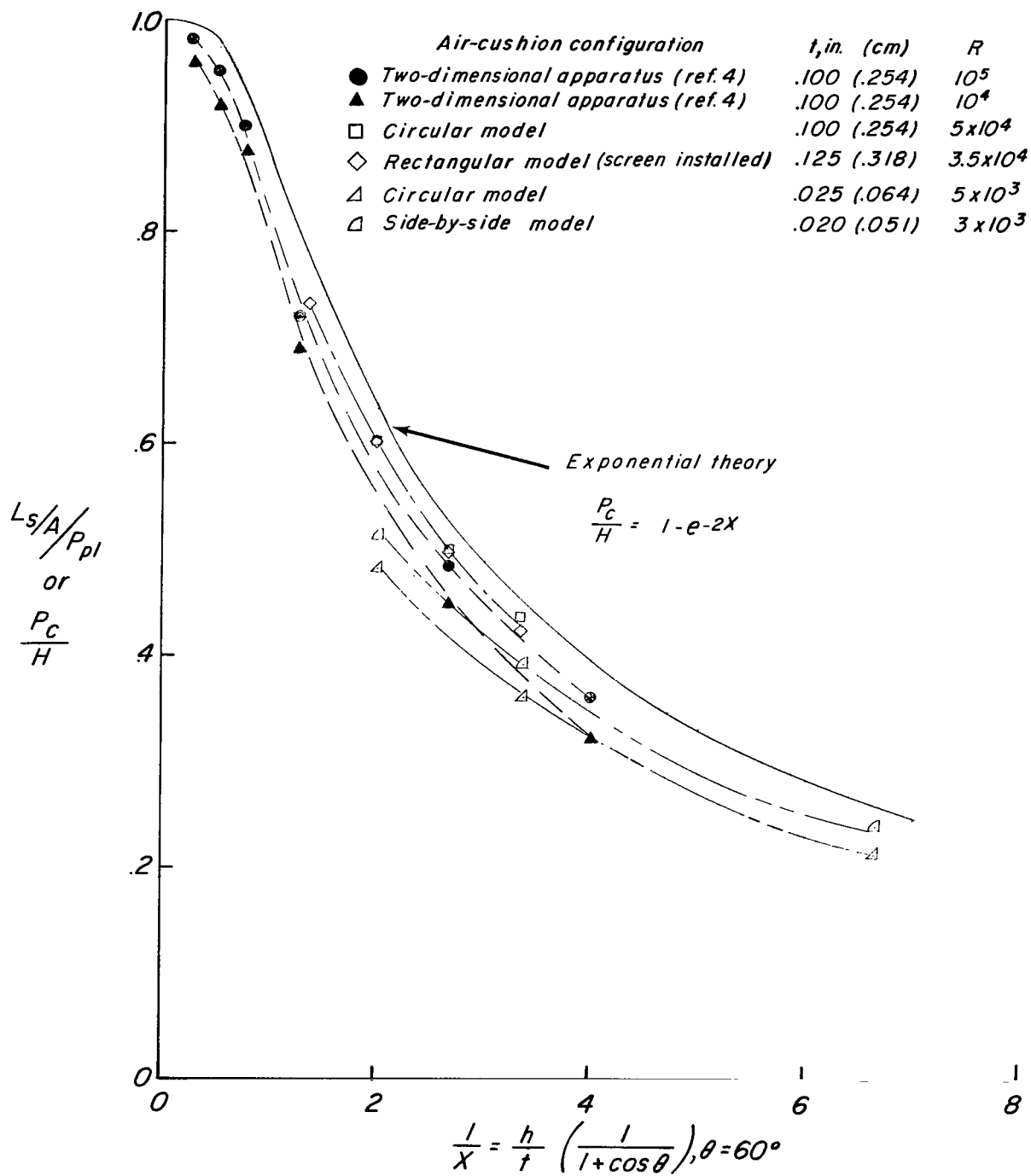


Figure 11.- Summary comparison of cushion effectiveness at zero speed including data from previous tests (ref. 4).



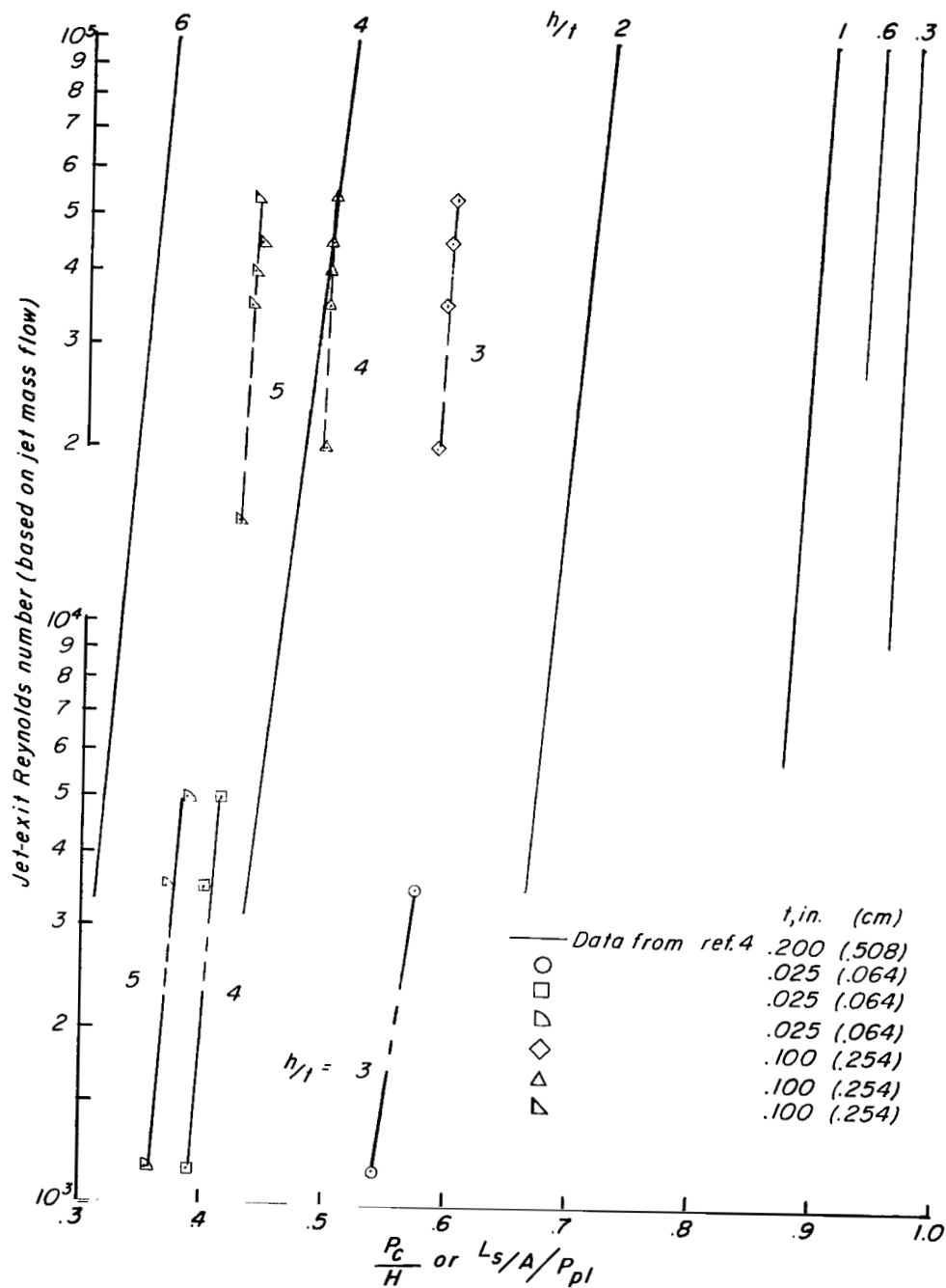


Figure 12.- Effect of Reynolds number on cushion pressure for circular model compared with Reynolds number effects from two-dimensional tests of reference 4.

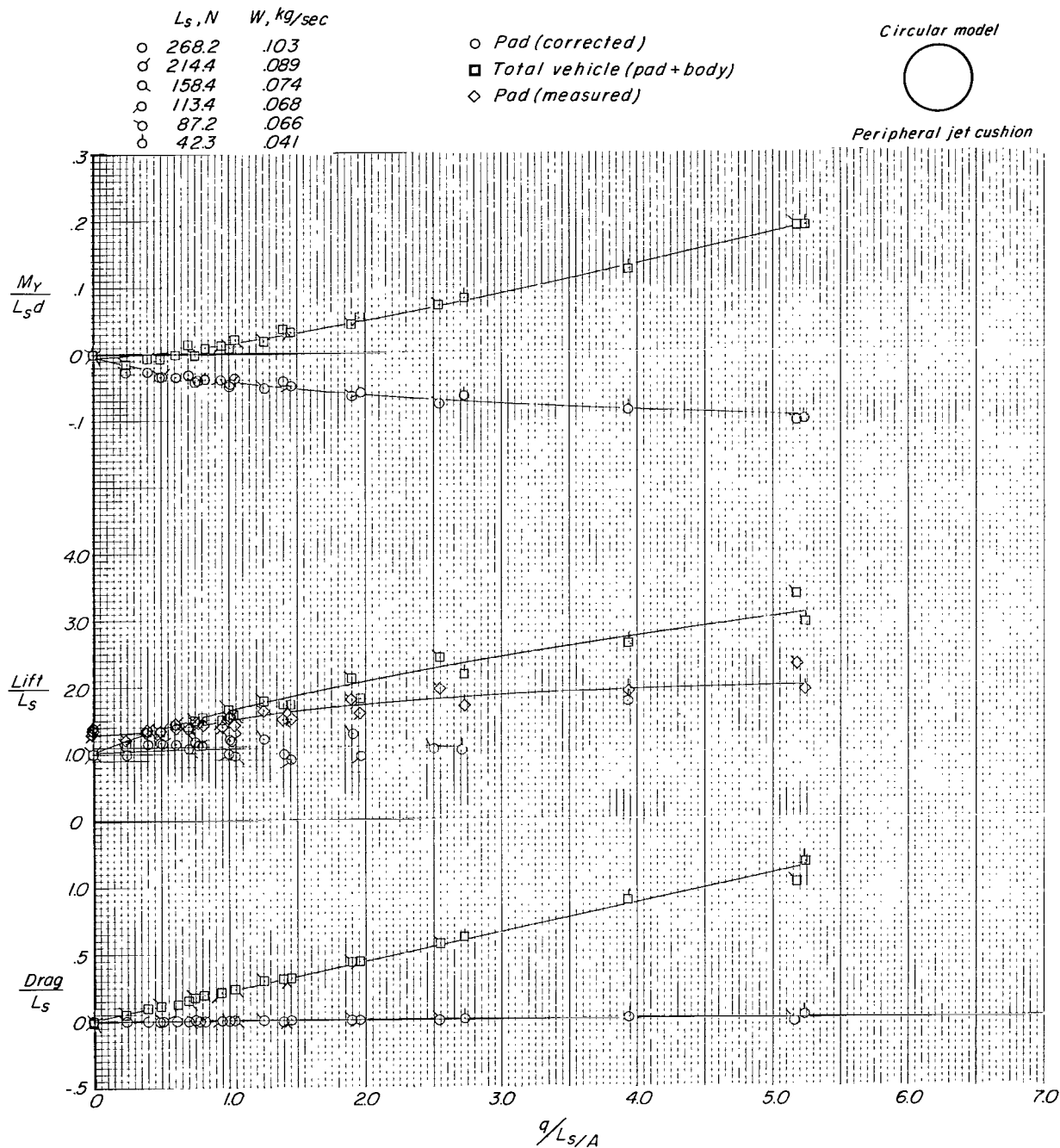
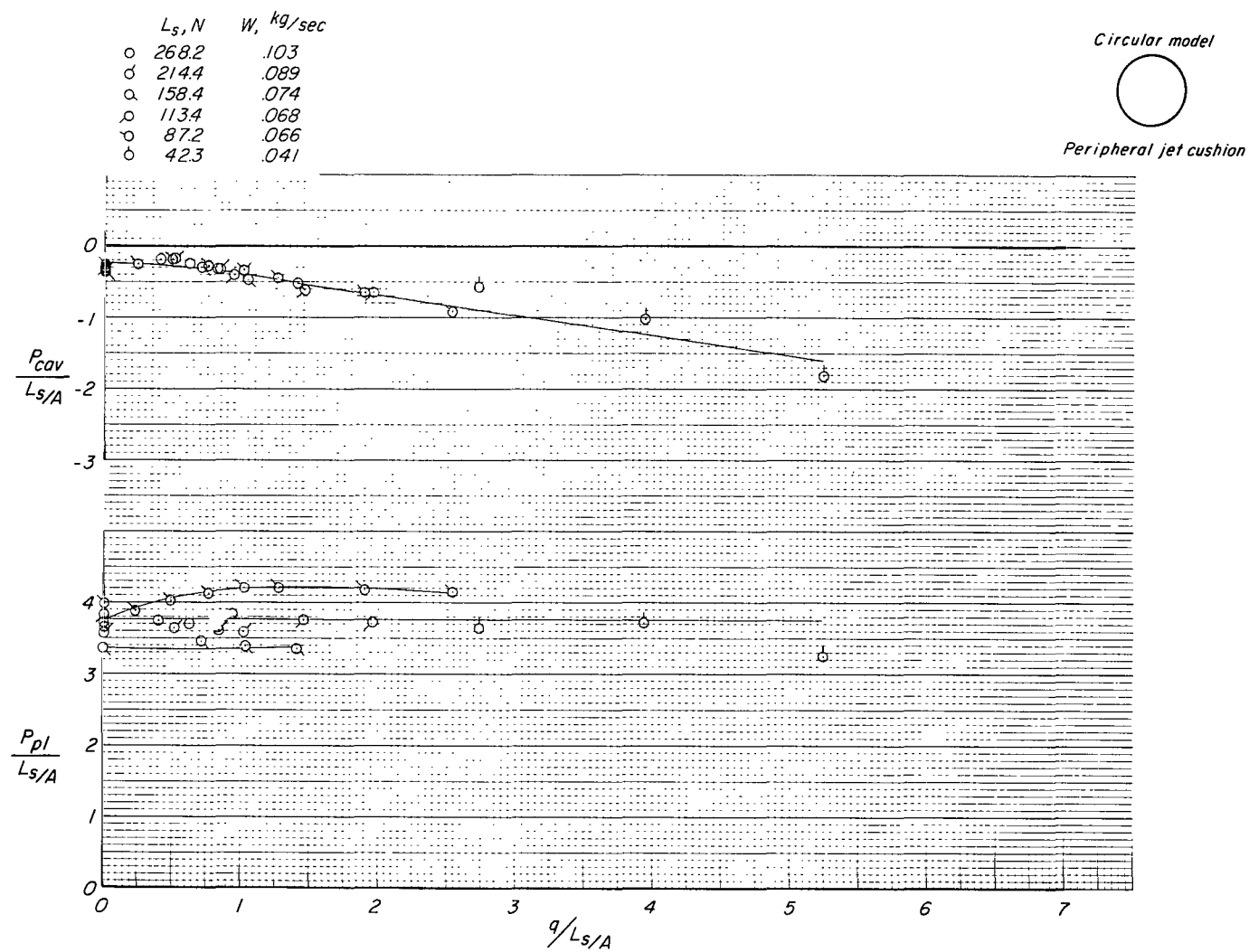


Figure 13.- Effect of forward speed on aerodynamic characteristics of circular model (peripheral jet). Belt moving;  $h/d = 0.00412$ .



(b) Cavity pressure and plenum pressure.

Figure 13.- Concluded.

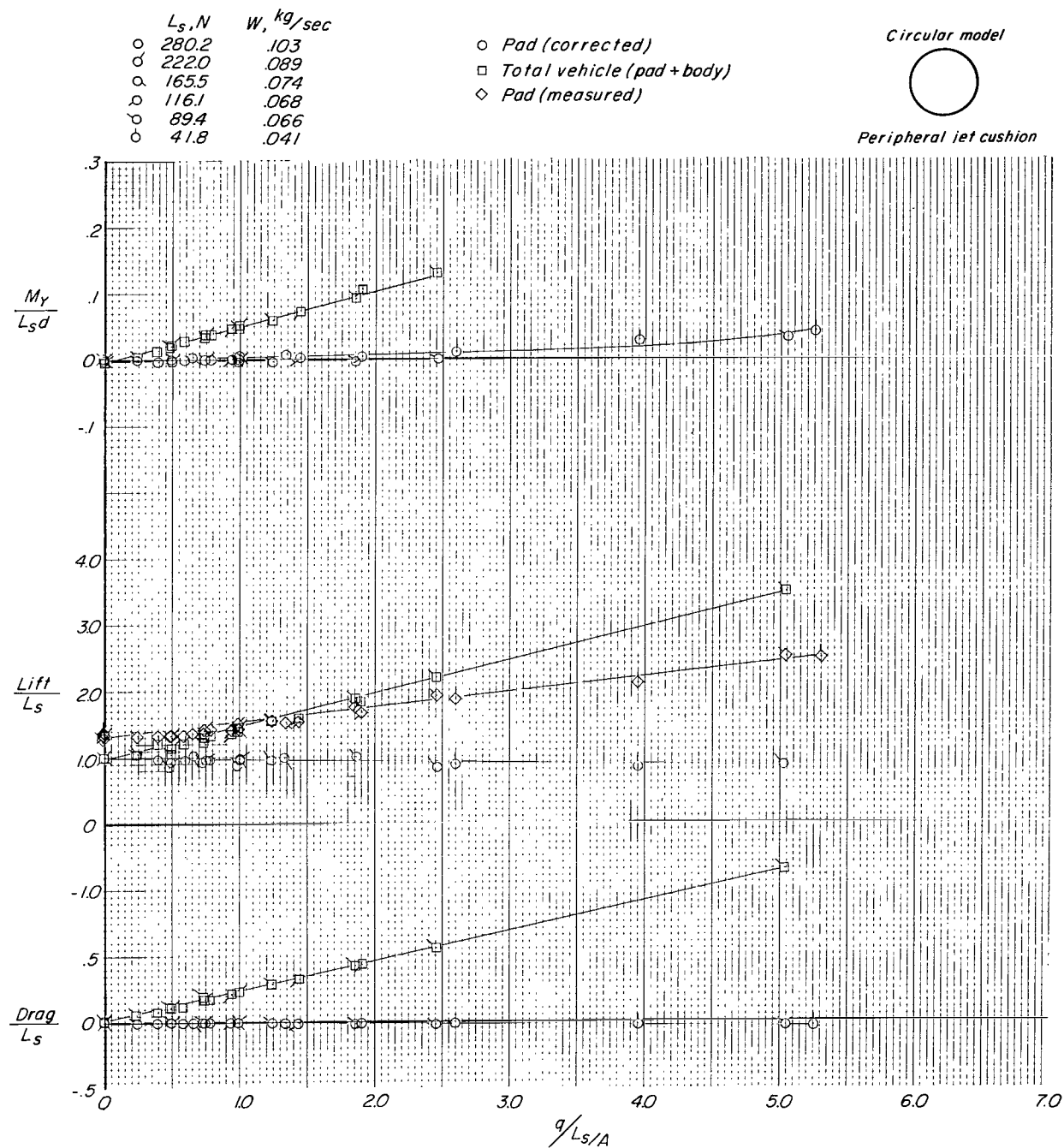
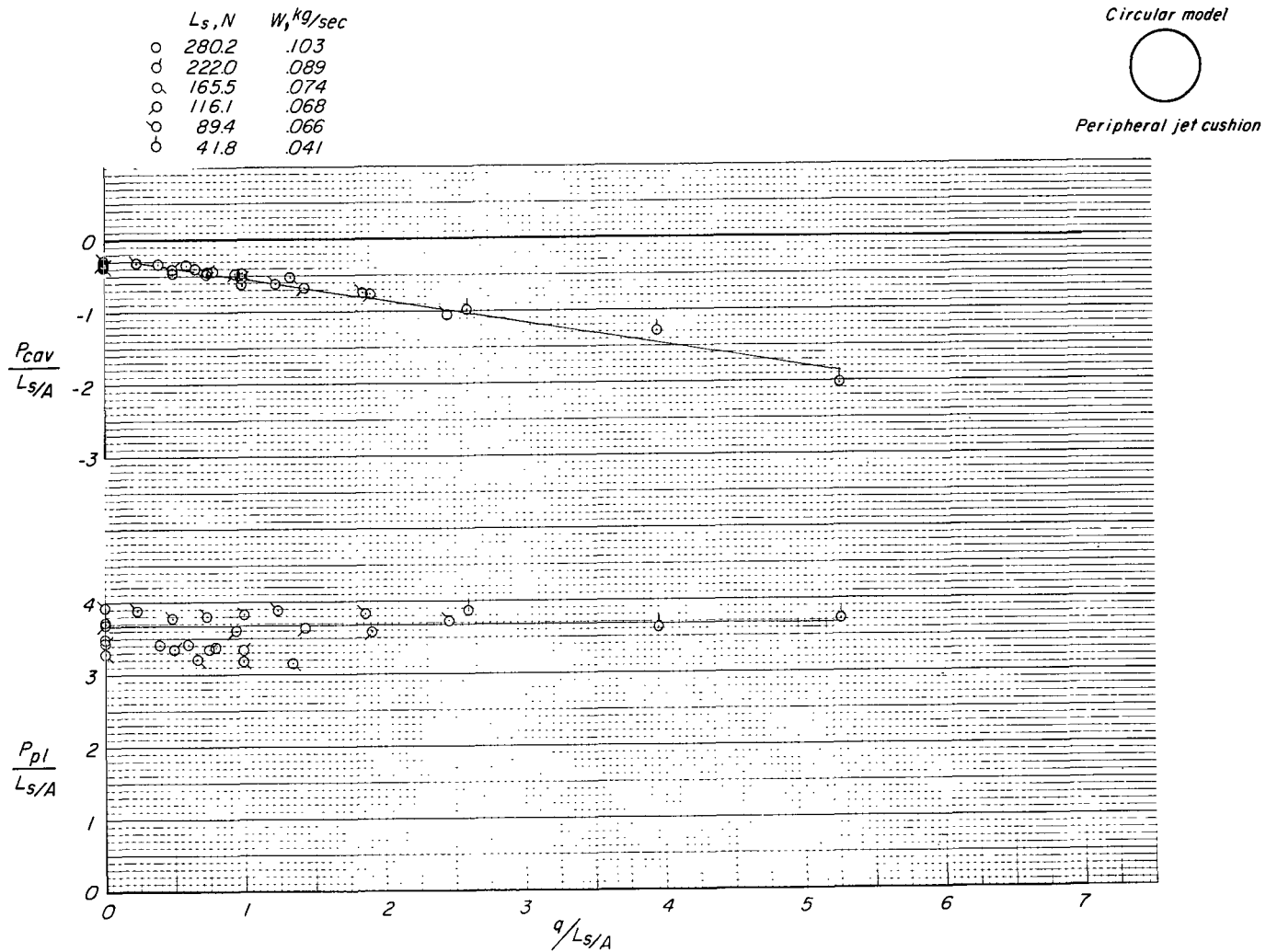


Figure 14.- Effect of forward speed on aerodynamic characteristics of circular model (peripheral jet). Belt stopped;  $h/d = 0.00412$ .



(b) Cavity pressure and plenum pressure.

Figure 14.- Concluded.

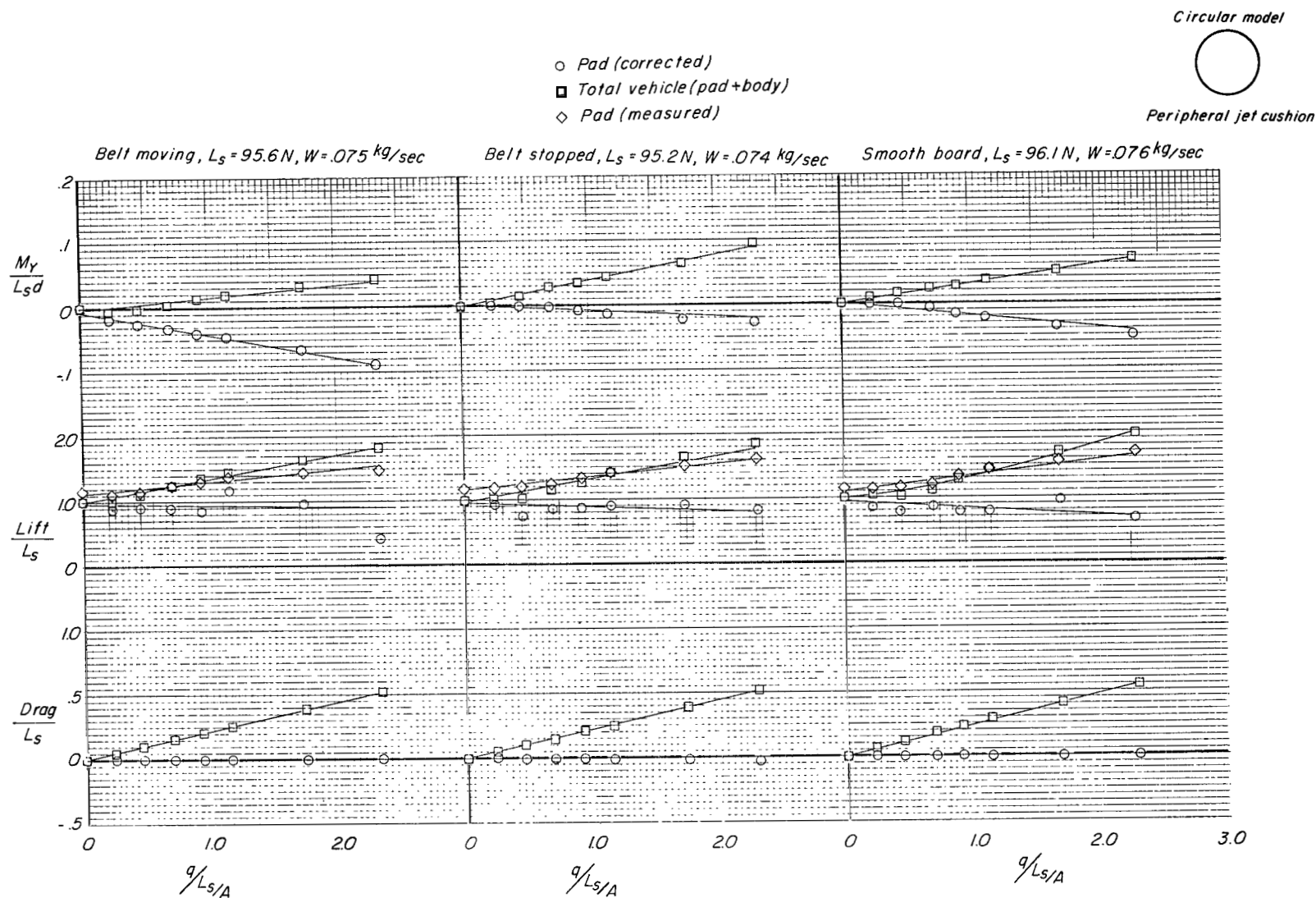


Figure 15.- Effect of moving ground belt on aerodynamic characteristics of circular model (peripheral jet).  
 $h/d = 0.00825$ .

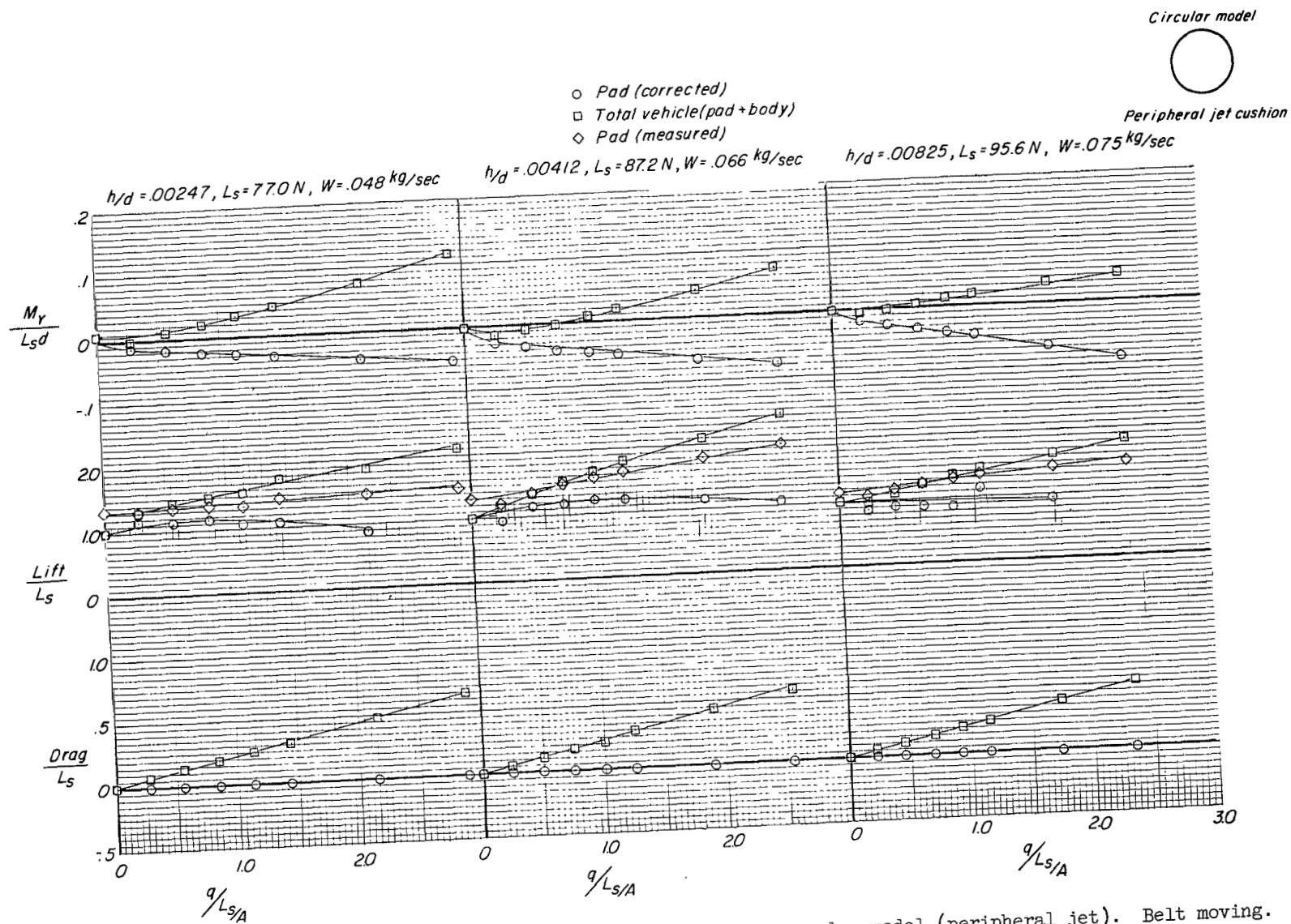


Figure 16.- Effect of height on aerodynamic characteristics of circular model (peripheral jet). Belt moving.

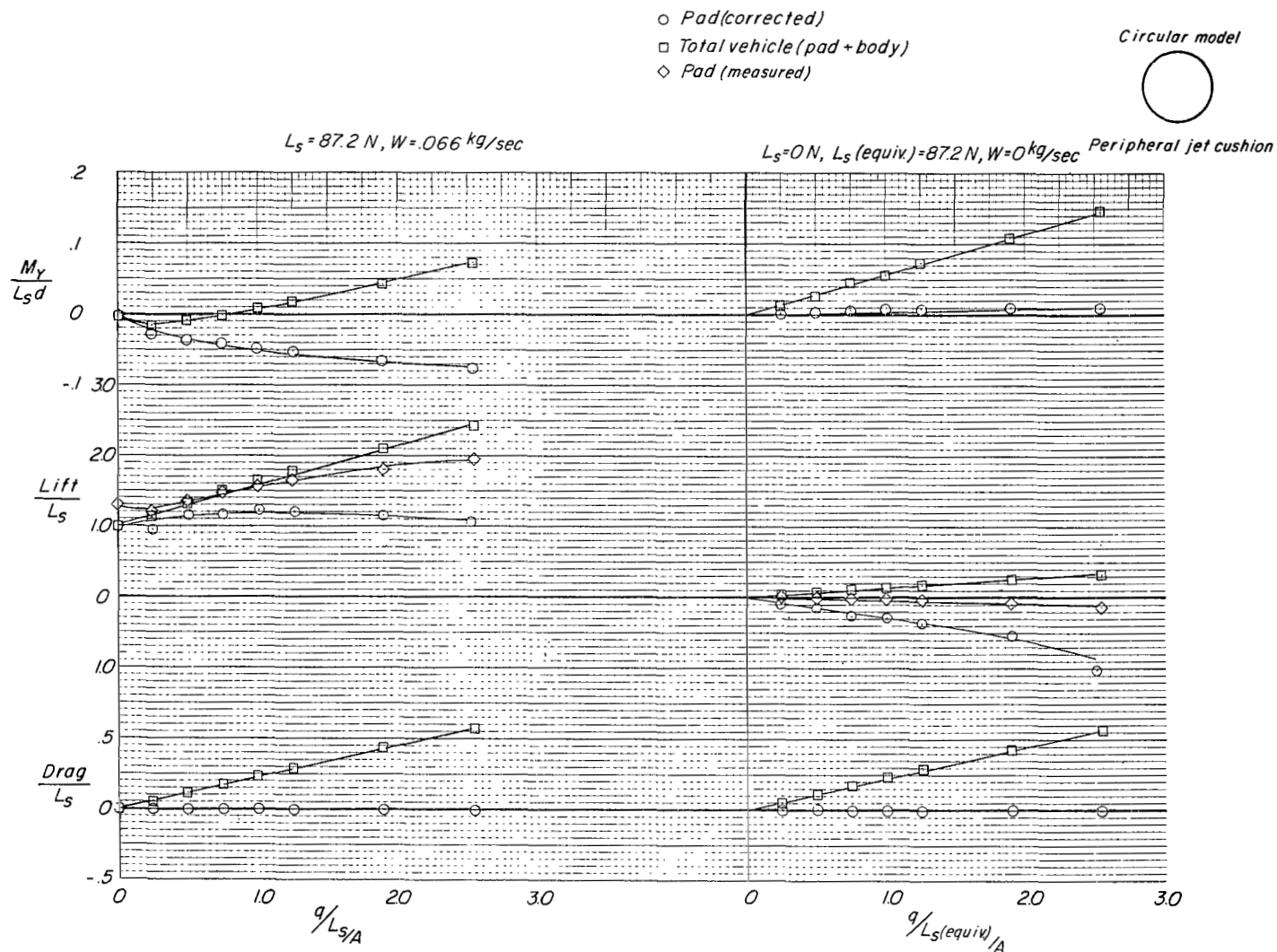


Figure 17.- Comparison of aerodynamic characteristics of powered air cushion with those of unpowered cushion for circular model (peripheral jet). Belt moving;  $h/d = 0.00412$ .



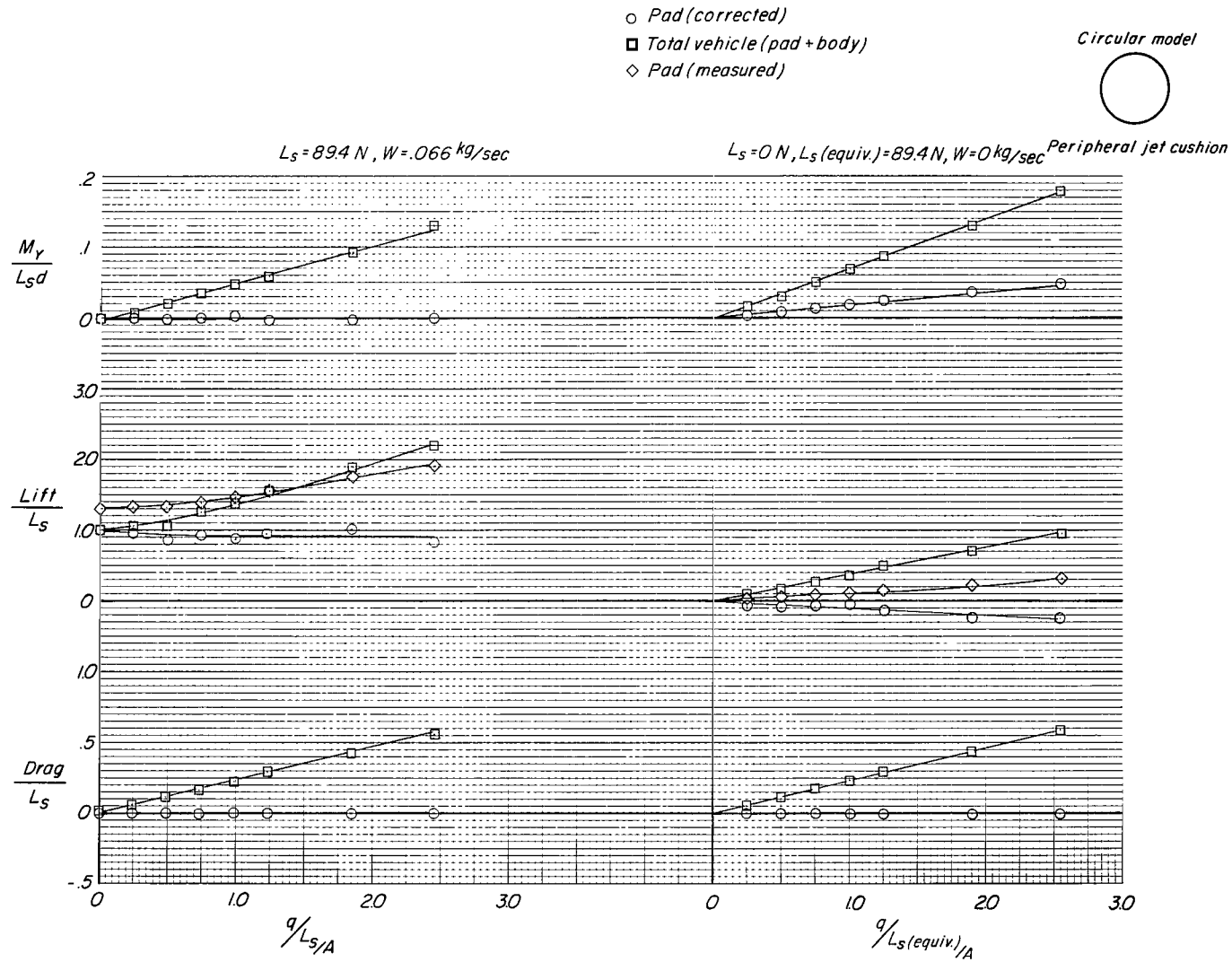


Figure 18.- Comparison of aerodynamic characteristics of powered air cushion with those of unpowered cushion for circular model (peripheral jet). Belt stopped;  $h/d = 0.00412$ .

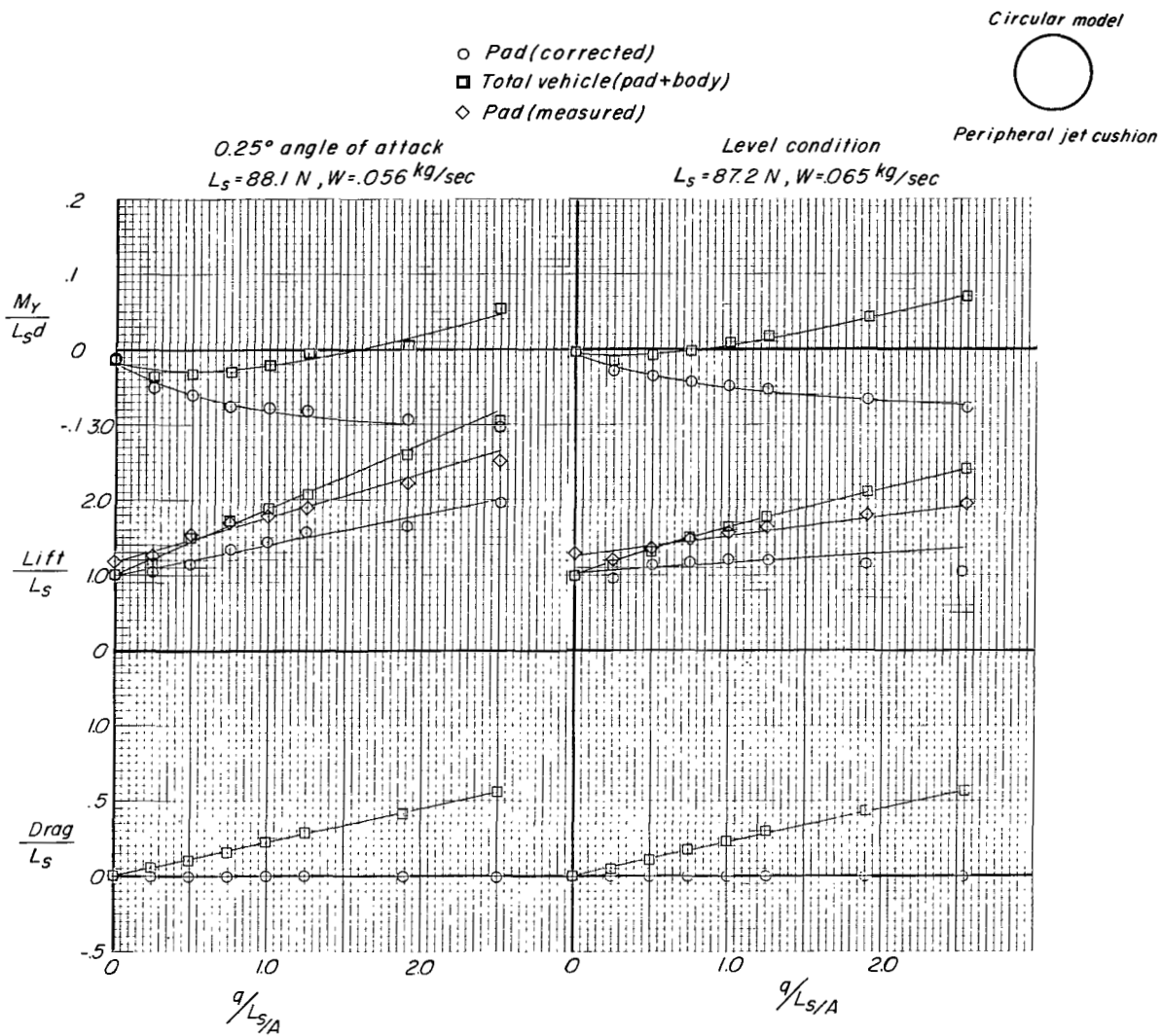


Figure 19.- Comparison of model in level attitude with model at 0.25° angle of attack.  
 Belt moving;  $h/d = 0.125$  (nominal).

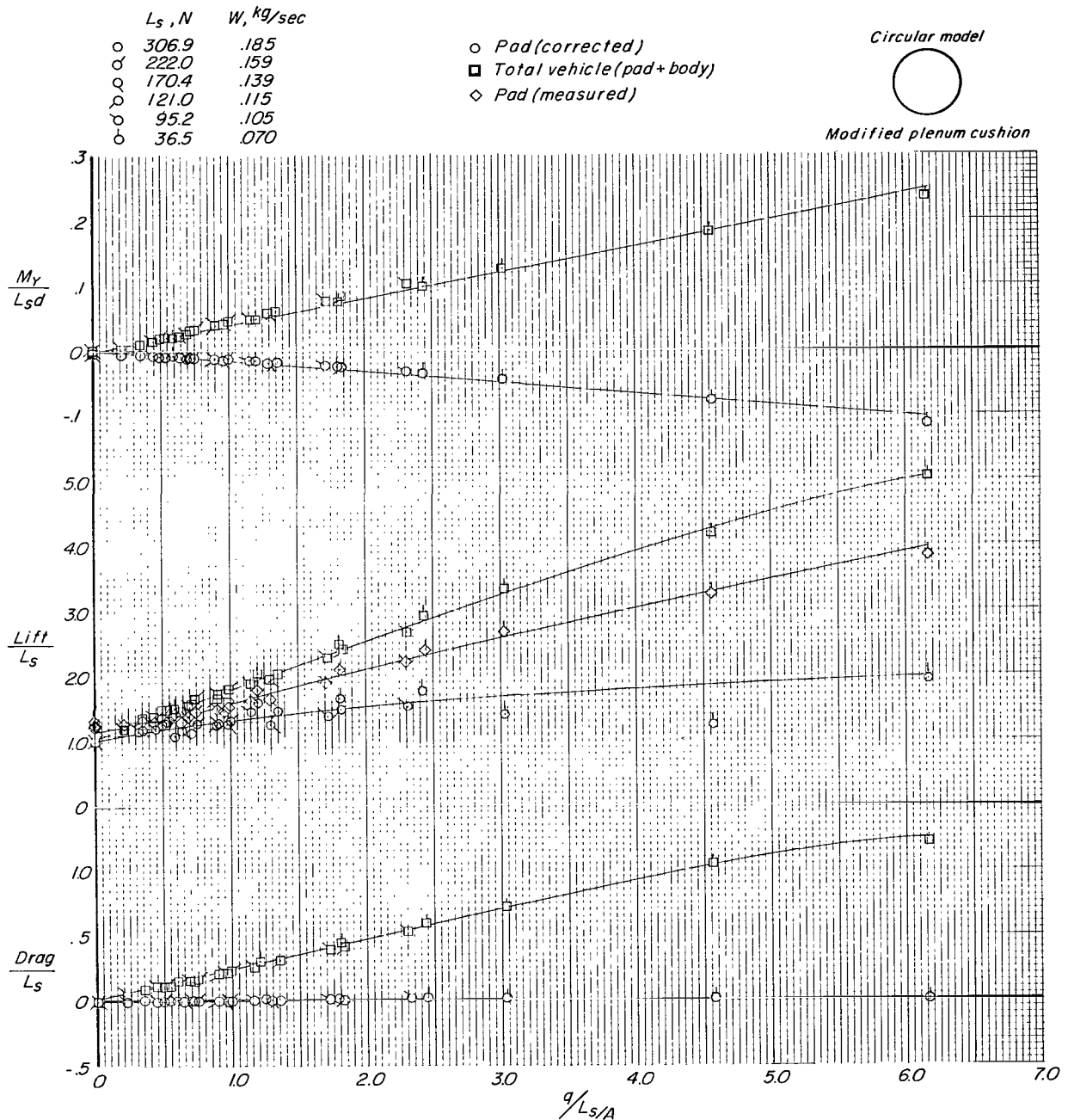
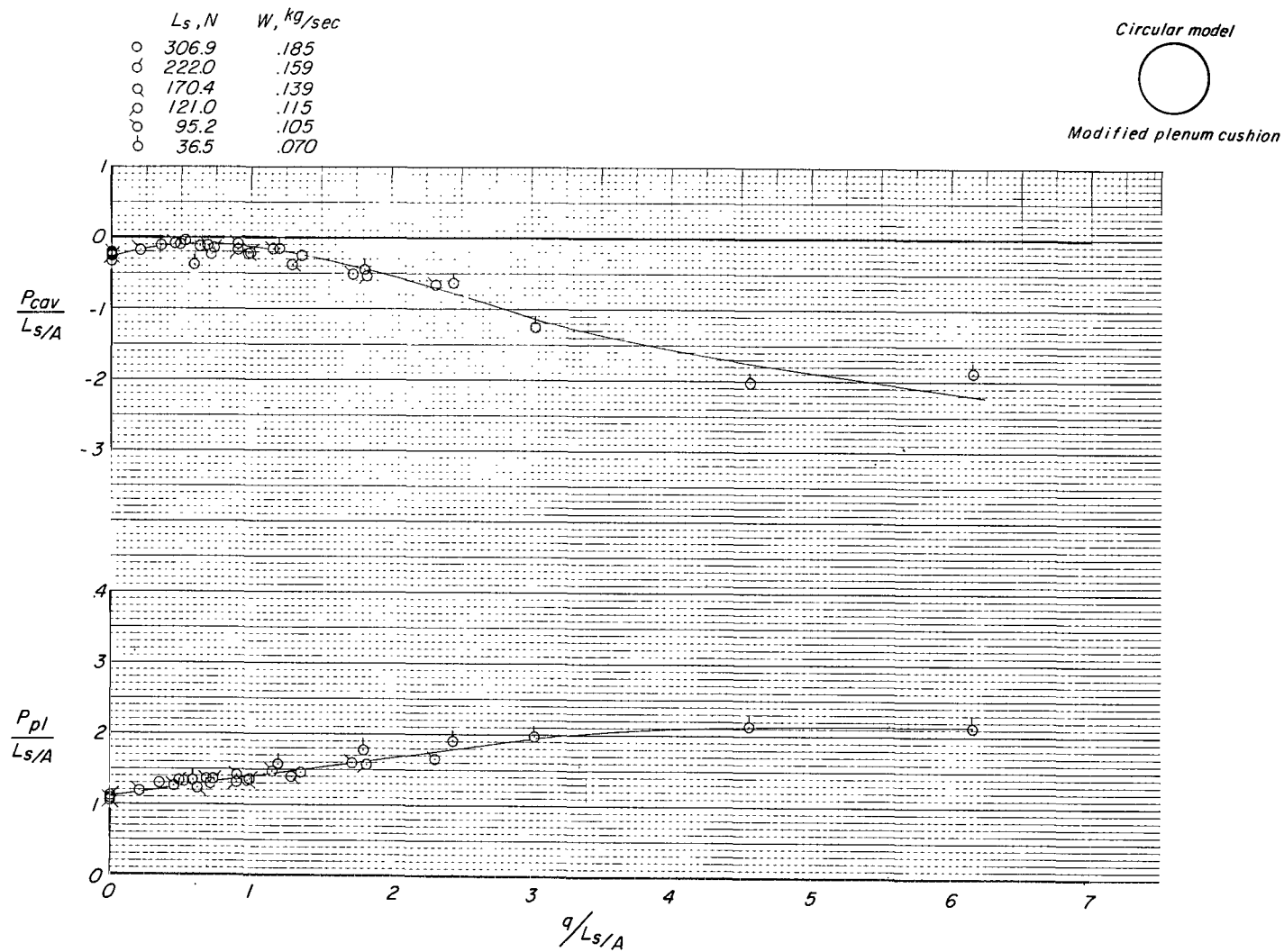


Figure 20.- Effect of forward speed on aerodynamic characteristics of circular model (modified plenum). Belt moving;  $h/d = 0.00412$ .



(b) Cavity pressure and plenum pressure.

Figure 20.- Concluded.

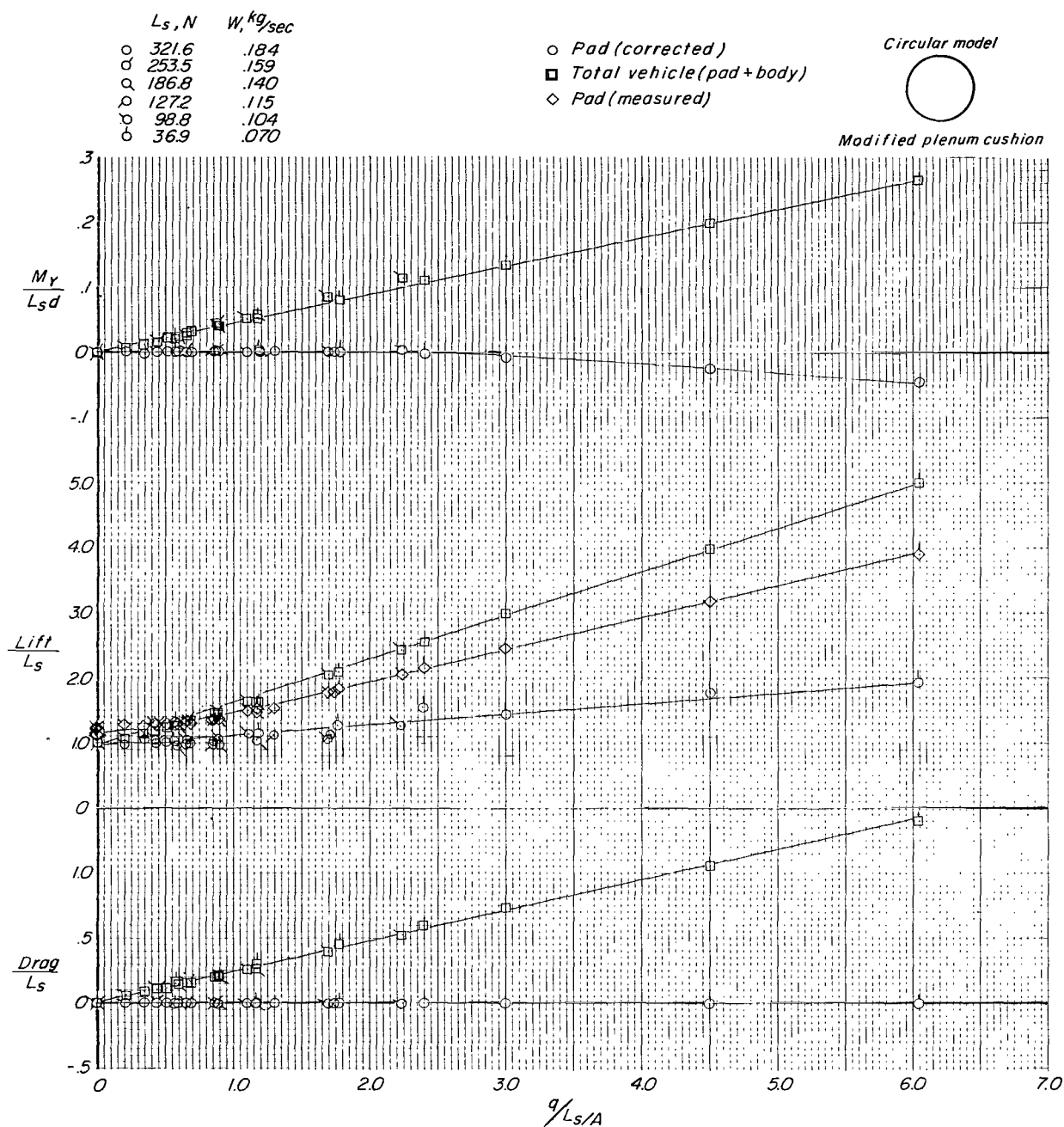
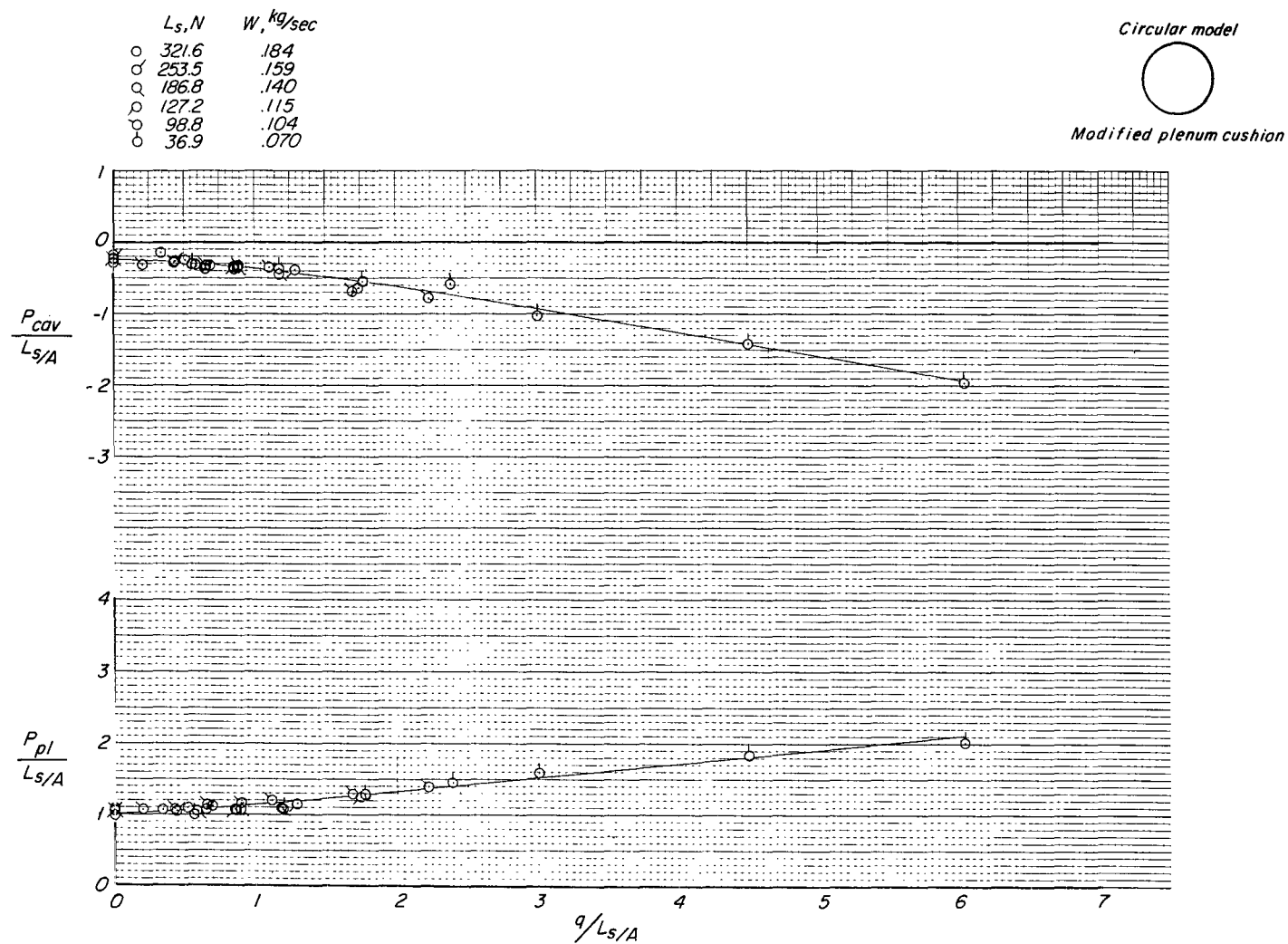


Figure 21.- Effect of forward speed on aerodynamic characteristics of circular model (modified plenum). Belt stopped;  $h/d = 0.00412$ .



(b) Cavity pressure and plenum pressure.

Figure 21.- Concluded.

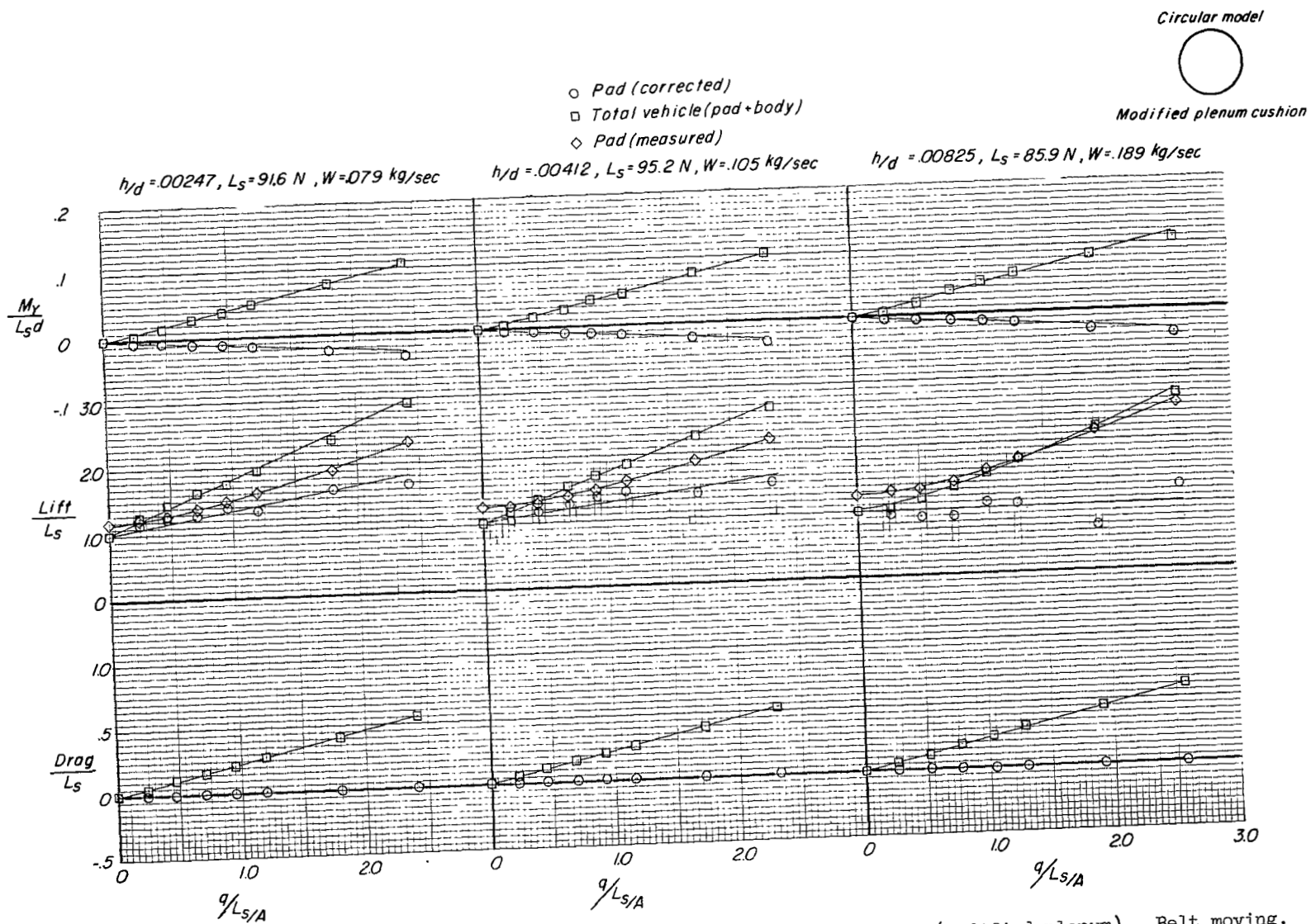


Figure 22.- Effect of height on aerodynamic characteristics of circular model (modified plenum). Belt moving.

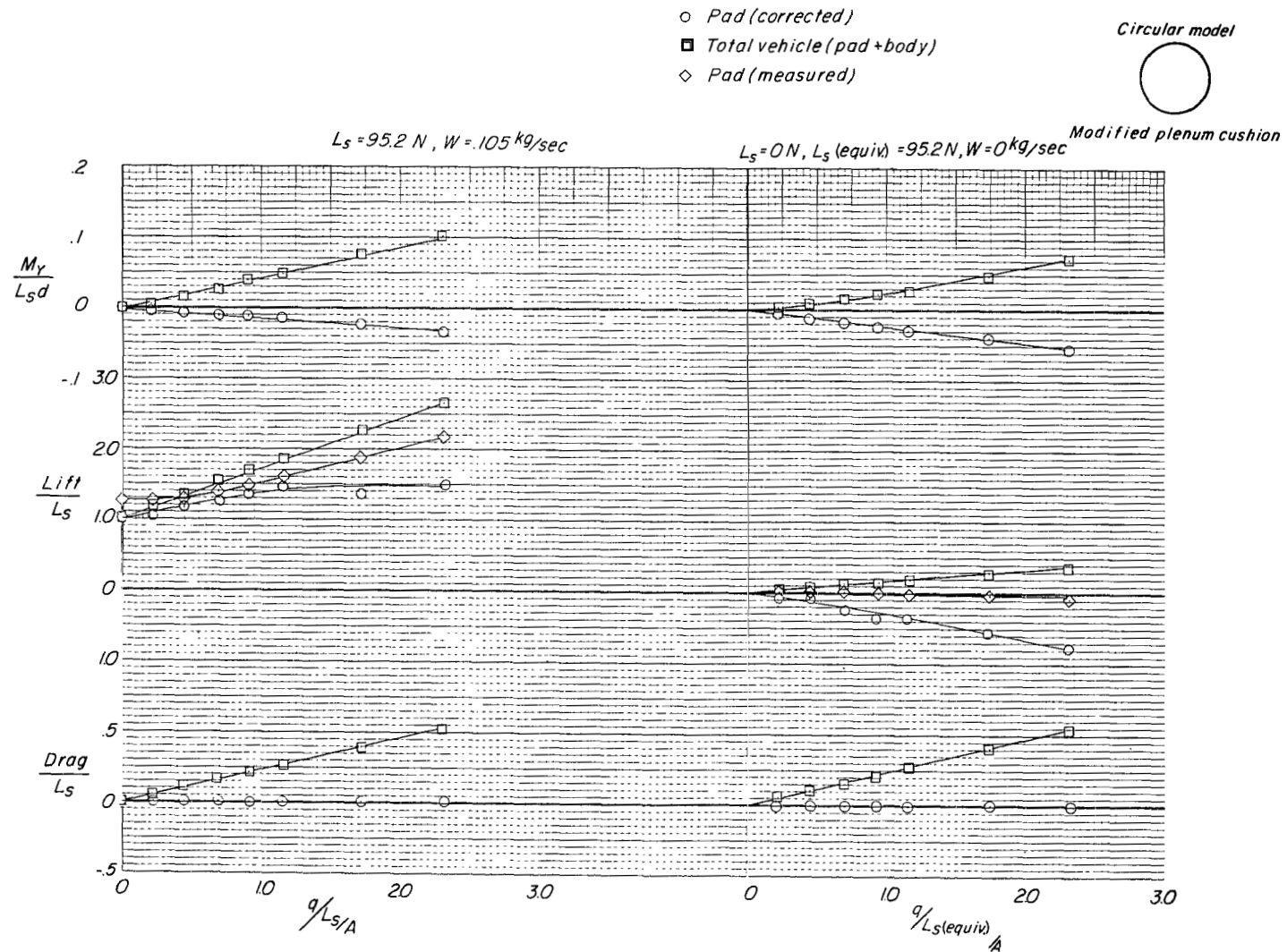


Figure 23.- Comparison of aerodynamic characteristics of powered air cushion with those of unpowered cushion for circular model (modified plenum). Belt moving;  $h/d = 0.00412$ .



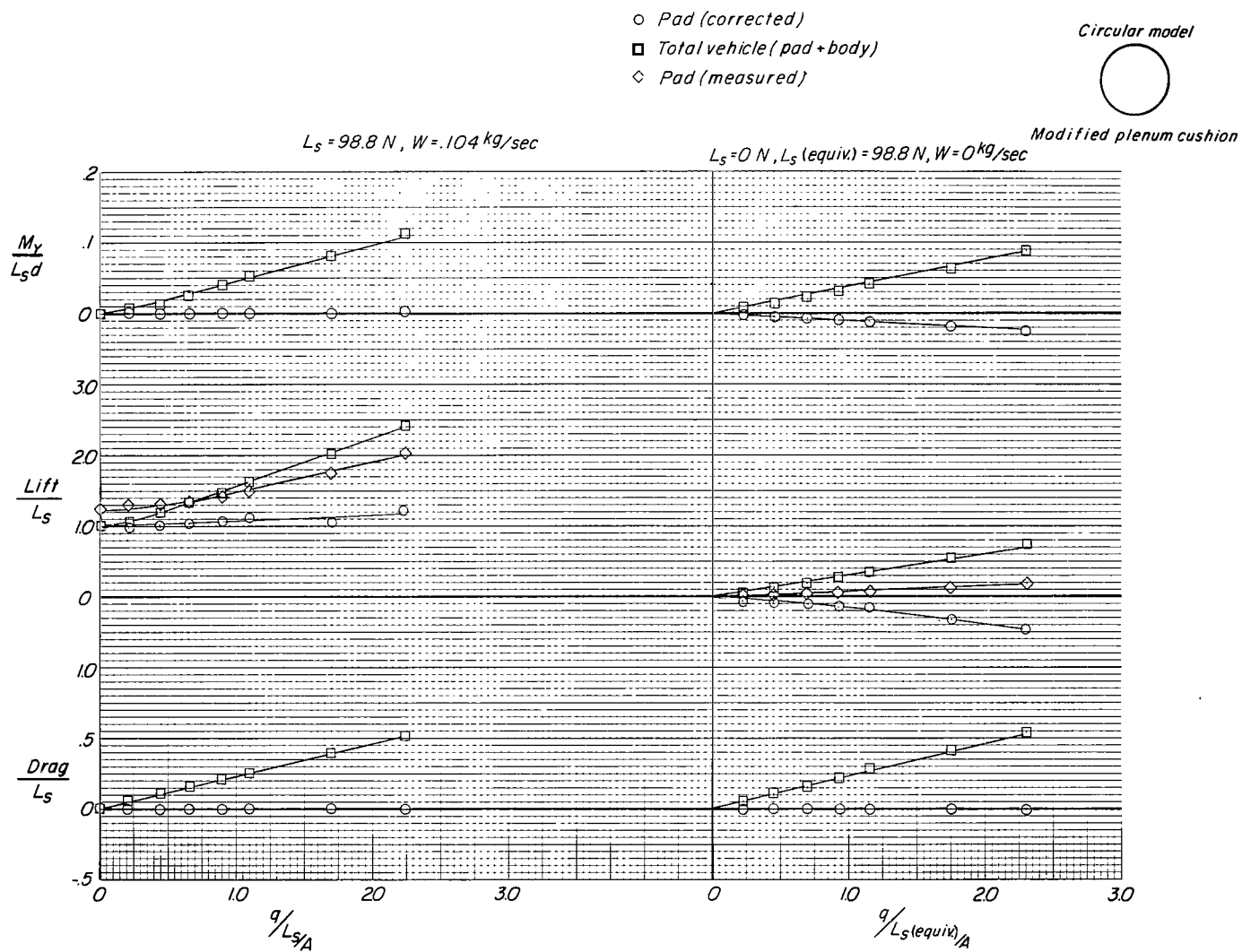
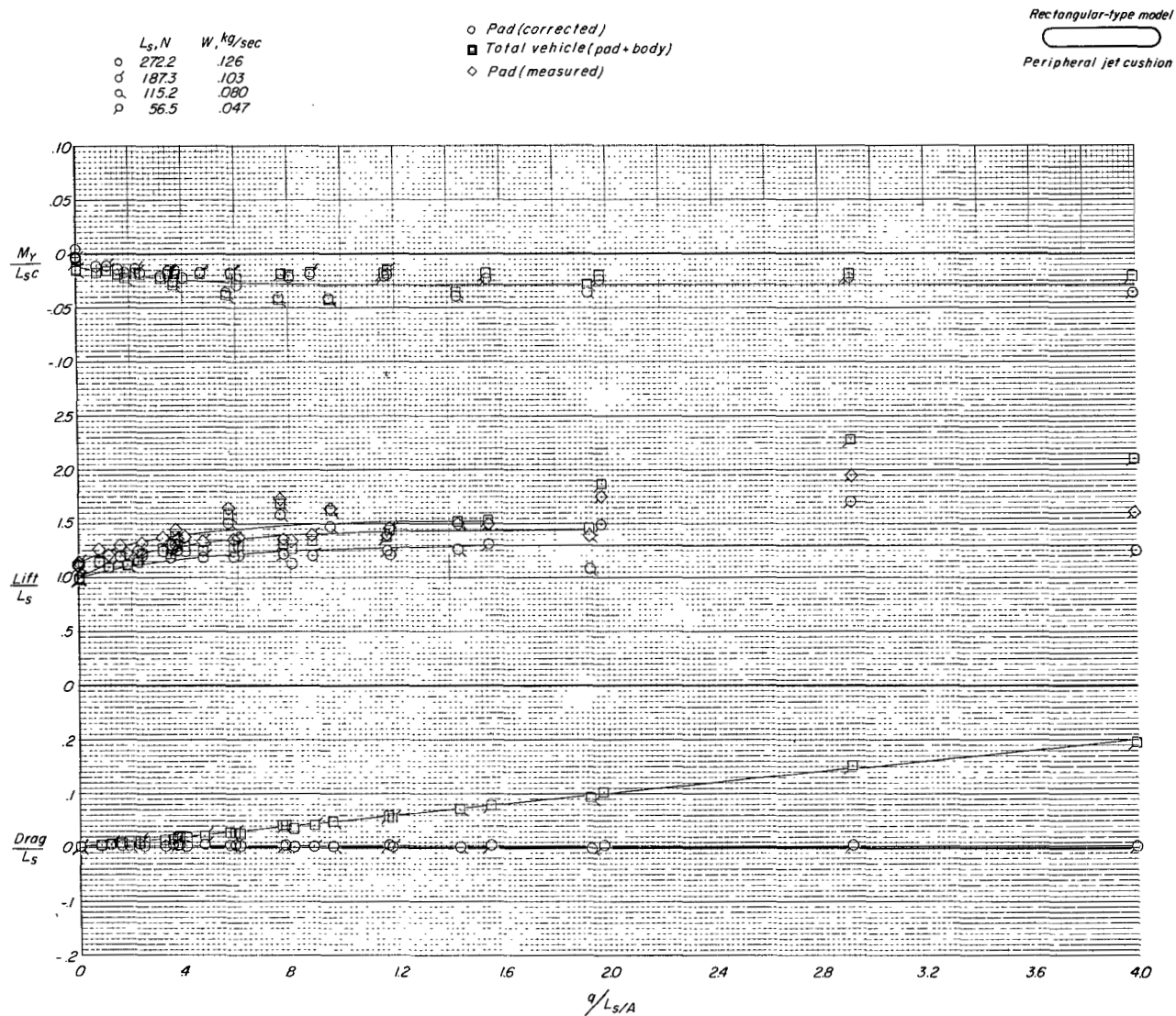
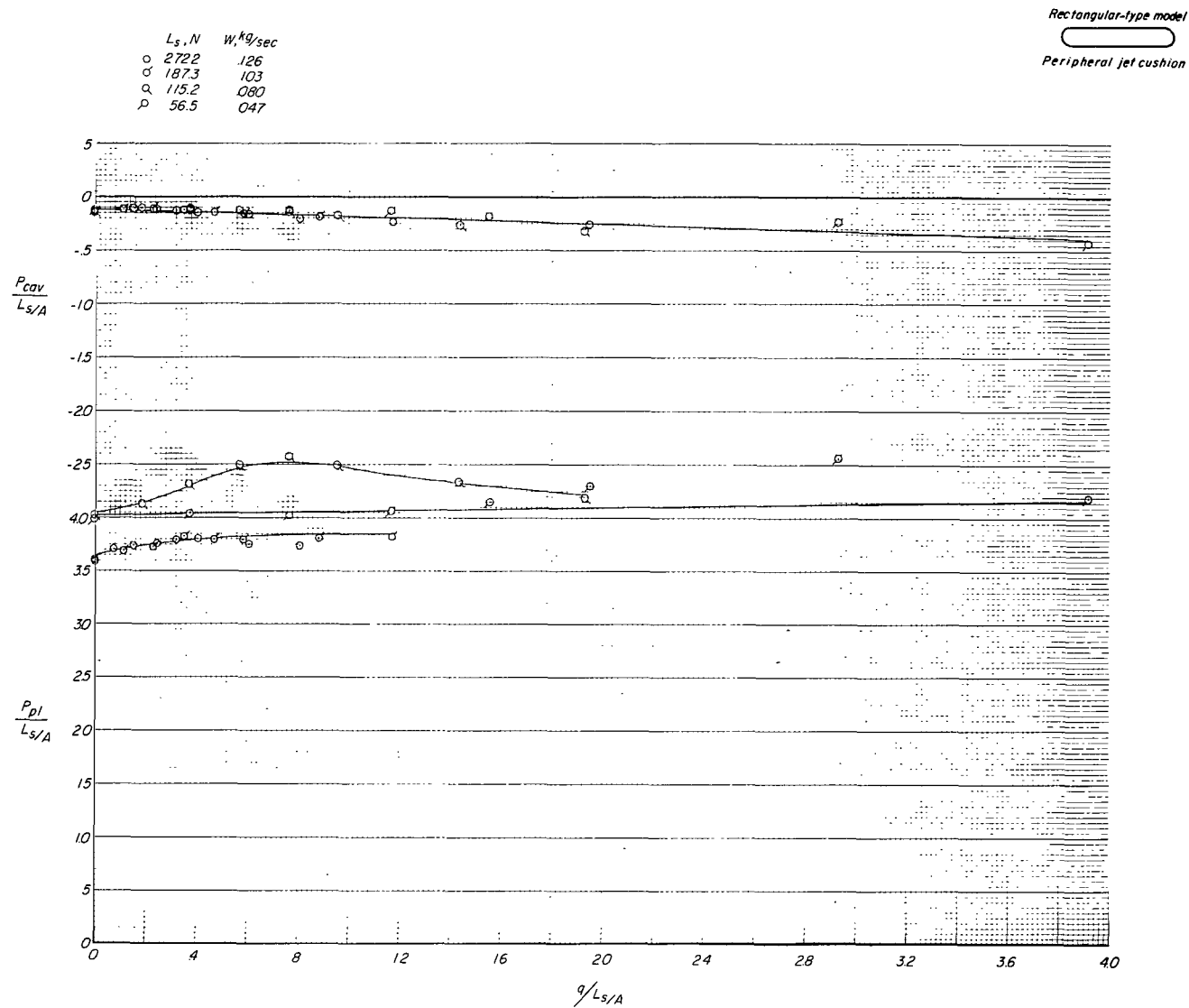


Figure 24.- Comparison of aerodynamic characteristics of powered air cushion with those of unpowered cushion for circular model (modified plenum). Belt stopped;  $h/d = 0.00412$ .



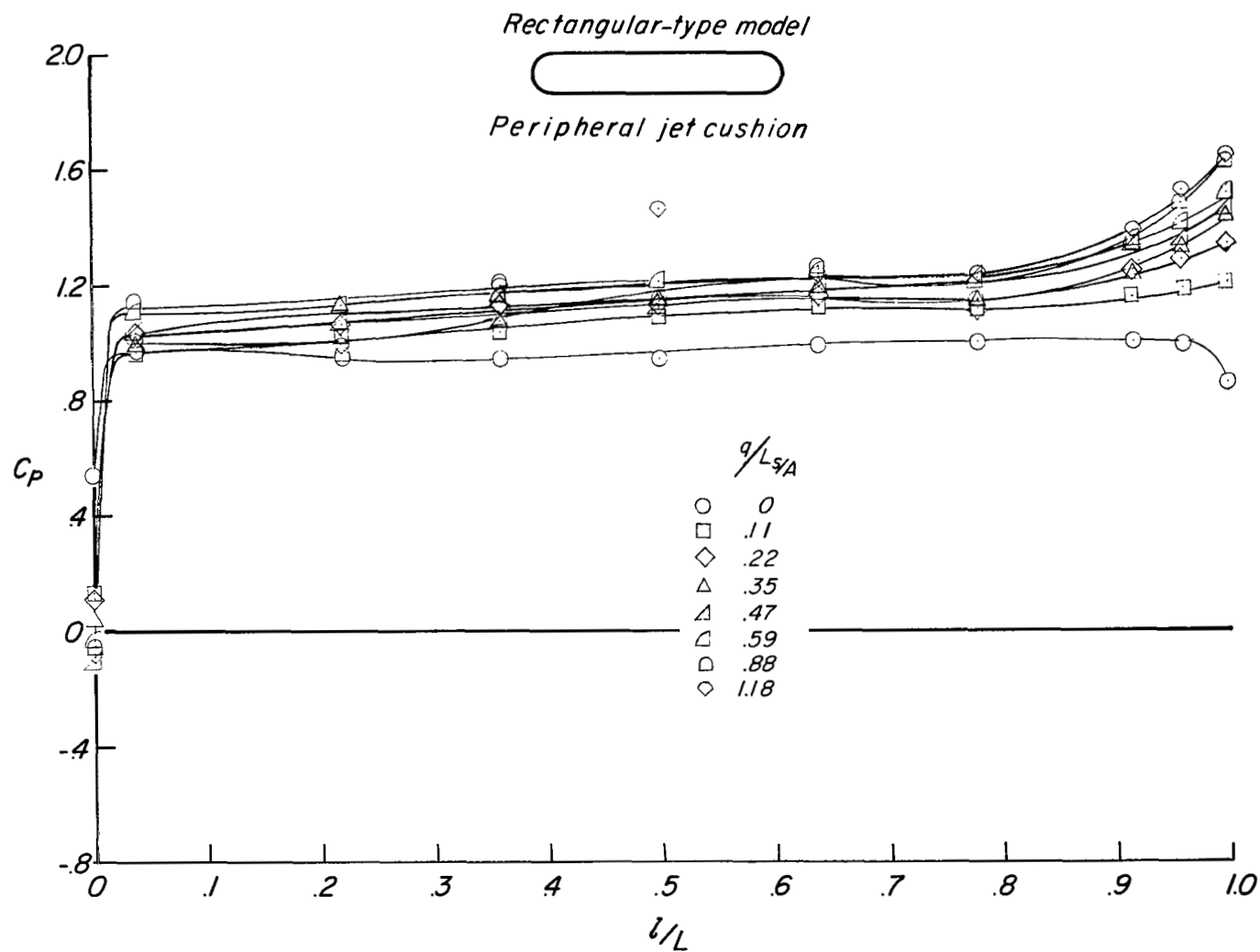
(a) Lift, drag, and pitching moment.

Figure 25.- Effect of forward speed on aerodynamic characteristics of rectangular-type model (peripheral jet). Belt moving;  $h/d_e = 0.0033$ .



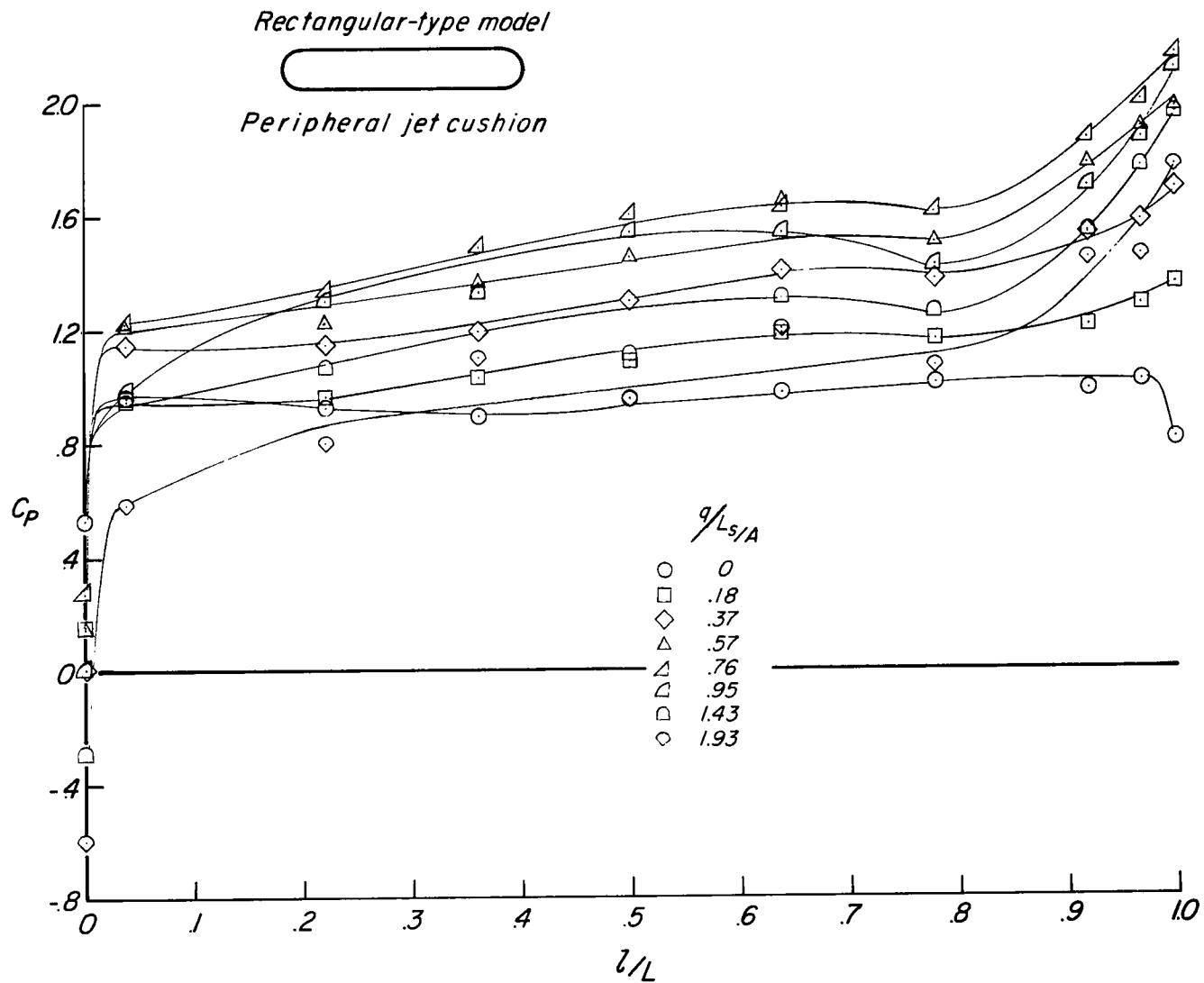
(b) Cavity pressure and plenum pressure.

Figure 25.- Continued.



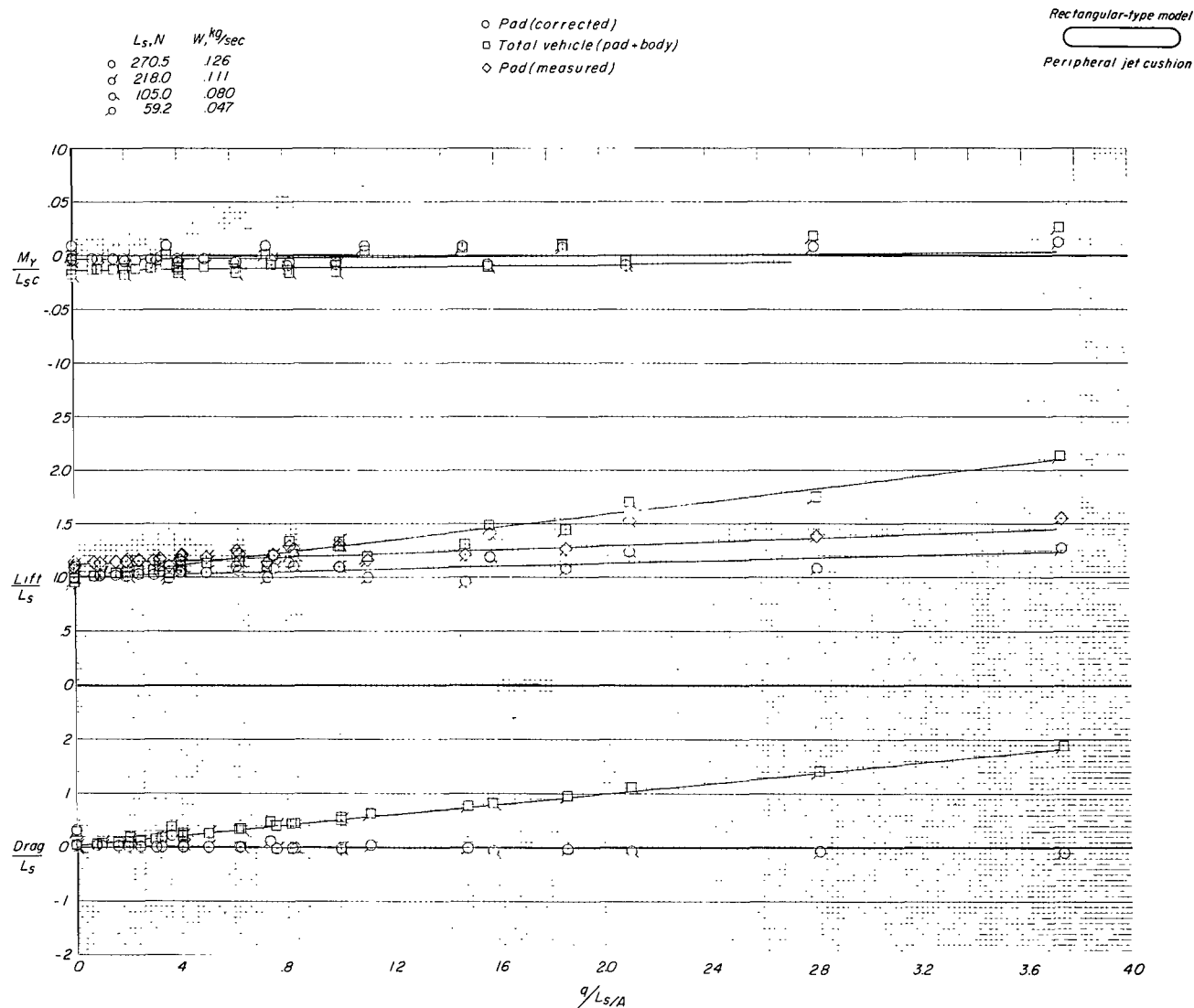
(c) Pressure coefficient along center line of air cushion.  $L_g = 187.3 \text{ N}$ ;  $W = 0.103 \text{ kg/sec}$ .

Figure 25.- Continued.



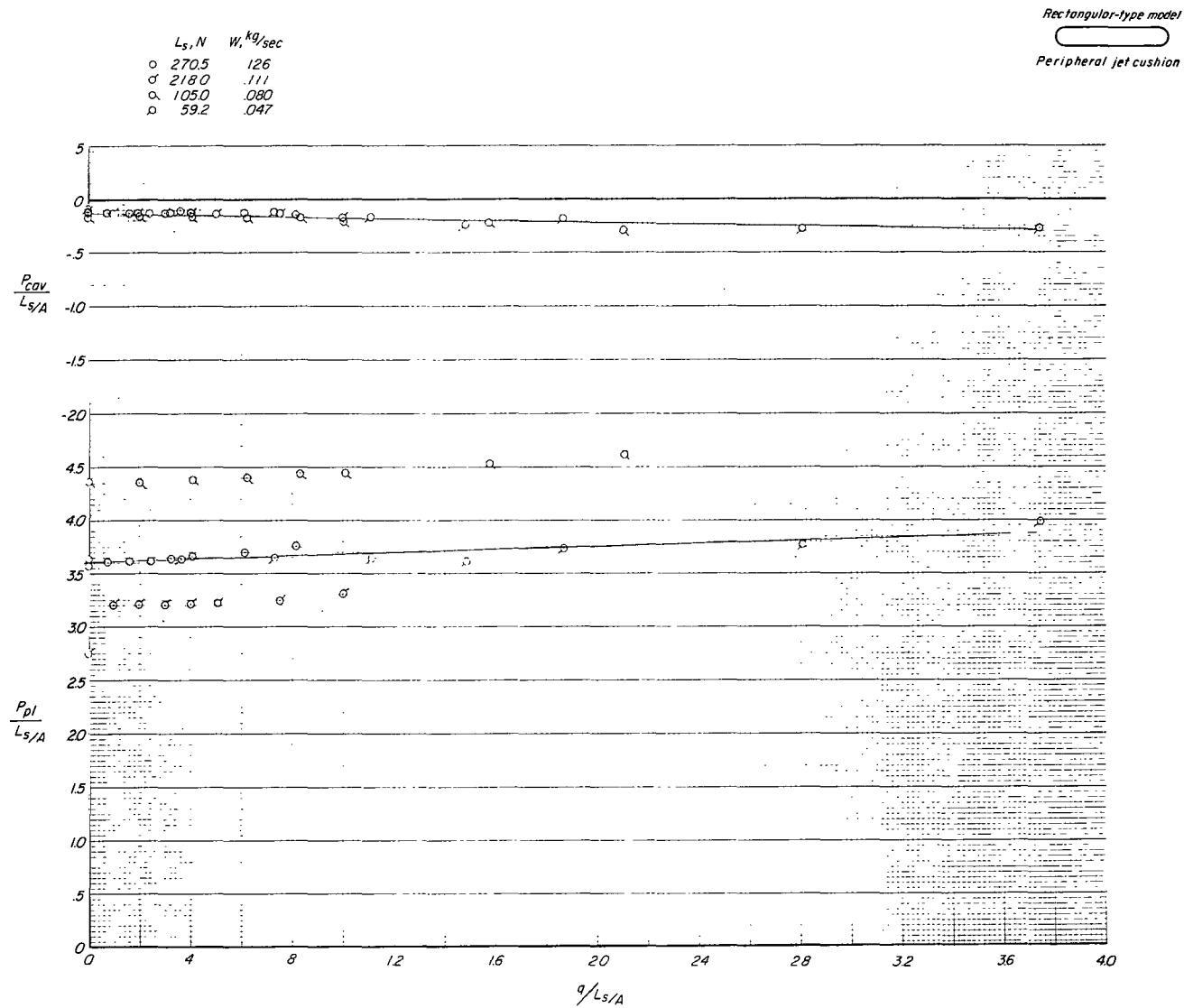
(d) Pressure coefficient along center line of air cushion.  $L_s = 115.2$  N;  $W = 0.080$  kg/sec.

Figure 25.- Concluded.



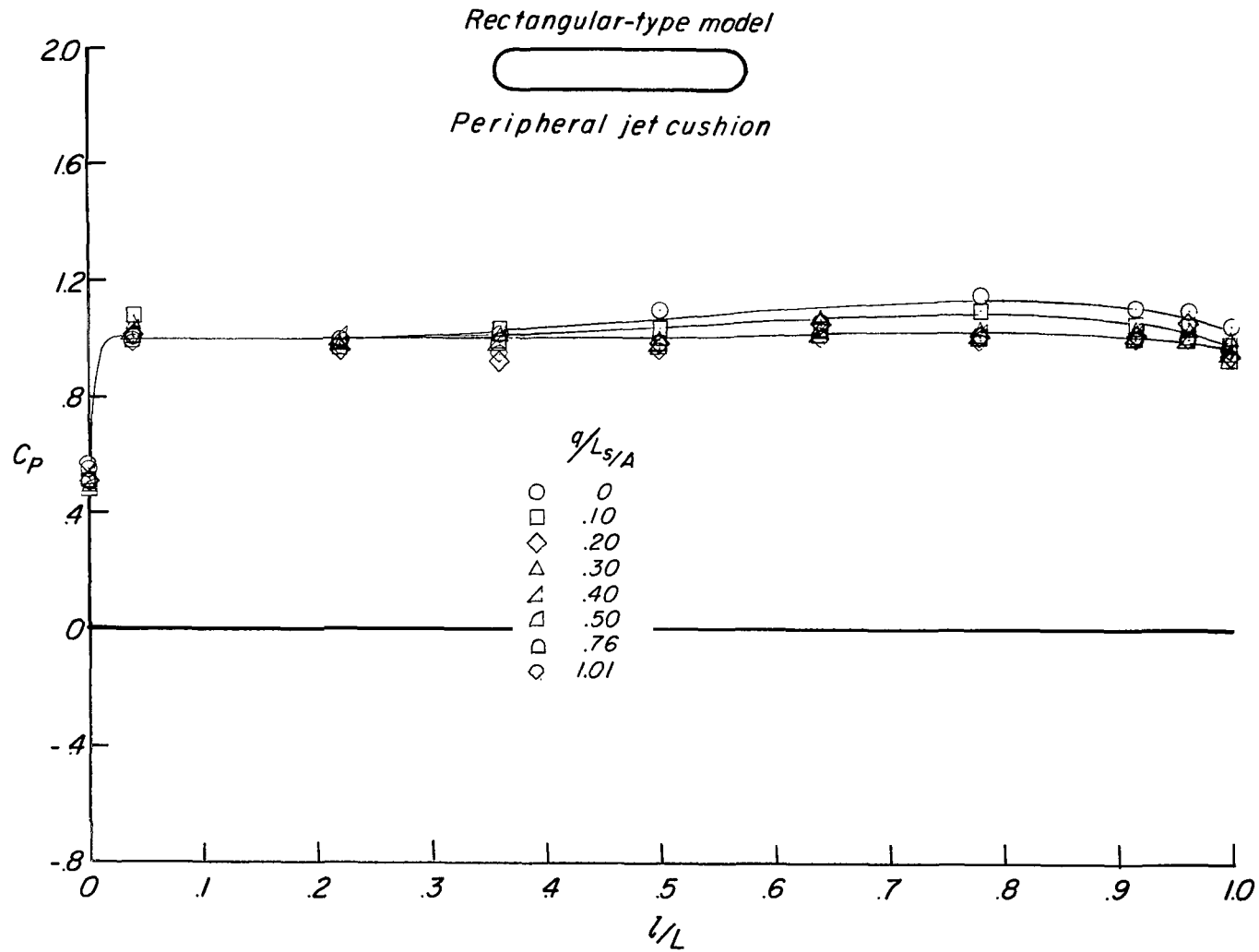
(a) Lift, drag, and pitching moment.

Figure 26.- Effect of forward speed on aerodynamic characteristics of rectangular-type model (peripheral jet). Belt stopped;  $h/d_e = 0.0033$ .



(b) Cavity pressure and plenum pressure.

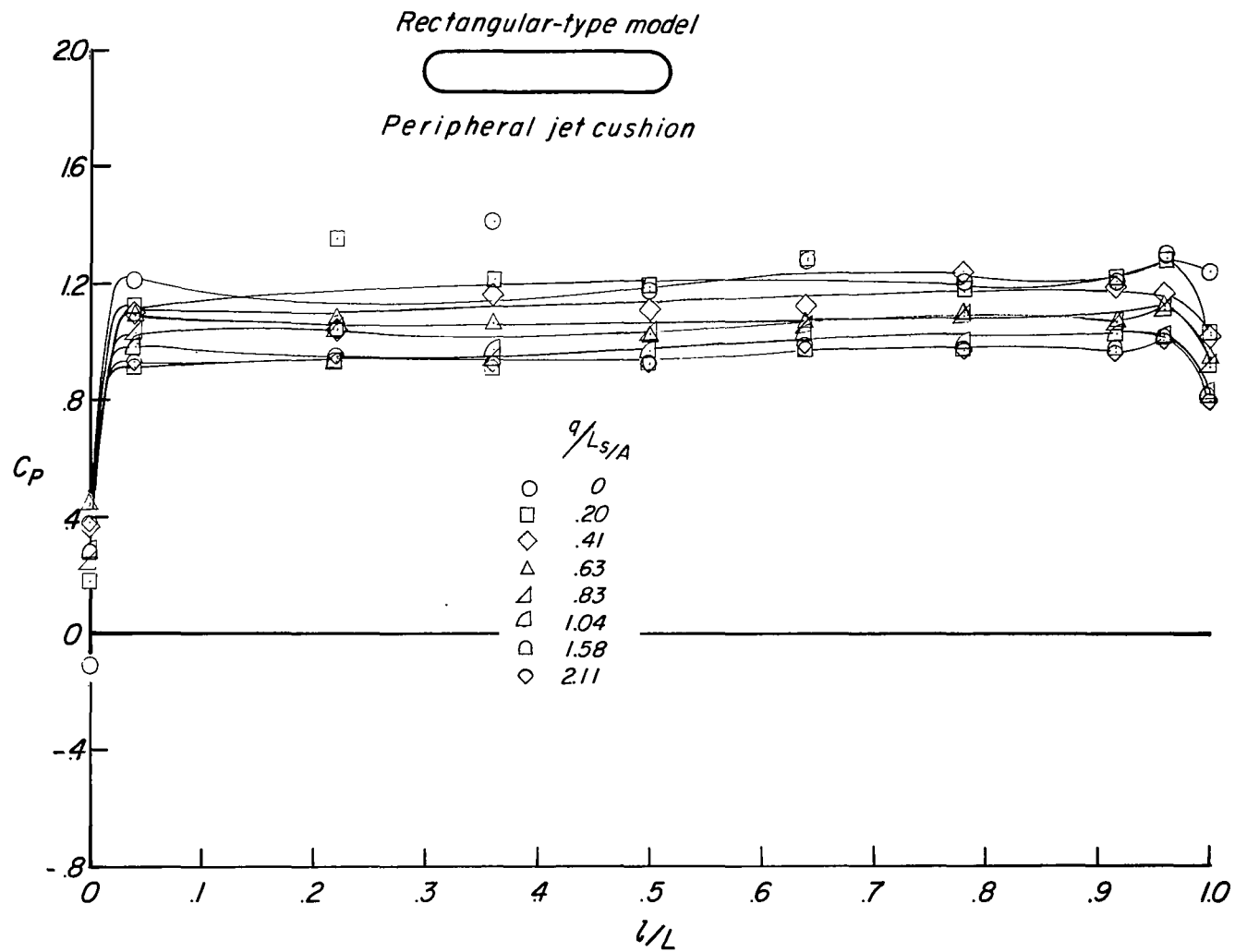
Figure 26.- Continued.



(c) Pressure coefficient along center line of air cushion.  $L_s = 218.0$  N;  $W = 0.111$  kg/sec.

Figure 26.- Continued.





(d) Pressure coefficient along center line of air cushion.  $L_s = 105.0$  N;  $W = 0.080$  kg/sec.

Figure 26.- Concluded.

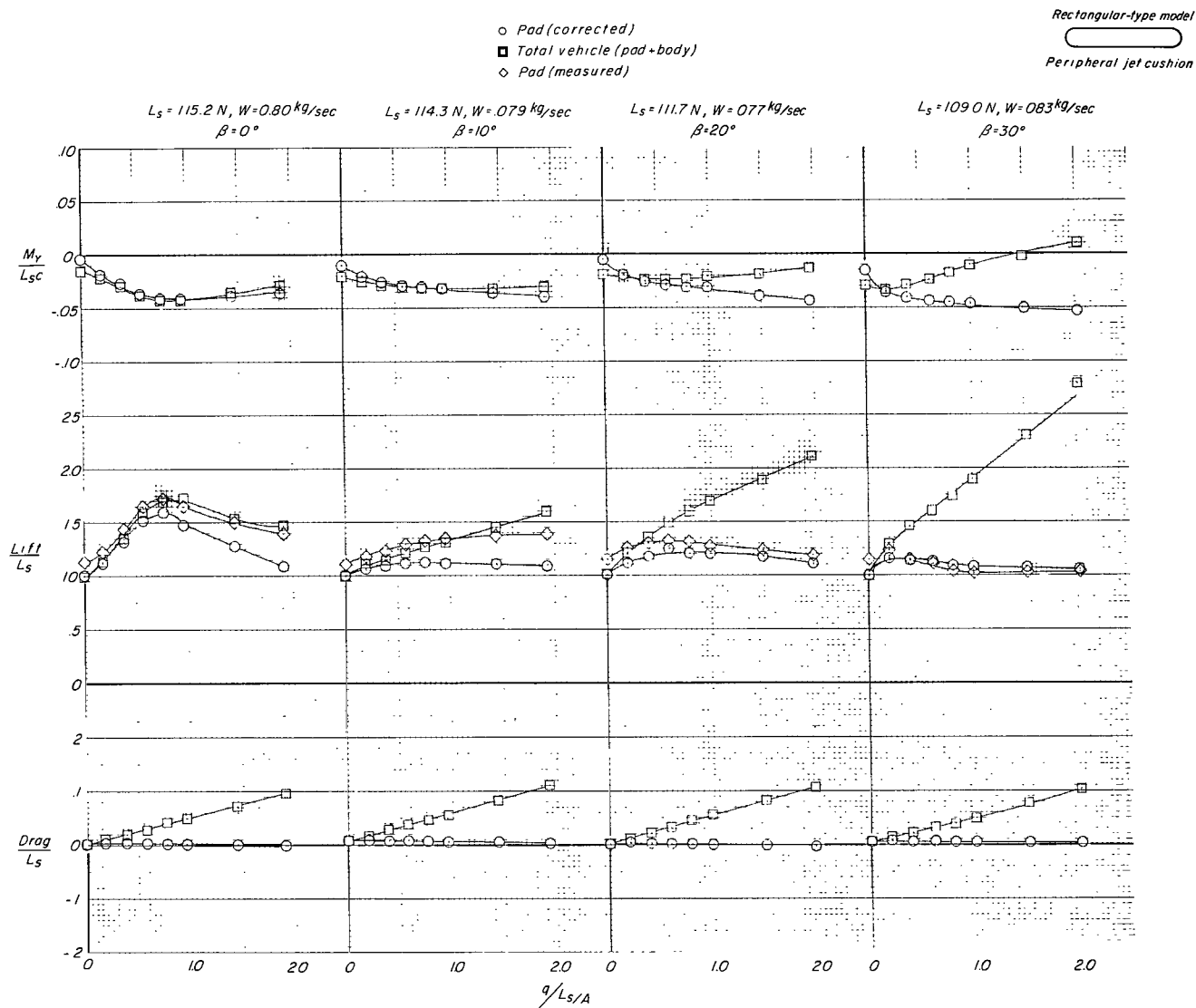
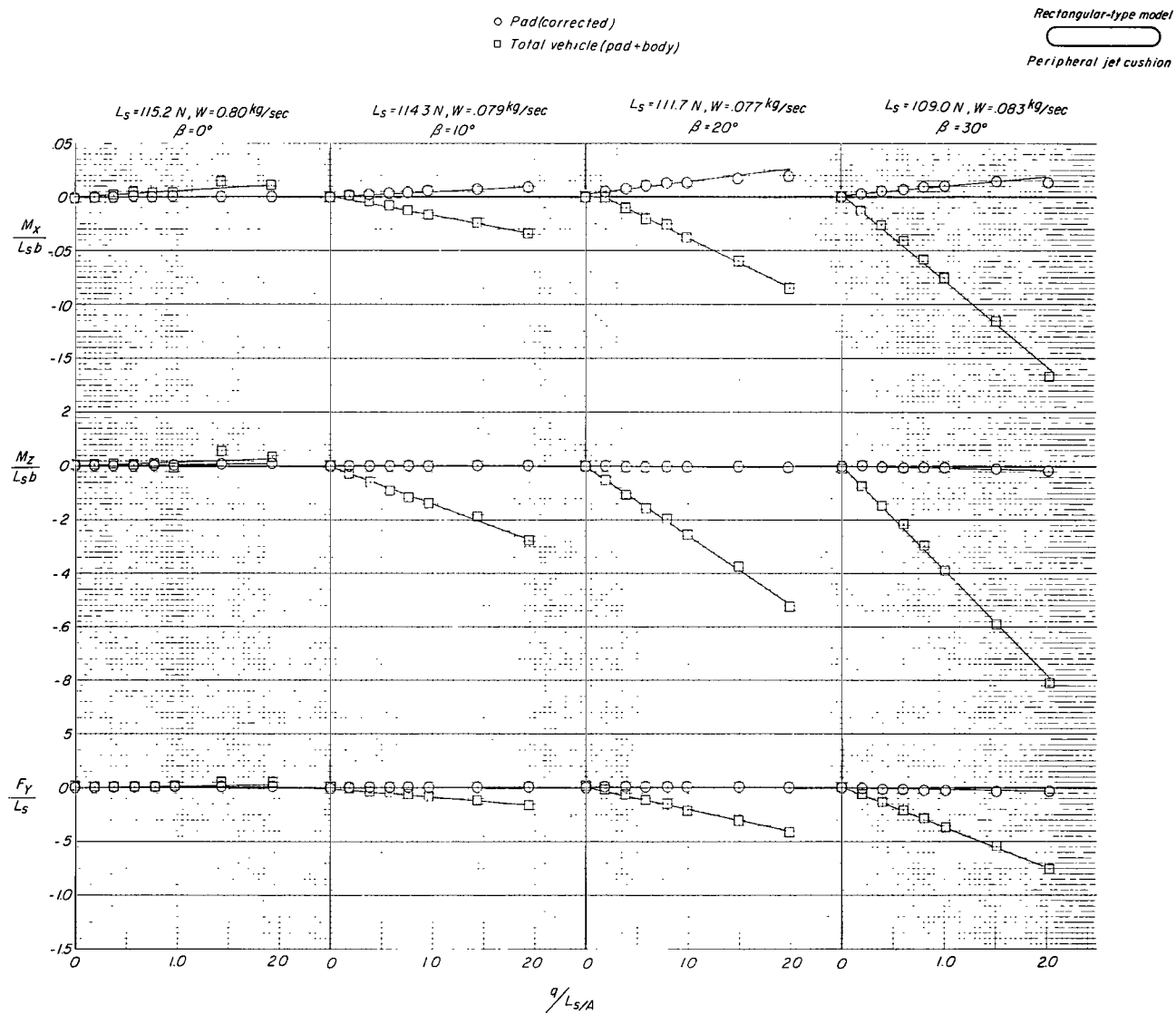
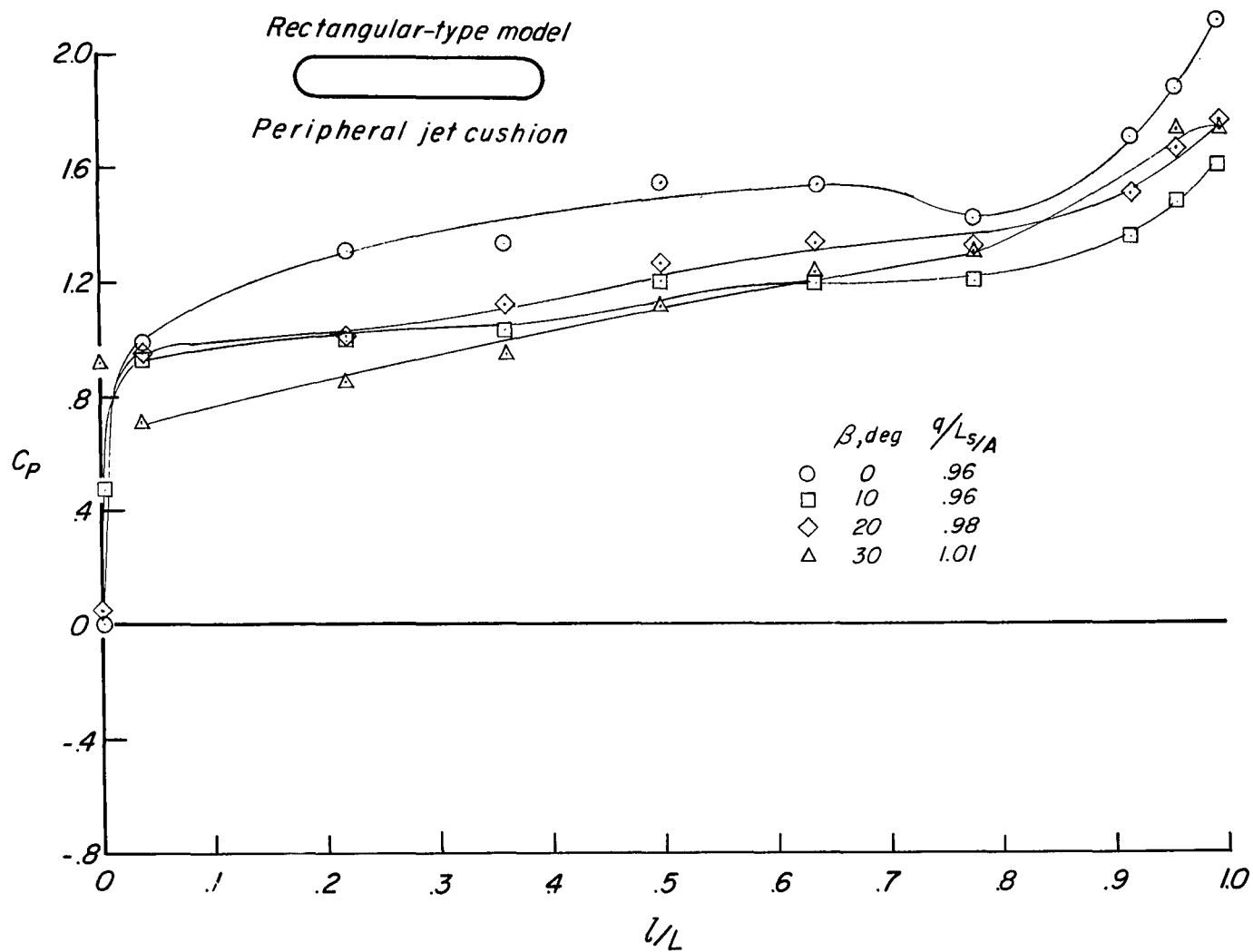


Figure 27.- Effect of sideslip on aerodynamic characteristics of rectangular-type model (peripheral jet). Belt moving;  $h/d_e = 0.0033$ .



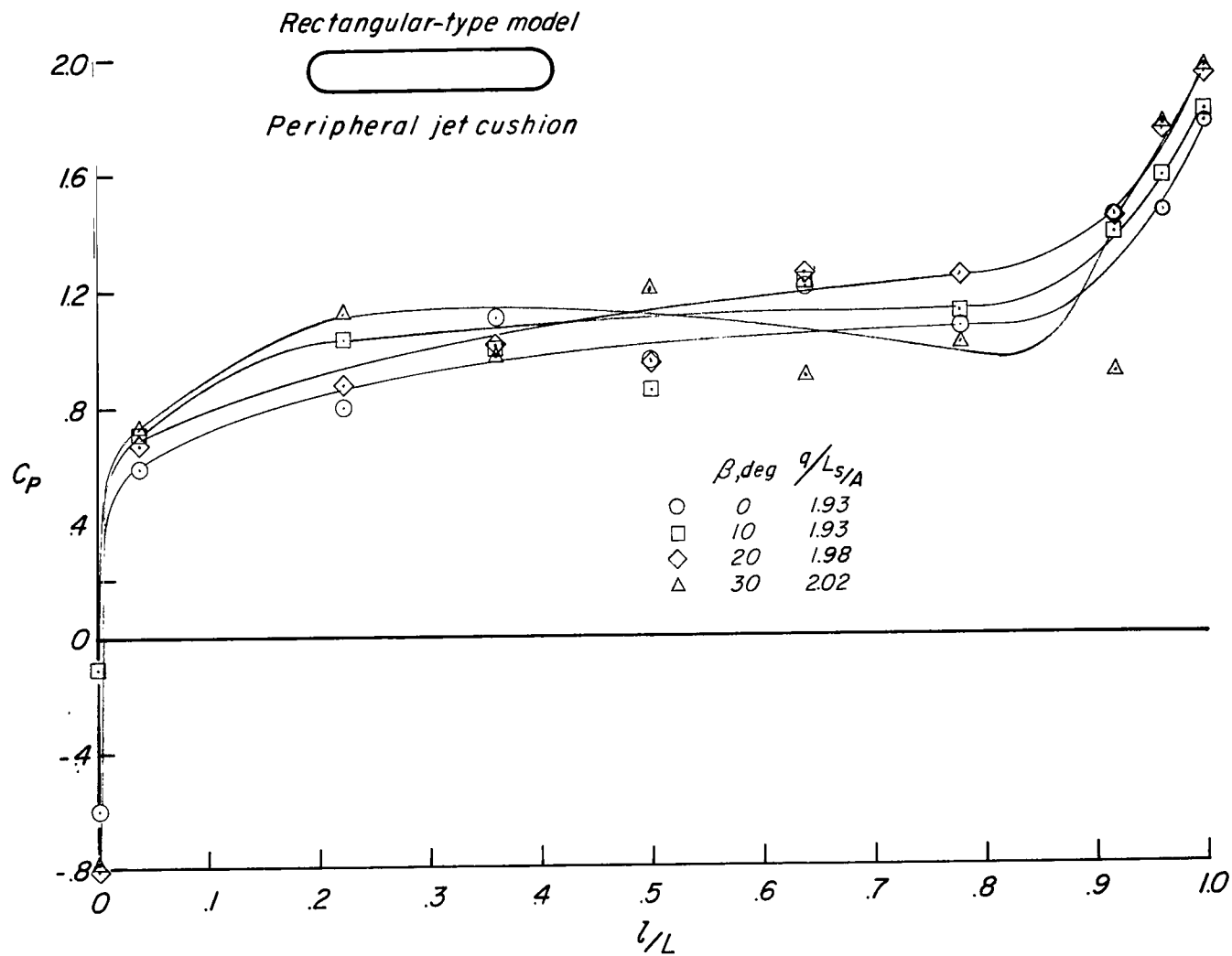
(b) Roll, yaw, and side force.

Figure 27.- Continued.



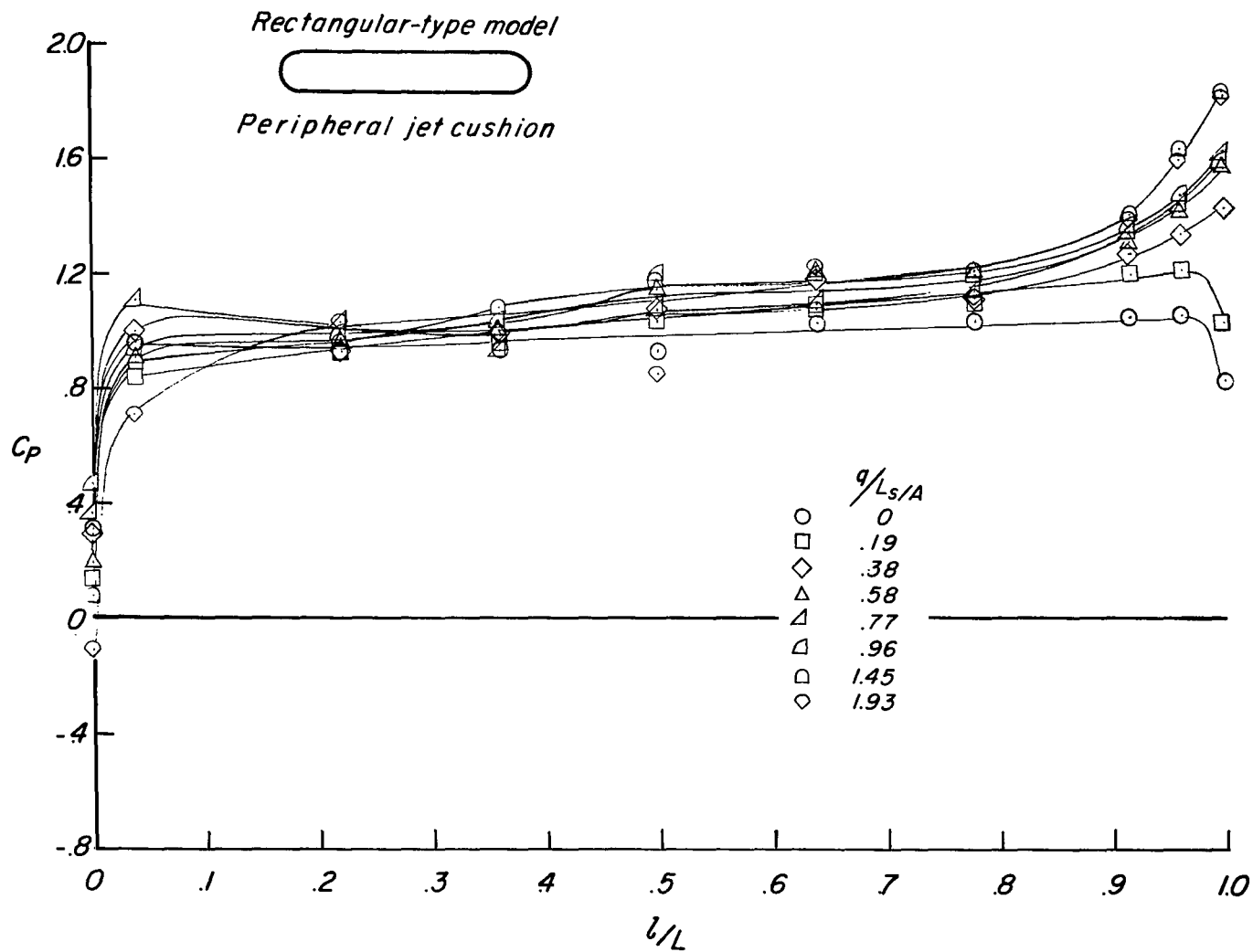
(c) Pressure coefficient along center line of air cushion at  $q/L_s/A \approx 1.00$ .

Figure 27.- Continued.



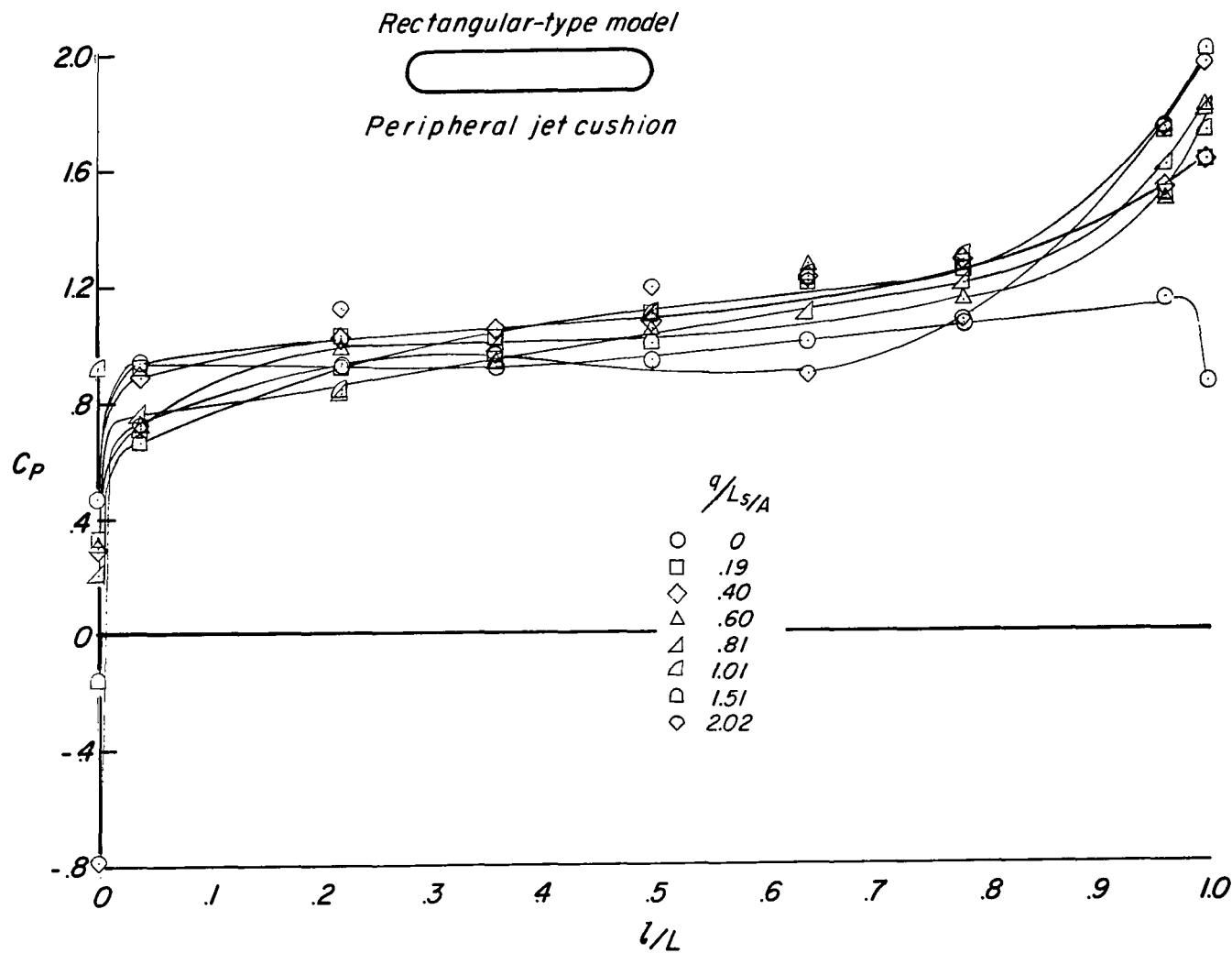
(d) Pressure coefficient along center line of air cushion at  $q/L_s/A \approx 2.00$ .

Figure 27.- Continued.



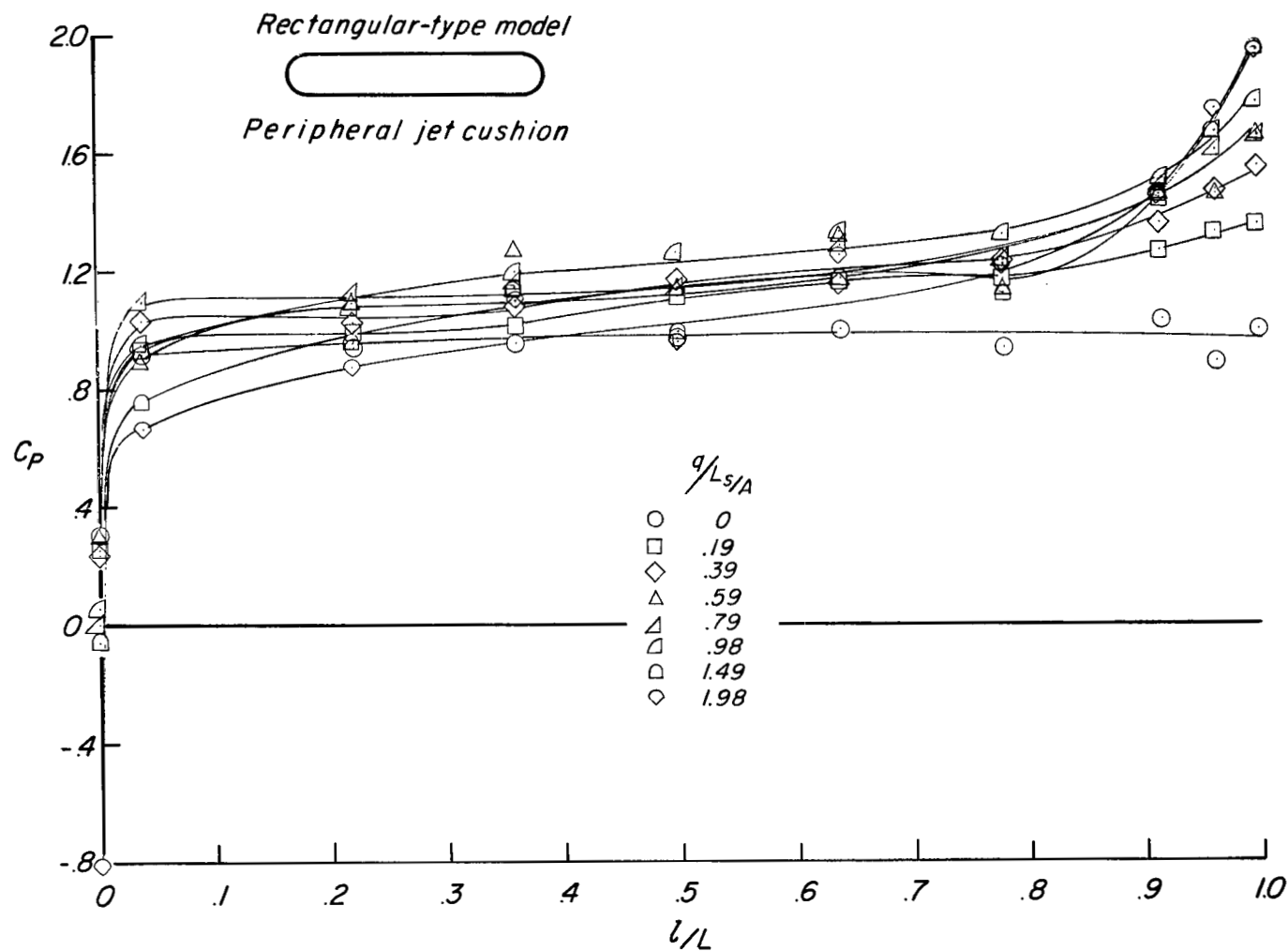
(e) Pressure coefficient along center line of air cushion.  $L_s = 114.3$  N;  $W = 0.079$  kg/sec;  $\beta = 10^\circ$ .

Figure 27.- Continued.



(f) Pressure coefficient along center line of air cushion.  $L_s = 111.7 \text{ N}$ ;  $W = 0.077 \text{ kg/sec}$ ;  $\beta = 20^\circ$ .

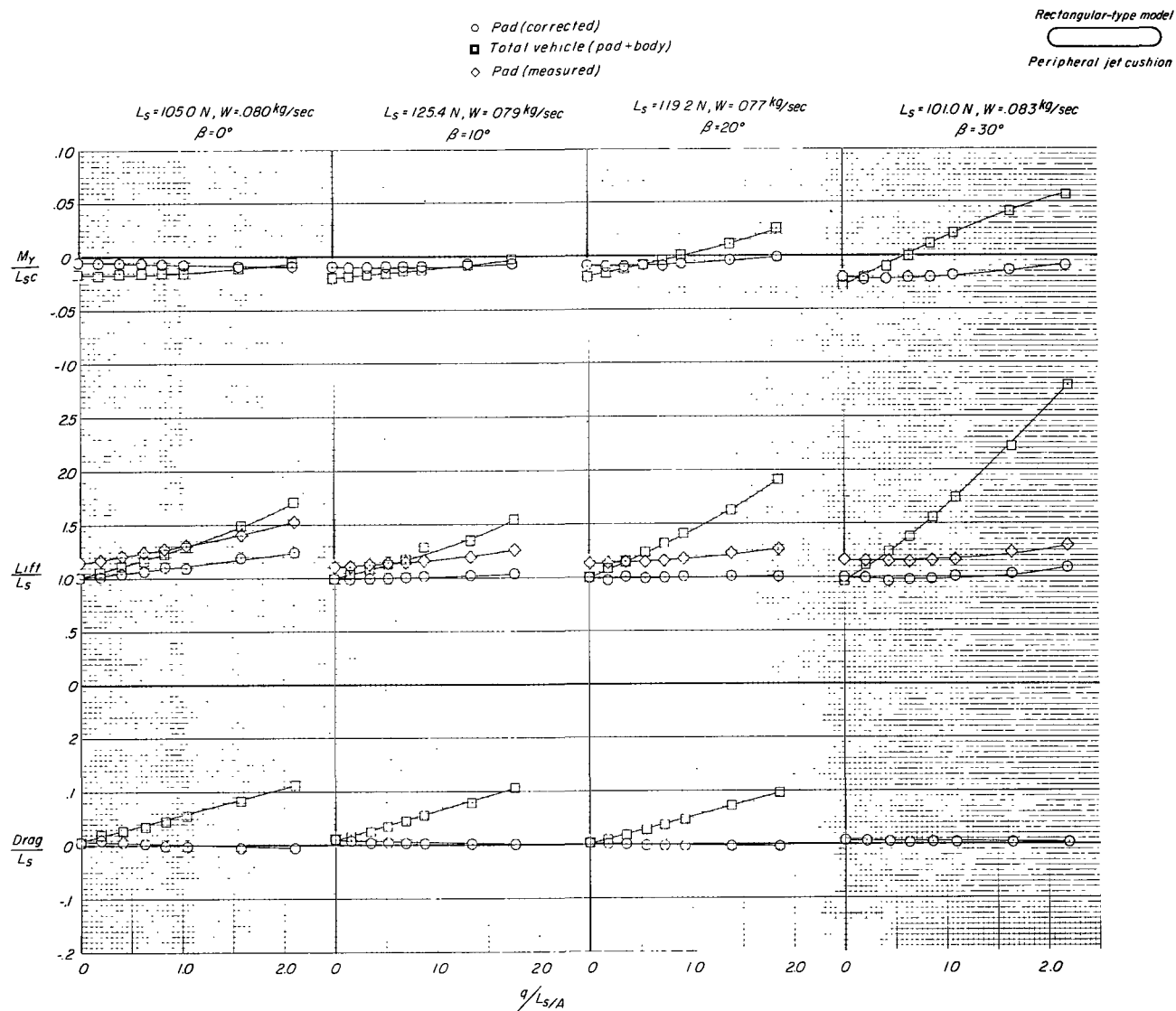
Figure 27.- Continued.



(g) Pressure coefficient along center line of air cushion.  $L_s = 109.0$  N;  $W = 0.083$  kg/sec;  $\beta = 30^\circ$ .

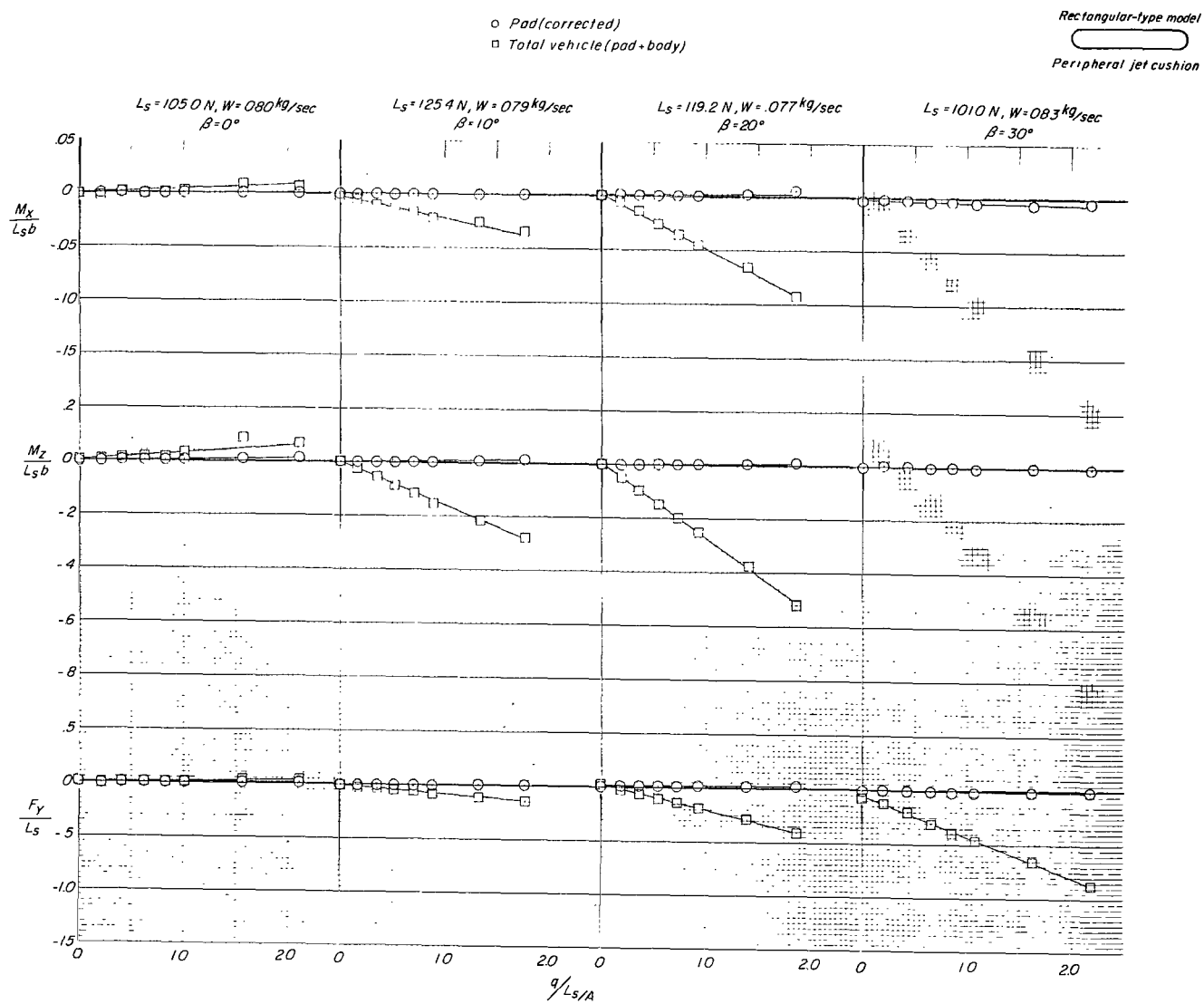
Figure 27.- Concluded.





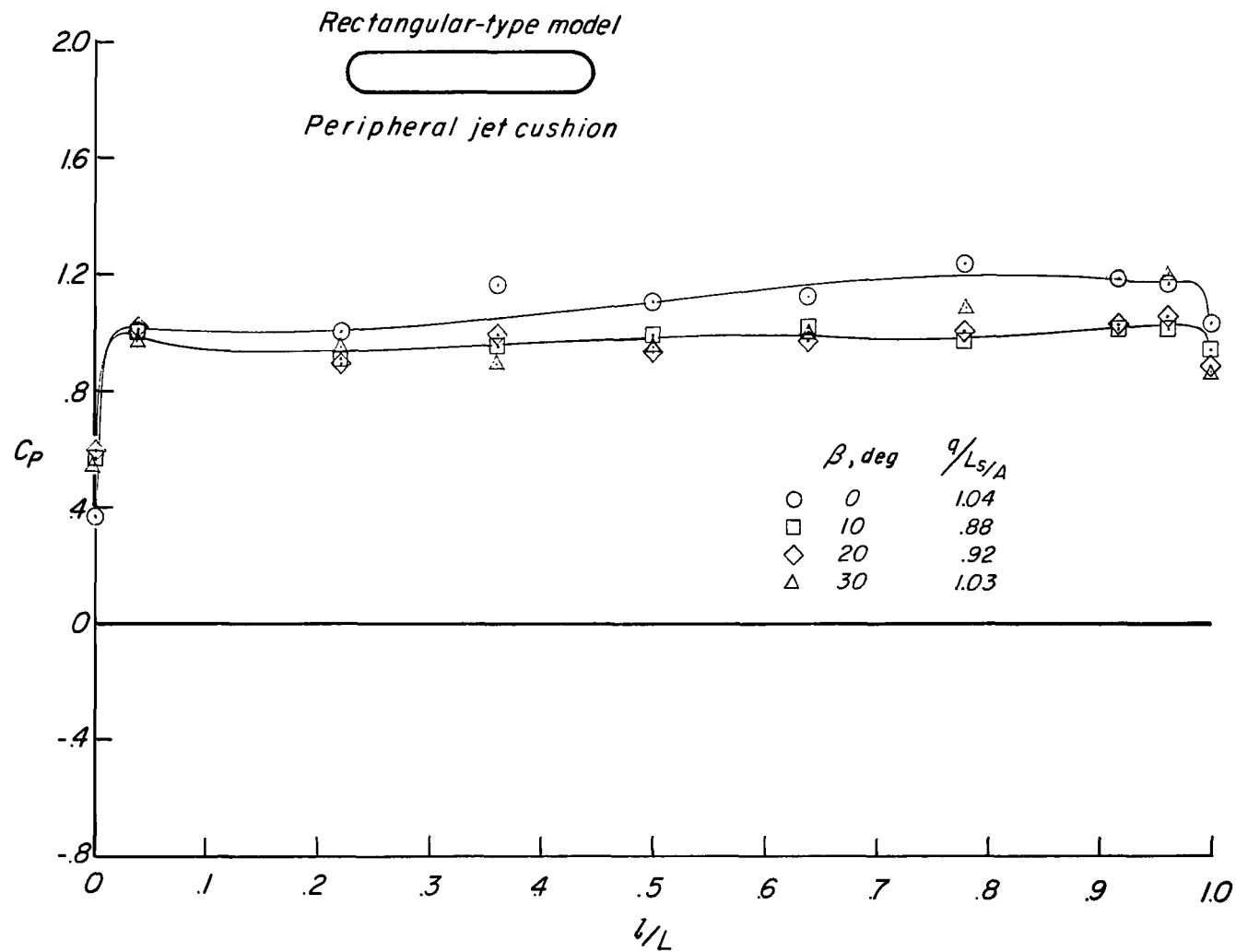
(a) Lift, drag, and pitching moment.

Figure 28.- Effect of sideslip on aerodynamic characteristics of rectangular-type model (peripheral jet). Belt stopped;  $h/d_e = 0.0033$ .



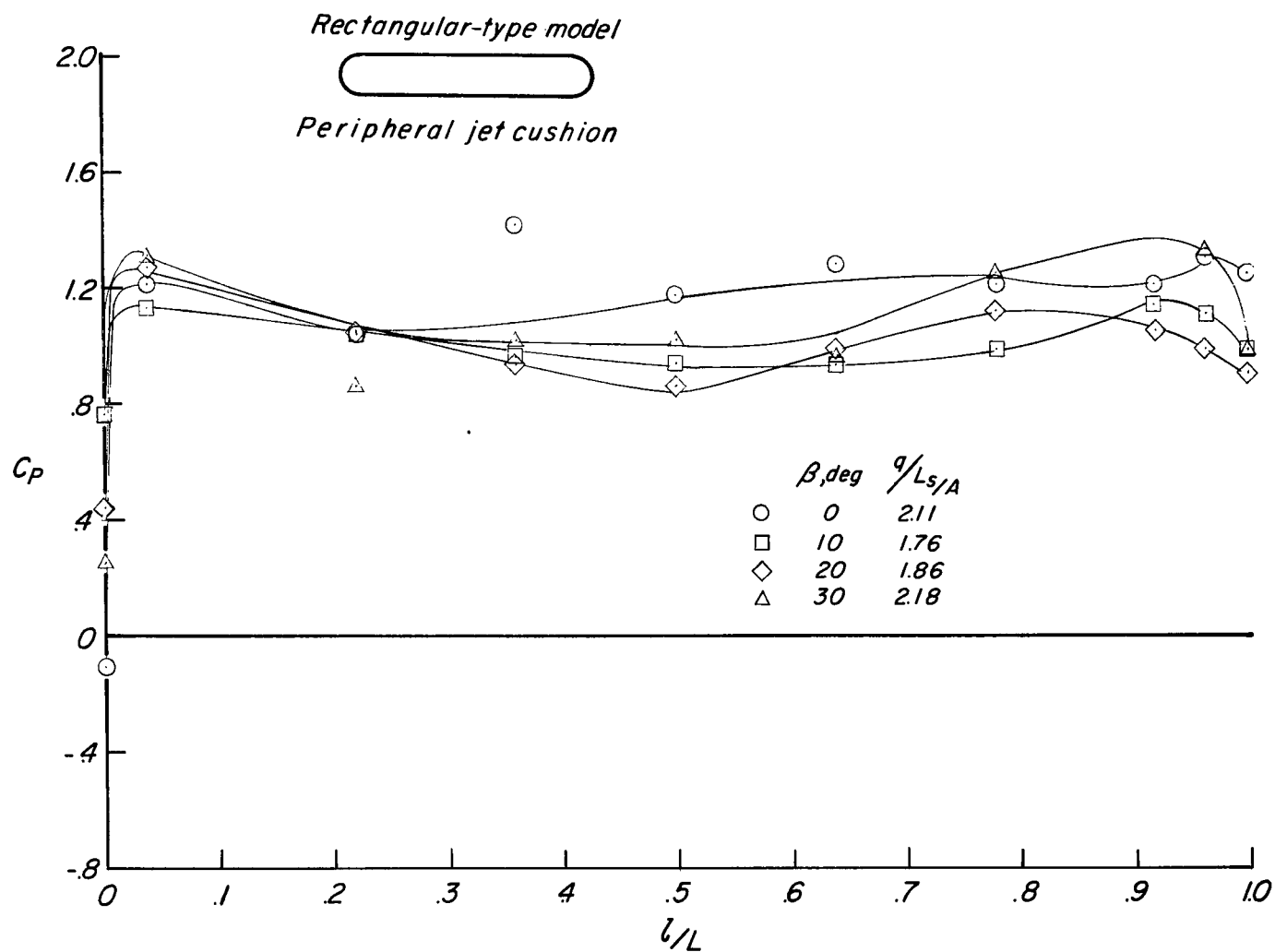
(b) Roll, yaw, and side force.

Figure 28.- Continued.



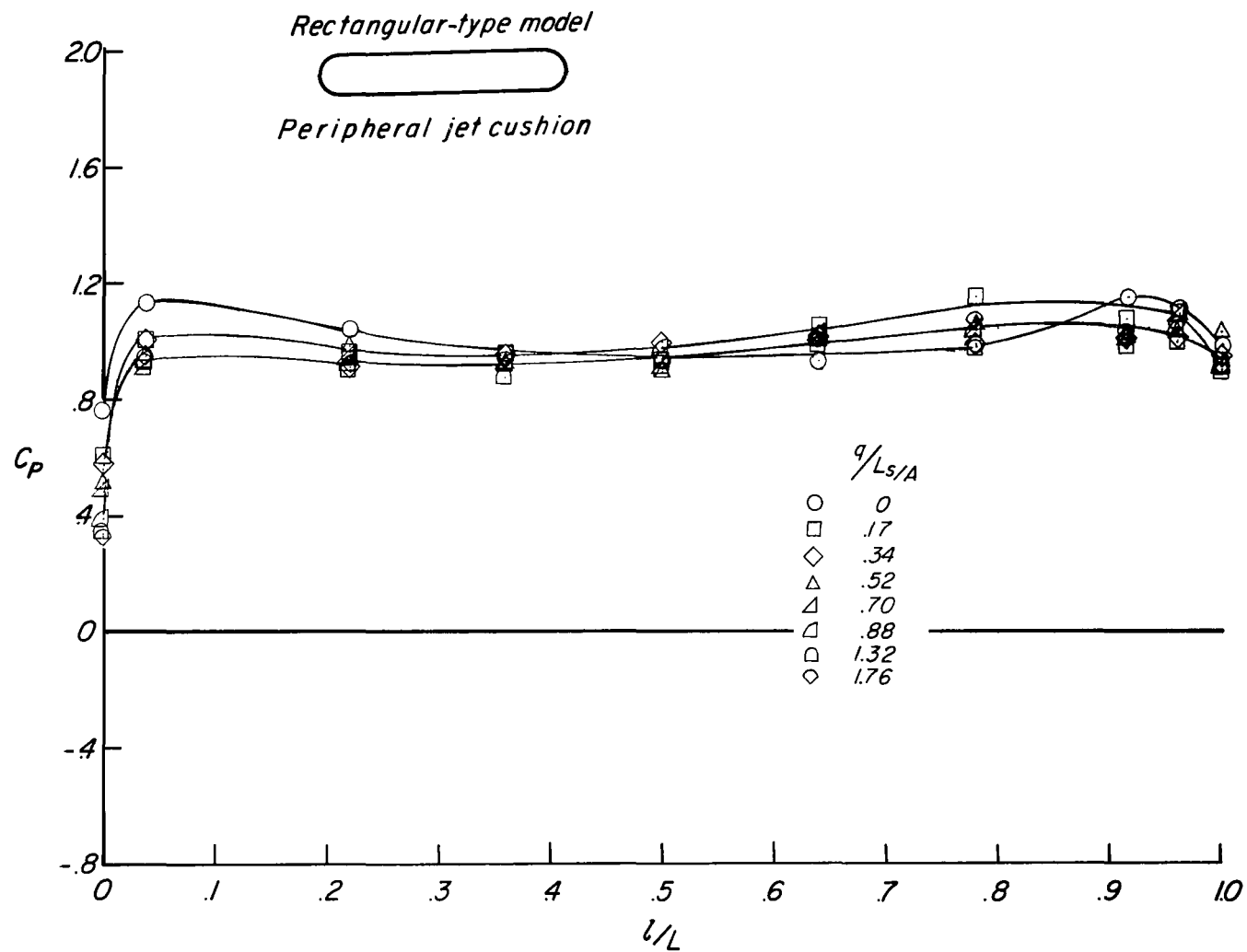
(c) Pressure coefficient along center line of air cushion at  $q/L_s/A \approx 1.00$ .

Figure 28.- Continued.



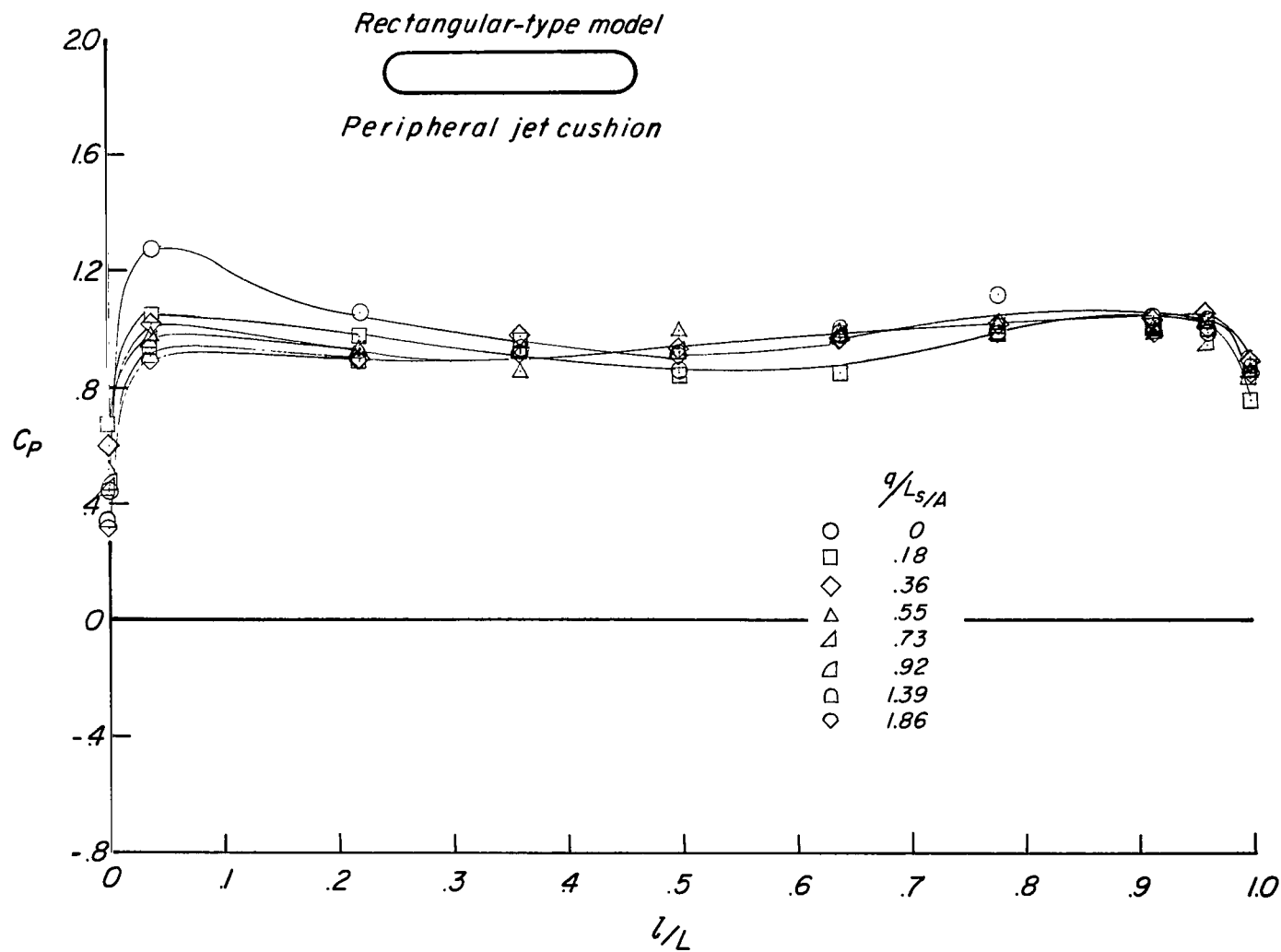
(d) Pressure coefficient along center line of air cushion at  $q/L_s/A \approx 2.00$ .

Figure 28.- Continued.



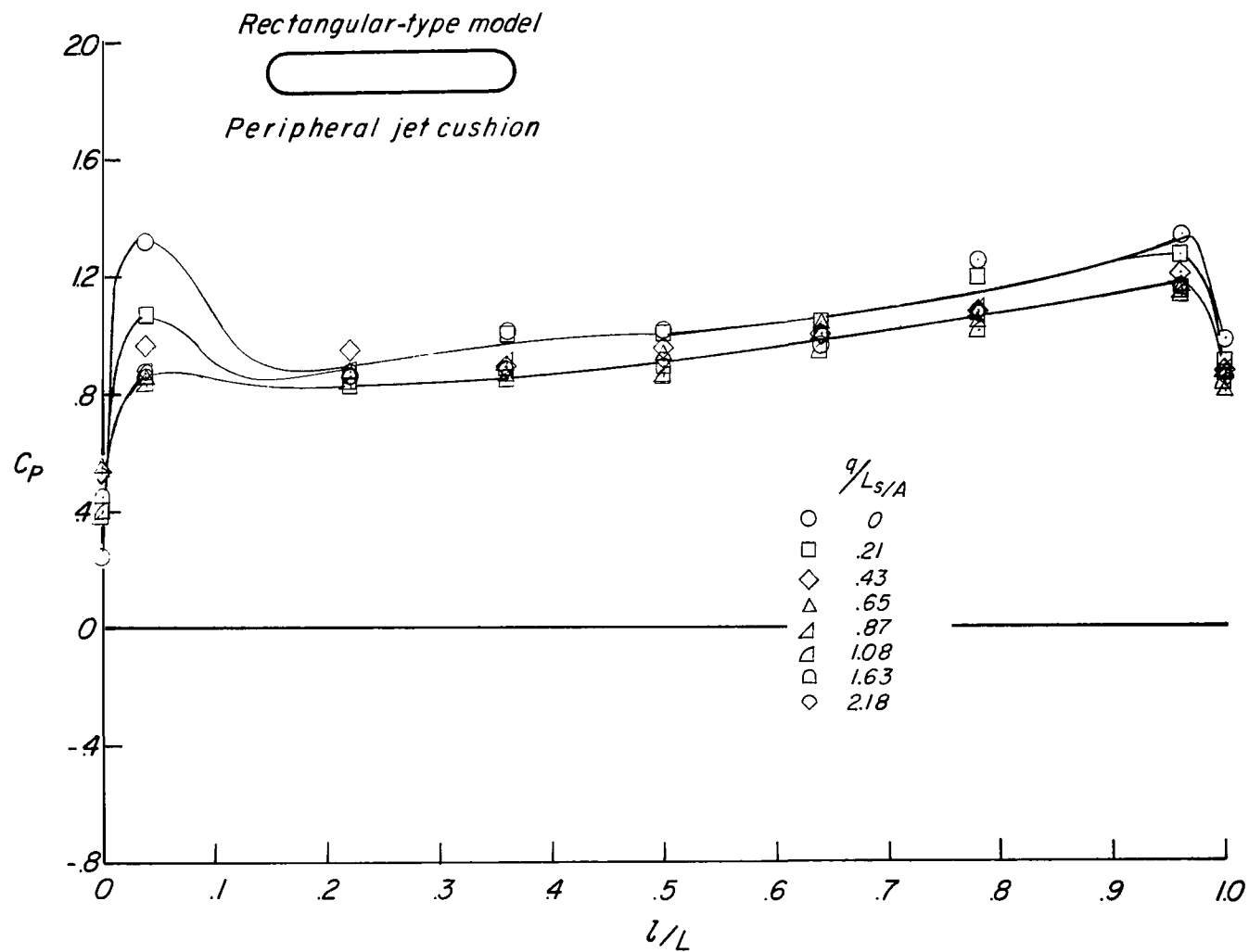
(e) Pressure coefficient along center line of air cushion.  $L_s = 125.4$  N;  $W = 0.079$  kg/sec;  $\beta = 10^\circ$ .

Figure 28.- Continued.



(f) Pressure coefficient along center line of air cushion.  $L_s = 119.2$  N;  $W = 0.077$  kg/sec;  $\beta = 20^\circ$ .

Figure 28.- Continued.



(g) Pressure coefficient along center line of air cushion.  $L_s = 101.0$  N;  $W = 0.083$  kg/sec;  $\beta = 30^\circ$ .

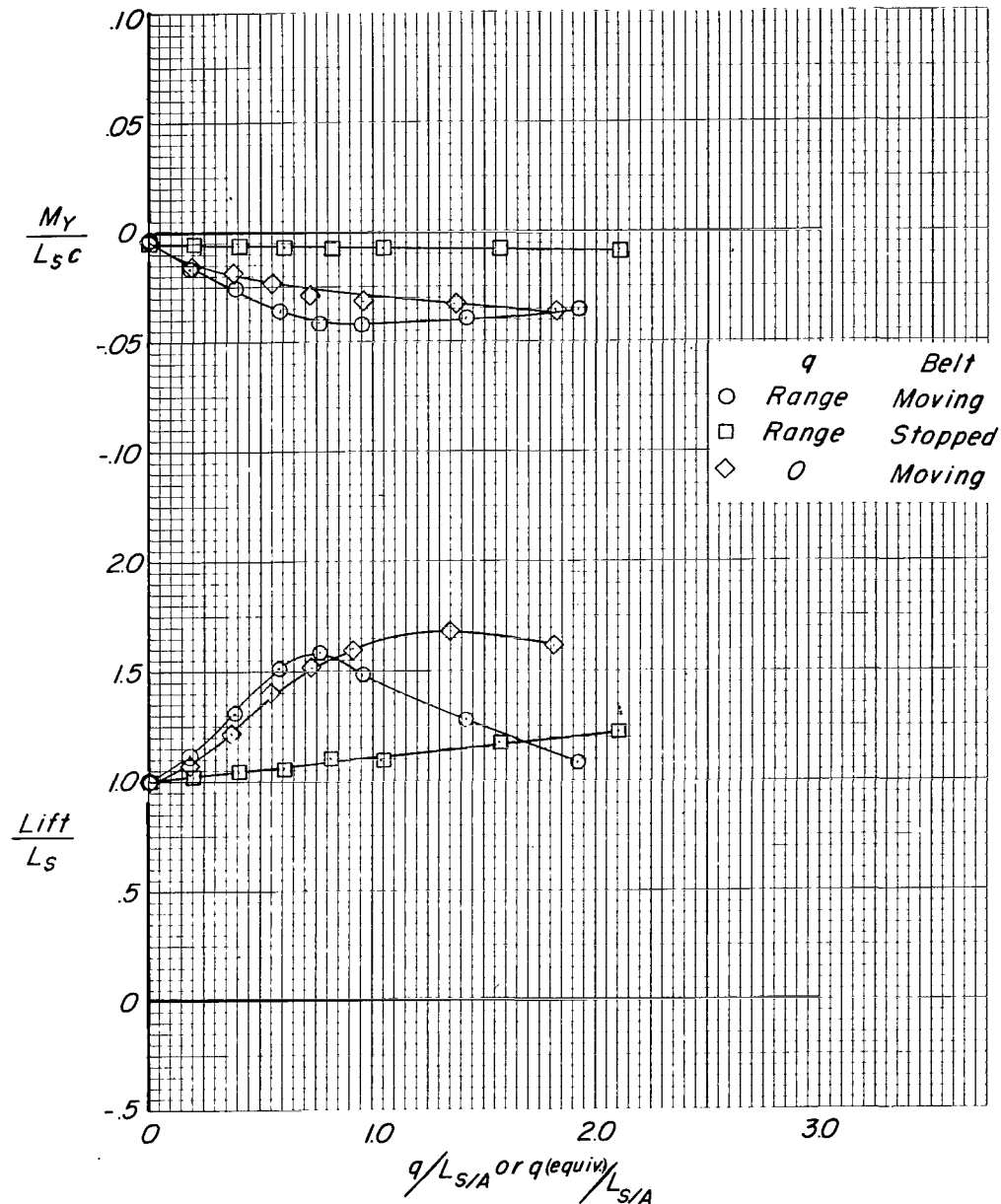
Figure 28.- Concluded.

Rectangular-type model



Peripheral jet cushion

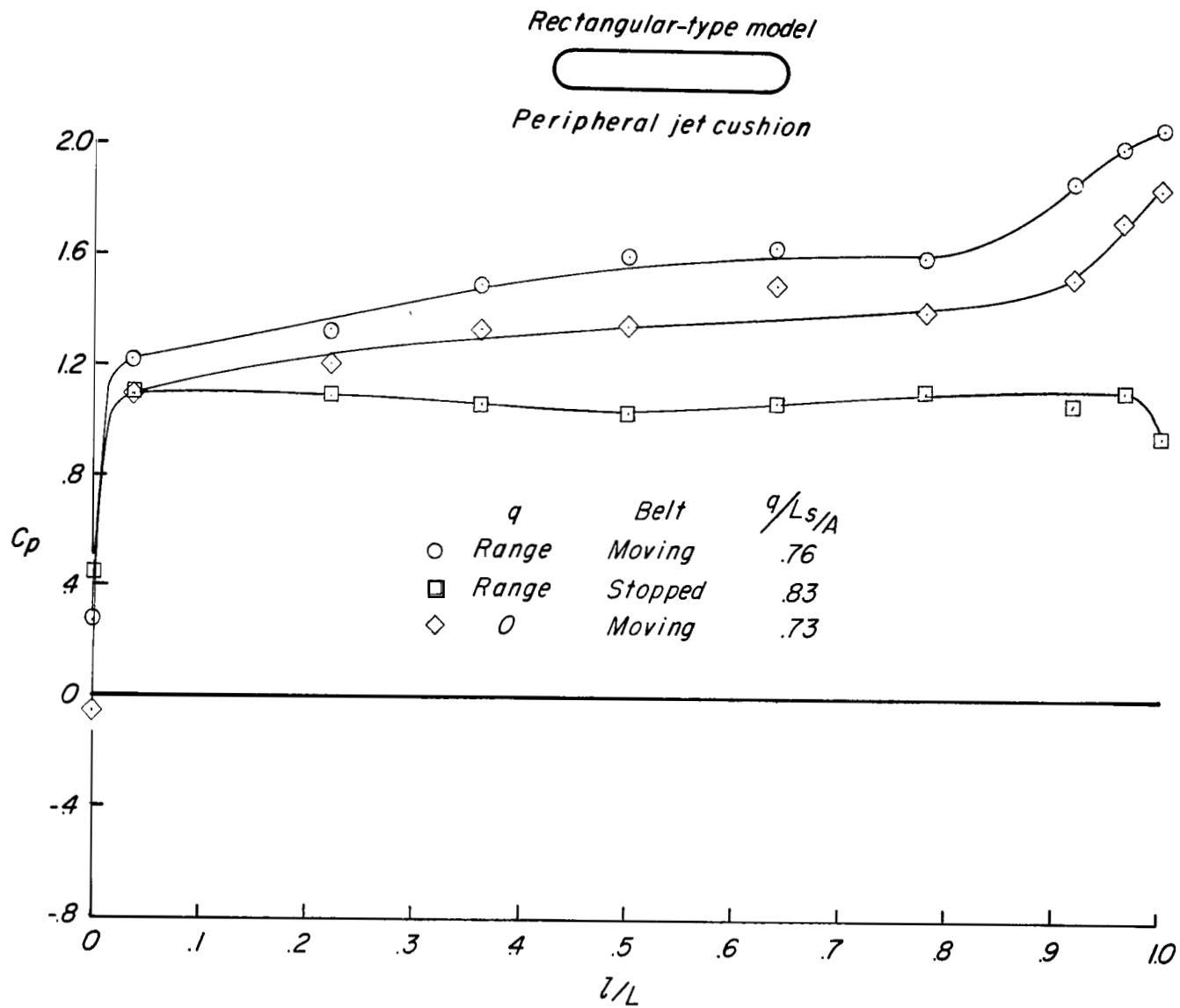
Air-cushion pad (corrected)



(a) Lift and pitching moment as a function of pressure ratio.

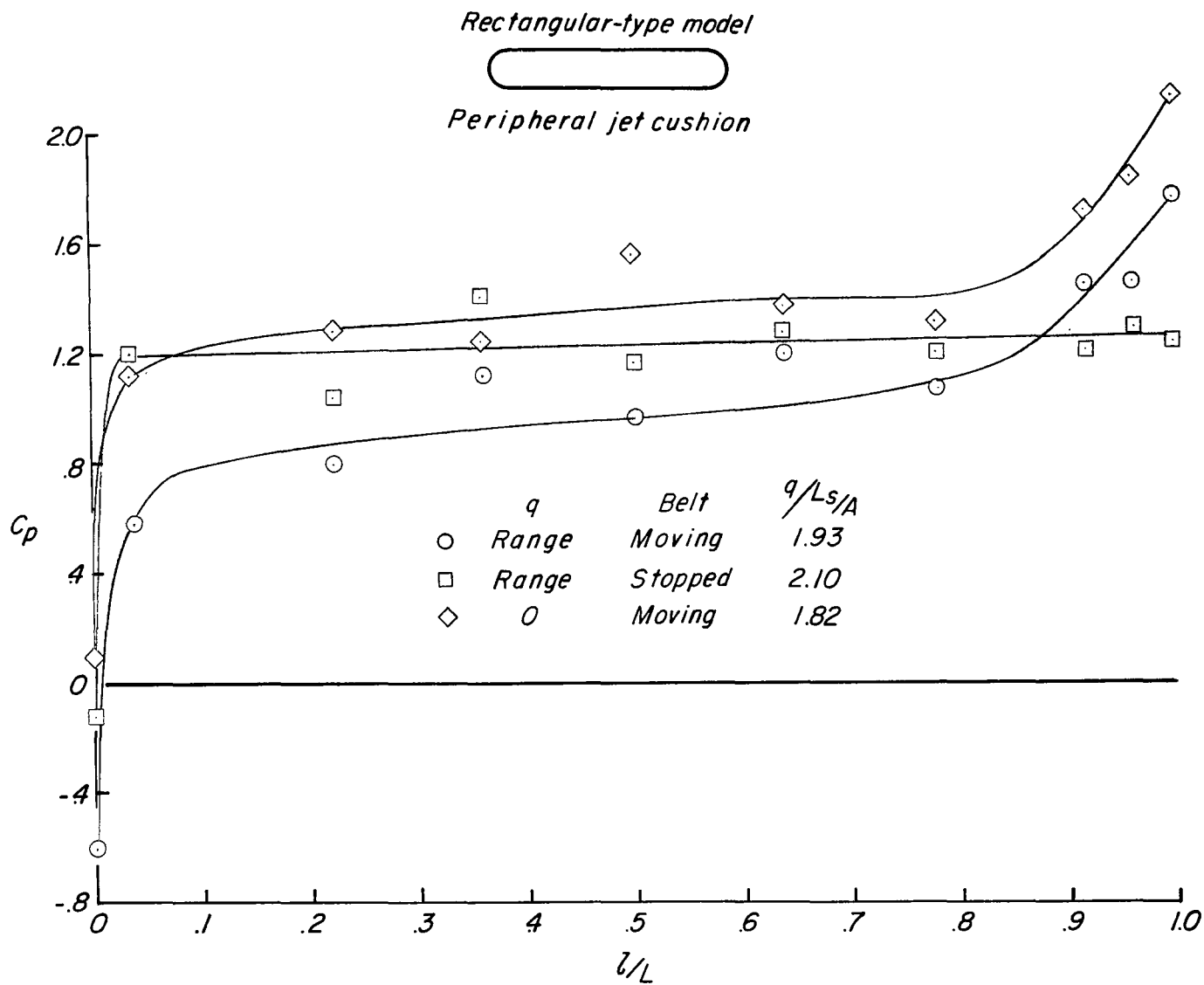
Figure 29.- Effect of moving ground belt on aerodynamic characteristics of rectangular-type model (peripheral jet).  $h/d_e = 0.0033$ ;  $\beta = 0^\circ$ .





(b) Pressure coefficient along center line of air cushion at  $q/Ls/A \approx 0.77$ .

Figure 29.- Continued.

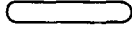


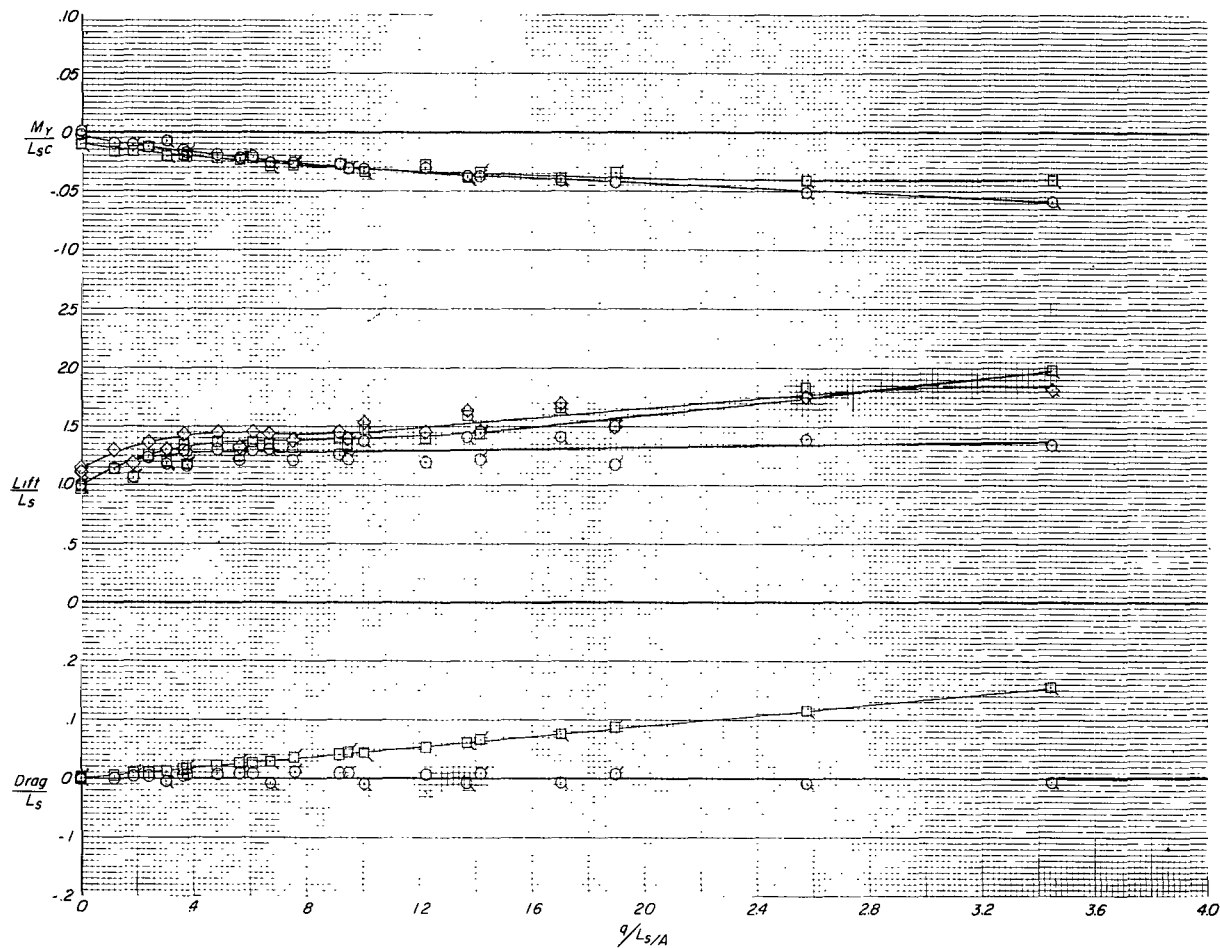
(c) Pressure coefficient along center line of air cushion at  $q/Ls/A \approx 1.95$ .

Figure 29.- Concluded.

$L_s, N$	$W, kg/sec$
180.6	.227
116.5	.176
64.1	.125

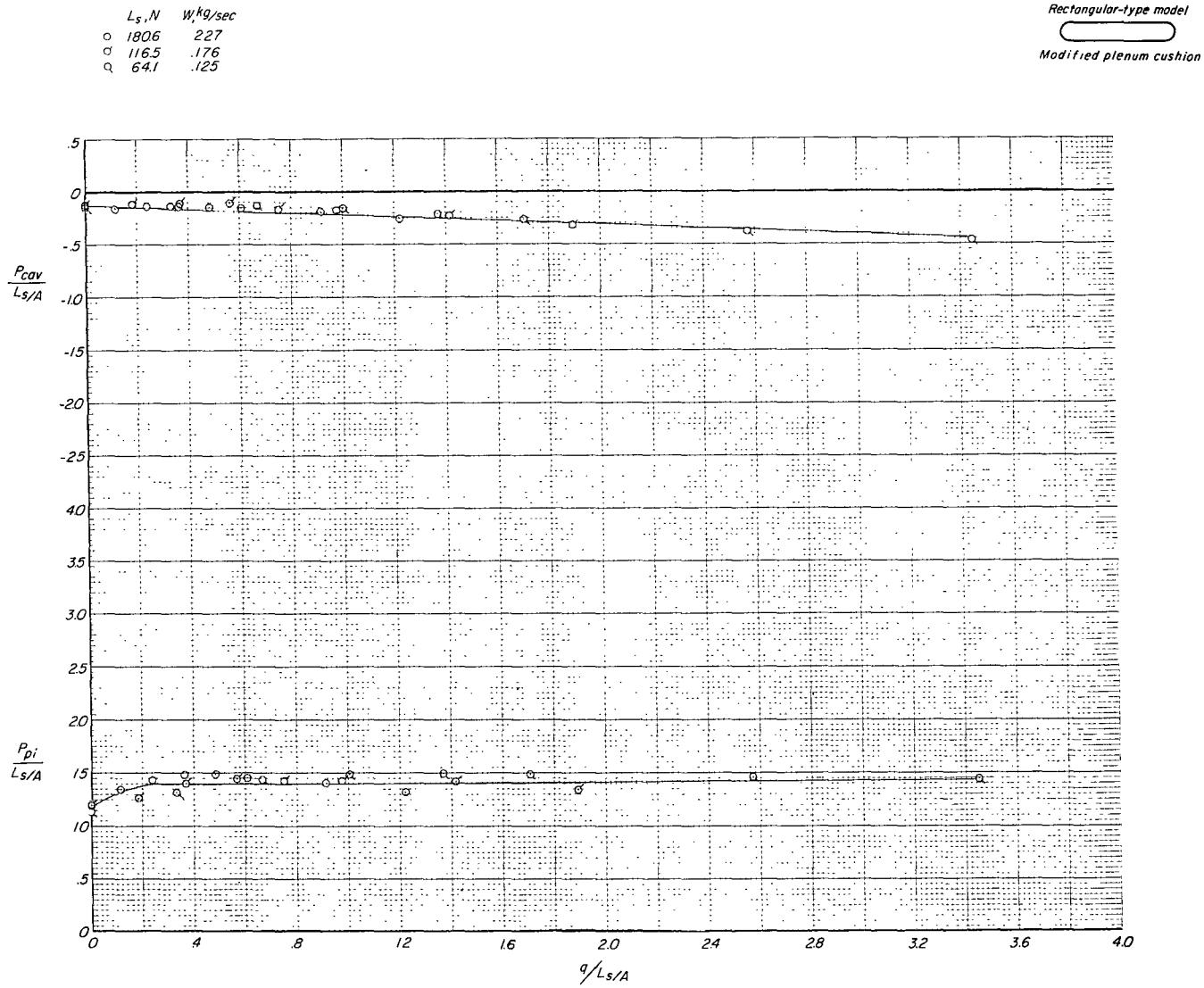
$\circ$	Pad (corrected)
$\square$	Total vehicle (pad + body)
$\diamond$	Pad (measured)

Rectangular-type model  
  
 Modified plenum cushion



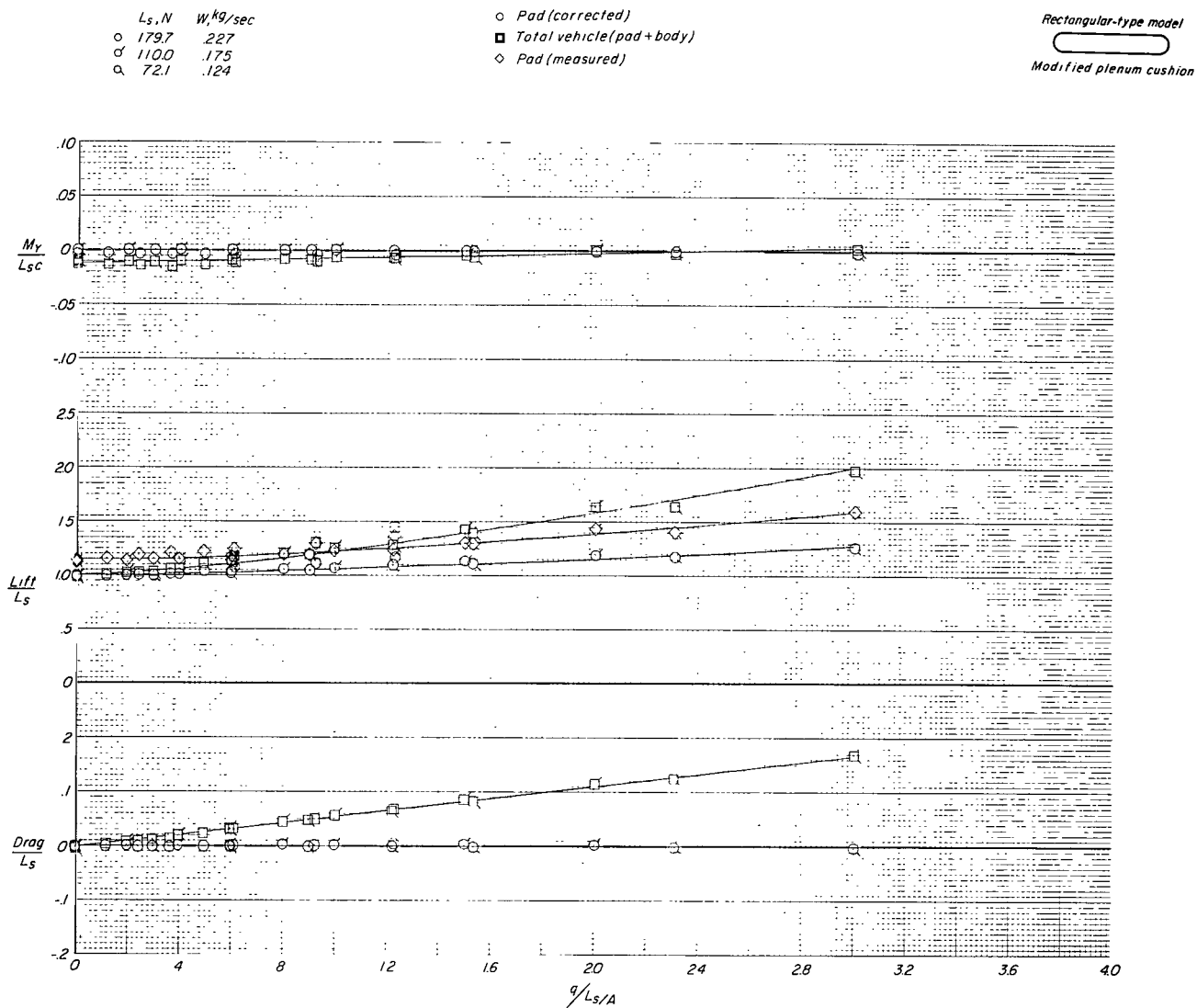
(a) Lift, drag, and pitching moment.

Figure 30.- Effect of forward speed on aerodynamic characteristics of rectangular-type model (modified plenum). Belt moving;  $h/d_e = 0.0033$ .



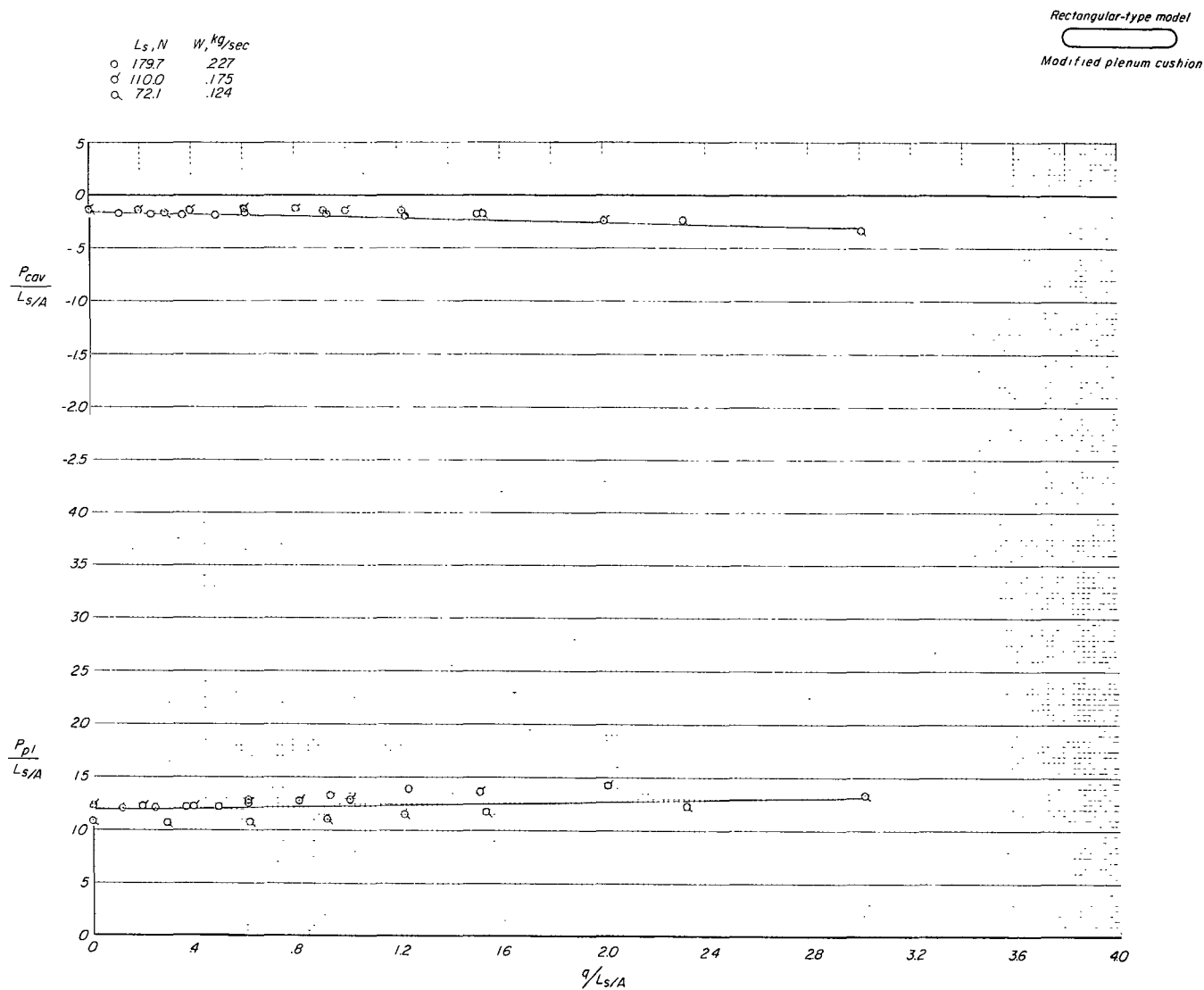
(b) Cavity pressure and plenum pressure.

Figure 30.- Concluded.



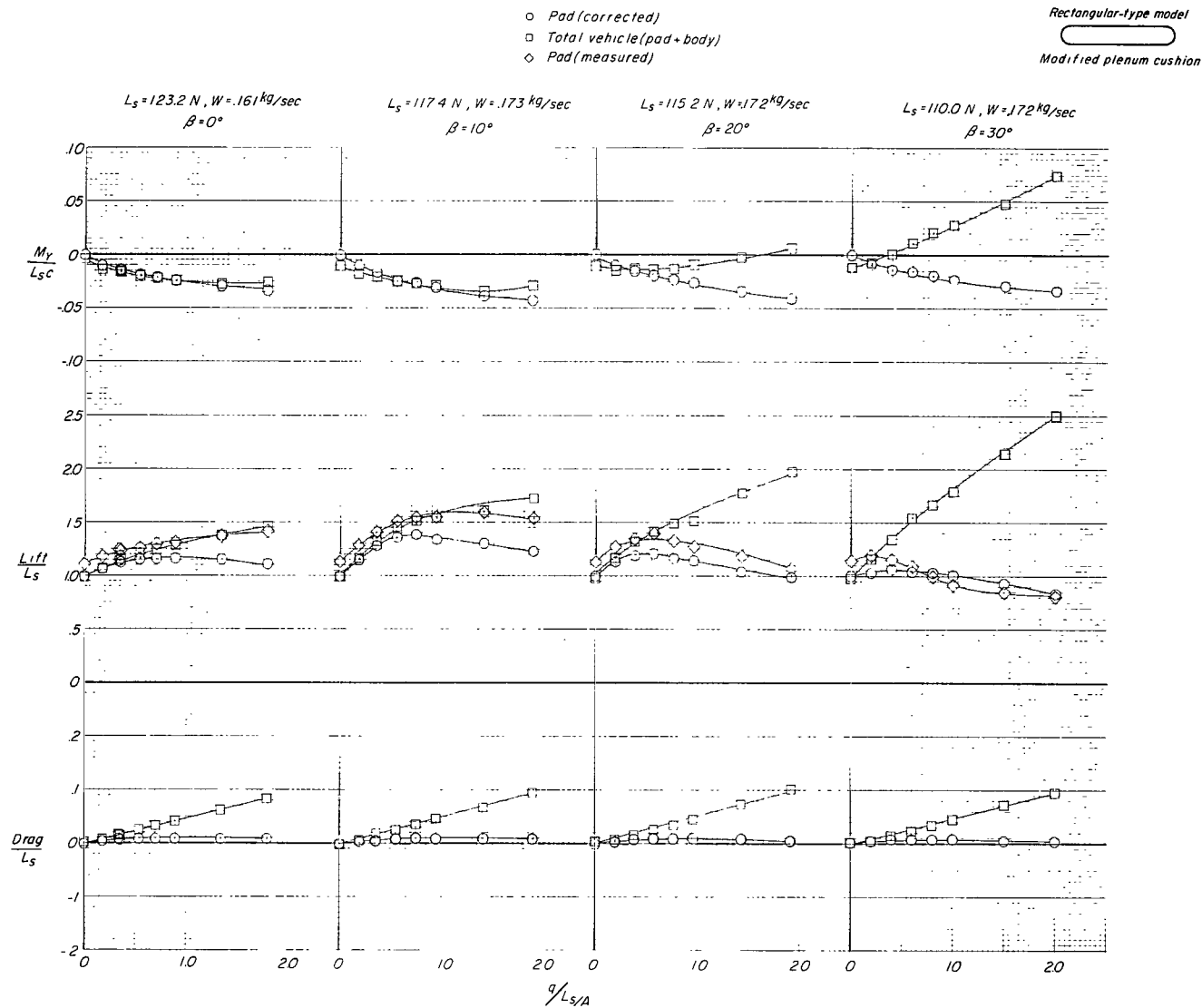
(a) Lift, drag, and pitching moment.

Figure 31.- Effect of forward speed on aerodynamic characteristics of rectangular-type model (modified plenum). Belt stopped;  $h/d_e = 0.0033$ .



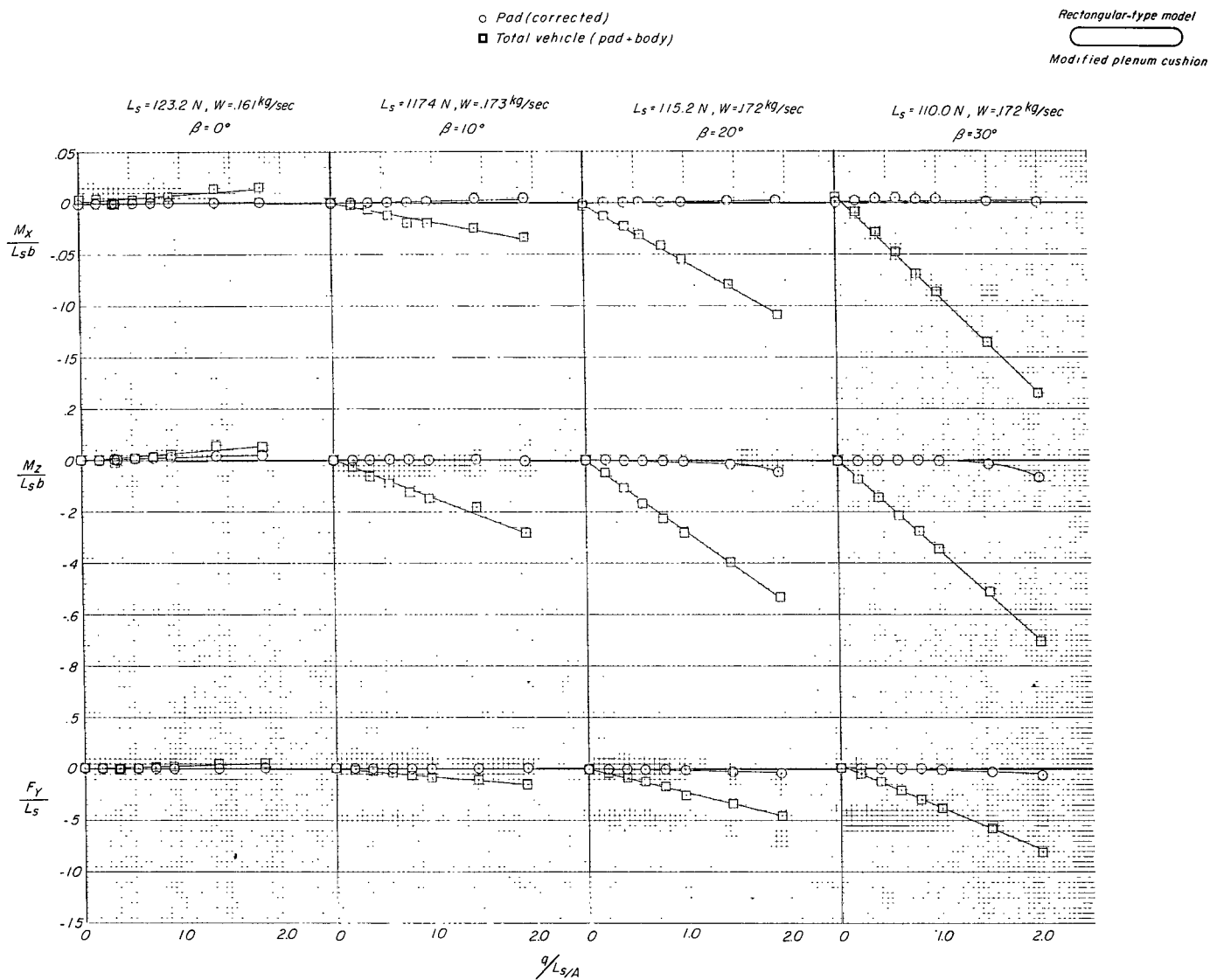
(b) Cavity pressure and plenum pressure.

Figure 31.- Concluded.



(a) Lift, drag, and pitching moment.

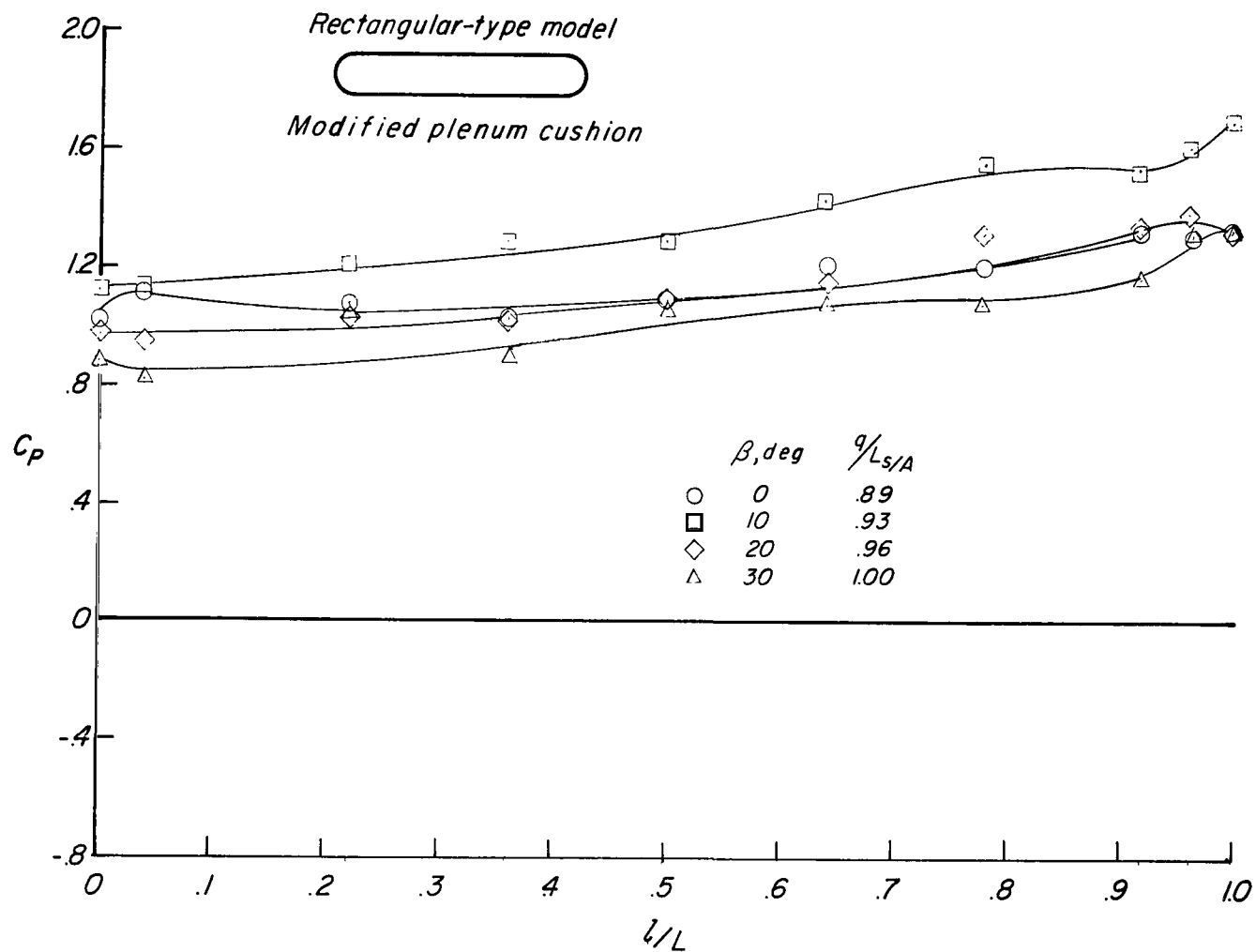
Figure 32.- Effect of sideslip on aerodynamic characteristics of rectangular-type model (modified plenum). Belt moving;  $h/d_e = 0.0033$ .



(b) Roll, yaw, and side force.

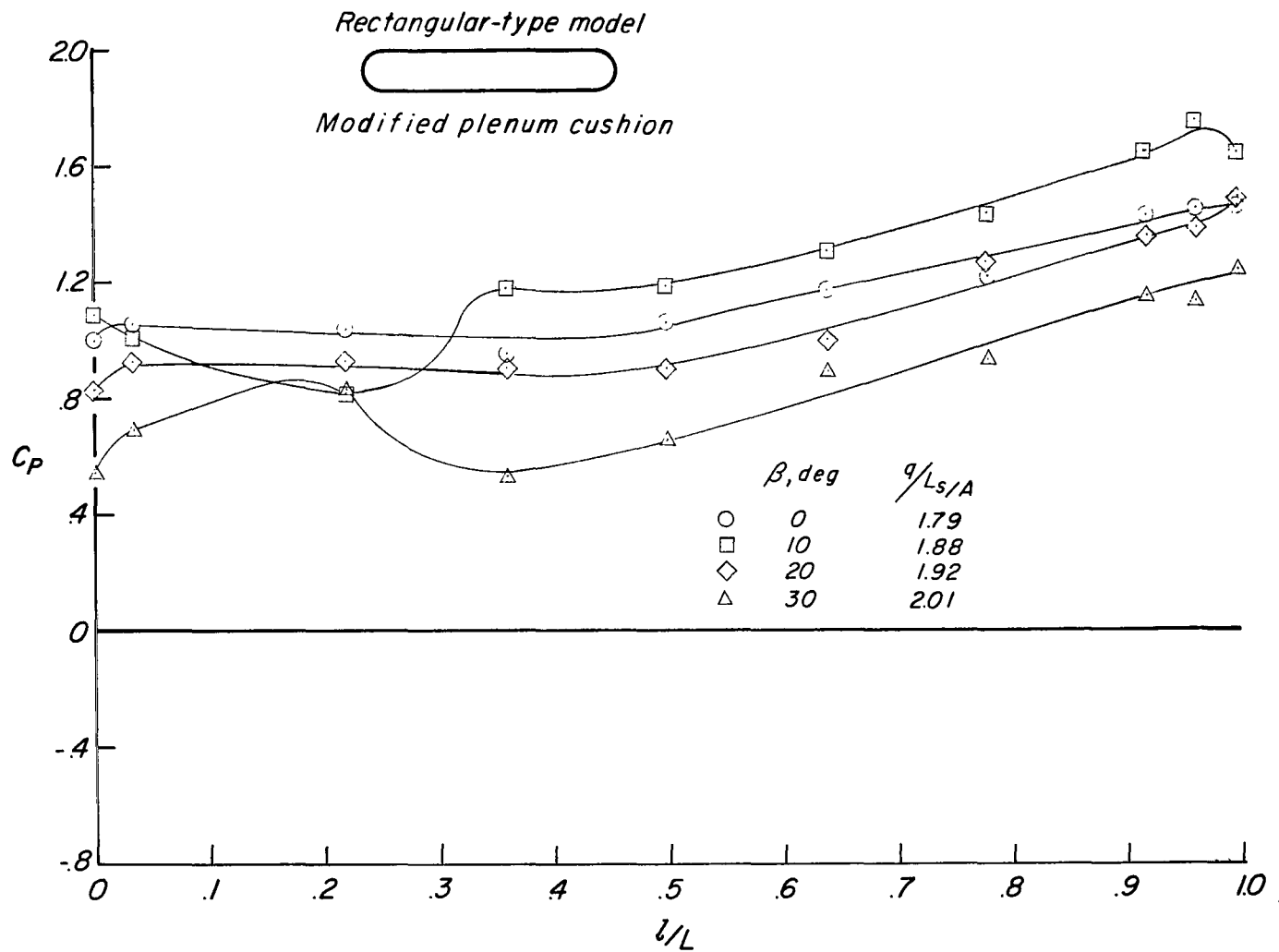
Figure 32.- Continued.





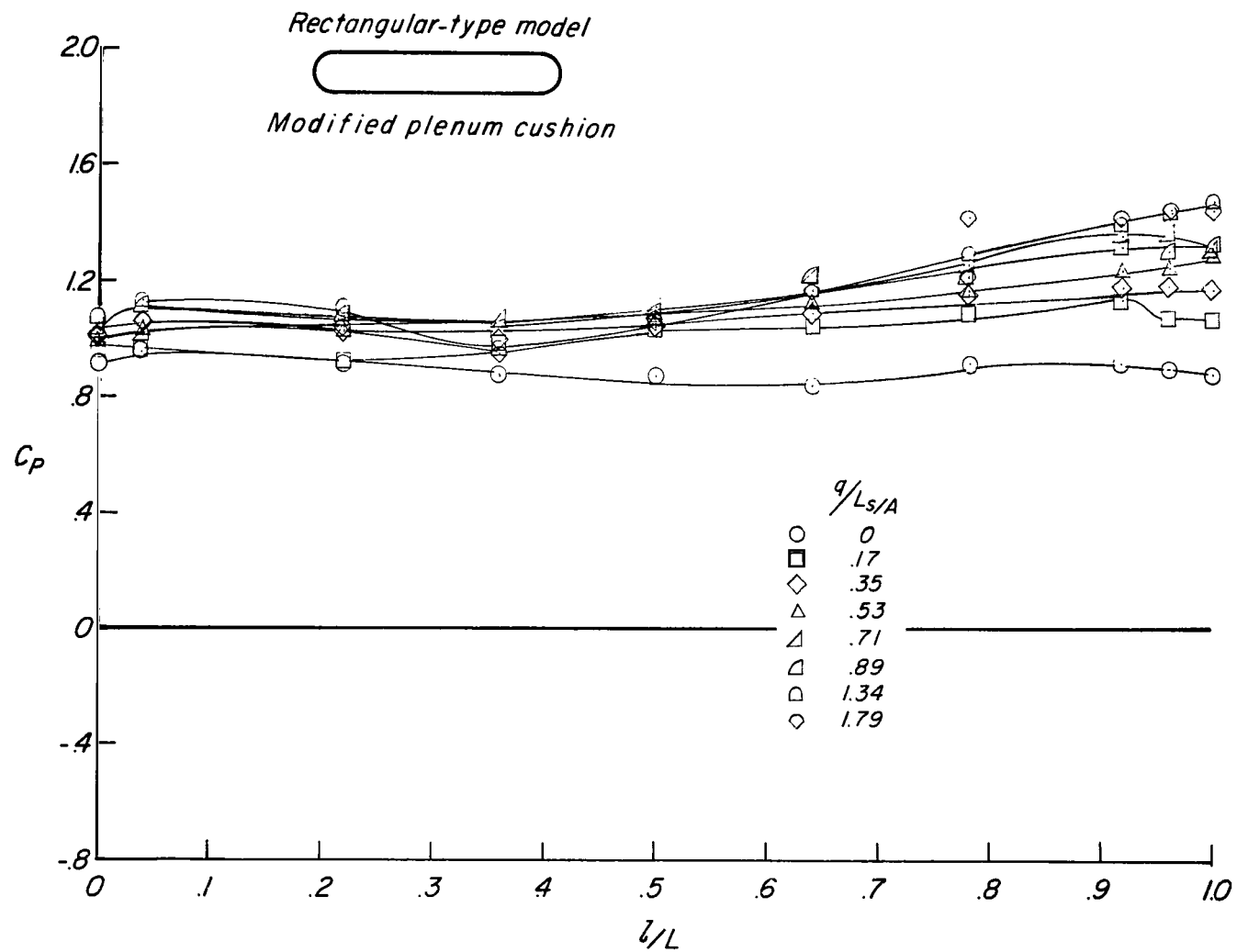
(c) Pressure coefficient along center line of air cushion at  $q/L_s/A \approx 1.00$ .

Figure 32.- Continued.



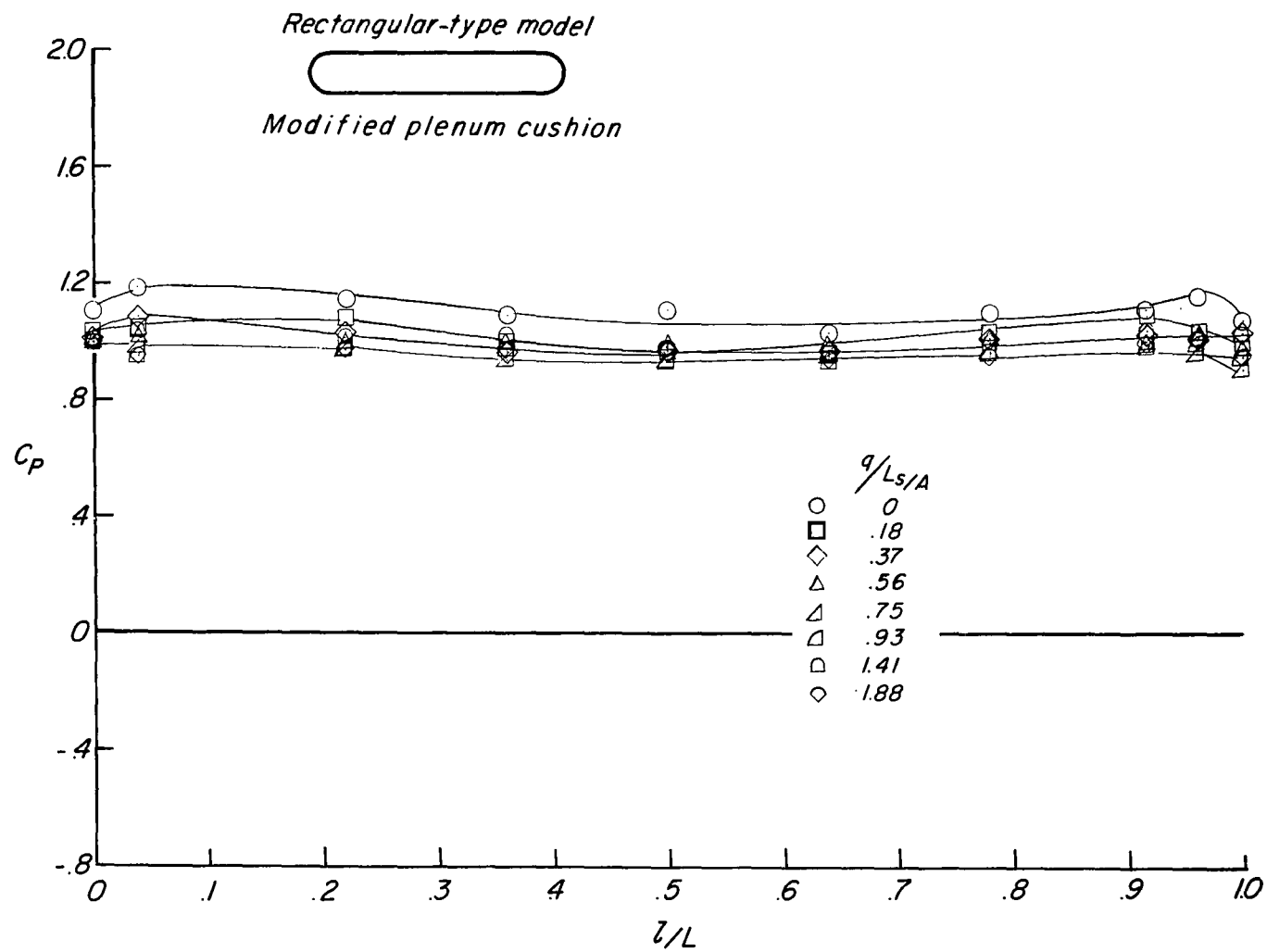
(d) Pressure coefficient along center line of air cushion at  $q/L_s/A \approx 2.00$ .

Figure 32.- Continued.



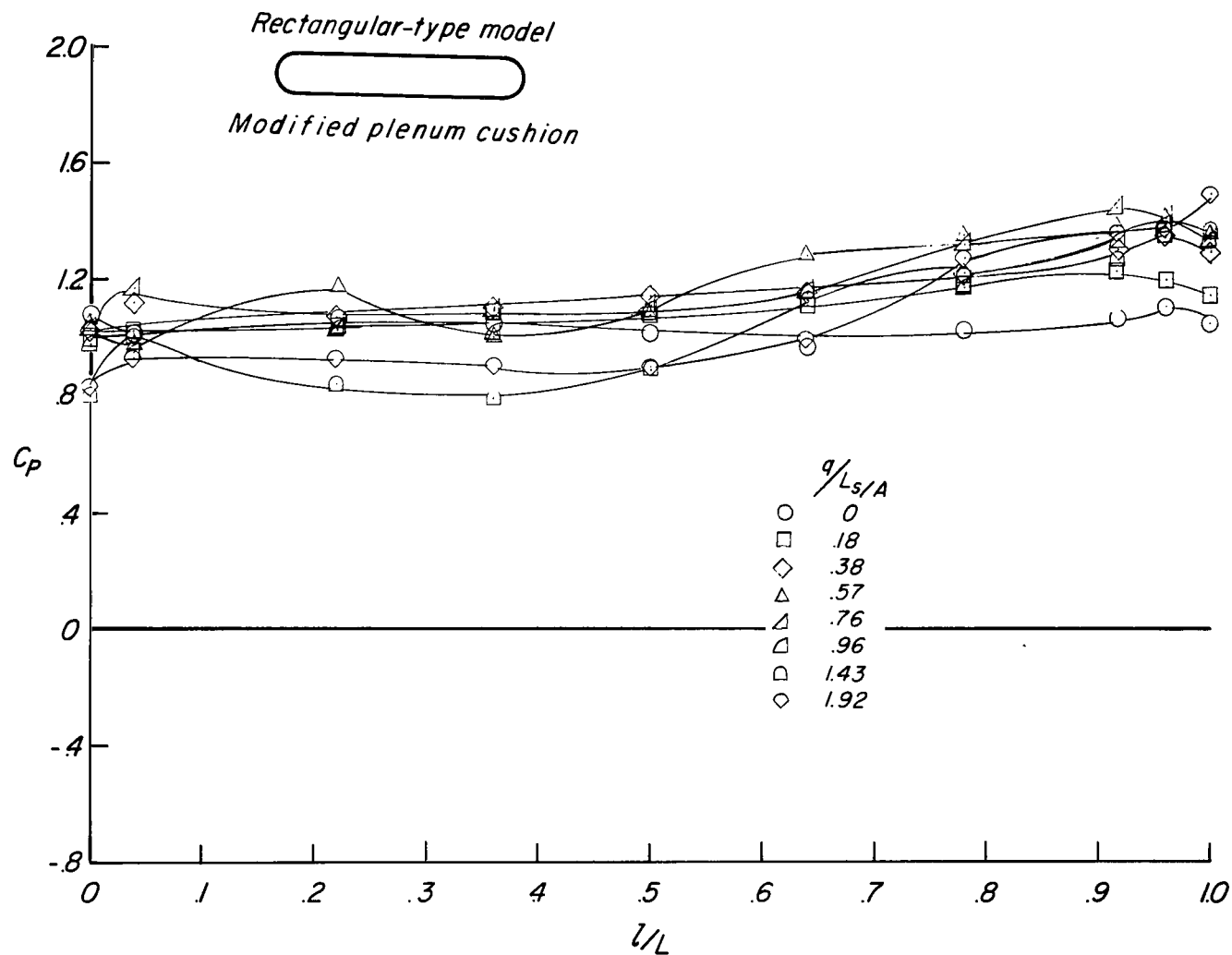
(e) Pressure coefficient along center line of air cushion.  $L_s = 123.2$  N;  $W = 0.161$  kg/sec;  $\beta = 0^\circ$ .

Figure 32.- Continued.



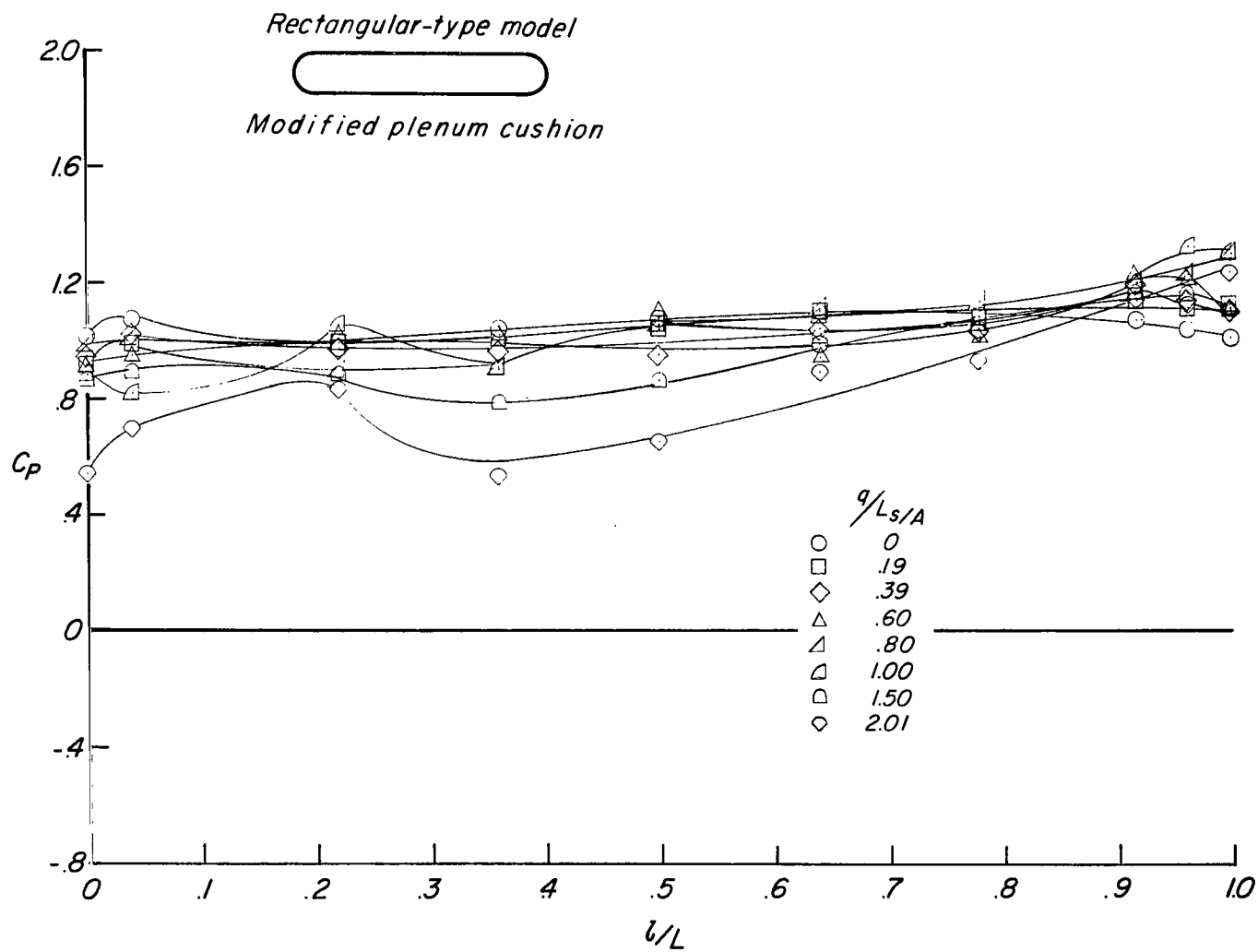
(f) Pressure coefficient along center line of air cushion.  $L_s = 117.4$  N;  $W = 0.173$  kg/sec;  $\beta = 10^\circ$ .

Figure 32.- Continued.



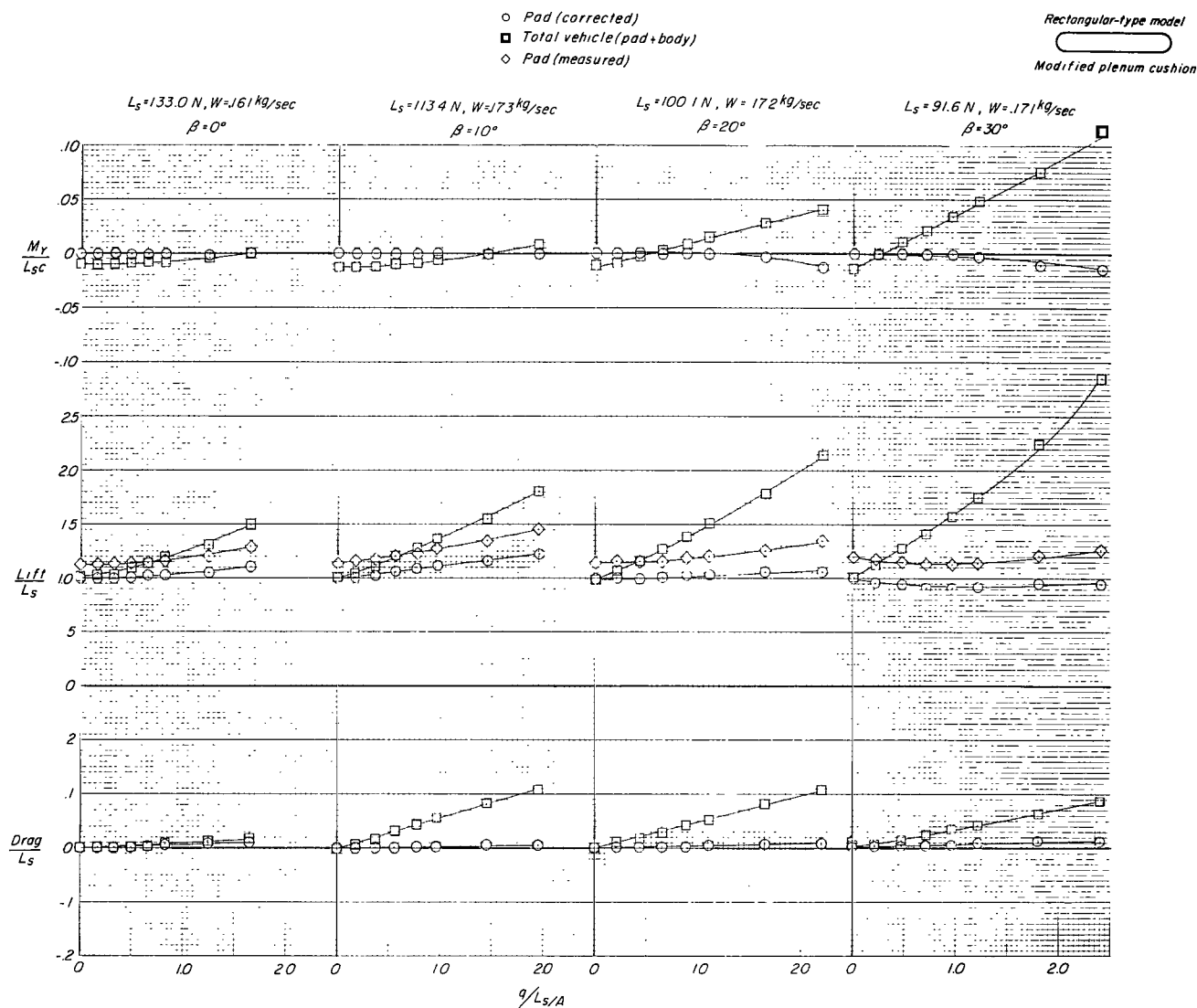
(g) Pressure coefficient along center line of air cushion.  $L_s = 115.2$  N;  $W = 0.172$  kg/sec;  $\beta = 20^\circ$ .

Figure 32.- Continued.



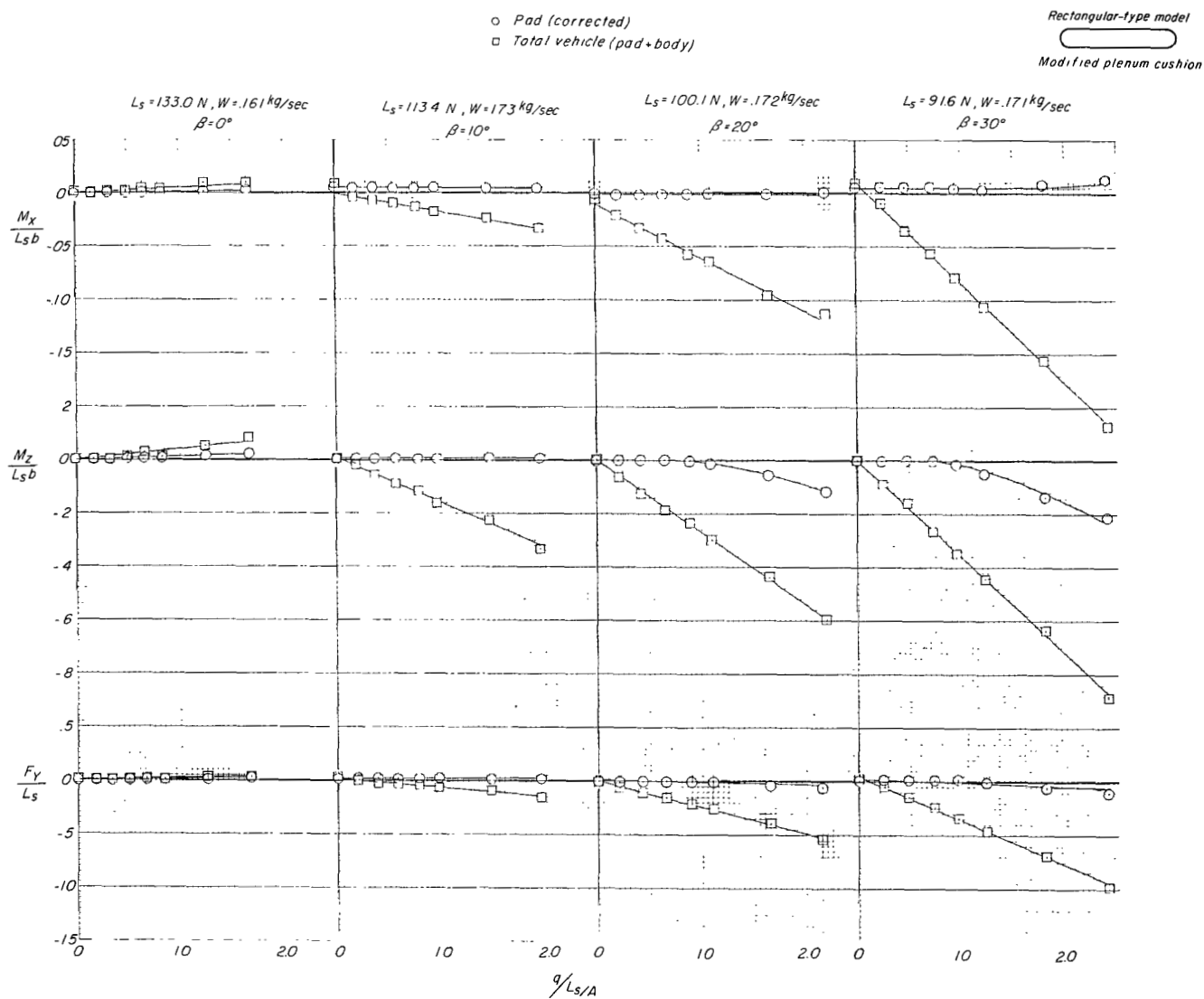
(h) Pressure coefficient along center line of air cushion.  $L_s = 110.0$  N;  $W = 0.172$  kg/sec;  $\beta = 30^\circ$ .

Figure 32.- Concluded.



(a) Lift, drag, and pitching moment.

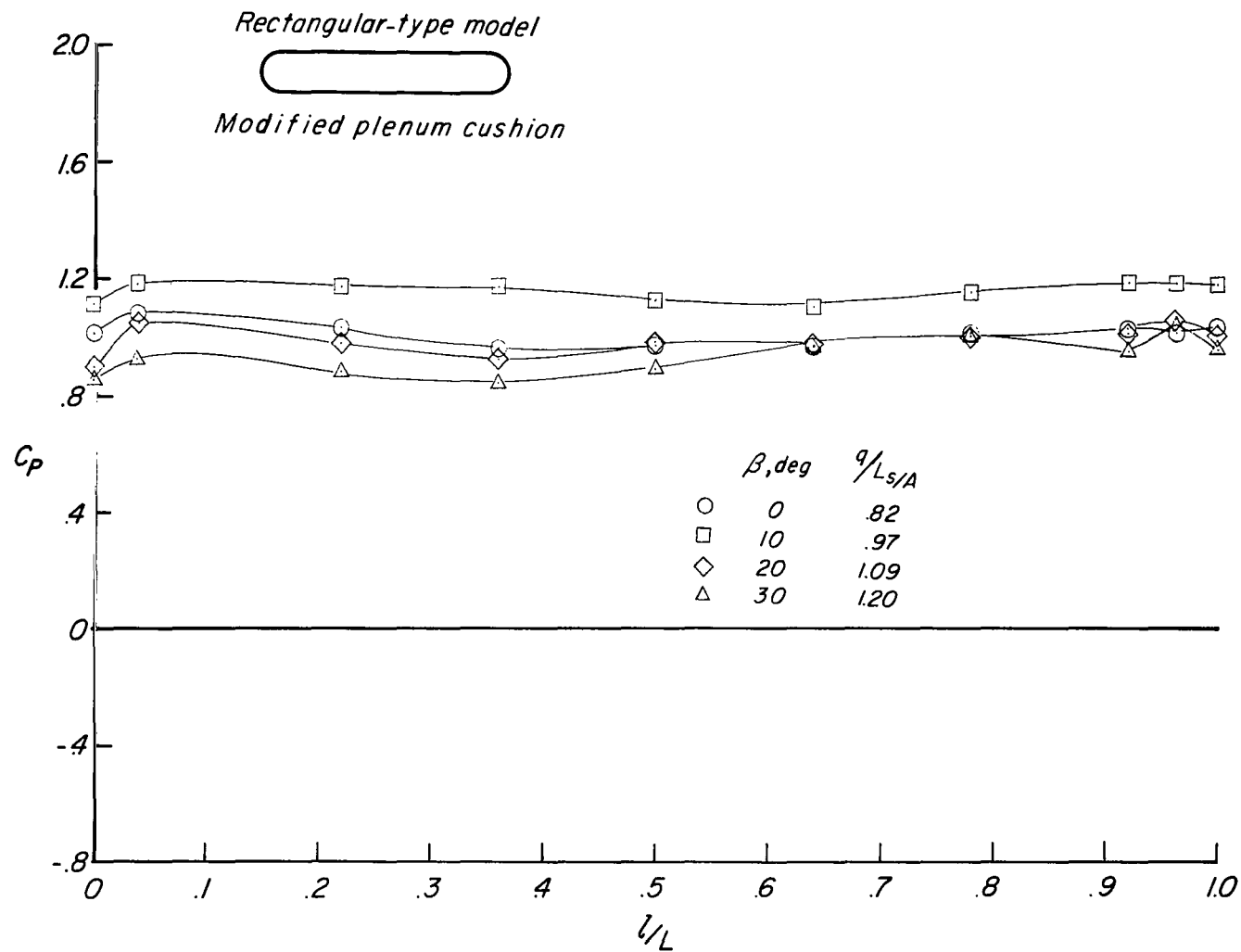
Figure 33.- Effect of sideslip on aerodynamic characteristics of rectangular-type model (modified plenum). Belt stopped;  $h/a_e = 0.0033$ .



(b) Roll, yaw, and side force.

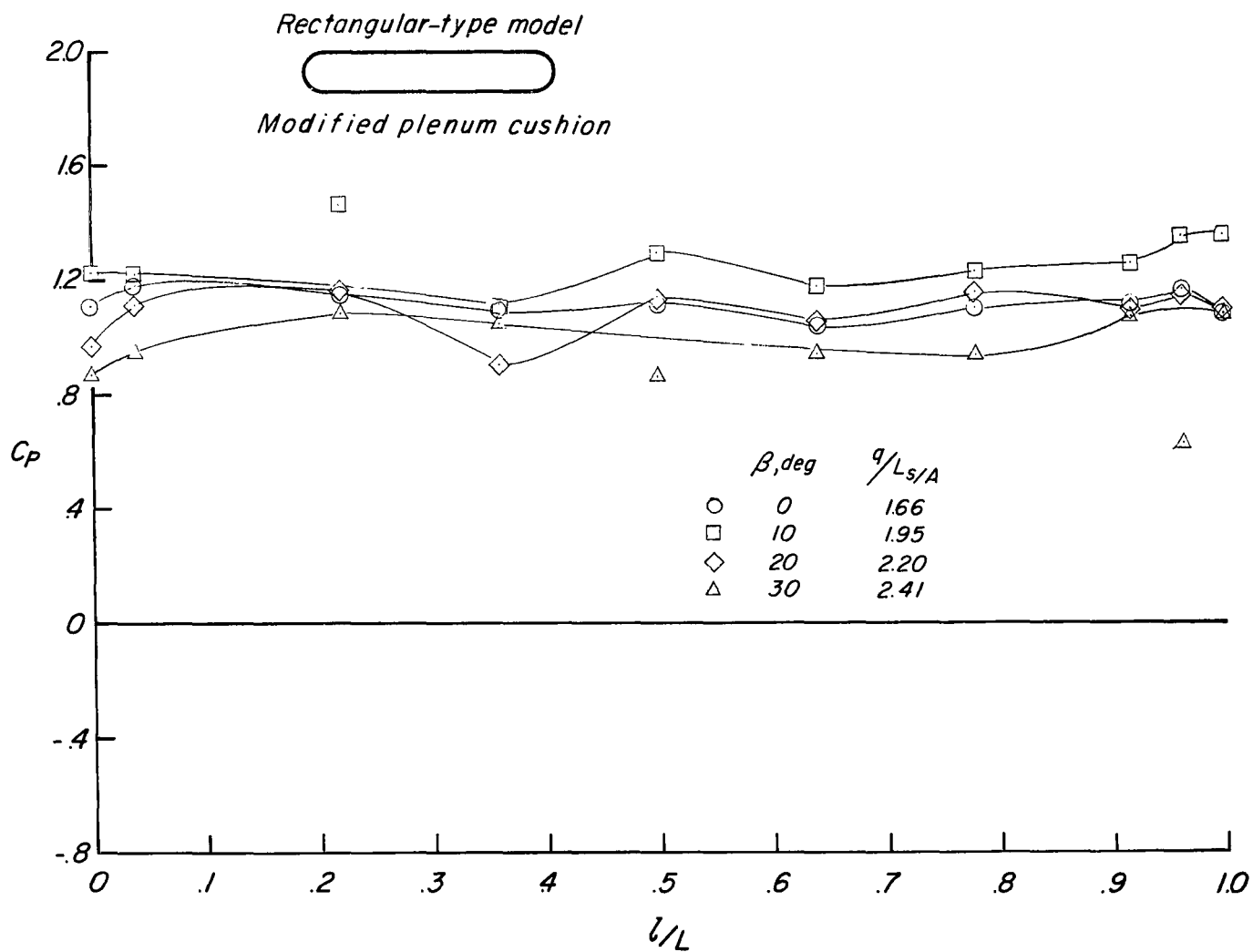
Figure 33.- Continued.





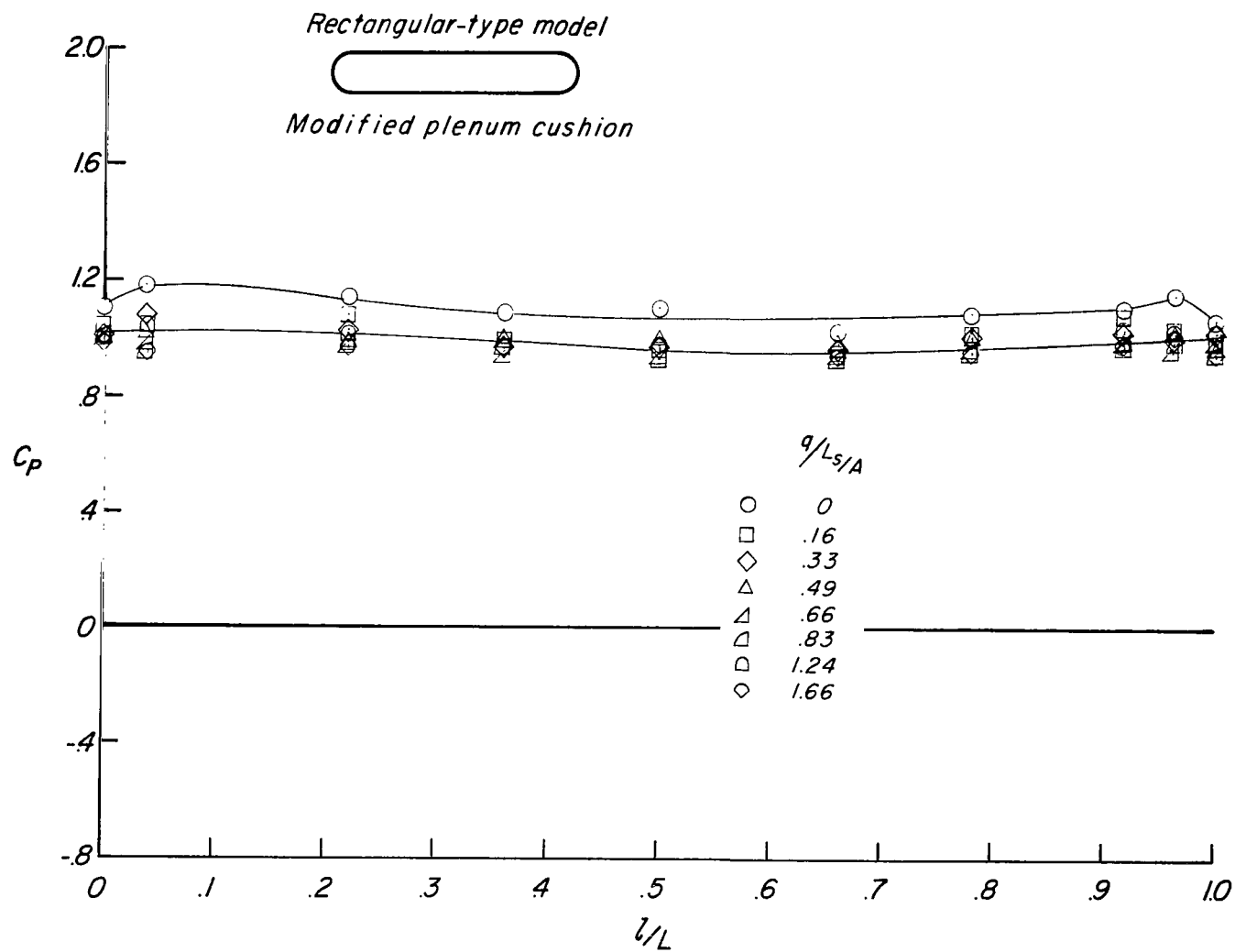
(c) Pressure coefficient along center line of air cushion at  $q/L_s/A \approx 1.00$ .

Figure 33.- Continued.



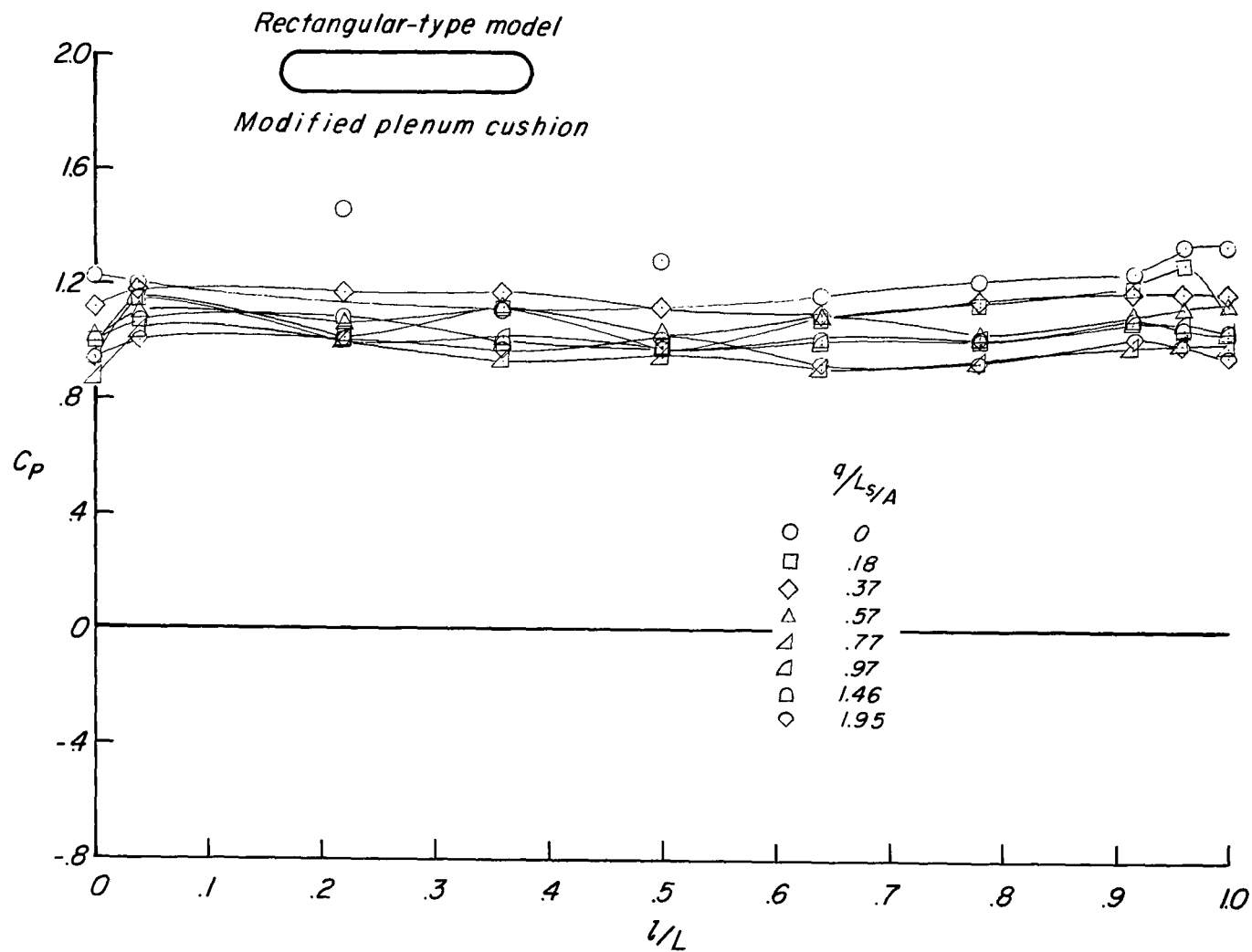
(d) Pressure coefficient along center line of air cushion at  $q/L_s/A \approx 2.00$ .

Figure 33.- Continued.



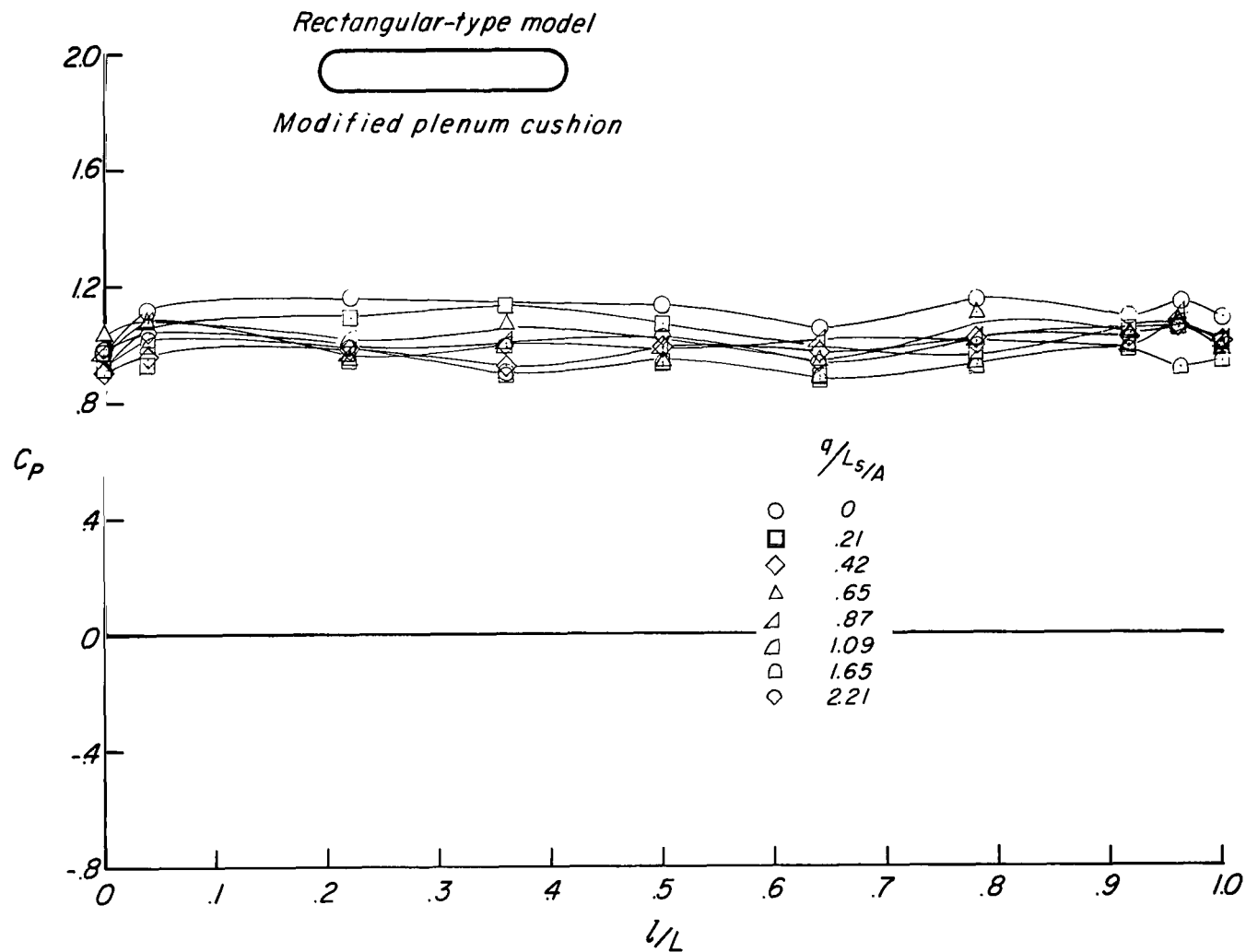
(e) Pressure coefficient along center line of air cushion.  $L_s = 133.0$  N;  $W = 0.161$  kg/sec;  $\beta = 0^\circ$ .

Figure 33.- Continued.



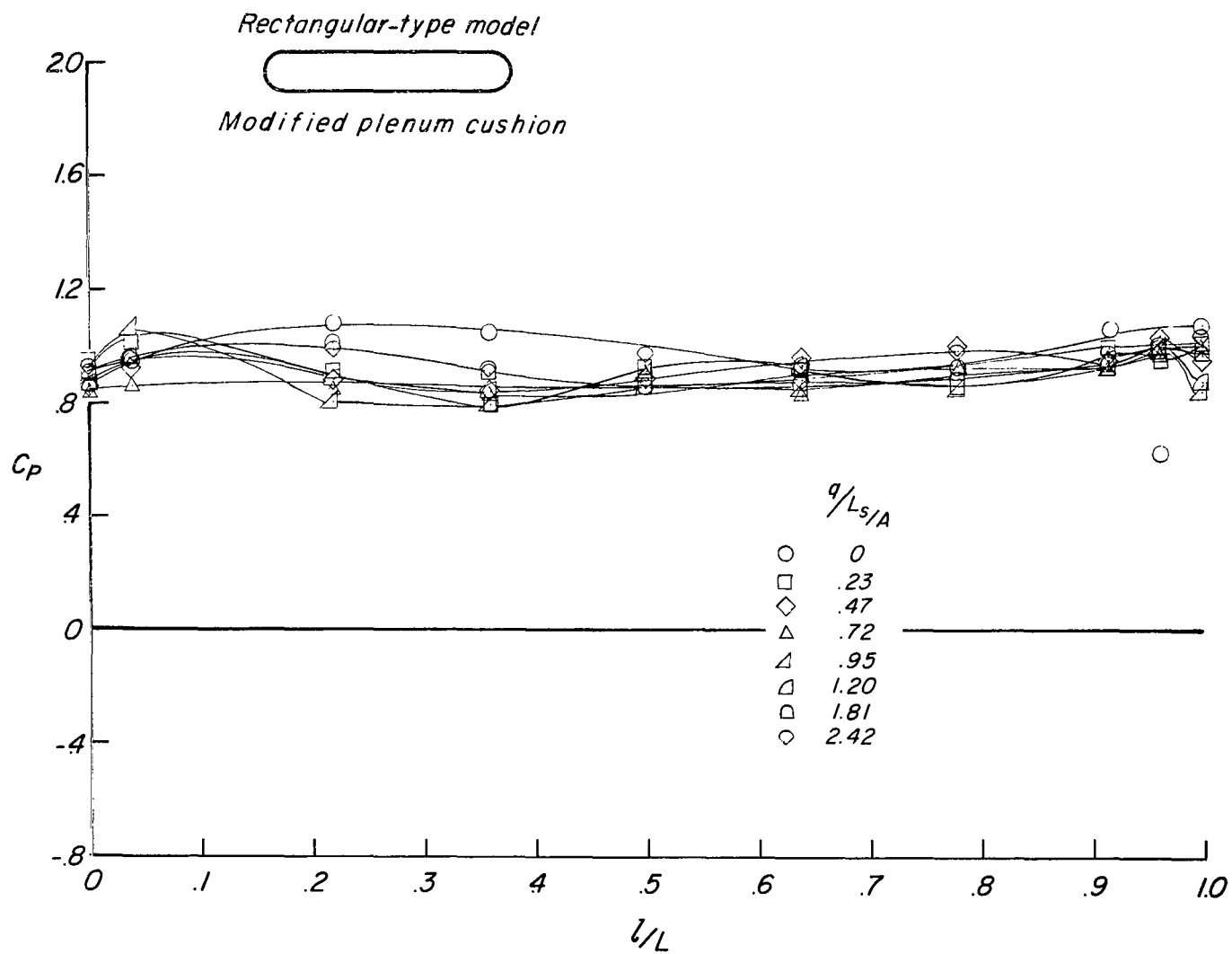
(f) Pressure coefficient along center line of air cushion.  $L_s = 113.4$  N;  $W = 0.173$  kg/sec;  $\beta = 10^\circ$ .

Figure 33.- Continued.



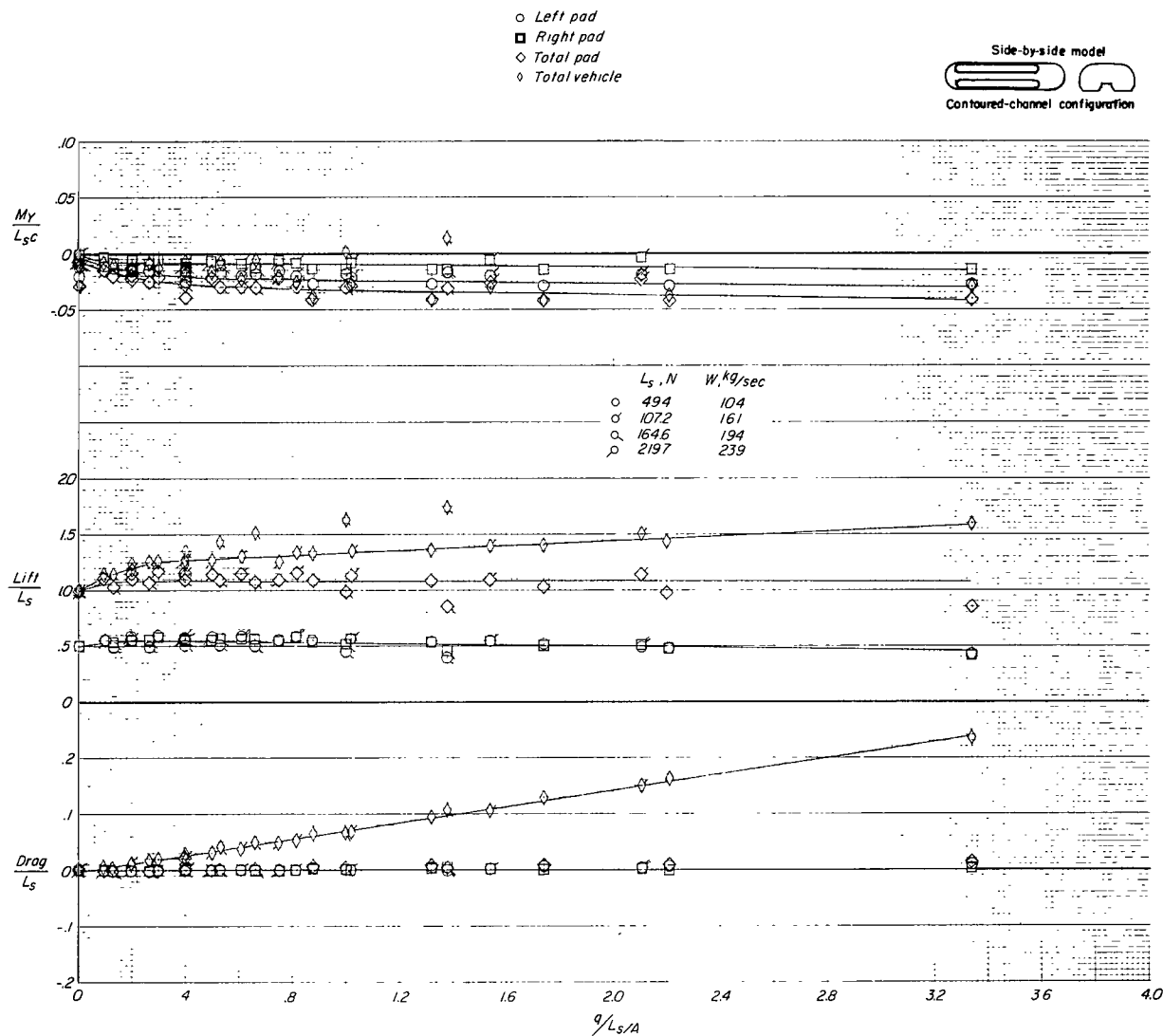
(g) Pressure coefficient along center line of air cushion.  $L_s = 100.1$  N;  $W = 0.172$  kg/sec;  $\beta = 20^\circ$ .

Figure 33.- Continued.



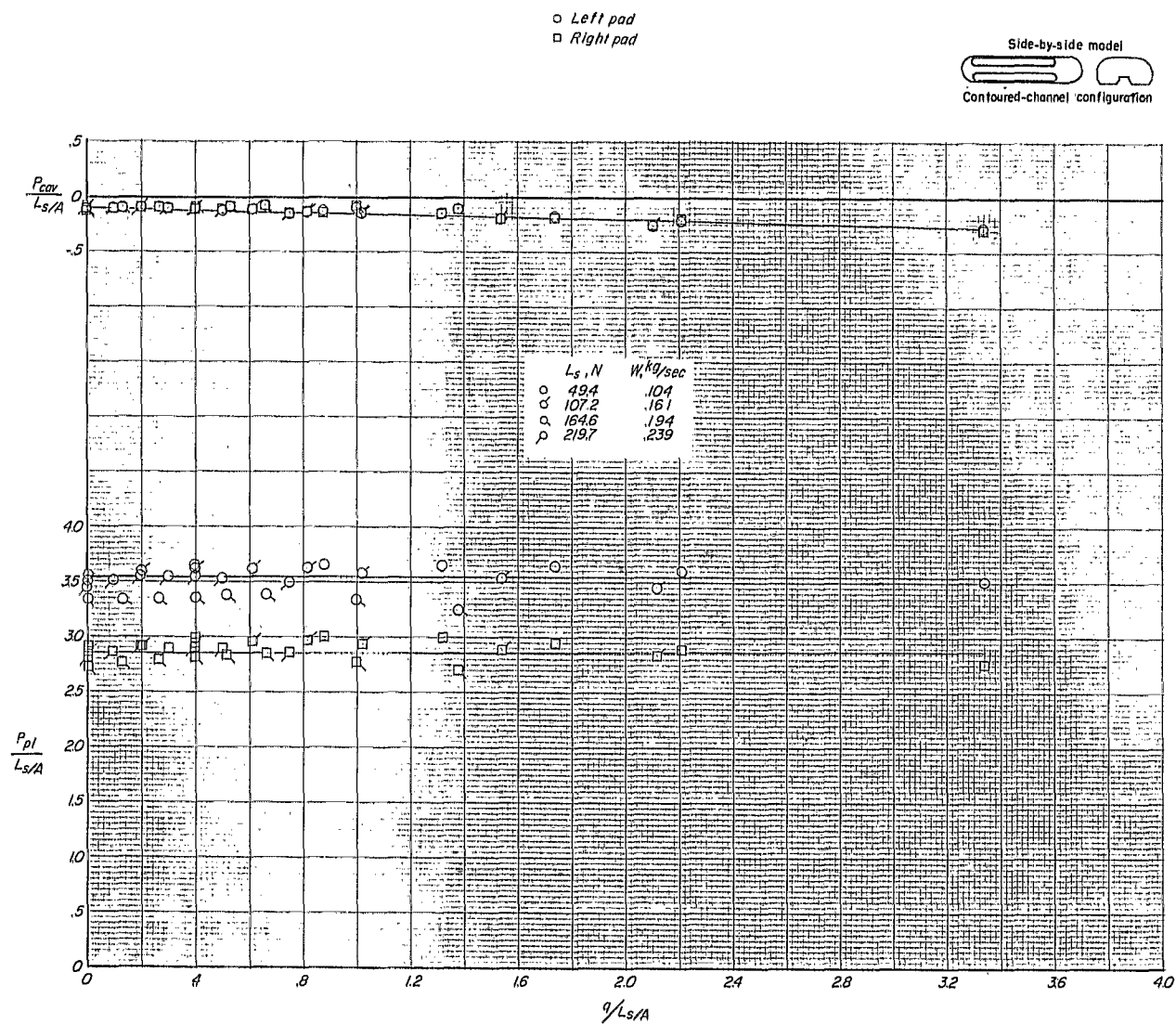
(h) Pressure coefficient along center line of air cushion.  $L_s = 91.6$  N;  $W = 0.171$  kg/sec;  $\beta = 30^\circ$ .

Figure 33.- Concluded.



(a) Lift, drag, and pitching moment as a function of pressure ratio.

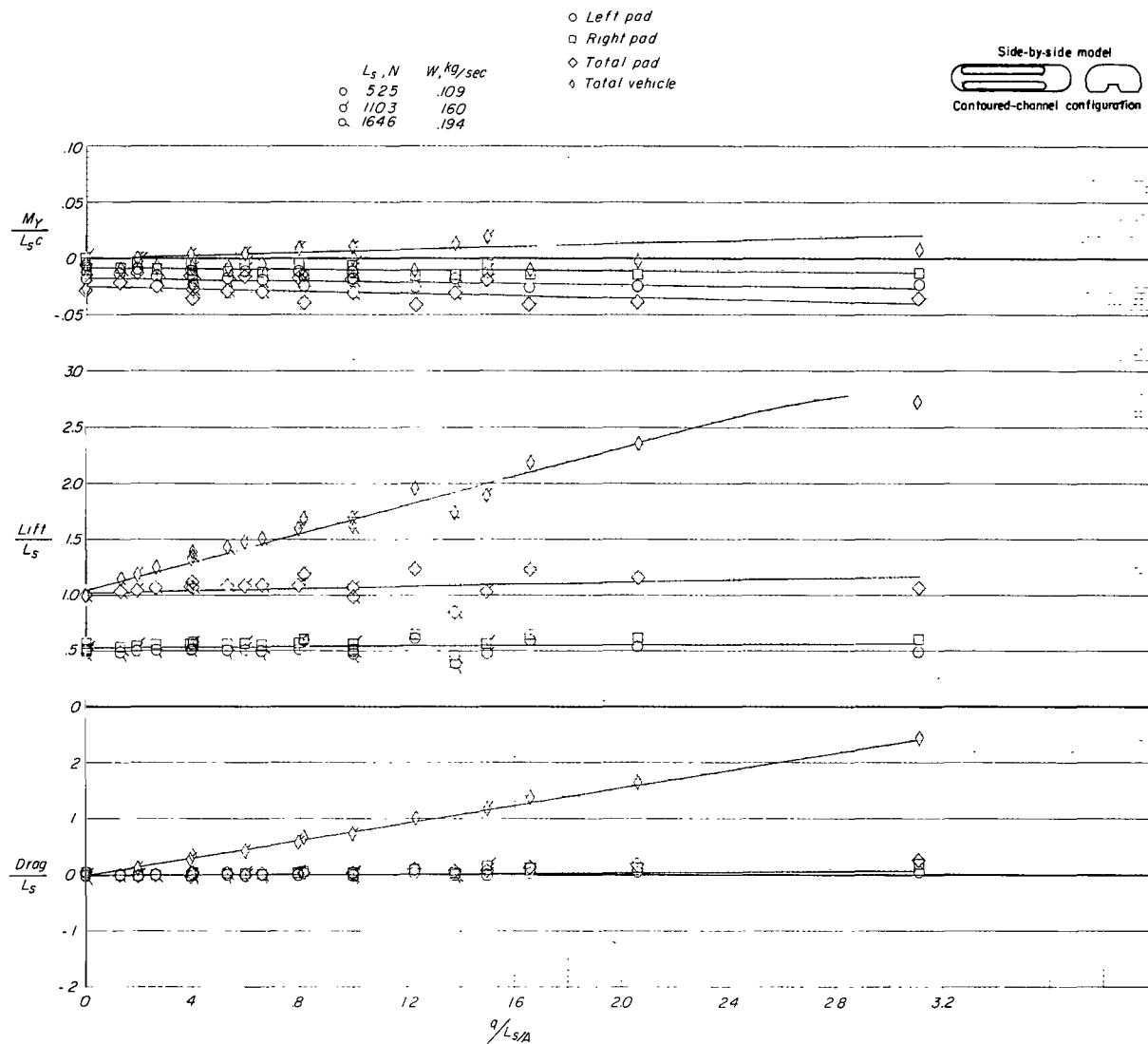
Figure 34.- Effect of forward speed on aerodynamic characteristics of side-by-side model (contoured channel). Belt moving;  $h/d_e = 0.0033$ ;  $\beta = 0^\circ$ .



(b) Cavity pressure and plenum pressure as a function of pressure ratio.

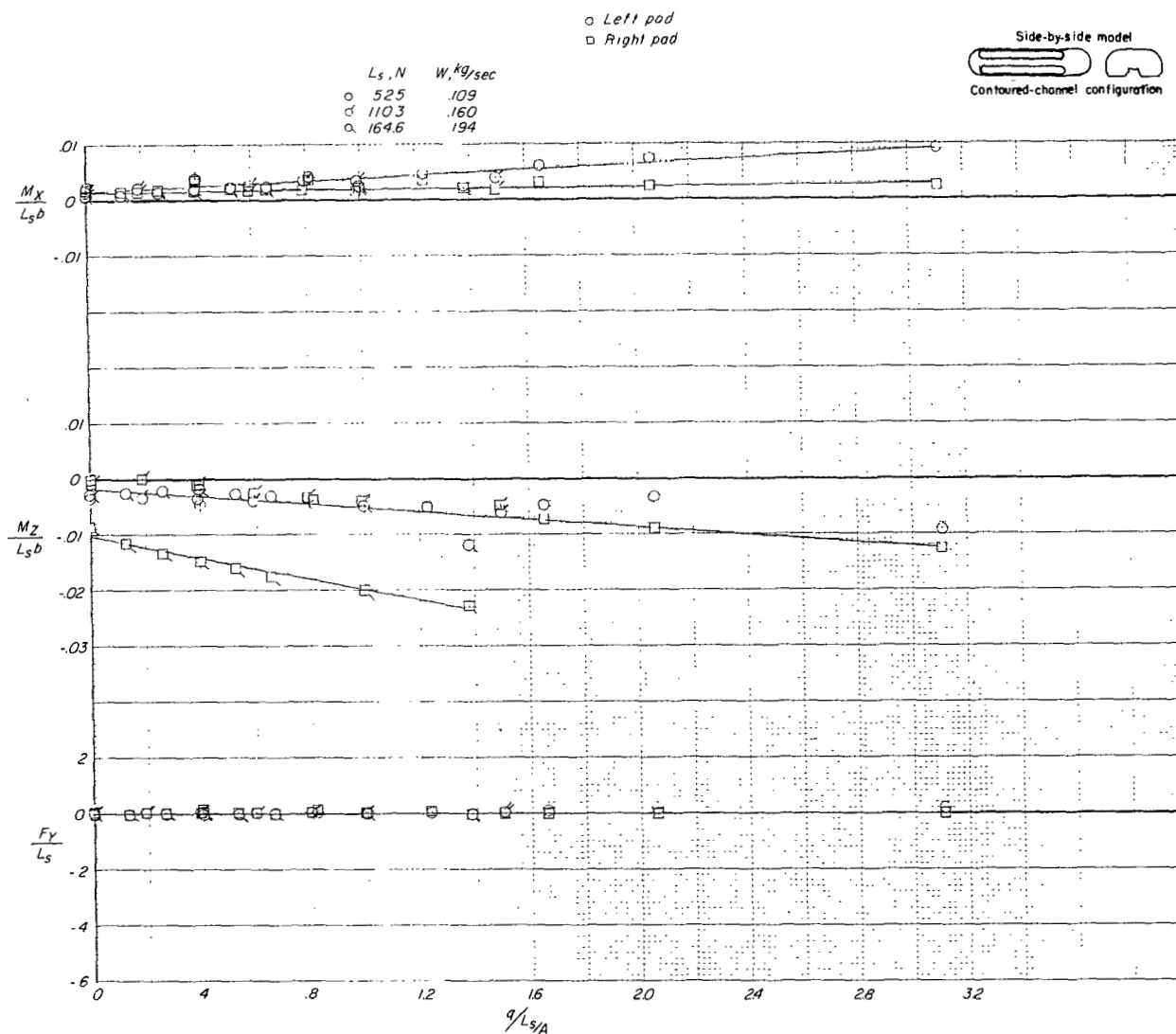
Figure 34.- Concluded.





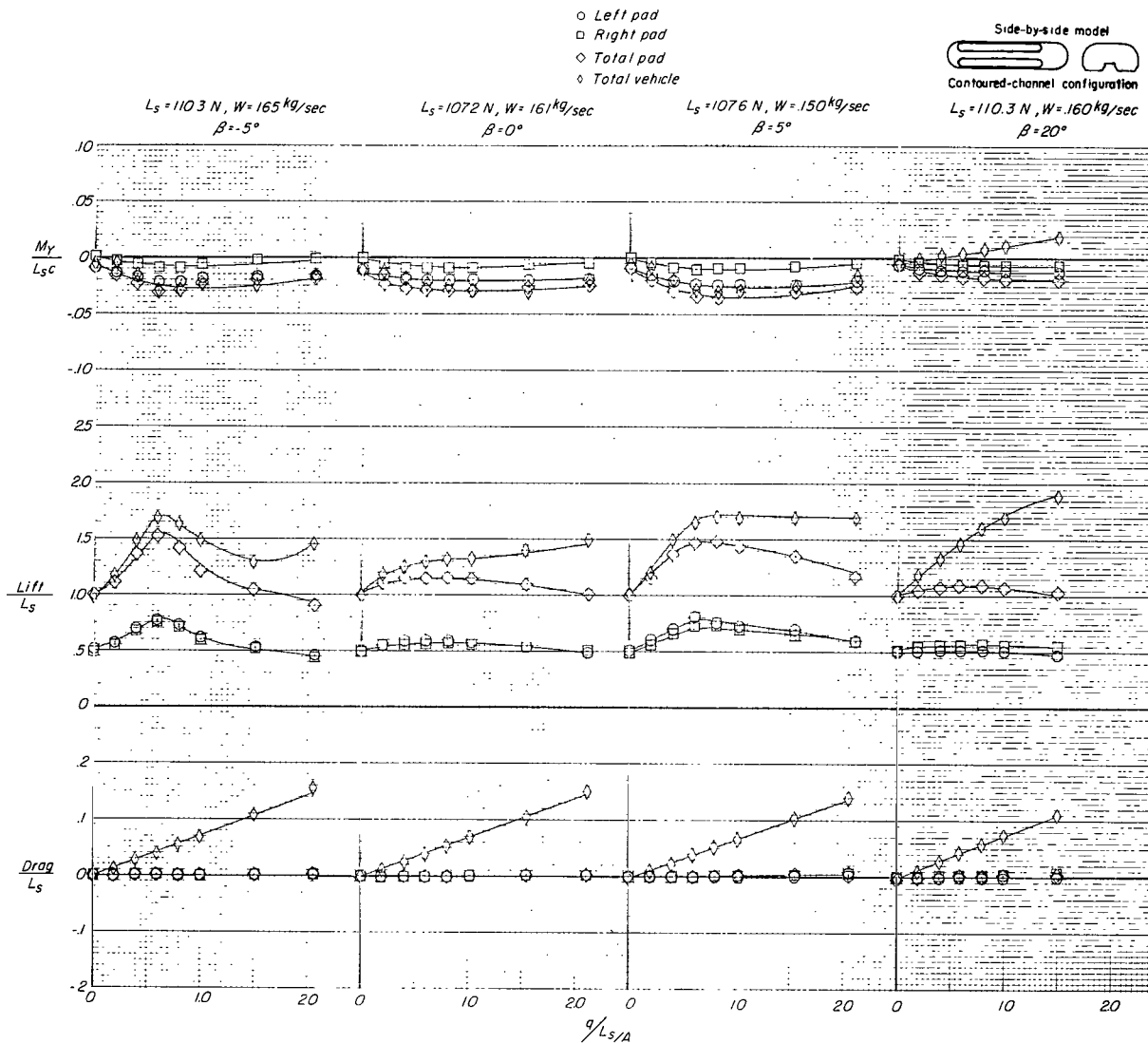
(a) Lift, drag, and pitching moment as a function of pressure ratio.

Figure 35.- Effect of forward speed on aerodynamic characteristics of side-by-side model (contoured channel). Belt moving;  $h/a_e = 0.0033$ ;  $\beta = 20^\circ$ .



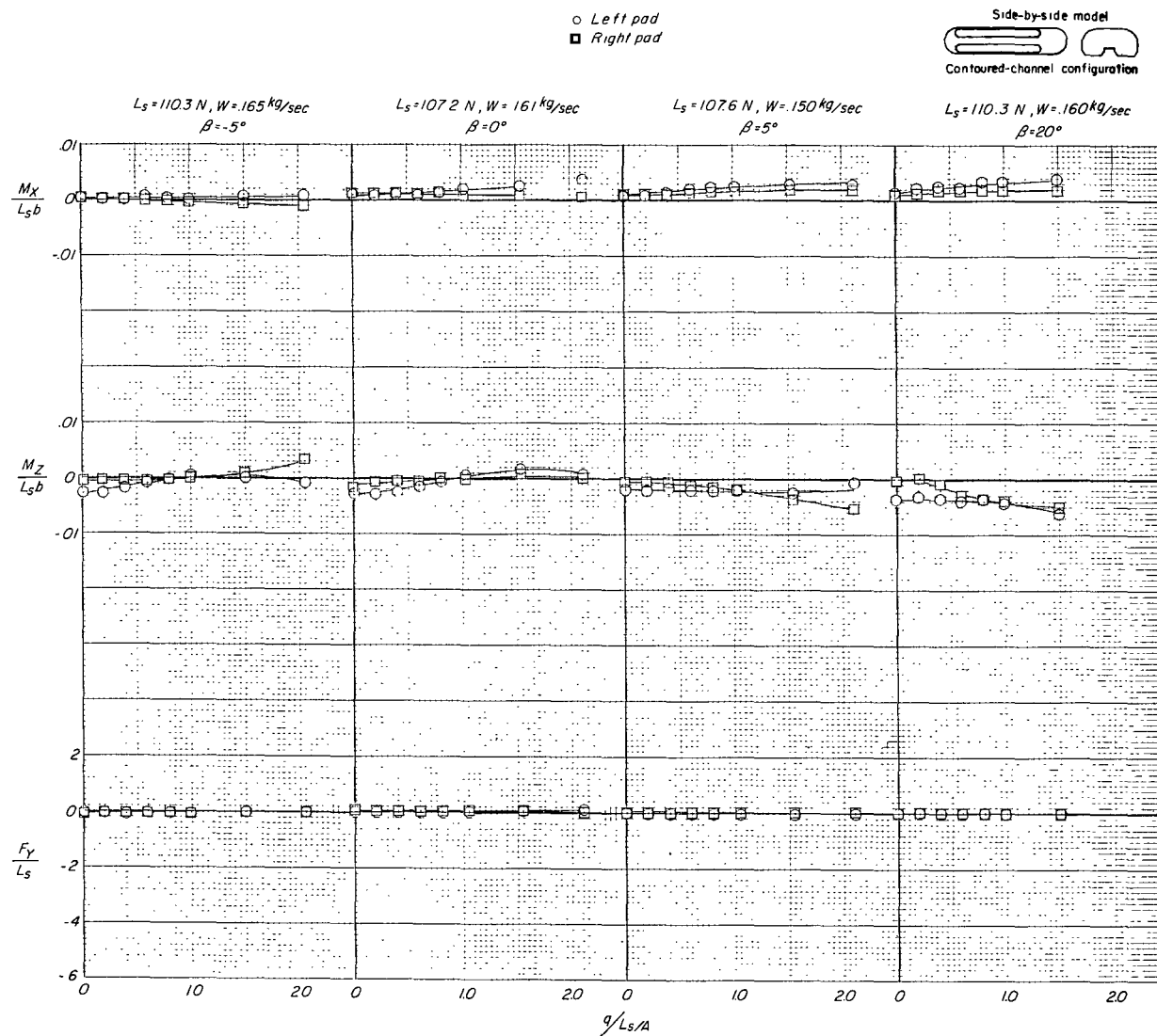
(b) Cavity pressure and plenum pressure as a function of pressure ratio.

Figure 35.- Concluded.



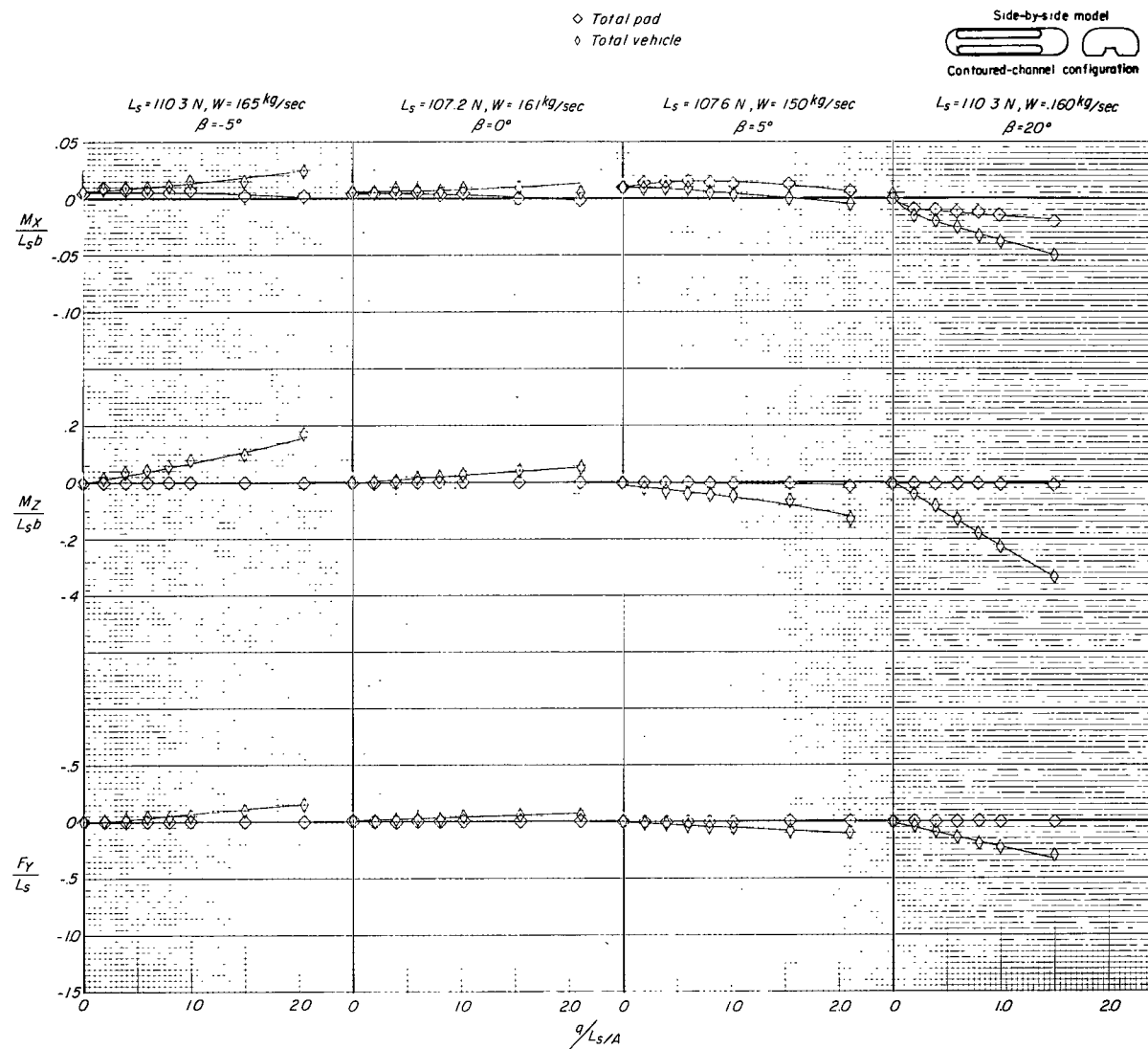
(a) Lift, drag, and pitching moment as a function of pressure ratio.

Figure 36.- Effect of sideslip on aerodynamic characteristics of side-by-side model (contoured channel). Belt moving;  $h/a_e = 0.0033$ .



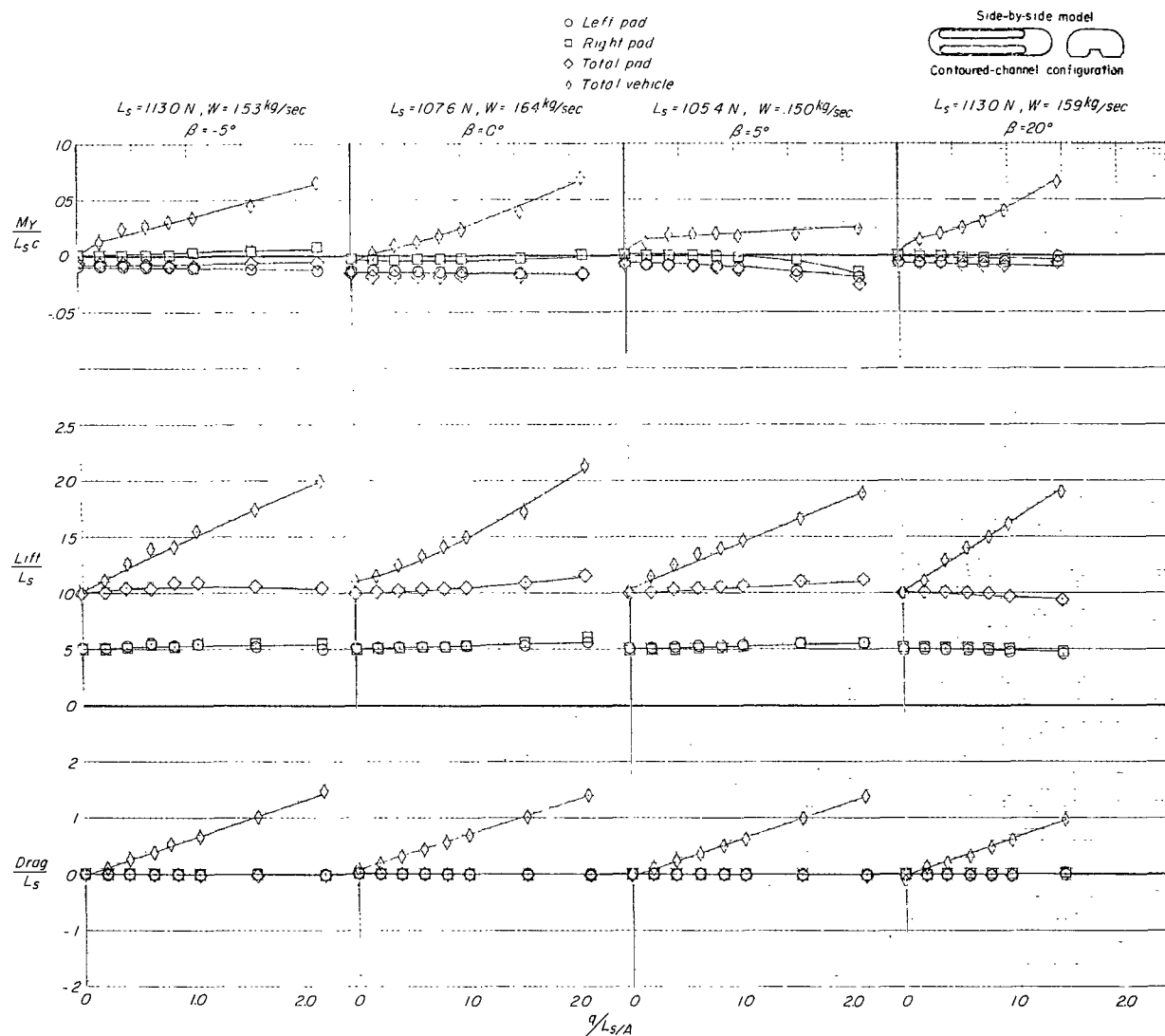
(b) Roll, yaw, and side force of each air cushion as a function of pressure ratio.

Figure 36.- Continued.



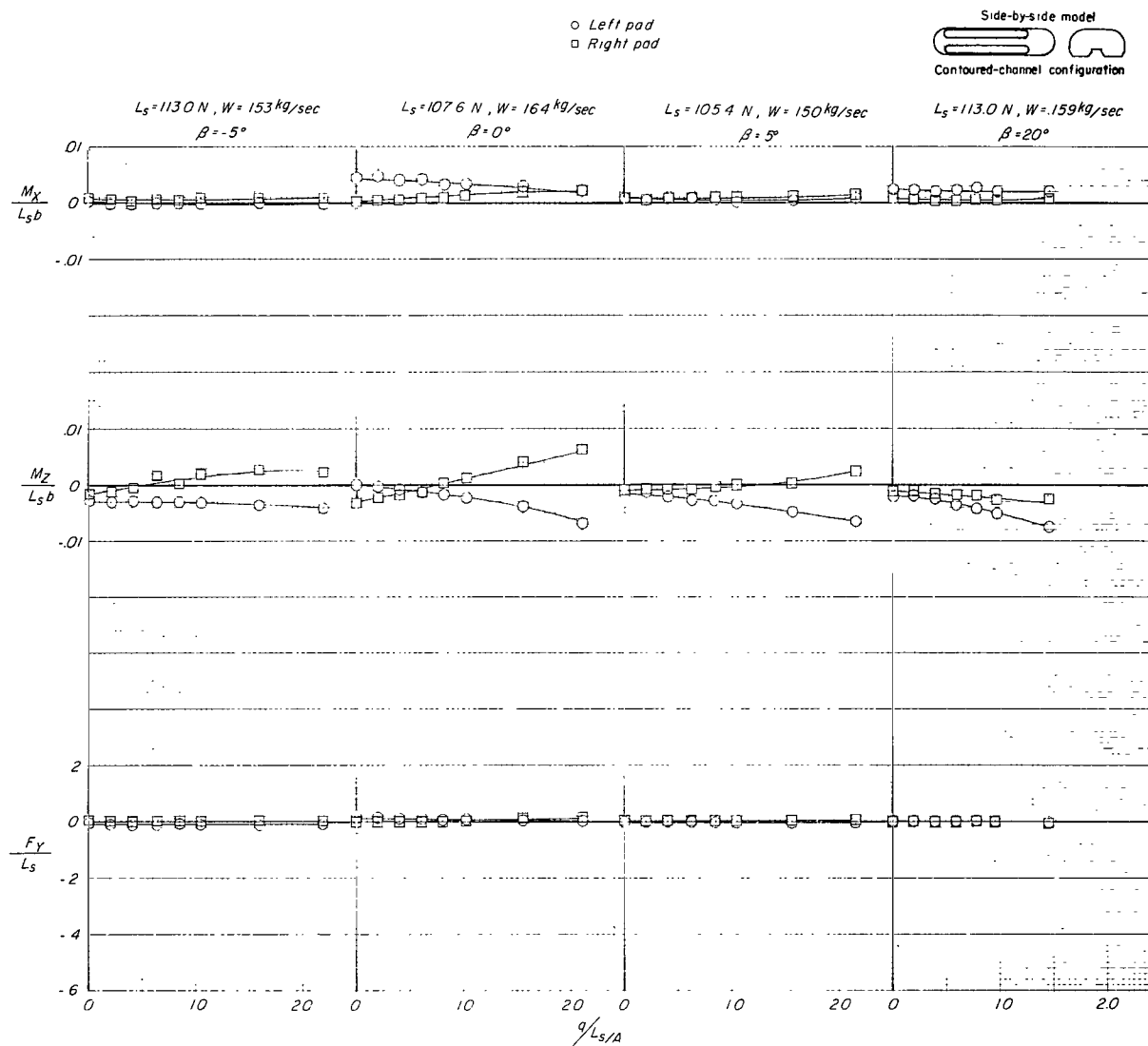
(c) Roll, yaw, and side force, total of both air cushions and total for entire vehicle, as a function of pressure ratio.

Figure 36.- Concluded.



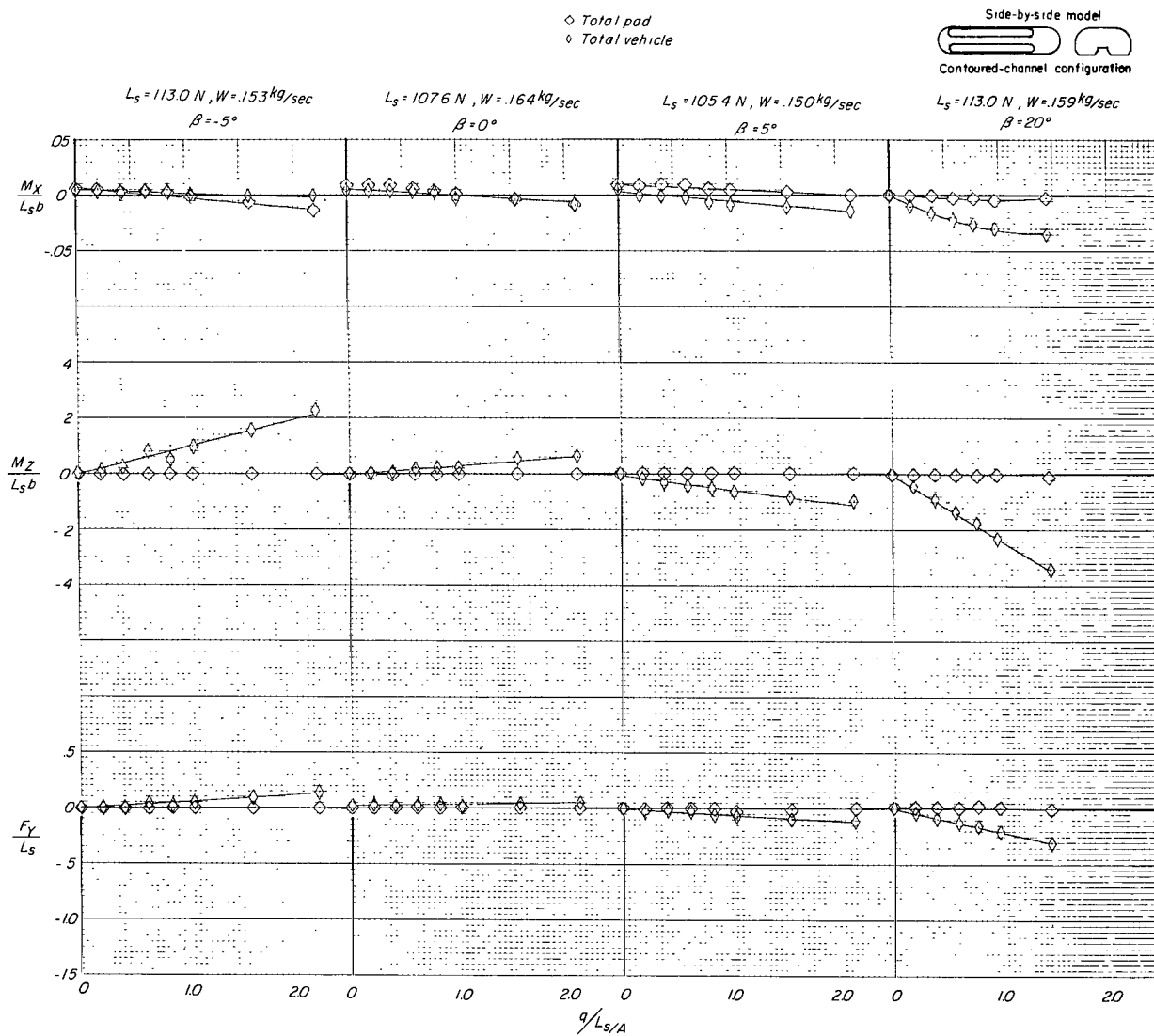
(a) Lift, drag, and pitching moment as a function of pressure ratio.

Figure 37.- Effect of sideslip on aerodynamic characteristics of side-by-side model (contoured channel). Belt stopped;  $h/d_e = 0.0033$ .



(b) Roll, yaw, and side force of each air cushion as a function of pressure ratio.

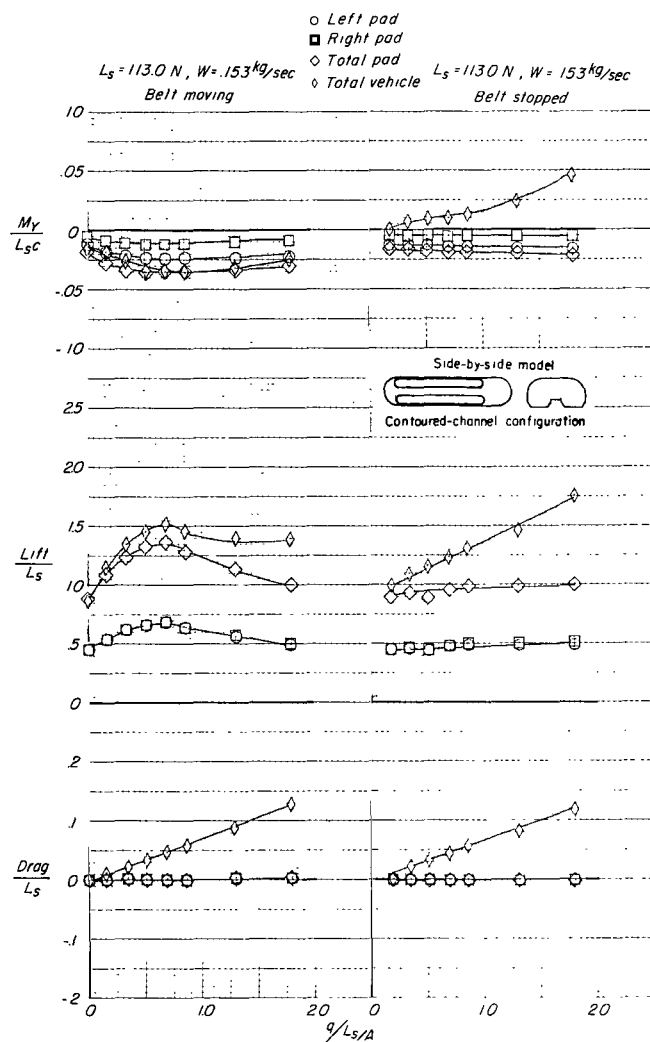
Figure 37.- Continued.



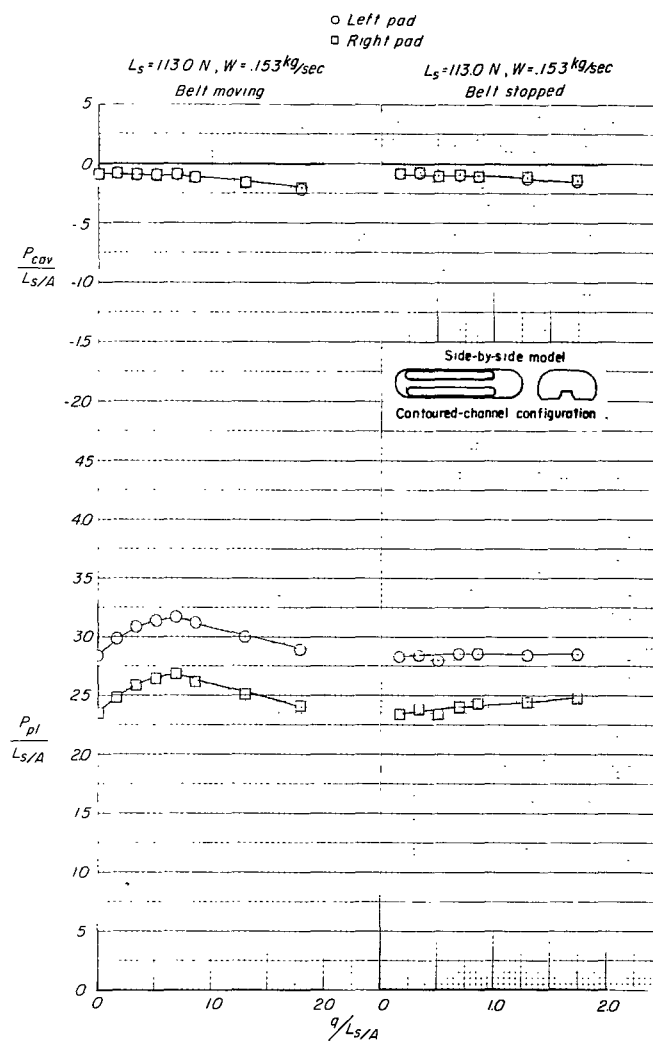
(c) Roll, yaw, and side force, total for both air cushions and total for entire vehicle, as a function of pressure ratio.

Figure 37.- Concluded.



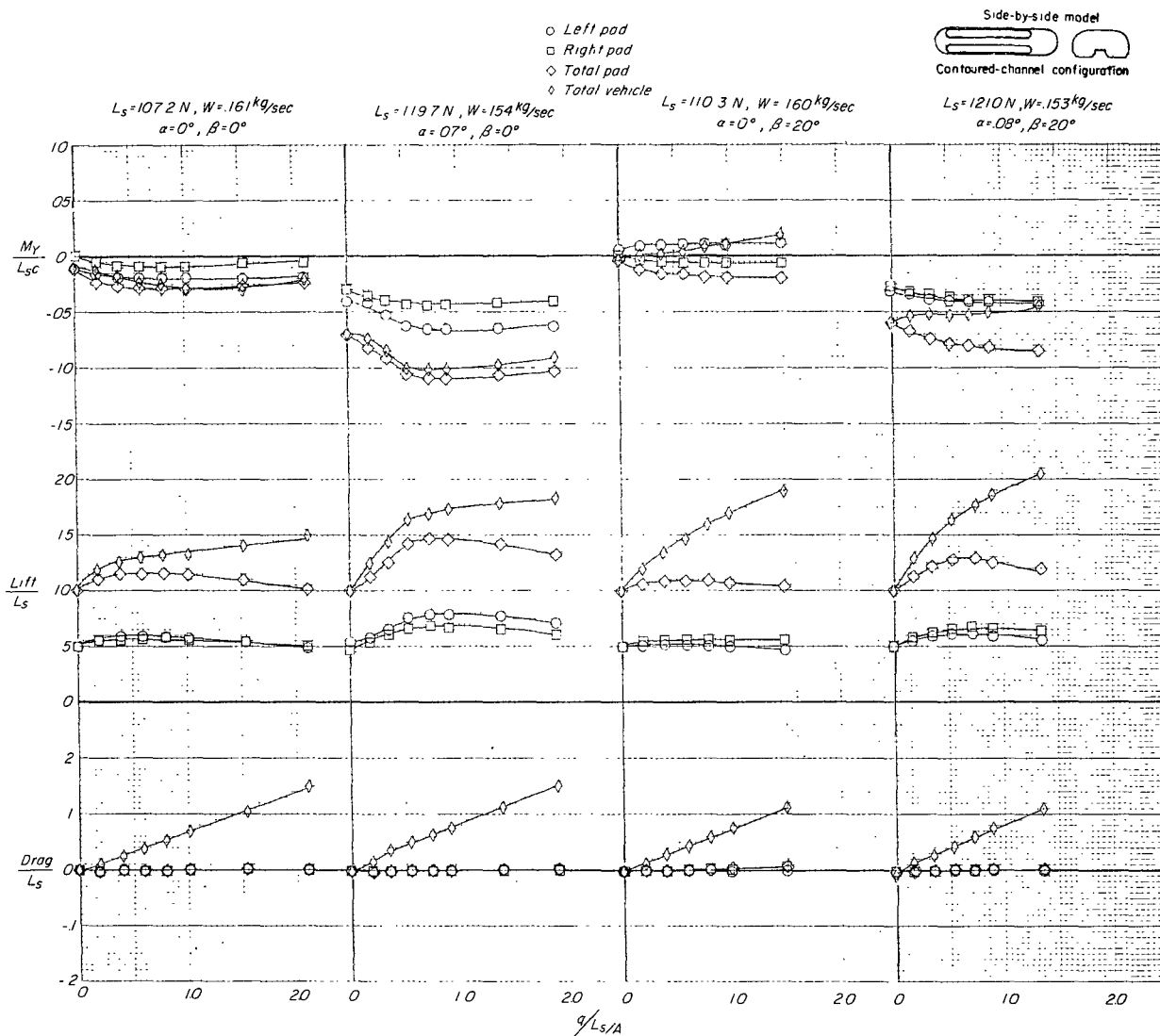


(a) Lift, drag, and pitching moment as a function of pressure ratio.



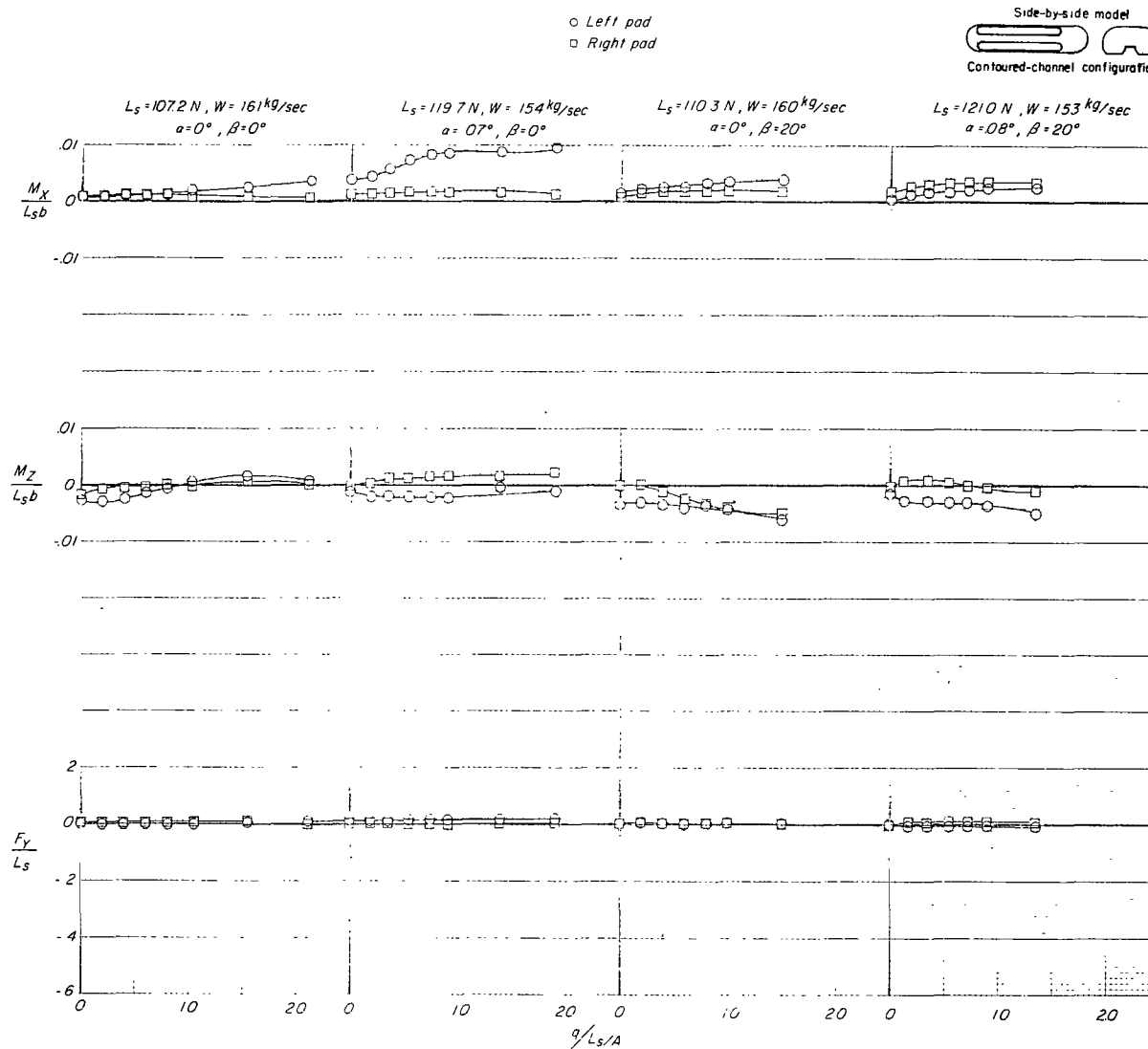
(b) Cavity pressure and plenum pressure as a function of pressure ratio.

Figure 38.- Effect of moving ground belt on aerodynamic characteristics of side-by-side model (contoured channel).  $h/d_e = 0.0033$ ;  $\beta = 0^\circ$ .



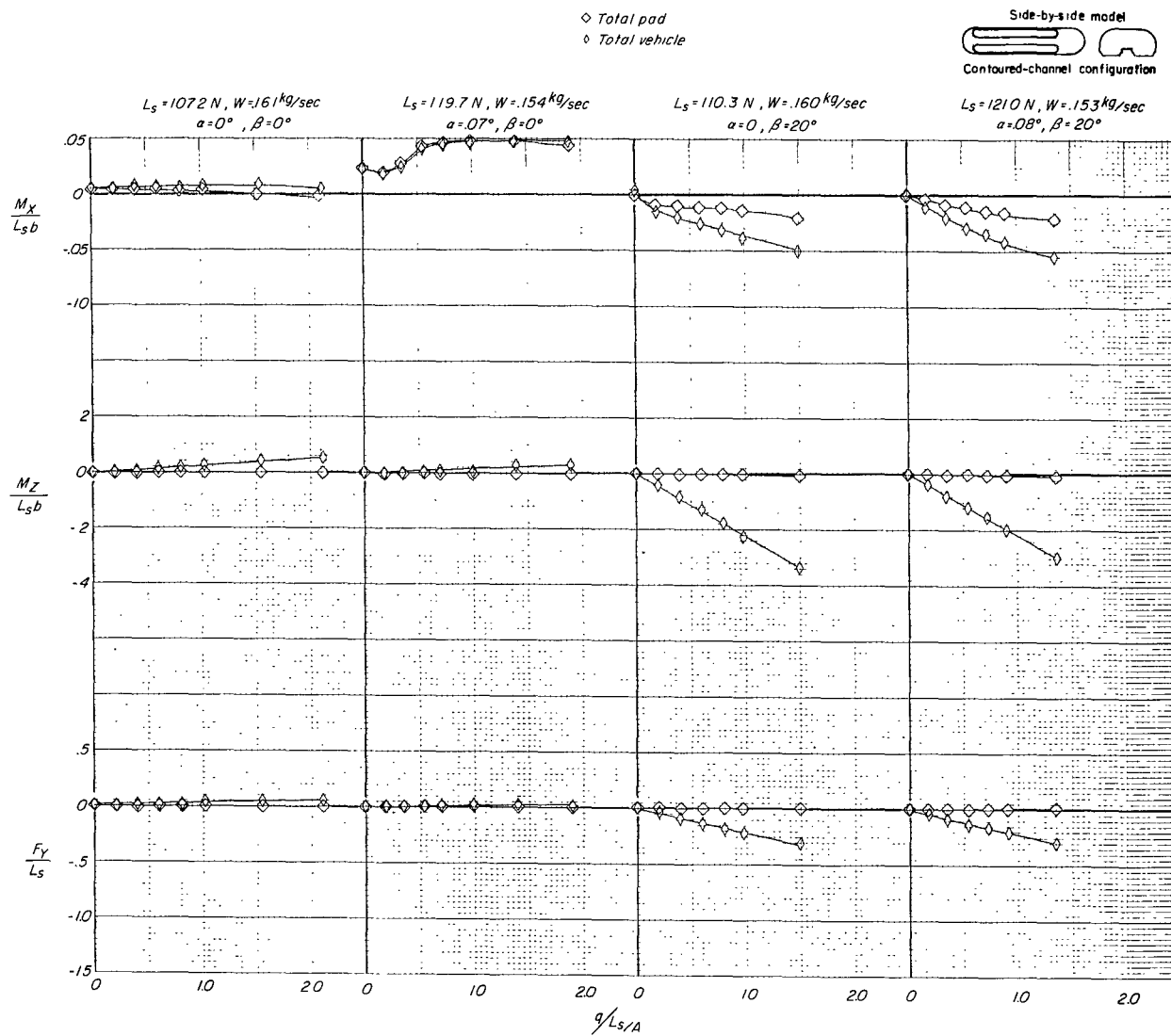
(a) Lift, drag, and pitching moment as a function of pressure ratio.

Figure 39.- Comparison of model in level attitude with model at small angles of attack.  
 $h/a_e = 0.0033$ ; ground belt moving.



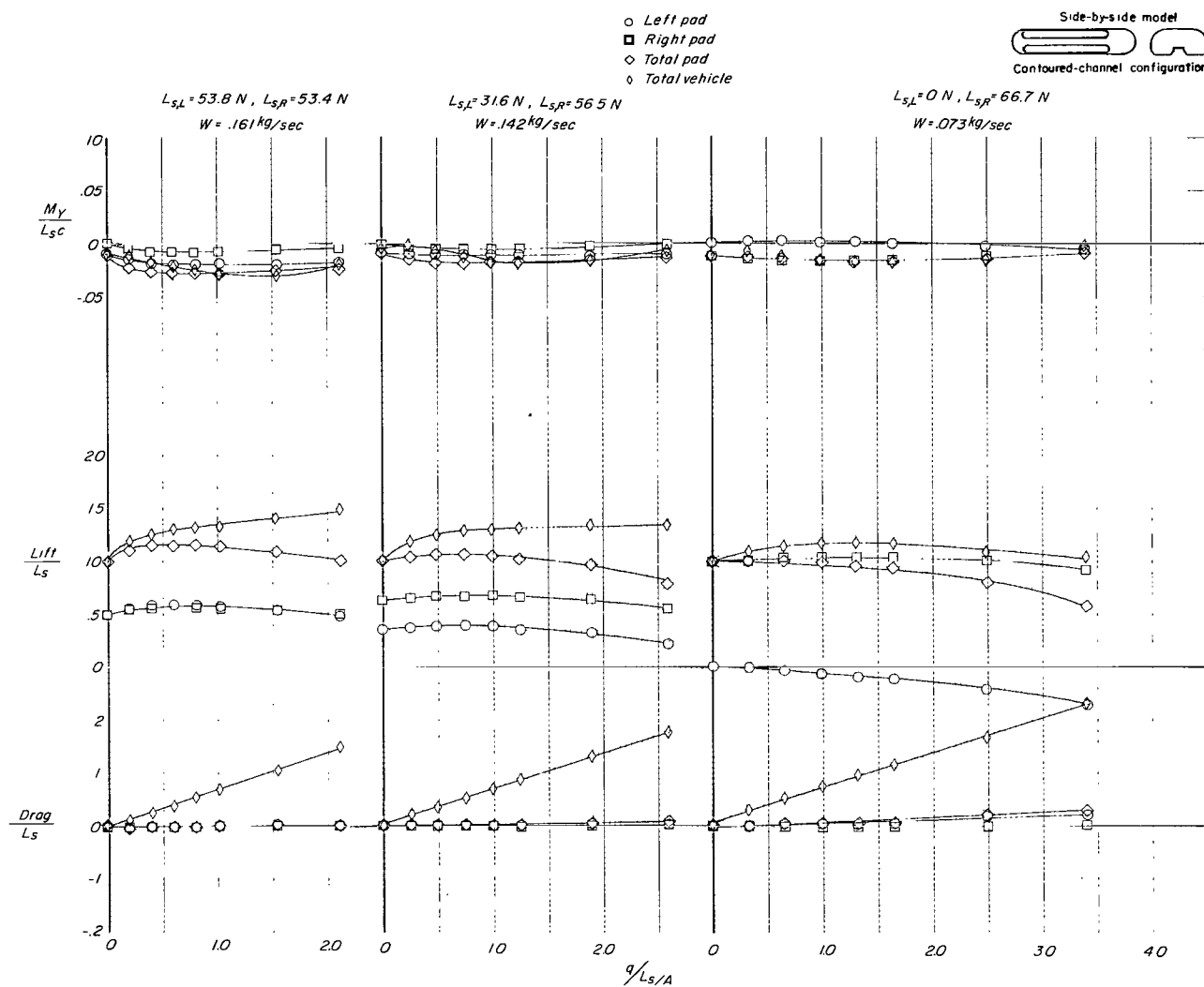
(b) Roll, yaw, and side force of each air cushion as a function of pressure ratio.

Figure 39.- Continued.



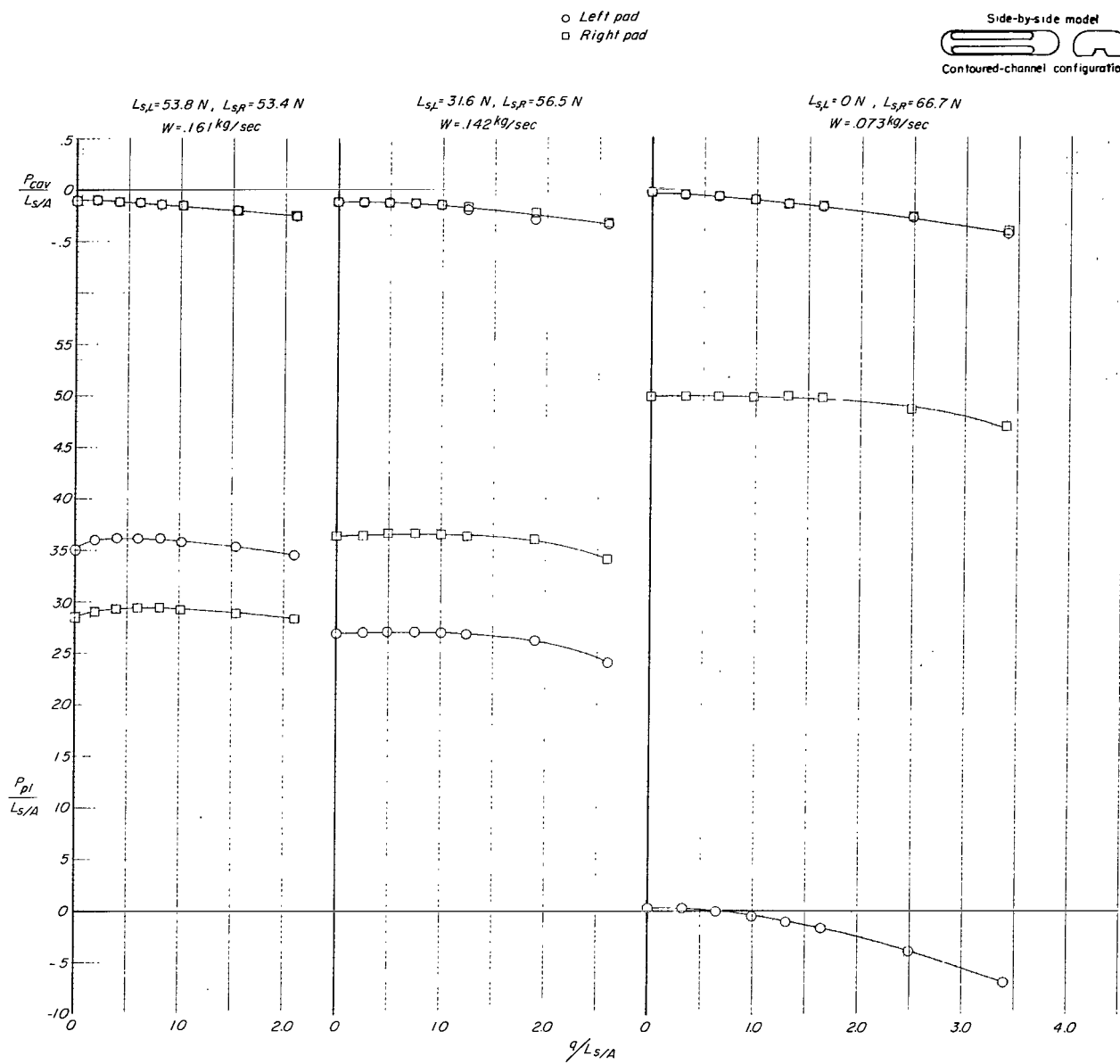
(c) Roll, yaw, and side force, total of both air cushions and total for entire vehicle, as a function of pressure ratio.

Figure 39.- Concluded.



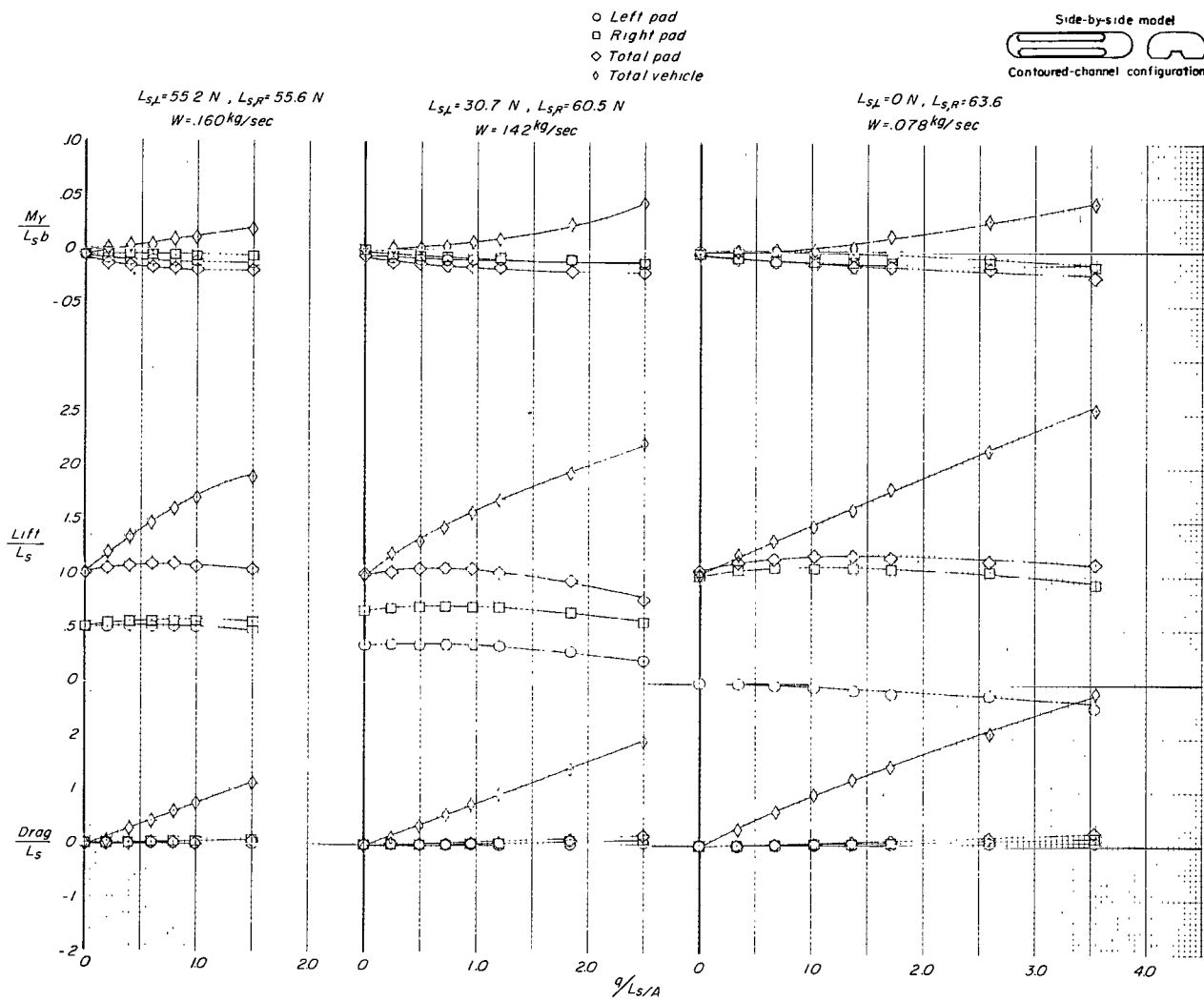
(a) Lift, drag, and pitching moment as a function of pressure ratio.

Figure 40.- Effect of differential pad pressure.  $h/d_e = 0.0033$ ;  $\beta = 0^\circ$ .



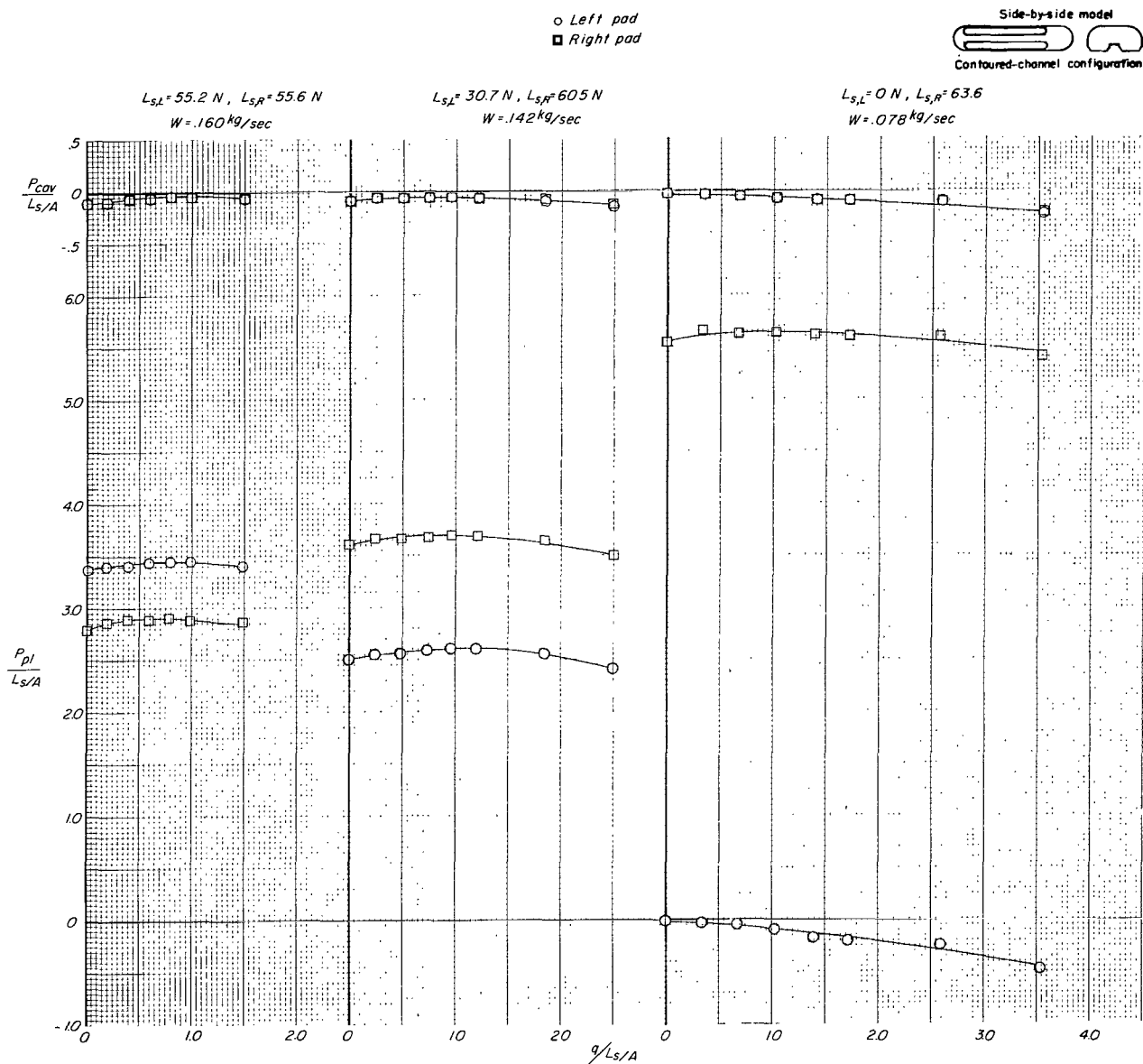
(b) Cavity pressure and plenum pressure as a function of pressure ratio.

Figure 40.- Concluded.



(a) Lift, drag, and pitching moment as a function of pressure ratio.

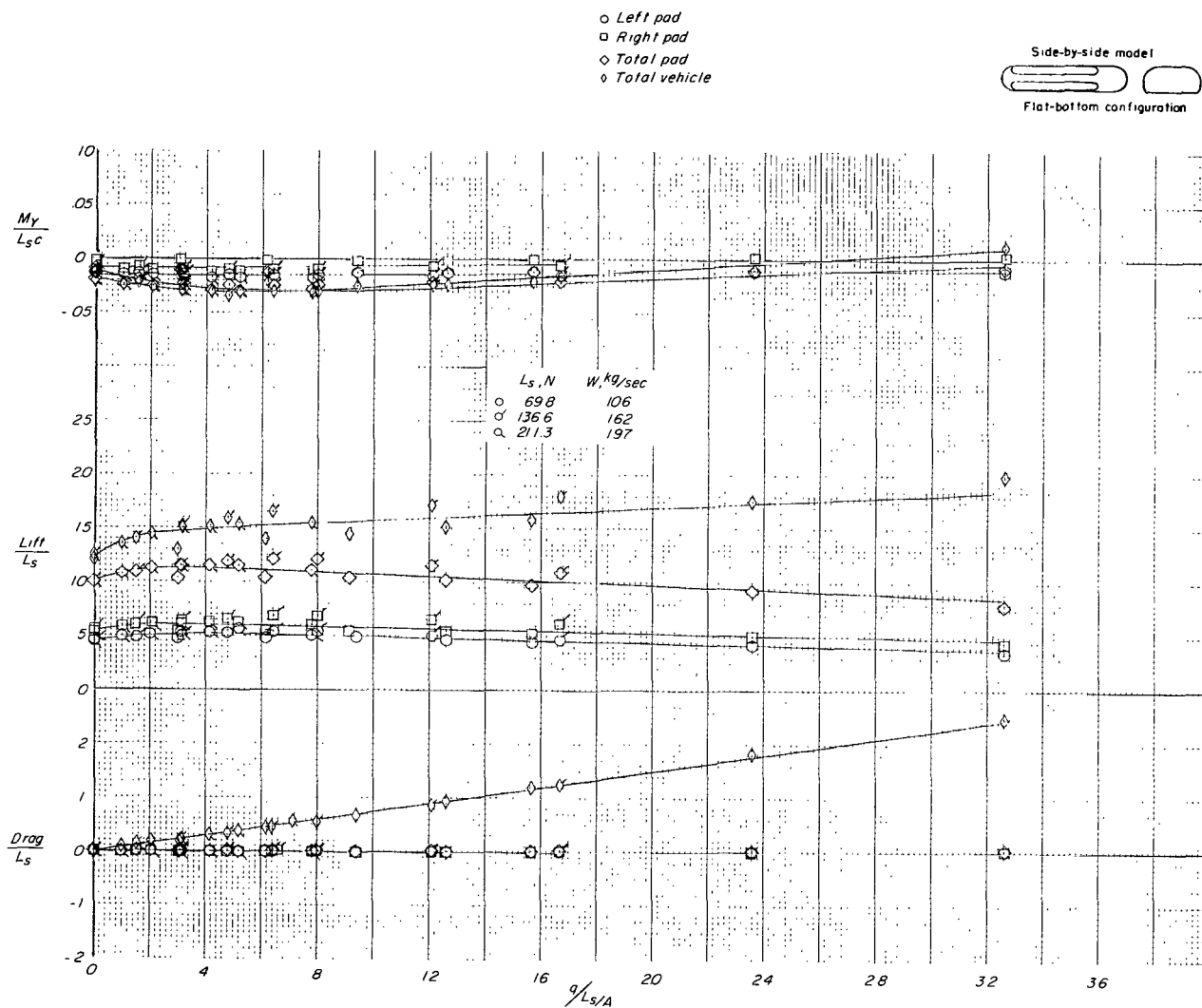
Figure 41.- Effect of differential pad pressure.  $h/d_e = 0.0033$ ;  $\beta = 20^\circ$ .



(b) Cavity pressure and plenum pressure as a function of pressure ratio.

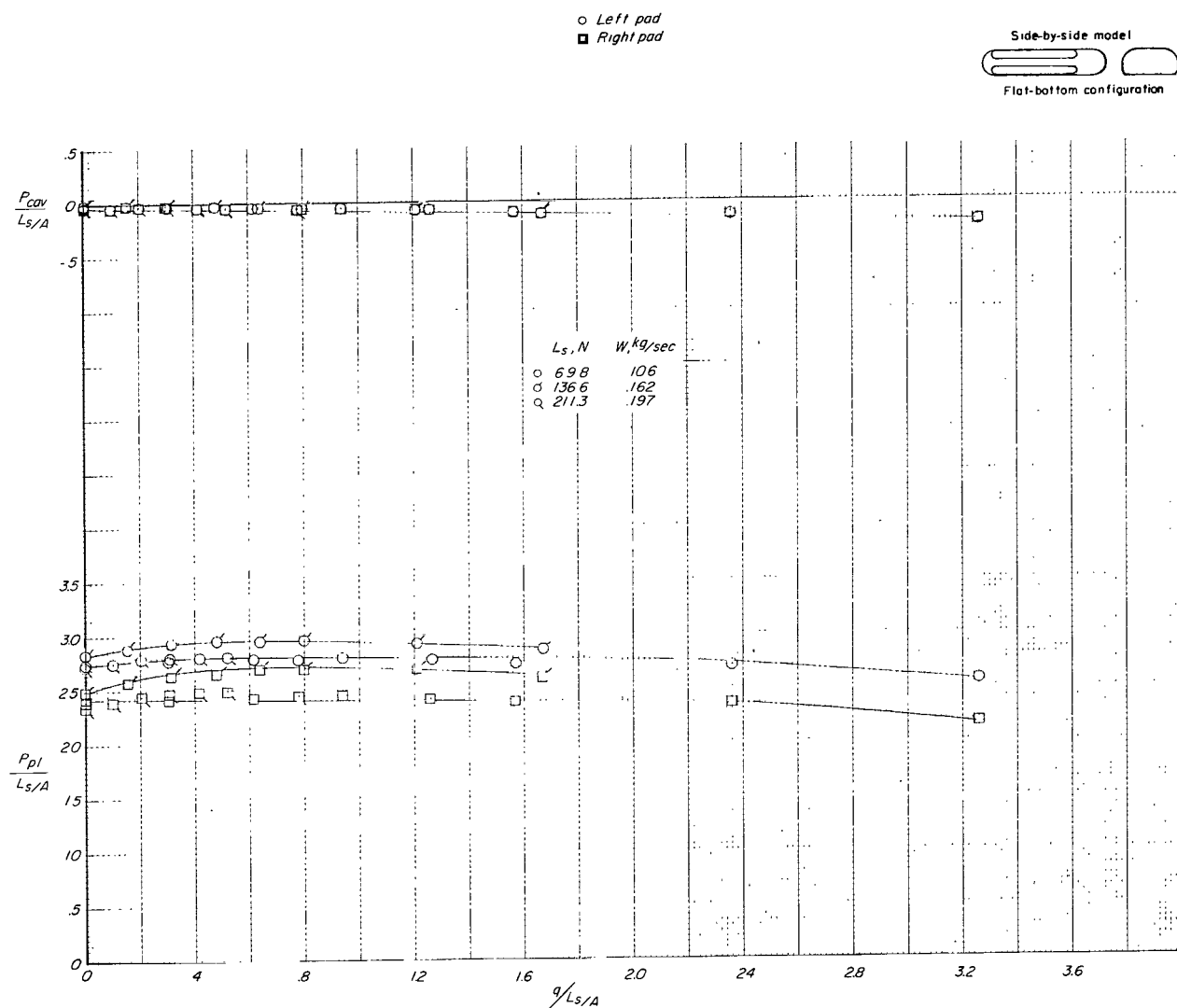
Figure 41.- Concluded.





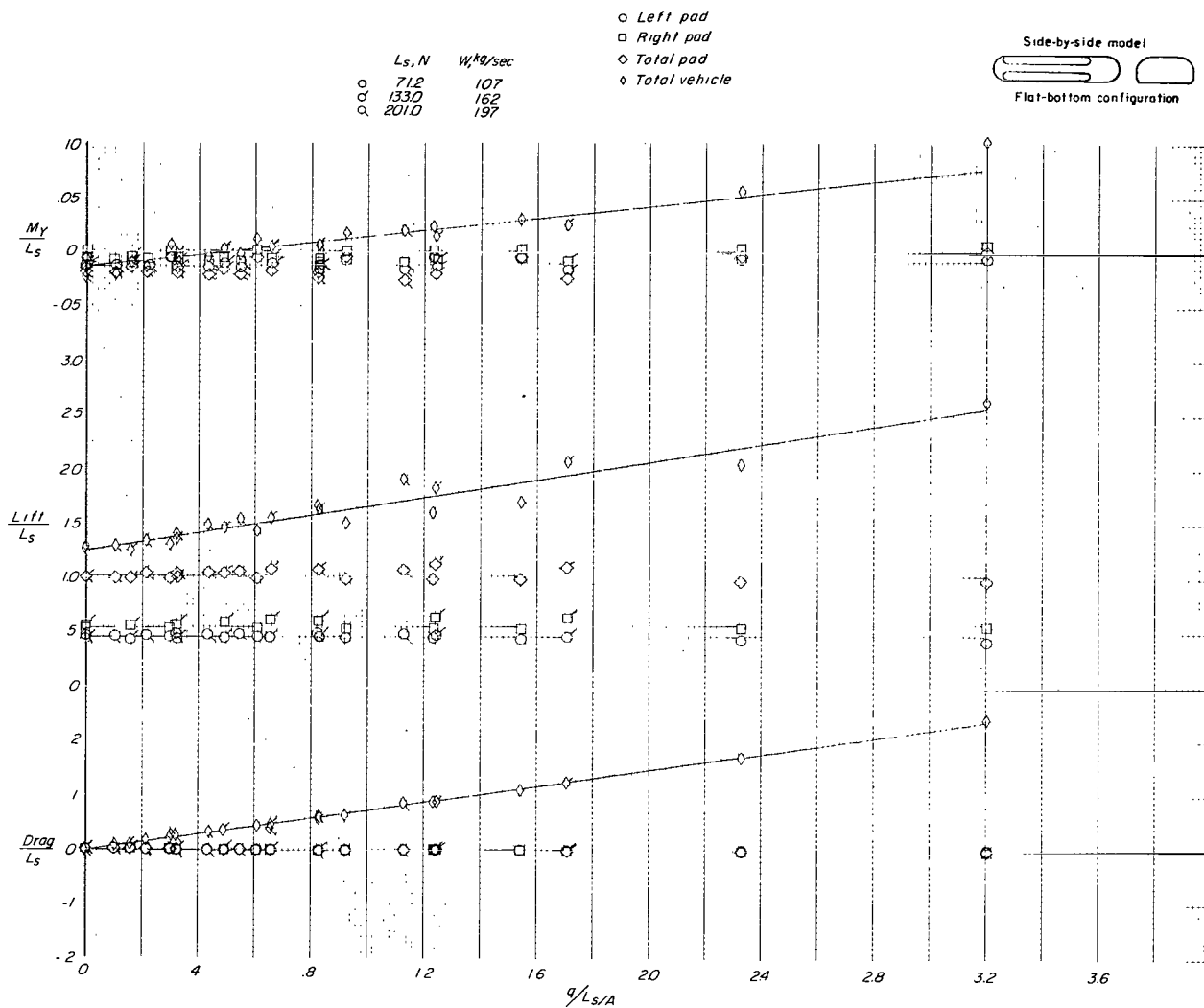
(a) Lift, drag, and pitching moment as a function of pressure ratio.

Figure 42.- Effect of forward speed on aerodynamic characteristics of side-by-side model (flat bottom). Belt moving;  $h/d_e = 0.0033$ ;  $\beta = 0^\circ$ .



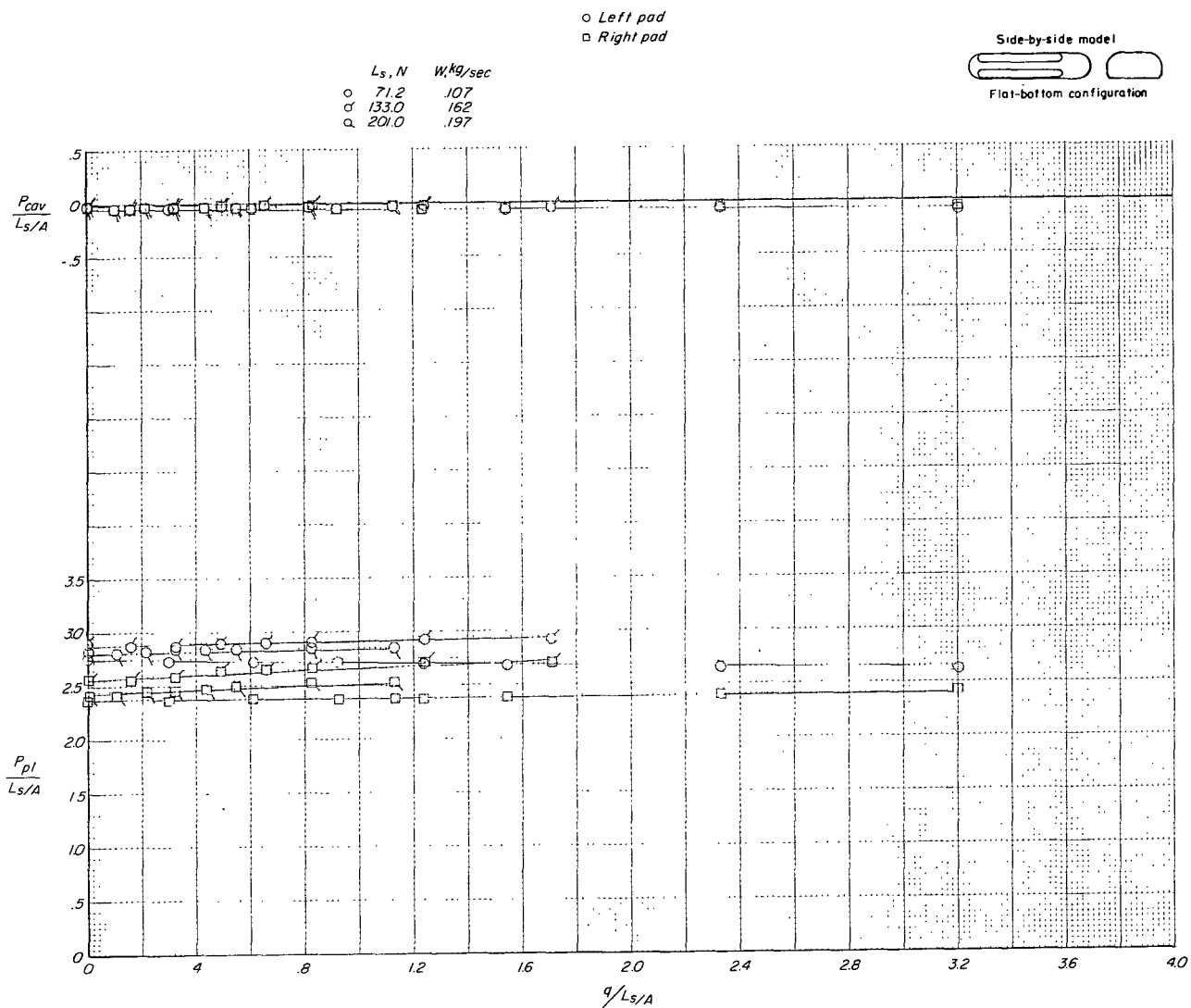
(b) Cavity pressure and plenum pressure as a function of pressure ratio.

Figure 42.- Concluded.



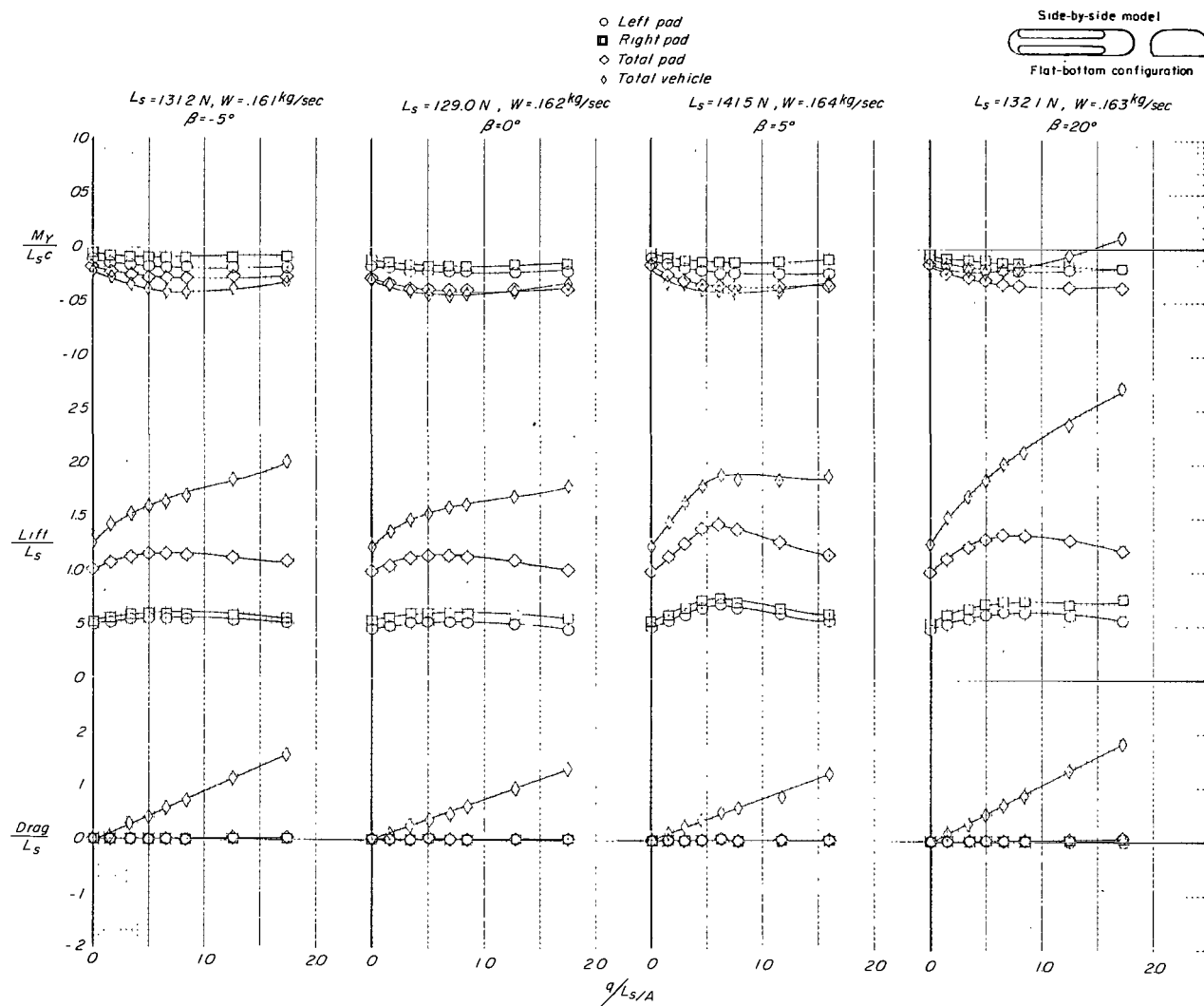
(a) Lift, drag, and pitching moment as a function of pressure ratio.

Figure 43.- Effect of forward speed on aerodynamic characteristics of side-by-side model (flat bottom). Belt stopped;  $h/d_e = 0.0033$ ;  $\beta = 0^\circ$ .



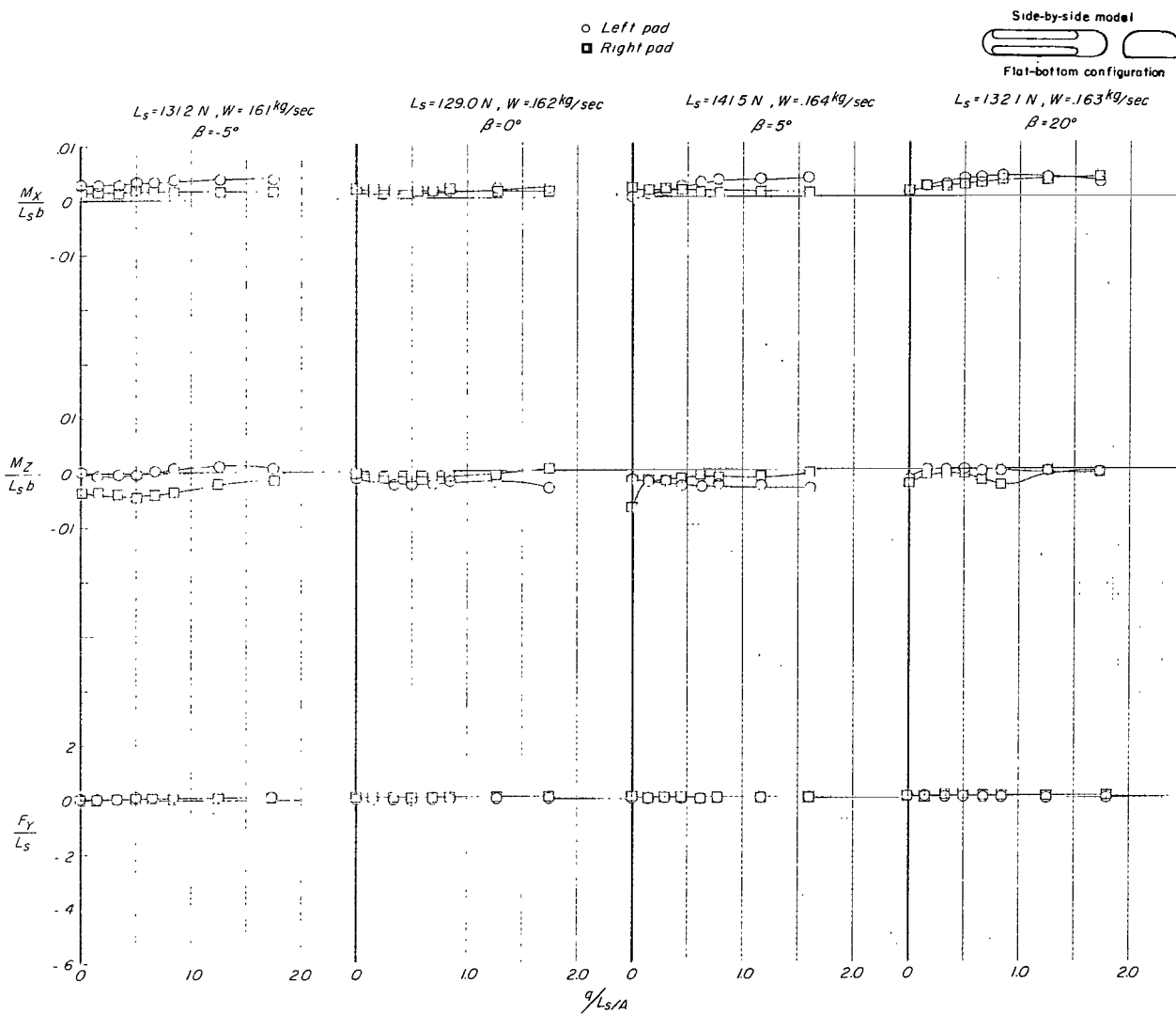
(b) Cavity pressure and plenum pressure as a function of pressure ratio.

Figure 43.- Concluded.



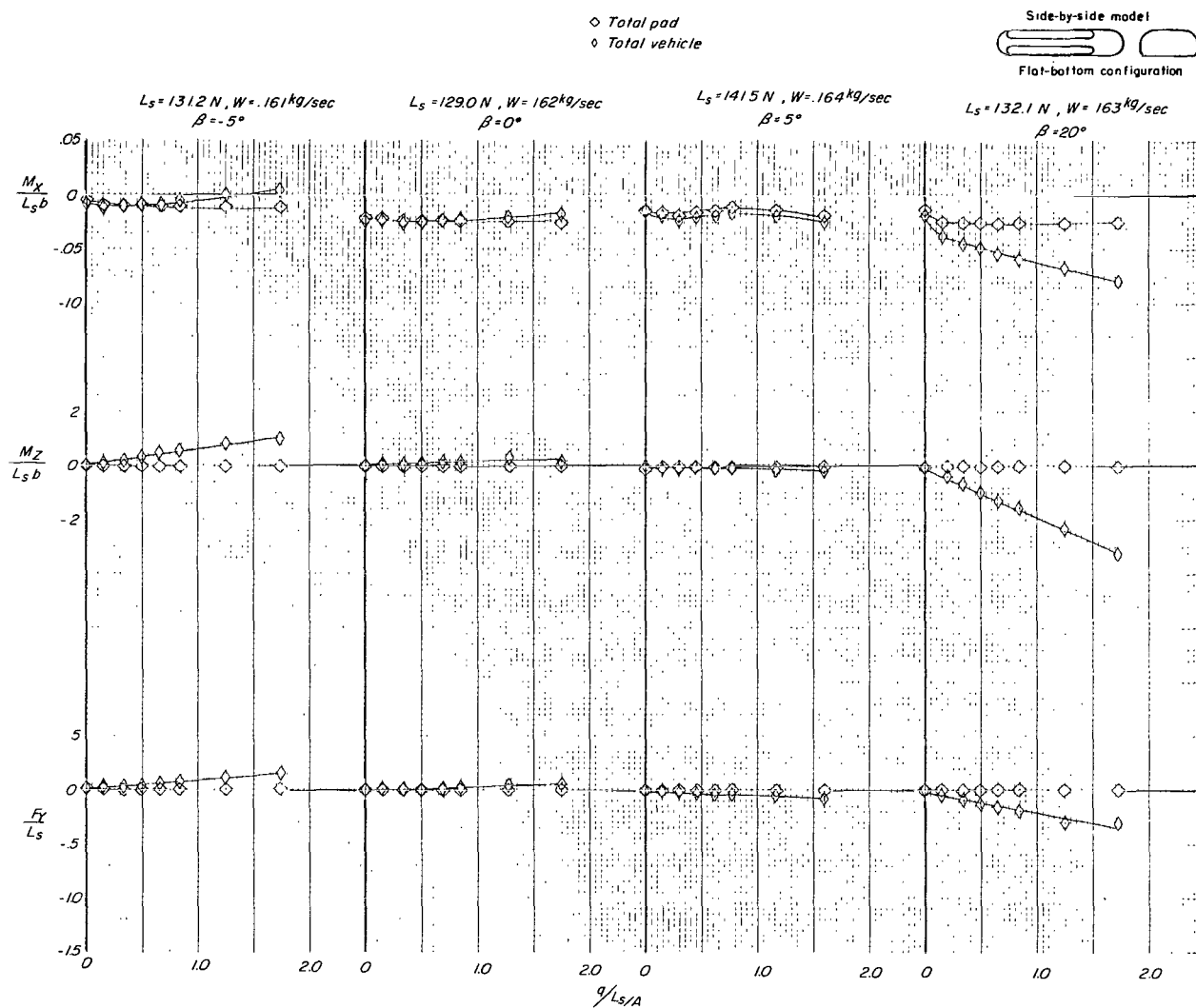
(a) Lift, drag, and pitching moment as a function of pressure ratio.

Figure 44.- Effect of sideslip on aerodynamic characteristics of side-by-side model (flat bottom). Belt moving;  $h/a_e = 0.0033$ .



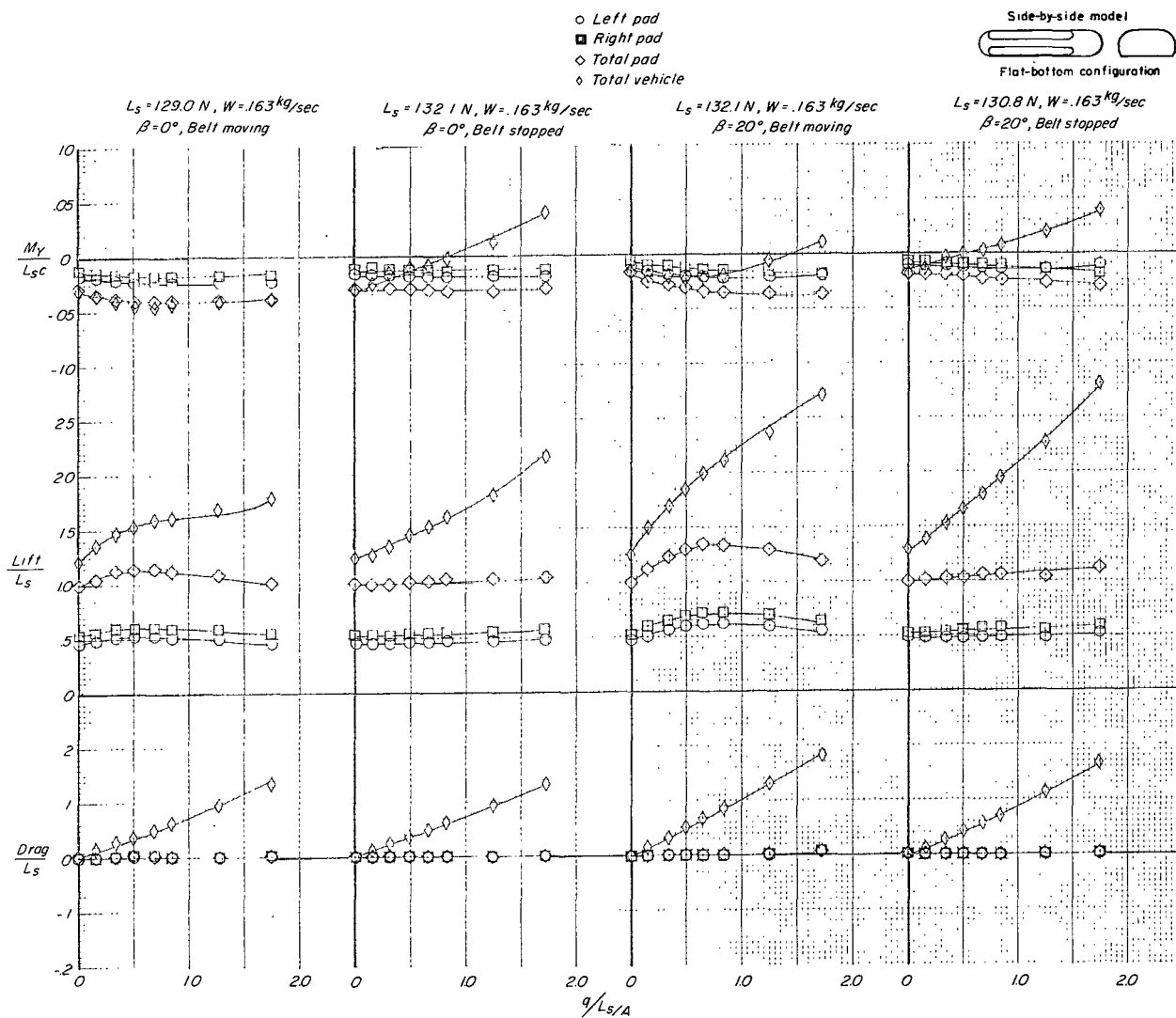
(b) Roll, yaw, and side force of each air cushion as a function of pressure ratio.

Figure 44.- Continued.



(c) Roll, yaw, and side force, total of both air cushion and total for entire vehicle, as a function of pressure ratio.

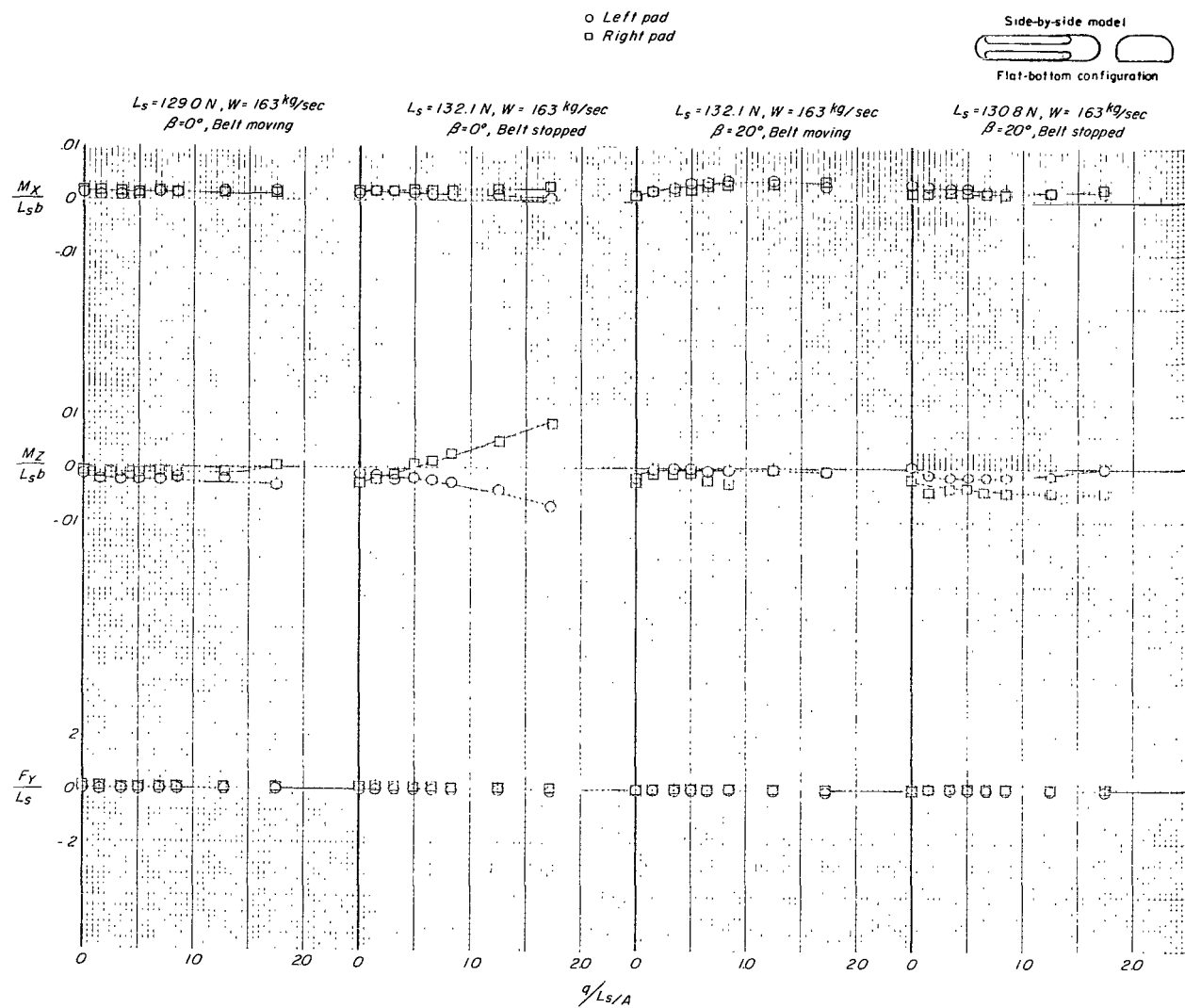
Figure 44.- Concluded.



(a) Lift, drag, and pitching moment as a function of pressure ratio.

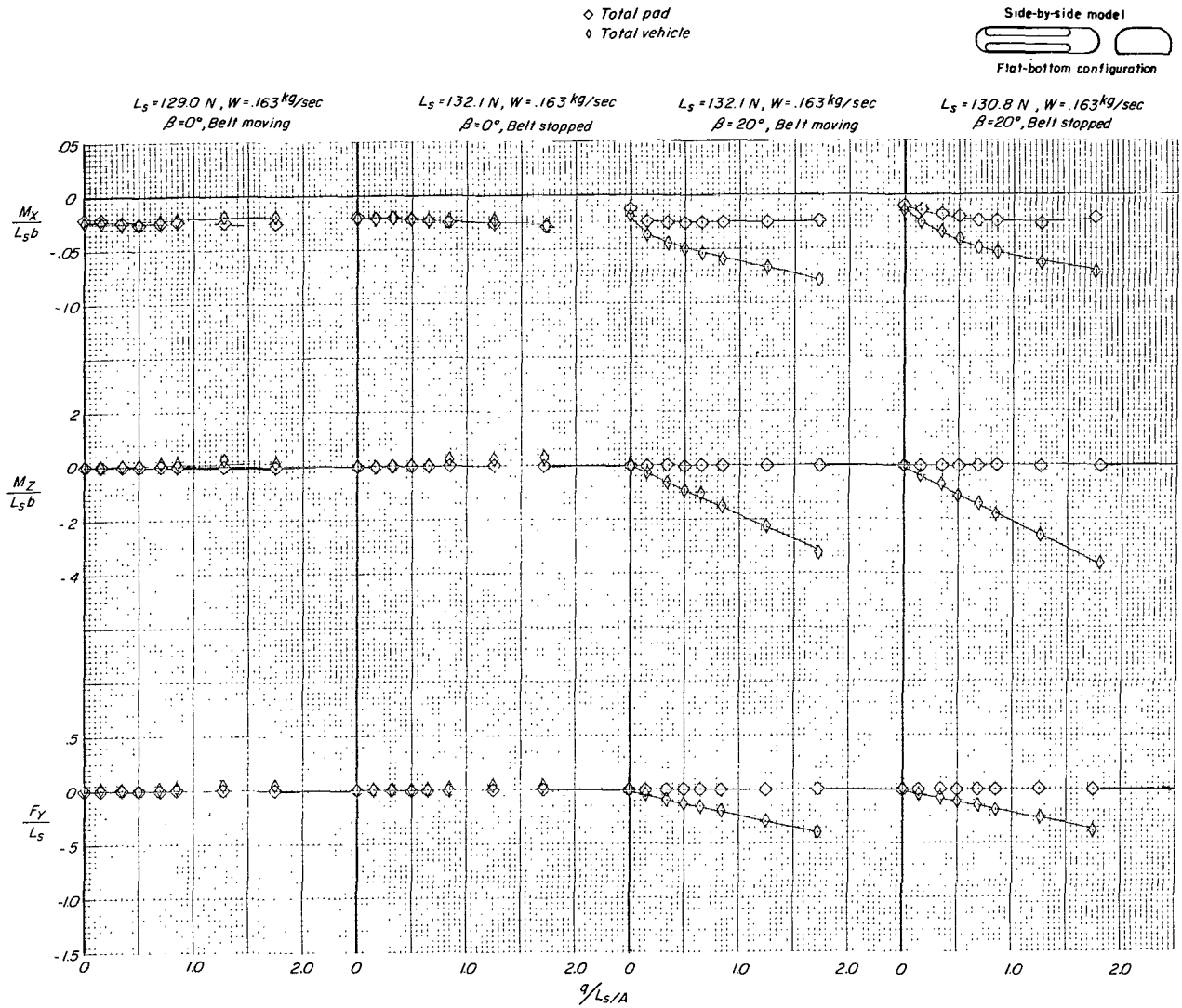
Figure 45.- Effect of moving ground belt on aerodynamic characteristics of side-by-side model (flat bottom).  $h/d_e = 0.0033$ .





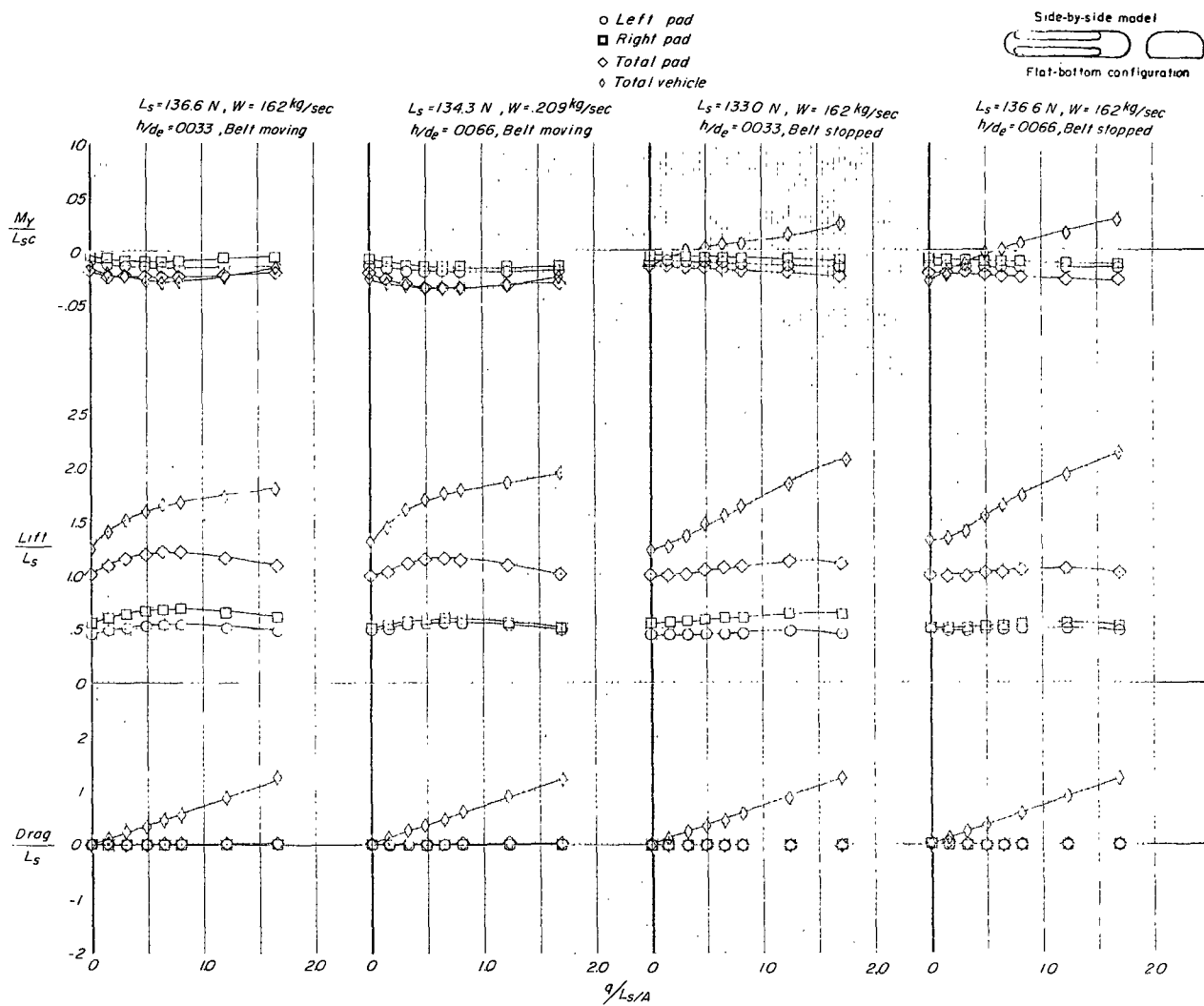
(b) Roll, yaw, and side force of each air cushion as a function of pressure ratio.

Figure 45.- Continued.



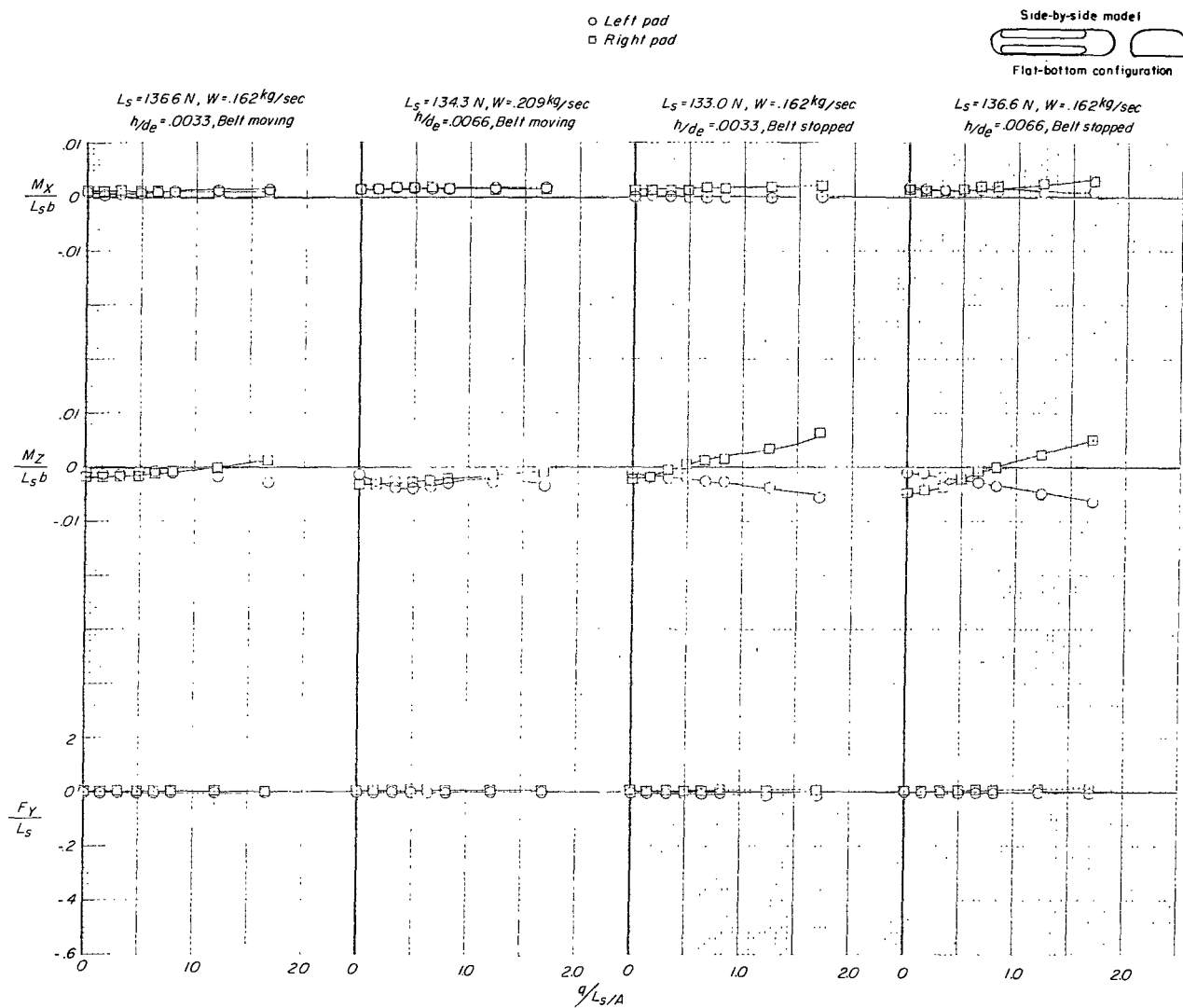
(c) Roll, yaw, and side force, total of both air cushions and total for entire vehicle, as a function of pressure ratio.

Figure 45.- Concluded.



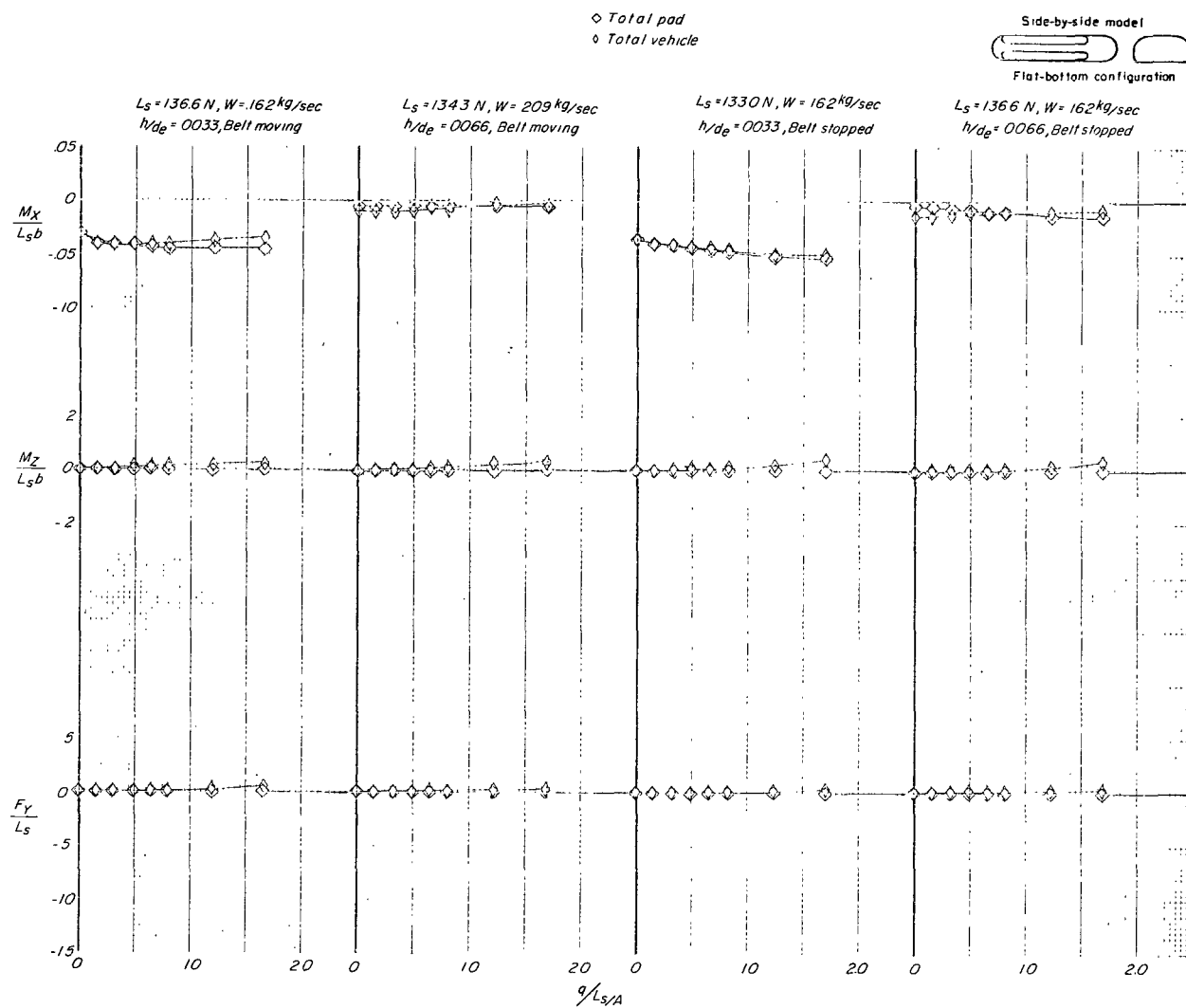
(a) Lift, drag, and pitching moment as a function of pressure ratio.

Figure 46.- Effect of height on aerodynamic characteristics for moving-belt and stopped-belt conditions at  $\beta = 0^\circ$ .



(b) Roll, yaw, and side force of each air cushion as a function of pressure ratio.

Figure 46.- Continued.



(c) Roll, yaw, and side force, total for both air cushions and total for entire vehicle, as a function of pressure ratio.

Figure 46.- Concluded.

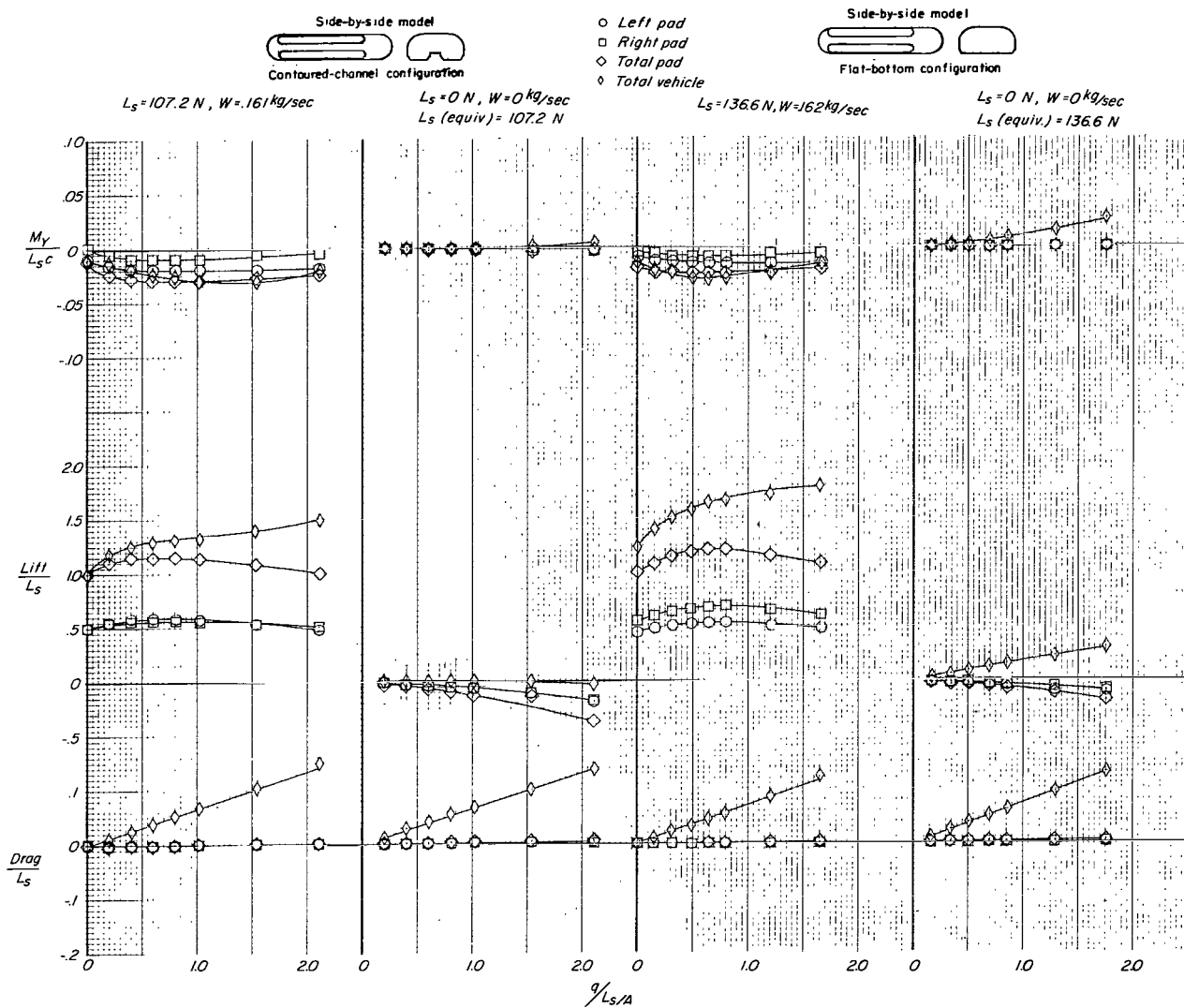
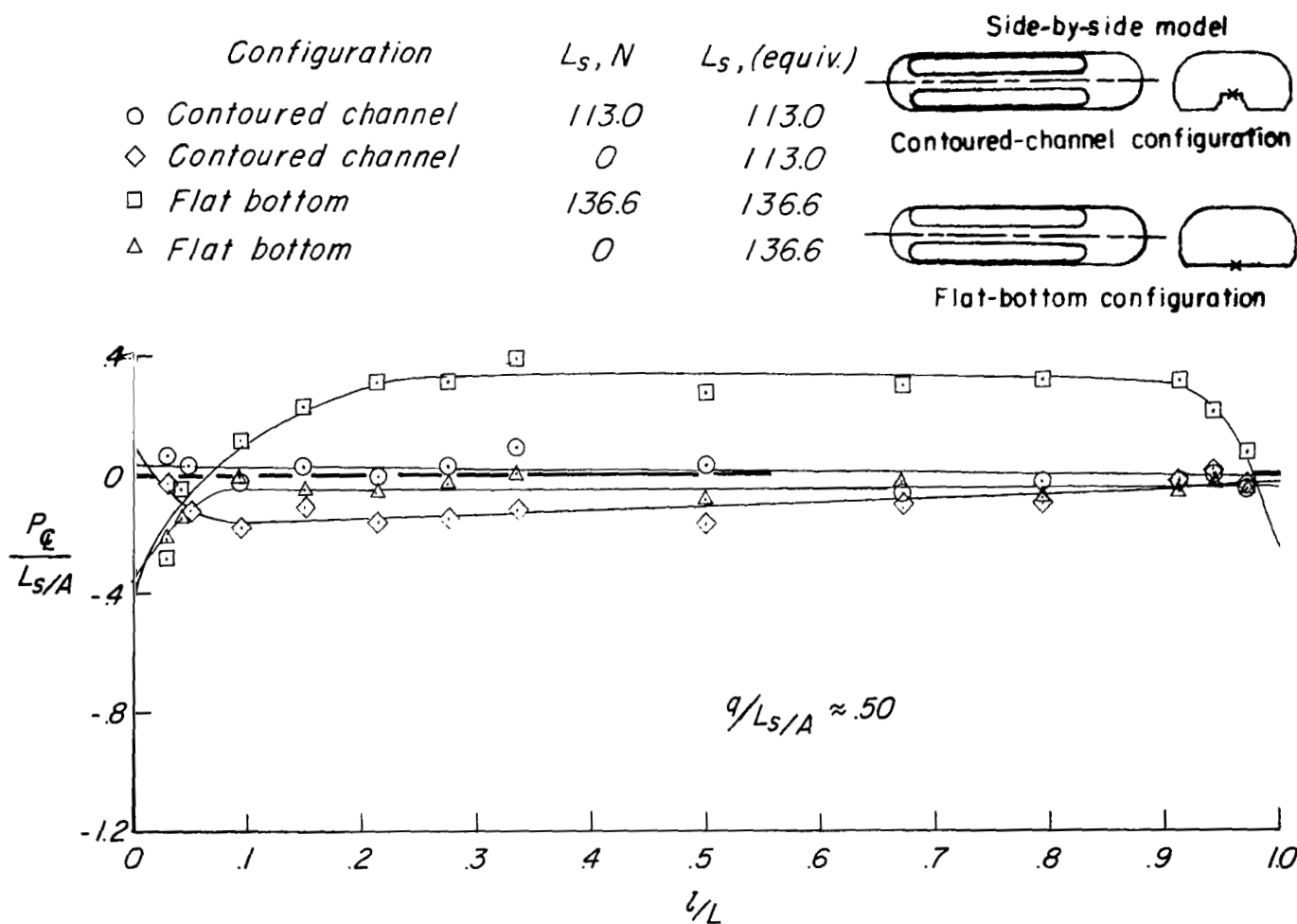
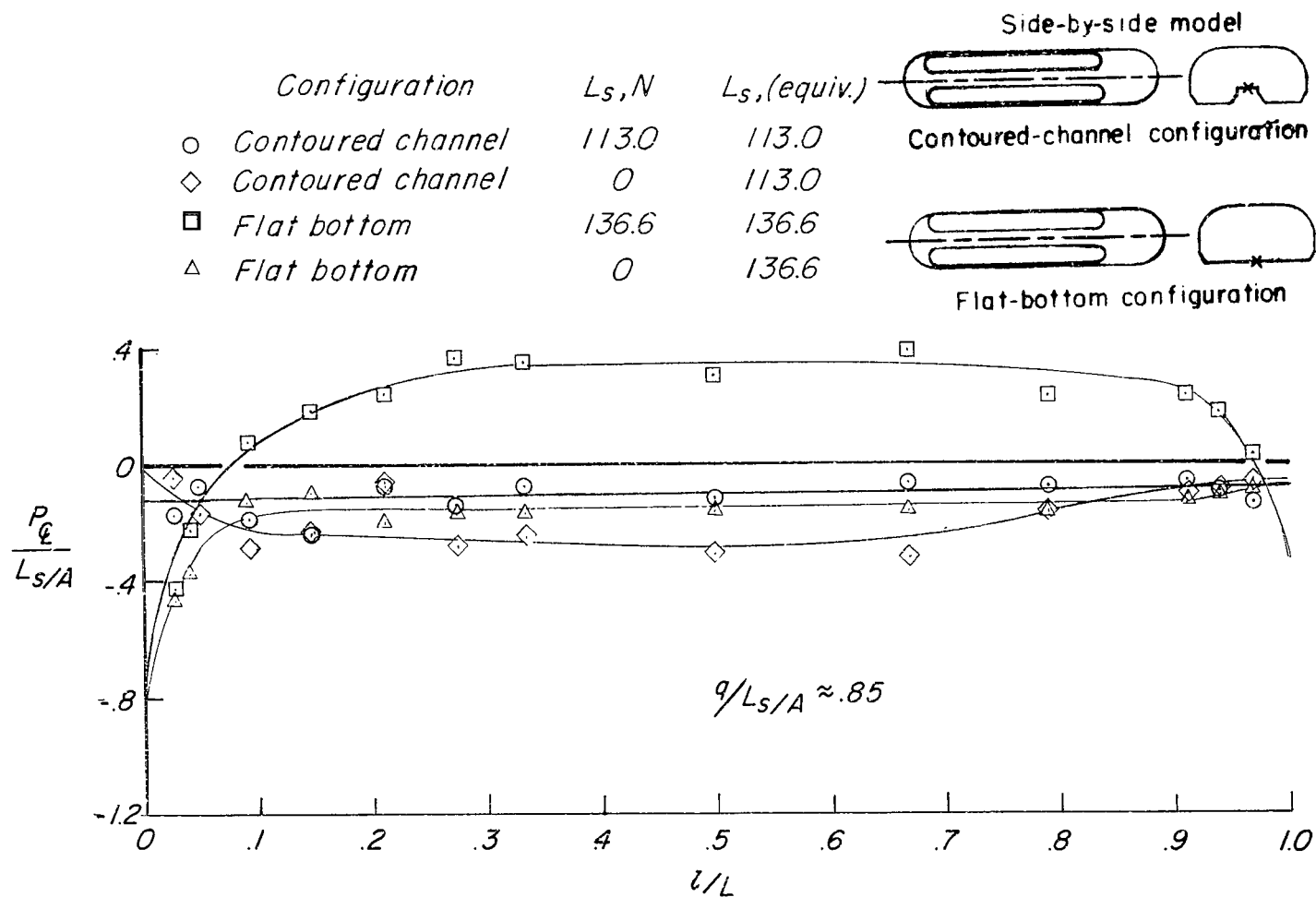


Figure 47.- Comparison of longitudinal aerodynamic characteristics of powered air cushion with those of unpowered cushion as a function of pressure ratio. Belt moving;  $h/d_e = 0.0033$ ;  $\beta = 0^\circ$ .



(a)  $q/L_s/A \approx 0.50$ .

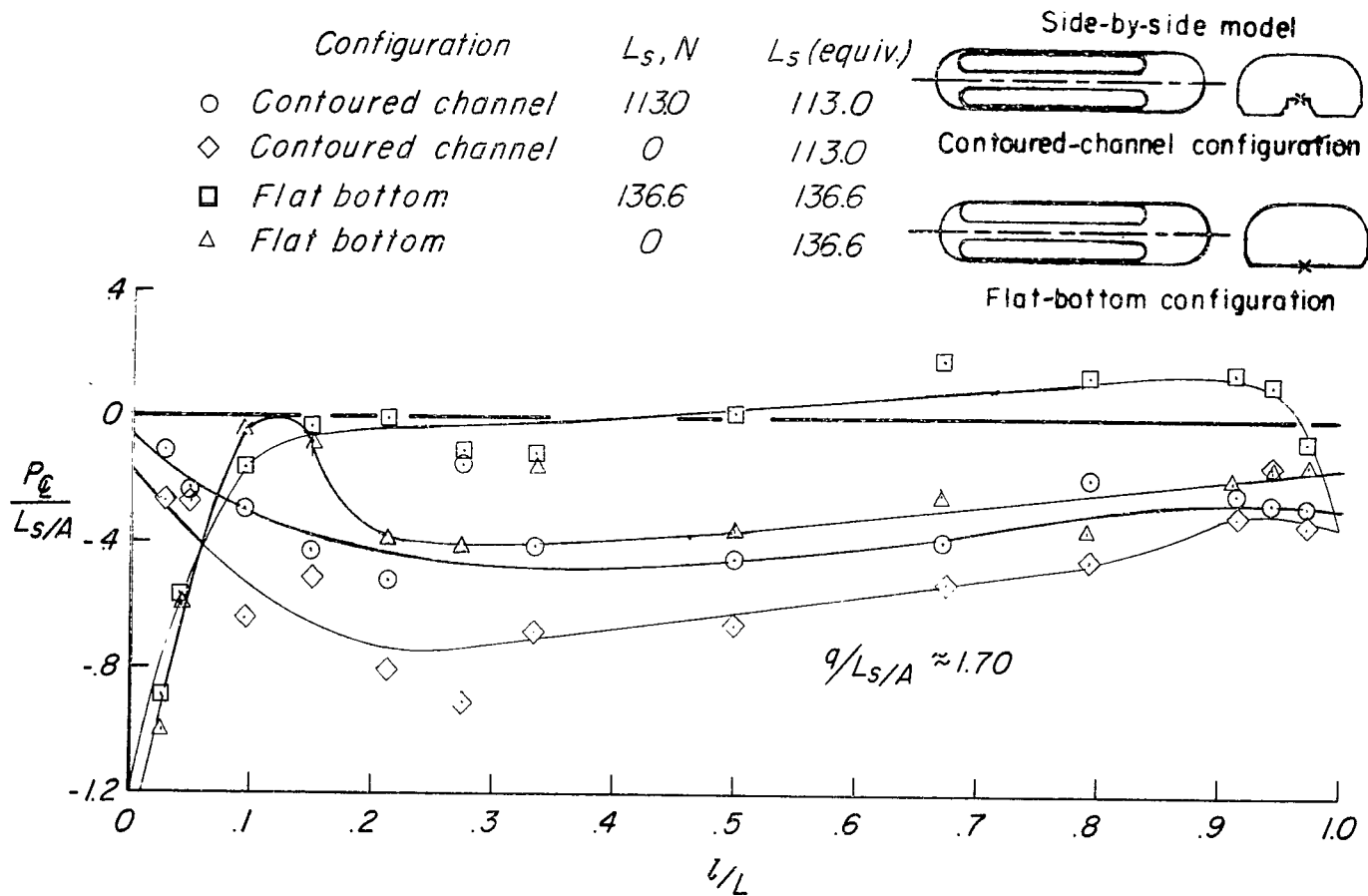
Figure 48.- The pressure distribution along center-line base of bottom of side-by-side models at various  $q/L_s/A$  values. (See fig. 6 for details.)



(b)  $q/L_s/A \approx 0.85$ .

Figure 48.- Continued.





(c)  $q / L_s / A \approx 1.70$ .

Figure 48.- Concluded.

NATIONAL AERONAUTICS AND SPACE ADMINISTRATION  
WASHINGTON, D. C. 20546  
OFFICIAL BUSINESS

FIRST CLASS MAIL



POSTAGE AND FEES PAID  
NATIONAL AERONAUTICS AND  
SPACE ADMINISTRATION

07U 001 26 51 3DS 70286 00903  
AIR FORCE WEAPONS LABORATORY /WLOL/  
KIRTLAND AFB, NEW MEXICO 87117

ATT E. LOU BOWMAN, CHIEF, TECH. LIBRARY

POSTMASTER: If Undeliverable (Section 158  
Postal Manual) Do Not Return

*"The aeronautical and space activities of the United States shall be conducted so as to contribute . . . to the expansion of human knowledge of phenomena in the atmosphere and space. The Administration shall provide for the widest practicable and appropriate dissemination of information concerning its activities and the results thereof."*

— NATIONAL AERONAUTICS AND SPACE ACT OF 1958

## NASA SCIENTIFIC AND TECHNICAL PUBLICATIONS

**TECHNICAL REPORTS:** Scientific and technical information considered important, complete, and a lasting contribution to existing knowledge.

**TECHNICAL NOTES:** Information less broad in scope but nevertheless of importance as a contribution to existing knowledge.

**TECHNICAL MEMORANDUMS:** Information receiving limited distribution because of preliminary data, security classification, or other reasons.

**CONTRACTOR REPORTS:** Scientific and technical information generated under a NASA contract or grant and considered an important contribution to existing knowledge.

**TECHNICAL TRANSLATIONS:** Information published in a foreign language considered to merit NASA distribution in English.

**SPECIAL PUBLICATIONS:** Information derived from or of value to NASA activities. Publications include conference proceedings, monographs, data compilations, handbooks, sourcebooks, and special bibliographies.

**TECHNOLOGY UTILIZATION PUBLICATIONS:** Information on technology used by NASA that may be of particular interest in commercial and other non-aerospace applications. Publications include Tech Briefs, Technology Utilization Reports and Notes, and Technology Surveys.

*Details on the availability of these publications may be obtained from:*

SCIENTIFIC AND TECHNICAL INFORMATION DIVISION  
NATIONAL AERONAUTICS AND SPACE ADMINISTRATION  
Washington, D.C. 20546